SURFACE MODIFICATIONS OF CELLULOSE NANOMATERIALS: MECHANISMS, KINETICS AND THEIR APPLICATIONS

Ana Oberlintner

Doctoral Dissertation
Jožef Stefan International Postgraduate School
Ljubljana, Slovenia

Supervisor: Asst. Prof. Dr. Uroš Novak, Department of Catalysis and Chemical Reaction Engineering, National Institute of Chemistry, Ljubljana, Slovenia
Co-Supervisor: Assoc. Prof. Dr. Blaž Likozar, Department of Catalysis and Chemical Reaction Engineering, National Institute of Chemistry, Ljubljana, Slovenia

Evaluation Board:
Prof. Dr. Uroš Cvelbar, Chair, Jožef Stefan International Postgraduate School, Ljubljana, Slovenia
Assoc. Prof. Dr. Urška Vrabič Brodnjak, Member, Faculty of Natural Sciences and Engineering, University of Ljubljana, Ljubljana, Slovenia
Assoc. Prof. Dr. Irena Pulko, Member, Faculty of Polymer Technology, Slovenj Gradec, Slovenia
Dr. Milica Velimirović, Member, Flemish Institute for Technological Research (Dutch: Vlaamse Instelling voor Technologisch Onderzoek or *VITO*), Mol, Belgium

MEDNARODNA PODIPLOMSKA ŠOLA JOŽEFA STEFANA
JOŽEF STEFAN INTERNATIONAL POSTGRADUATE SCHOOL

Ana Oberlintner

SURFACE MODIFICATIONS OF CELLULOSE NANOMATERIALS: MECHANISMS, KINETICS AND THEIR APPLICATIONS

Doctoral Dissertation

POVRŠINSKE MODIFIKACIJE CELULOZNIH NANOMATERIALOV: MEHANIZMI, KNETIKA IN NJIHOVE APLIKACIJE

Doktorska disertacija

Supervisor: Asst. Prof. Dr. Uroš Novak

Co-Supervisor: Assoc. Prof. Dr. Blaž Likozar

Ljubljana, Slovenia, July 2023

To everyone who made this possible.

Acknowledgments

First and foremost, I would like to express my sincere gratitude to my supervisor Asst. Prof. Dr. Uroš Novak for all the knowledge he shared with me and his guidance throughout my PhD journey. I really appreciate the freedom he gave me and his trust in my (research) skills to explore the topic in my own ways, while providing me the support to bring my ideas to life. I am also extending my gratefulness to Assoc. Prof. Dr. Blaž Likozar for his guidance, inputs on the manuscripts, but most importantly for being a great and open-minded boss and leader.

I am also genuinely grateful to Dr. Vasyl Shvalya, Dr. Neelakandan Marath Santhosh, Dr. Aswathy Vasudevan, Dr. Andrea Jurov, Martin Košiček, and Prof. Dr. Uroš Cvelbar from, what I feel was my "second lab", the Department of Gaseous Electronics at the Jožef Stefan Institute for sharing their equipment and extensive knowledge on plasma treatments as well as on surface analyses with me.

Special thanks go to Helena Spreitzer and Dr. Ivan Jerman for letting me use their tensiometer, which was one of the crucial tools for analyses in my thesis.

I am thankful to L'Oréal-UNESCO for awarding me the 'For Women in Science Fellowship'.
Slovenian Research and Innovation Agency is acknowledged for funding my studies through the Young Researcher program.

Big shout out goes to all of my amazing colleagues from the Department of Catalysis and Chemical Reaction Engineering, who made this roller-coaster ride less scary and quite enjoyable.

Thank you, my dear family and friends, for bearing with me over this journey, cheering my ups and supporting me during my downs. Thank you, Sheena, for always being there for me and offering the soft comfort. Finally, Žiga – the other half of the Dream Team, gargantuan thanks for your unlimited support in all aspects of life, without which these words would not see the light of day.

Abstract

Synthesized in green plants, cellulose is the most abundant natural biopolymer on the planet and is thus widely available, cheap and renewable. Furthermore, its hierarchical structure allows extraction of nanosized particles in the form of cellulose nanocrystals (CNCs), obtained with hydrolysis or cellulose nanofibrils (CNFs), isolated through chemical, biological pretreatment and mechanical fibrillation. The latter can also be produced by some bacteria, yielding bacterial nanocellulose (BNC). All cellulose nanomaterials exhibit high specific surface and mechanical strength, that are highly desirable in numerous applications.

In the dissertation, firstly, all three types of cellulose nanomaterials were used as primary biopolymer for film fabrication or as a reinforcing agent in chitosan and alginate-based composite films. To indicate their potential as sustainable packaging material, technical specifications of the films were evaluated: tensile strength (TS) and elongation-at-break (ε), together with oxygen permeability (OTR), water vapor transmission (WVT) and water contact angle (WCA). To enable broader applications, improvement towards the water resistance through functionalization of either cellulose nanomaterials prior to their incorporation in natural biopolymer matrix or by surface treatment of the already fabricated biopolymer film is needed.

Literature on hydrophobization of cellulose nanomaterials was thoroughly reviewed to determine possible approaches to modifications as well as to identify gaps in knowledge. While routes of chemical functionalizations (esterification, silylation, carbamation, etherification and click chemistry) are well known and researched, there is a lack of thorough studies on mechanisms and kinetics of these reactions, the understanding of which is crucial in transfer to industrial scale. Furthermore, the comprehensive review revealed that although the use of plasma treatment is fast and effective for hydrophobization of cellulose (nano)materials, only very limited available scientific contributions have been presented.

With this in mind, the films based on CNFs were processed with fluorocarbon plasma, resulting in a drastic increase of WCA from initial 46° to 130° in already 30 s of treatment due to newly formed C-F_3, C-F_2, and C-F bonds that were identified with high resolution C 1s XPS, Raman and ATR-FTIR spectroscopy. The treatment was extended to chitosan-based films with incorporated CNCs, studying stability of properties relevant for packaging applications as well (TS, ε, WVT and WCA) over the course of 30 days after hydrophobization. Additionally, no leaching of fluorine components into liquid environments was found through LC-MS analysis. While the treatment with RF-generated plasma in fluorocarbon was found to be ultrafast and providing stable hydrophobic coating, fluorinated compounds might cause a disturbance in metabolism at higher concentrations, therefore in this work we aimed to find a substitute gas. It was discovered that plasma generated in N_2 provides the same result of hydrophobic surface while avoiding fluorine-related compounds.

To fulfil the other objective, contribution to the knowledge on mechanisms and kinetics of functionalization reactions, an esterification reaction of cellulose nanomaterials with acetic anhydride in the presence of pyridine was revisited. A combined computational and experimental study of this reaction was carried out on both CNCs and CNFs, indicated two competitive reaction mechanisms and yielded kinetic parameters through microkinetic modelling of both materials. To demonstrate the practical use of surface acetylation of cellulose nanomaterials, modified CNCs of various degrees of substitution were incorporated into alginate and chitosan films that were subjected to various environmental humidity to evaluate its effect on TS, ε, moisture content and WVT. Finally, to gain an insight into the end-of-life of such films, biodegradation of alginate and chitosan-based with pristine and acetylated CNCs in activated sludge was followed through the course of 5 days through respirometry in OxiTop system.

Povzetek

Celuloza, ki jo sintetizirajo zelene rastline, je najbolj razširjen naravni biopolimer na planetu, zaradi česar je široko dostopna, poceni in hitro obnovljiva. Poleg tega nam njena hierarhična struktura omogoča ekstrakcijo nanodelcev v obliki celuloznih nanokristalov (CNC) preko hidrolize ali celuloznih nanofibrilov (CNF), pridobljenih s kemijsko in biološko obdelavo in mehansko fibrilacijo. Eno izmed oblik slednje lahko proizvedejo tudi nekatere bakterije, pri čemer nastane bakterijska nanoceluloza (BNC). Vsi ti celulozni nanomateriali imajo visoko specifično površino in mehansko trdnost, ki sta zelo zaželeni v številnih aplikacijah.

V disertaciji smo najprej uporabili vse naštete vrste celuloznih nanomaterialov kot primarne biopolimeri za izdelavo filmov ali kot ojačevalce v kompozitnih filmih na osnovi hitozana in alginata. Da bi pokazali njihov potencial kot trajnostni embalažni material, smo ocenili tehnične specifikacije folij - natezno trdnost (TS), raztezek ob pretrganju (ε), prepustnost kisika (OTR), prepustnost vodne pare (WVT) in kontaktni kot z vodo (WCA). Za širšo uporabo je potrebno izboljšanje odpornosti na vodo, kar je mogoče doseči s funkcionalizacijo celuloznih nanomaterialov pred njihovo vključitvijo v naraven biopolimer ali s površinsko obdelavo že izdelanega biopolimernega filma.

Literatura s področja hidrofobizacije celuloznih nanomaterialov je bila temeljito pregledana, da bi določili možne pristope k modifikacijam in odkrili vrzeli v znanju. Medtem ko so možnosti kemičnih funkcionalizacij (esterifikacija, sililacija, karbamacija, eterifikacija in klik-kemija) dobro raziskane, primanjkuje temeljitih študij o mehanizmih in kinetiki teh reakcij, razumevanje katerih je ključnega pomena za prenos na industrijsko skalo. Poleg tega je celovit pregled pokazal, da čeprav je uporaba plazemske tehnologije hitra in učinkovita za hidrofobizacijo celuloznih (nano)materialov, je število objavljenih študij omejeno.

Z ozirom na to so bili filmi na osnovi CNF obdelani s fluorogljikovo plazmo, kar je drastično povečalo WCA z začetnih 46° na 130° že v prvih 30 s obdelave. Razlog za spremembo leži v novonastalih C-F_3, C-F_2 in C-F vezeh, ki so bile identificirane z visokoločljivostnim C 1s XPS, Ramansko spektroskopijo in ATR-FTIR. Takšna obdelava je bila razširjena na filme na osnovi hitozana z dodanimi CNC-ji, pri čemer smo preučevali stabilnost lastnosti, ki so pomembne za pakirano embalažo (TS, ε, WVT in WCA) v 30 dneh po hidrofobizaciji. Poleg tega z analizo LC-MS ni bilo ugotovljeno izpiranje komponent fluora v različne tekočine. Čeprav obdelava biopolimernih filmov z RF-generirano plazmo v fluorogljiku zelo hitra in zagotavlja stabilno hidrofobno prevleko, lahko fluorirane spojine povzročijo motnje v presnovi v višjih koncentracijah. V nadaljnjem delu smo zato iskali alternativen plin, ki bi nadomestil fluorogljike. Ugotovljeno je bilo, da plazma, ustvarjena v N_2, zagotavlja enak rezultat hidrofobne površine, pri čemer se izognemo uporabi fluorovih spojin.

Za izpolnitev drugih ciljev – prispevek k znanju o mehanizmih in kinetiki funkcionalizacijskih reakcij – je bila obravnavana reakcija esterifikacije celuloznih nanomaterialov z anhidridom ocetne kisline v prisotnosti piridina. Kombinirana računalniška in eksperimentalna študija te reakcije, ki je bila izvedena na CNC in CNF, nakazuje na dva konkurenčna reakcijska mehanizma in podaja kinetične parametre preko mikrokinetičnega modeliranja obeh materialov. Za prikaz praktične uporabe površinske acetilacije celuloznih nanomaterialov so bili CNC modificirani do različnih stopenj substitucije in vgrajeni v filme na osnovi alginata in hitozana. Ti so bili nato izpostavljeni okoljem različnih vlažnosti, da bi ocenili njihov učinek na TS, ε, vsebnost vlage in WVT. Za vpogled v dogajanje ob koncu življenjske dobe filmov so bile izvedene študije biorazgradnje alginata in hitozana na osnovi nemodificiranih in acetiliranih CNC v aktivnem blatu, kjer smo biorazgradnjo spremljali 5 dni preko respirometrije v sistemu OxiTop.

Contents

List of Figures

List of Tables

Abbreviations

CNCs	. . .	Cellulose nanocrystals
CNFs	. . .	Cellulose nanofibrils
BNC	. . .	International Postgraduate School
GlcNAc	. . .	N-acetylated-D-glucosamine
GlcN	. . .	D-glucosamine
LDPE	. . .	Low density polyethylene
AGU	. . .	Anhydroglucopyranose unit
PLA	. . .	Polylactic acid
WCA	. . .	Water contact angle
SEM	. . .	Scanning electron microscope
TEM	. . .	Transmission electron microscope
XRD	. . .	X-ray diffraction
NMR	. . .	Nuclear magnetic resonance
ATR-FTIR	. . .	Attenuated total reflection Fourier transform infrared
XPS	. . .	X-ray photoelectron spectroscopy
RF	. . .	Radiofrequency
LC-MS	. . .	Liquid chromatography-mass spectroscopy
DBD	. . .	Dielectric barrier discharge

Chapter 1

Introduction

1.1 In Search of Materials of the Future

In the last century, plastic materials have found their way into all aspects of our daily life due to their toughness, durability and incredible versatility. However, in 2021, 44 % of altogether 390.7 million tons produced plastic was used for packaging sector, which is the application that also exhibits the shortest lifetime as it is in use for only half a year on average and thus generating the most plastic waste (Geyer, Jambeck, and Law 2017). In light of raising awareness of plastic pollution and its potential health risks caused by microplastics, eco-friendly and non-hazardous alternatives are needed and in focus of research. The solution is seen in biodegradable, biocompatible and non-toxic biopolymers, originating from renewable biomass. Still, such materials should be comparable to conventional packaging or even better in shielding of product from environmental conditions by exhibiting suitable mechanical strength, water vapor and oxygen barrier, thermal resistance and antimicrobial activity. Furthermore, it is crucial for the material to be lightweight and flexible. This chapter introduces chitosan, alginate and cellulose nanomaterials, the main biopolymers used in the thesis, in terms of structure, isolation from raw biomass and potential applications with a focus on the packaging industry.

1.1.1 Chitin and Chitosan

After cellulose, chitin is the second most abundant biopolymer in nature. It is found in shells of crustaceans, exoskeletons of insects, skeletons of mollusk or cell walls of some fungi (Ji et al. 2022). It is a linear polymer consisting of β-(1,4)-N-acetylglucosamine (GlcNAc) units connected through glycoside bonds (Song, Shang, and Ratner 2012). The production of chitin from raw biomass consists of demineralization, deproteinization and decolorization as depicted in Figure 1, with the side products of each step having economic value (Vicente et al. 2022). By deacetylation D-glucosamine (GlcN) is formed and with degree of deacetylation (molar ratio of GlcN compared to all (GlcN and GlcNAc) units in the polymer) reaching at least 50 %, a derivative called chitosan is obtained, which is also a threshold for solubility in acidic media (Jiang et al. 2017). Additionally, chitin is a semi-crystalline biopolymer with crystallinity around 70 %, which decreases with deacetylation to about 30 % (Ji et al. 2022). Molecular weight (which also defines viscosity) and functional properties of chitosan are predominantly determined by the source of chitin, reaction conditions during the isolation process and degree of deacetylation (Oladzadabbasabadi et al. 2022).

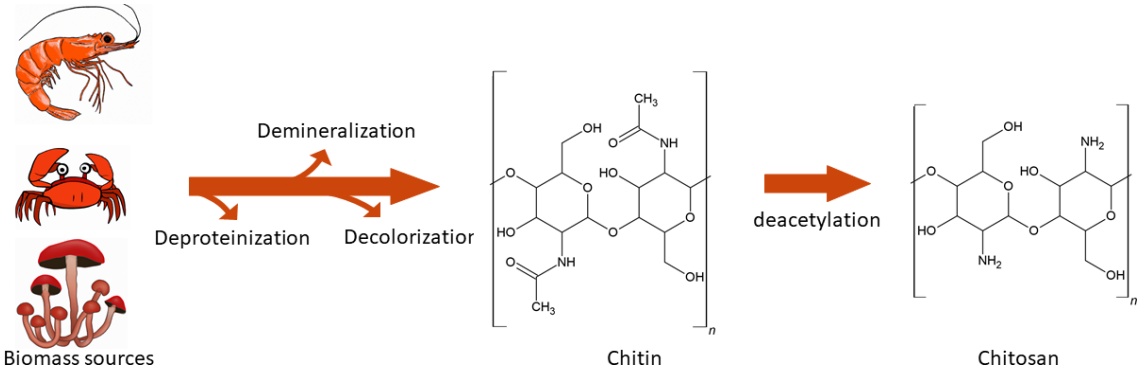

Figure 1: Production of chitosan from biomass with depicted chitin and chitosan structural formulas.

Its non-toxicity, pH sensitivity, biodegradability, antioxidant, antibacterial and chelating properties, solubility in green solvents and biocompatibility have brought chitosan to be seen as a high potential material in various fields. Chitosan and its derivatives can be fabricated in the form of films, hydrogels, sponges, electrospun membranes and asymmetric membranes (Cao et al. 2022; Heimbuck et al. 2019; Hosseini et al. 2022; Ji et al. 2022; Zhang et al. 2021) and as such used in numerous applications in various fields: in biotechnology for enzyme immobilization (Verma et al. 2020), biomedicine (wound dressing, tissue engineering) (Kalantari et al. 2019), pharmacy (drug delivery) (Murthy et al. 2020), agriculture to manage plant diseases (Riseh et al. 2022), food as a gelling, thickening and stabilizing agent (Agulló et al. 2003), cosmetics (skin care, hair care and gum and teeth health) (Aranaz et al. 2018) and environment (dye and oil absorbent from waste waters) (Oladzadabbasabadi et al. 2022). Commercially, chitosan is already used as a wound dressing and food supplement (Biranje et al. 2021; Ji et al. 2022).

Chitosan presents a promising biopolymer as matrix or only component of packaging applications. Various methods were used to prepare chitosan-based films or coatings: direct casting or solvent casting, coating, dipping or layer-by-layer assembly. Chitosan packaging materials can be obtained through extrusion as well, though in this case, chitosan is added as an additive to a non-biobased matrix such as low density polyethylene (LDPE) or polycaprolactone (Wang, Qian, and Ding 2018). Natural antimicrobial and antioxidative activity of chitosan-based films can be enhanced by the addition of various plan extracts rich in antioxidants such as hop (Bajić, Jalšovec, et al. 2019), chestnut (Bajić, Ročnik, et al. 2019), oak (Bajić, Ročnik, et al. 2019), turmeric (Kalaycıoğlu et al. 2017), thyme (Talón et al. 2017), etc. Furthermore, such films were shown to be biodegradable in terrestrial environment (Oberlintner et al. 2020). Regarding barrier properties, chitosan-based films exhibit sufficiently low permeability for oxygen, while their high sensitivity to water prevents them to perform well in humid environments (Gällstedt and Hedenqvist 2002).

1.1.2 Alginate

Alginate, an anionic polymer composing up to 40 % of dry matter of brown marine algae such as *Ascophyllum nodosum*, *Laminaria hyperborean,* and *Macrocytis pyrifera*, is built of β-D-mannuronate (M block) and α-L-guluronate (G block) that are linked by 1-4 glycosidic bonds (Hay et al. 2013). In nature, it is found as a gel in the intercellular matrix and contains Na^+, Ca^{2+}, Mg^{2+}, Sr^{2+} and Ba^{2+} ions and is as such not soluble in water. To extract it from biomass ion-exchange is carried out first, usually by treatment with mineral acid. The product is then neutralized with Na_2CO_3 or NaOH forming sodium alginate, which is water soluble. Separation processes such as sifting, flotation, centrifugation and filtration are applied to separate sodium alginate from algal residues. Lastly, to obtain the dry form, Na-alginate is precipitated by alcohol, calcium chloride or mineral acid and then finally converted back to sodium form (Draget 2009). The process scheme of alginate production is shown in Figure 2.

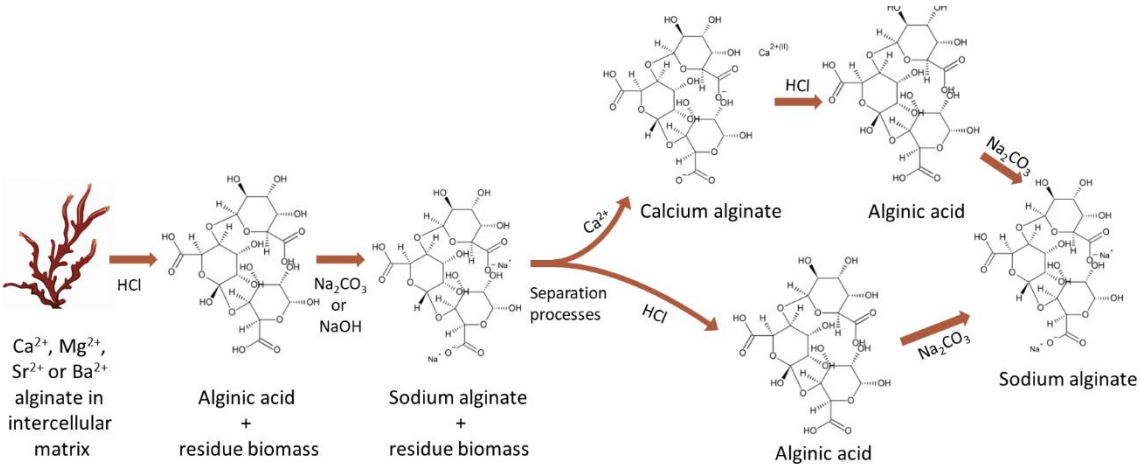

Figure 2: Schematic representation of extraction of alginate from marine biomass.

One of the most useful properties of alginate is its ability to form gels in the presence of bivalent ions (such as Ca^{2+}, Ba^{2+}, Cu^{2+}, $Sr^{2+}$and Zn^{2+}). The physicochemical properties of alginate, viscosity and its gelation behavior (shrinking, swelling, mechanical resistance of gels) are greatly influenced by molecular weight of alginate that depends on the biomass source and extraction process, typically falling between 32 and 400 kDa (Hu et al. 2021). Additionally, as only G blocks are involved in intermolecular crosslinking with divalent ions G/M blocks ratio their sequence and length of G blocks influence physical properties of hydrogels as well (Hu et al. 2021; Lee and Mooney 2012). On the other hand, in an environment free of crosslinking ions, alginate is soluble in water (Pawar and Edgar 2012).

Due to its gelation properties, alginate is commercially used as a food thickener and stabilizing agent as well as binder, gelling agent and wound dressing in pharmaceutical industry (Goh, Heng, and Chan 2012). Furthermore, alginate has shown to be useful in bone regeneration applications (dental molds, simulator of extracellular matrix proteins, tissue scaffolding) and cell culture (Goh et al. 2012; Hu et al. 2021).

Alginate exhibits high potential for use in food packaging industry as well. So far, the use of edible alginate-based films and coatings, possibly with incorporated antibacterial and antimicrobial active ingredients (lemongrass, cinnamon and rosemary oil, silver nanoparticles), were shown to prolong shelf-life of various foods such as button mushrooms (Jiang 2013), fresh-cut carrots (Costa et al. 2012), chicken meat (Raeisi et al. 2016) and various fruits (Maftoonazad, Ramaswamy, and Marcotte 2008). Yet, its full potential has not been fully exploited commercially in the field of packaging as poor water vapor barrier properties and high sensitivity to water that causes swelling of the film pose as a limitation (Kontominas 2020).

1.1.3 Cellulose and Cellulose Nanomaterials

1.1.3.1 Sources and Structure of Cellulose

Cellulose is the most abundant biopolymer on the planet and is therefore cheap and easily accessible around the world. It is found mostly in cell walls of green plants and is harvested in the form of lignocellulosic biomass, which consists of cellulose (35 %–50 %), hemicellulose (20 %–35 %) and lignin (10 %–25 %) as well as smaller fractions of proteins, oils and ash (Wei et al. 2017). Cellulose is obtained through pulping process in which lignin is dissolved and removed from the biomass (Aravamuthan 2004). Besides plants, some prokaryotes (*Achromobacter Alcaligenes, Acetobacter, Aerobacter, Agrobacterium, Azotobacter, Escherichia, Klebsiella, Pseudomonas, Salmonella, Sarcina)*, archaea (*Thermoplasma, Ferroplasma*) and eukaryotes (*Cyanobacter, Green algae, Rhizobium, Tunicates*) produce cellulose as well (Raghavendran, Asare, and Roy 2020). It is called bacterial cellulose and is, compared to plant cellulose, purer as it contains no lignin and hemicellulose (Heinze 2016; Raghavendran et al. 2020).

The basic building blocks of cellulose are D-anhydroglucopyranose units (AGUs) alternatively rotated for 180° along the chain axis linked through β-1,4 glyosidic bonds. As it is a product of

polycondensation reaction, the last units on both sides differentiate as one is a reducing end and the other one a non-reducing end. A single chain in native cellulose measures 500–15,000 nm in length. There are two secondary in-plane and one primary out-of-plane hydroxyl groups on each AGU that play several roles in the structure of cellulose. Firstly, inter- and intra-molecular bonding is formed between these hydroxyl groups, forming first cellulose nanofibrils, then macrofibrils and finally cellulose fibers as shown in Figure 3 (Heinze 2016; Yuan and Cheng 2015). A result of hydrogen bonding is also ordered crystalline arrangements, leading to four different crystalline allomorphs: cellulose I, II, III and IV. The basic form found in nature is cellulose I, from which then cellulose II can be obtained through alkali treatment or solubilization and subsequent recrystallization. Cellulose III_I and III_{II} are prepared from cellulose I and cellulose II by treatment with liquid ammonia, respectively. Lastly, cellulose IV_I and cellulose IV_{II} are formed upon heating of cellulose III_I and III_{II}, respectively (Zugenmeier 2021). Surface hydroxyl groups are also the reason behind inherent hydrophilicity of cellulose and its poor compatibility with polar solvents or matrices. However, they are also the most reactive part of cellulose molecule which enables surface modifications minimizing hydrophilicity (Heinze 2016).

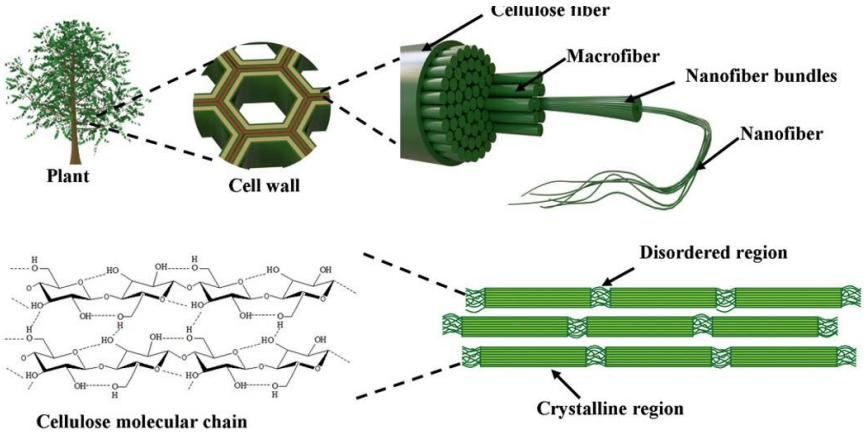

Figure 3: Schematic representation of hierarchical structure of cellulose from plant to molecular chains. Reproduced with permission from Pei et al. (2021).

1.1.3.2 Isolation of Cellulose Nanomaterials and Their Properties

Due to the hierarchical structure of cellulose, it is possible to isolate cellulose nanoparticles in two forms: cellulose nanocrystals (CNCs, also known as nanocrystalline cellulose NCC) or cellulose nanofibrils (CNFs, also known as nanofibrillated cellulose NFC). The two differentiate in shape and crystallinity, as well as isolation method.

CNCs are generally obtained through acid (usually by use of sulfuric or hydrochloric acid) hydrolyzation that penetrates into amorphous parts of cellulose fibers and dissolves them leaving highly crystalline rod-like nanoparticles with 3-50 nm in width and from 100 nm to several µm in length (International Organization for Standardization 2017; Vanderfleet and Cranston 2021). The exact dimensions and crystallinity depend on the cellulose source and treatment conditions that affect surface charge as well. CNCs isolated through hydrolyzation with sulfuric acid are negatively charged and tend to be more stable in suspensions compared to positively charged CNCs obtained with HCl hydrolyzation (Heinze 2016). CNCs exhibit an exceptionally high Young's modulus (143 GPa for a single CNC) and mechanical strength (approx. 10 GPa) (Shojaeiarani, Bajwa, and Chanda 2021; Šturcová, Davies, and Eichhorn 2005).

The second type of cellulose nanomaterials, CNFs, are in the form of long fibrilous network with diameter of a single fibril between 3 nm and 100 nm and up to 100 µm in length (International Organization for Standardization 2017). They are produced by mechanical disintegration (homogenization, grinding, refining, extrusion, ultrasonication, cryocrushing, steam explosion and ball milling), however to lower the cost of energy-intensive principle mechanical treatment, pretreatments such as blending, refining, grinding, enzymatic hydrolysis, 2,2,6,6-tetramethylpiperidine-N-oxyl)-mediated oxidation, etc. are carried out as well (Nechyporchuk, Belgacem, and Bras 2016). It is less crystalline than CNCs as it retains the

amorphous, less ordered regions of cellulose, enabling higher mobility. Tensile strength and Young's modulus were reported to be 0.8–10 GPa and 30–250 GPa for a single fiber, respectively (Jele, Lekha, and Sithole 2022).

1.1.3.3 Applications of Cellulose Nanomaterials

High mechanical strength and specific surface, light weight, biocompatibility and biodegradability of cellulose nanomaterials enable their use in a broad range of applications, such as electronics (as a substitute of plastic or glass for flexible display panels and electronic devices or as highly bendable microelectrodes in small electronic devices) (Dufresne 2019; Kim et al. 2018), construction (for insulation purposes, concrete) (Aziz, Zubair, and Saleem 2021), energy storage (as an alternative to separator in lithium-ion batteries or as supercapacitors) (Wang et al. 2017), biomedicine (scaffold for growth of cell cultures, drug delivery, blood vessels, soft tissues, cartilage and bone tissue) (Dufresne 2019) and packaging, which are in focus in this thesis.

Cellulose nanomaterials can be applied in the packaging industry as a standalone biopolymer (typically CNFs) or incorporated into other (bio)polymer matrices (CNCs or CNFs). Both types of cellulose nanomaterials were shown to decrease oxygen permeability when incorporated in matrices such as polylactic acid (PLA) and polycaprolactone (Espino-Pérez et al. 2018; Khan et al. 2013). Low oxygen permeability is important especially in food packaging applications, as oxidation of lipids is a major factor in food spoilage (Saedi et al. 2021). Important role of packaging materials is also to protect their contents from damages during distribution, therefore the advantage of cellulose nanomaterials lies in their high mechanical strength and stiffness. Their addition to high density polyethylene, LDPE, polycaprolactone and polypropylene has resulted in an increase of Young's modulus (Abdelmouleh et al. 2007; Ahmadi, Behzad, and Bagheri 2017; Ferreira et al. 2019; Inukai, Kurokawa, and Hotta 2020). Furthermore, in certain polymers (PLA and polyvinyl acetate), incorporation of cellulosic fibers decreased water vapor permeability, an important parameter in evaluation of product protection from environment (Saedi et al. 2021). However, in their natural form, cellulose nanomaterials generally exhibit high hydrophilicity and water sensitivity and low compatibility with most of conventional packaging matrices, preventing full exploitation of their potentials. To overcome this issue, the surface of cellulose nanomaterials before incorporation into the biocomposite or surface of already produced biopolymer composite films can be hydrophobically modified.

1.1.3.4 Surface Modifications of Cellulose Nanomaterials or Polysaccharide Composite Films

Surface is considered to be hydrophobic when water contact angle (WCA), a demonstrative measurement of surface hydrophilicity/hydrophobicity, is higher than 90°. The hydrophilic/hydrophobic character is governed by two parameters: surface free energy and surface topology. The latter is not applicable in modification of CNCs or CNFs as they are already nanostructures, but is an important parameter when decreasing hydrophilicity of films. Due to the presence of hydroxyl groups (each AGU contains two secondary (C2 and C3) and one primary (C6) alcohols) on the surface of cellulose nanomaterials that are the reason behind hydrophilicity, most approaches for surface modification target their decrease. These hydroxyl groups can be substituted with a more hydrophobic species or grafted with polymer chains (Kargarzadeh et al. 2018). It is important to note that not all three of them are equally reactive, as the primary alcohol group is more exposed and prone to reactions. Because CNCs tend to aggregate and CNFs arrange themselves in entangled fibrilous networks, the exposure of hydroxyl groups can be as low as 2 % (Dufresne 2012). Further, while modifying the surface of cellulose nanomaterials, it is crucial not to impact their size or crystallinity.

Generally, there are two different approaches to decreasing surface free energy: covalent and non-covalent modification. Taking the covalent modification approach, hydrophobic functional groups or polymer chains can be grafted to the surface of cellulose nanomaterials through esterification, carbamation, silylation etherification or click chemistry reactions (Kargarzadeh et al. 2018). Non-covalent hydrophobization includes adsorption of surfactants, oligomers or copolymers that hinder hydroxyl groups and induce hydrophobicity by prevention of hydrogen bonds formation (Habibi 2014). Detailed description of hydrophobization

techniques of cellulose nanomaterials with an emphasis on mechanisms and kinetics with an intent to identify knowledge gap is one of the objectives of the thesis and can be found in Chapter 3.

Regarding surface hydrophobization of biopolymer-based films, both chemical and morphological modifications can be applied. Biopolymer films were hydrophobized by using acid chloride and acid anhydride (Tangpasuthadol, Pongchaisirikul, and Hoven 2003), silane (Oyekanmi et al. 2021; Surya et al. 2022), pentafluorobenzoyl chloride (Cunha et al. 2007) and dodecyl aldehyde (Zheng et al. 2014). Besides chemical modification, hydrophobicity of surfaces of solid materials can be further increased through topology, by increasing surface roughness (Kim et al. 2007). Researchers have tried mimicking nature and its hierarchical microstructures with which, together with wax, plant leaves exhibit (super)hydrophobic behavior with WCAs over 160° (Ensikat et al. 2011). Attempts of such surface manipulation are described mostly on conventional polymers. Polystyrene, for example, was modified by the means of electrohydrodynamics (Jiang, Zhao, and Zhai 2004), electrospinning (Zhu et al. 2006) or structure of polytetrafluoroethylene was manipulated by using filter paper as a template (Hou and Wang 2009) or by direct molding technique (Lepore and Pugno 2011; Pereira et al. 2014) and polydimethylsiloxane with soft lithography process (Foday Jr et al. 2022), as well as C:H:Si:O coating with plasma (Kim et al. 2007). However, to the best of my knowledge, controlling hydrophobic properties with surface roughness of biopolymers is not documented in the literature.

1.2 Motivation, Hypotheses, Thesis Objectives and Novelty

The main motivation of this thesis is to explore the role of cellulose nanomaterials in polysaccharide flexible film materials, their hydrophobic modifications, mechanisms and kinetics of such reactions and impact of such treatments on its applicative properties. Development of new, sustainable materials should be in line with 12 principles of green chemistry defined by Anastas and Warner (Anastas and Warner 1998): 1) prioritizing prevention to cleaning up the waste, 2) maximizing incorporation of materials used during the process into the final product (atom economy), 3) use of non-toxic and less hazardous chemicals, 4) designing safer products, 5) reducing use of solvents and use of benign solvents and auxiliaries, 6) maximizing energy efficiency, 7) use of renewable feedstocks, 8) reducing derivatives, 9) favorizing catalysts to stoichiometric reagents, 10) designing the product to degrade, 11) development of real-time analytics and 12) use of substances that minimize accident probability. The thesis follows the guidelines where applicable, as further described in Sections from 1.2.1 to 1.2.5.

With this in mind, five objectives and four hypotheses were defined that are discussed in Chapters 2 - 5. For clarity, the outline of the dissertation is schematically presented in Figure 4.

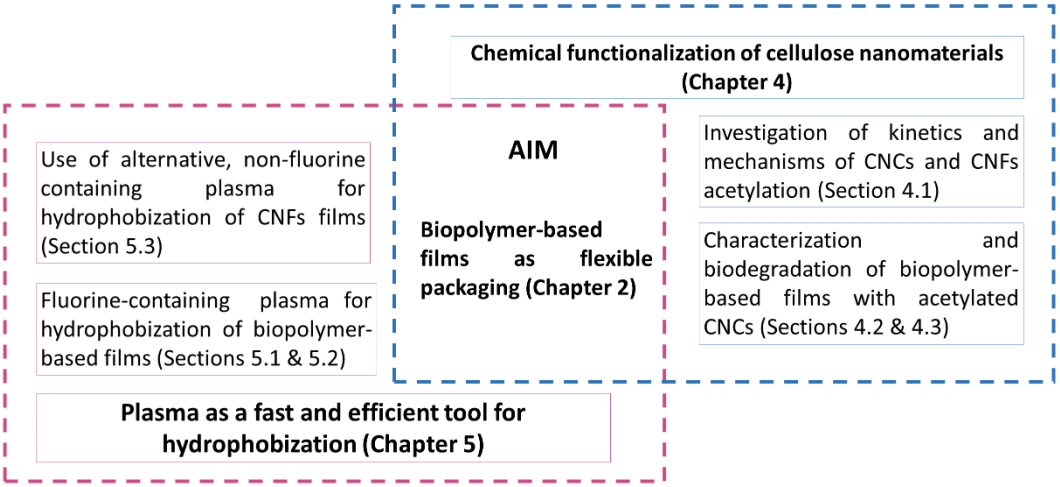

Figure 4: Schematic representation of the structure of the doctoral dissertation.

1.2.1 Objective 1: Fabrication and Evaluation of Alginate, Chitosan, Cellulose Nanomaterials and Their Composite Films

Film forming ability of chitosan and alginate was taken advantage of to produce alginate, chitosan, cellulose nanomaterials and their biocomposite films that exhibit high potential to be used as an alternative to conventional single-use packaging materials. The first hypothesis of the dissertation is that the use of nanosized cellulose in biocomposites improves mechanical and barrier properties and brings biopolymer-based flexible films closer to being comparable with conventional packaging. Therefore, the first objective is to evaluate such films in terms of morphology, mechanical resistance, water vapor and oxygen barrier capability and their interactions with water interactions (water contact angle, water uptake). Based on these results, the best compositions of biopolymer-based films will be selected and further studied throughout the thesis. Several principles of green chemistry are followed by this research: non-toxic and less hazardous renewable feedstocks are used with the goal to produce a safe and degradable final product. Furthermore, non-toxic, non-hazardous and benign solvents such as water and aqueous solution of lactic acid are used. Finally, such films employ waste biomass from food processing facilities (chitosan) or renewable biomass that is not competing with food production (alginate and cellulose nanomaterials).

Novelty of this work: The research concerning this objective systematically compares films based on chitosan, alginate and cellulose nanomaterials respect to properties relevant for packaging applications for the first time and offers the suitable formulations for such applications.

The results regarding this objective are discussed in Chapter 2.

1.2.2 Objective 2: Comprehensive Review of Hydrophobic Modifications of Cellulose Nanomaterials and Identification of Knowledge Gaps

To overcome the drawbacks such as poor compatibility, hydrophilicity, high water permeability and overall water sensitivity in biocomposites, modification of surface hydroxyl groups on cellulose nanomaterials is widely researched. The second objective of this thesis is to provide a comprehensive review on the topic of cellulose nanomaterials hydrophobic modifications with the emphasis on reaction mechanisms and kinetics as the second hypothesis is that there is currently a lack of published literature concerning these two specific topics. The identified knowledge gaps will serve as a starting point for further research and will be covered throughout the dissertation.

Novelty of this work: In this part of thesis, the hydrophobic functionalization reactions are comprehensively reviewed, to the best of our knowledge for the first time, with emphasis on mechanistic and kinetic point of view.

Objective 2 is addressed in Chapter 3.

1.2.3 Objective 3: Determination of Kinetics and Mechanisms of Cellulose Nanomaterials Modification

Objective 3 is based on the findings of the literature review, demonstrating that the techniques to hydrophobization of cellulose nanomaterials are widely researched, however the exact mechanisms and kinetics remain unknown. To address this issue, a reaction of cellulose nanomaterials with acetic anhydride in the presence of pyridine, which was previously proposed in literature, will be examined closely in terms of mechanisms and kinetics. The study will be carried out with a joint experimentally-computational approach. Knowledge of exact mechanism and kinetic parameters are crucial to push cellulose nanomaterials to an industrial scale, taking into the account the approaches of green chemistry. By knowing the exact mechanism and kinetics of the reaction, atom economy (maximizing incorporation of all reagents and avoidance of side products) can be considered as well as optimization of reaction in terms of energy efficiency.

Novelty of this work: In this objective, the mechanism and kinetics of cellulose nanomaterials acetylation with acetic anhydride in presence of pyridine are scrutinized. For the first time, the mechanisms of this reaction are defined as a competitive mechanism of one-step (direct conversion) and two-step (through intermediate) reactions accompanied with development of a kinetic model that describes both types of cellulose nanomaterials.

Objective 3 is addressed in Chapter 4, Section 4.1.

1.2.4 Objective 4: Biopolymer-Based Films Reinforced with CNCs, Their Properties and Biodegradability in Activated Sludge Medium

The fourth objective is to demonstrate the applicability of acetylated cellulose nanomaterials by incorporating acetylated CNCs to various degrees of substitution, using reaction studied in Objective 3, into chitosan and alginate matrices to fabricate films suitable for packaging applications, concerning the next hypothesis, stating that acetylated cellulose nanocrystals can be used as a reinforcement in chitosan-based films. As packaging materials should withstand various environmental conditions, the mechanical properties of the fabricated biocomposites will be tested after incubation in environments with 33 %, 50 % and 75 % relative humidity (RH). Additionally, the effect of acetylation of CNCs on water vapor barrier as well as WCA will be studied.

Although it is intuitive that bio-based polymers are also biodegradable, it is important to study end-of-life of fabricated composites. Objective 4 therefore also covers the study of

biodegradation of chitosan/CNCs and alginate/CNCs in activated sludge medium. With this knowledge, the new materials can be tested and potentially adapted in order to reach degradation to benign products that do not persist in the environment as outlined in principles of green chemistry.

Novelty of this work: In frame of this objective, CNCs functionalized by previously studied method were incorporated into chitosan and alginate matrices in order to form films. Properties relevant for packaging materials were then simultaneously compared under various environmental conditions, to the best of our knowledge, for the first time. Lastly, biodegradation in activated sludge medium was followed and linked to physicochemical parameters of the fabricated films.

Objective 4 is addressed in Chapter 4, Sections 4.2 and 4.3.

1.2.5 Objective 5: Plasma as a Fast and Efficient Tool for Hydrophobization of Biopolymer-Based Composites

Following the completion of Objective 2, plasma was identified to have a high potential for fast and effective hydrophobization of cellulose nanomaterials surface. Furthermore, plasma presents several advantages as it does not require liquid solvents and therefore produces no liquid waste, and is a one-step hydrophobization, which is easy to handle and is very effective. The last and fourth hypothesis is that the use of plasma for hydrophobization of cellulose nanomaterials and their composites are not yet exploited to their full potential. Furthermore, it is speculated that besides fluorine plasma, there is a greener carrier gas that could be applied for such purposes. With this in mind, the main goal of objective 5 is to study various gases for hydrophobic functionalization and chemical changes on the surface of biopolymer-based films. Furthermore, safety of such films will be evaluated by the determination of possible leaching of toxic species into liquid environment.

Novelty of this work: In the last part of the thesis, plasma is employed for hydrophobization of nanostructured cellulose and its composite film. While fluorine plasma has been utilized for such purposes before, this works describes faster conversion of CNFs films to nearly superhydrophobic compared to existing literature and studies surface functionalization of chitosan/CNCs composite film, its properties, aging and potential leaching of fluorine into liquid environments. Lastly, nitrogen was used for hydrophobization of cellulose-based substrate for the first time.

Objective 5 is addressed in Chapter 5, Sections 5.1, 5.2 and 5.3.

Chapter 2

Functional Nanocellulose, Alginate and Chitosan Nanocomposites Designed as Active Film Packaging Materials

In this chapter, cellulose nanocrystals, cellulose nanofibrils, bacterial nanocellulose (BNC), alginate, chitosan and their composites are investigated regarding properties relevant as packaging materials. 25 different films with various combinations and concentrations of CNCs were produced and evaluated in terms of mechanical strength. For further analysis, 7 samples (alginate, alginate/CNCs composite, chitosan, chitosan/CNCs composite, BNC, BNC with glycerol, and CNFs film) exhibiting the highest mechanical strength were selected and their WCA, surface free energy, water vapor permeability, moisture uptake and morphology were evaluated. It was observed that upon the addition of CNCs into alginate and chitosan matrix decreased water vapor transmission by 15 % and 45 %, respectively. Oxygen barrier was shown to be better than commercial polymers such as (poly)lactic acid, polyethylene terephthalate, polyvinyl chloride and polyethylene. Based on the results it was concluded that biopolymer-based films would be suitable for packing foods with short storage time, for example pre-made foods such as sandwiches, or refrigerated vegetables such as broccoli, cauliflower, carrots and cucumbers.

The chapter addresses thesis Objective 1.

Regarding my contribution: I prepared various composite films with other co-authors, conducted analyses of water contact angle, film density and morphology, helped with the analysis of other results and co-wrote the paper.

2.1 Functional Nanocellulose, Alginate and Chitosan Nanocomposites Designed as Active Film Packaging Materials

polymers

MDPI

Article

Functional Nanocellulose, Alginate and Chitosan Nanocomposites Designed as Active Film Packaging Materials

Gregor Lavrič [1], Ana Oberlintner [2,3], Inese Filipova [4], Uroš Novak [2], Blaž Likozar [2] and Urška Vrabič-Brodnjak [5,*]

[1] Pulp and Paper Institute, Bogišićeva Ulica 8, 1000 Ljubljana, Slovenia; gregor.lavric@icp-lj.si
[2] National Institute of Chemistry, Hajdrihova 19, 1000 Ljubljana, Slovenia; ana.oberlintner@ki.si (A.O.); uros.novak@ki.si (U.N.); blaz.likozar@ki.si (B.L.)
[3] Jožef Stefan International Postgraduate School, Jamova Cesta 39, 1000 Ljubljana, Slovenia
[4] Latvian State Institute of Wood Chemistry, Dzerbenes Street 27, LV-1006 Riga, Latvia; inese.filipova@kki.lv
[5] Department of Textiles, Graphic Arts and Design, Faculty of Natural Sciences and Engineering, University of Ljubljana, Snežniška 5, 1000 Ljubljana, Slovenia
* Correspondence: urska.vrabic@ntf.uni-lj.si; Tel.: +386-1-200-32-82

Abstract: The aim of the study was to characterize and compare films made of cellulose nanocrystals (CNC), nano-fibrils (CNF), and bacterial nanocellulose (BNC) in combination with chitosan and alginate in terms of applicability for potential food packaging applications. In total, 25 different formulations were made and evaluated, and seven biopolymer films with the best mechanical performance (tensile strength, strain)—alginate, alginate with 5% CNC, chitosan, chitosan with 3% CNC, BNC with and without glycerol, and CNF with glycerol—were selected and investigated regarding morphology (SEM), density, contact angle, surface energy, water absorption, and oxygen and water barrier properties. Studies revealed that polysaccharide-based films with added CNC are the most suitable for packaging purposes, and better dispersing of nanocellulose in chitosan than in alginate was observed. Results showed an increase in hydrophobicity (increase of contact angle and reduced moisture absorption) of chitosan and alginate films with the addition of CNC, and chitosan with 3% CNC had the highest contact angle, 108 ± 2, and 15% lower moisture absorption compared to pure chitosan. Overall, the ability of nanocellulose additives to preserve the structure and function of chitosan and alginate materials in a humid environment was convincingly demonstrated. Barrier properties were improved by combining the biopolymers, and water vapor transmission rate (WVTR) was reduced by 15–45% and oxygen permeability (OTR) up to 45% by adding nanocellulose compared to single biopolymer formulations. It was concluded that with a good oxygen barrier, a water barrier that is comparable to PLA, and good mechanical properties, biopolymer films would be a good alternative to conventional plastic packaging used for ready-to-eat foods with short storage time.

Keywords: carbohydrate; polysaccharide; nanocellulose; alginate; chitosan; film packaging material; functional active design; biomass-derived biomaterial nanocomposites; oxygen/air/water barrier properties; bio-based biopolymer composites for food

Citation: Lavrič, G.; Oberlintner, A.; Filipova, I.; Novak, U.; Likozar, B.; Vrabič-Brodnjak, U. Functional Nanocellulose, Alginate and Chitosan Nanocomposites Designed as Active Film Packaging Materials. *Polymers* **2021**, *13*, 2523. https://doi.org/10.3390/polym13152523

Academic Editors: Cédric Delattre and Paola Scarfato

Received: 14 June 2021
Accepted: 29 July 2021
Published: 30 July 2021

1. Introduction

According to estimates by the United Nations Joint Group of Experts on the Scientific Aspects of Marine Pollution (GESAMP), between 70 and 95% of waste will join millions of tons already present in seas, lakes, air, rivers, groundwater, crop fields, landfills, and cities. Most of this waste is coming from the traditional commercial food packaging materials with a petroleum-based origin such as polyethylene (PE), polypropylene (PP), and polystyrene (PS). Researchers have estimated that 31.9 million tonnes of mismanaged plastic waste enter the environment every year, with 4.8–12.7 million tonnes going into the oceans and significant quantities contaminating terrestrial ecosystems [1,2]. Still, it is expected that the demand for plastics will continue to grow in the future to enable resource-efficient products

needed by society. One of the establishing trends is in designing mindful products from sources including recycled chemicals and renewable raw materials, and using processes powered by renewable energy in striving to establish an efficient circular economy [3]. To be in line with the UN sustainable development goals and sustainable plastic strategy, the global plastics industry's shift from a manufacturing system based predominantly on fossil fuels to sustainable and affordable alternatives is being envisioned [4,5].

Packaging materials are an essential part of product processing, therefore the number of investigations on the development and use of new alternatives has increased in recent times. That the transition towards non-virgin petrochemical and bio-based raw materials as alternative feedstocks should include recycled chemicals from plastics waste, sustainable biomass, industrial wastes such as CO_2, and modified biopolymers such as cellulose or starch, is suggested mainly due to the interest in minimizing the environmental impact caused using synthetic packaging materials. One of the most desired features expected in packaging is the capability of decomposing into carbon dioxide, methane, water, inorganic compounds, or biomass, the dominant mechanism of decomposition being the enzymatic action of microorganisms and that the resulting products can be obtained and measured in a period of a certain time [6]. The materials used to make biodegradable packaging can be biopolymers of natural origin (alginate, starch, gelatine, collagen, proteins, chitosan, (nano)cellulose, pectin) or of synthetic origins, such as polylactic acid, polycaprolactone, and polyvinyl alcohol [7,8]. Especially the materials of natural origin have recently (re)gained popularity, due to their special properties, which in many industries can become an alternative for fossil fuel-based plastic. However, high production costs, low performance, and not less important, ethical implications, still hinder the market penetration of plastics-free alternatives so far. One of the currently underutilized sources of feedstock for bio-based polymers can be found in the side streams of both agricultural and forest feedstock, which are a good source [9]. Cellulose, which exists in the lignocellulosic biomass, is the most abundant polysaccharide present in nature. It is encapsulated by lignin and hemicellulose and produces a linear polysaccharide with nanometre diameter by repeating the connection of β-d-glucose [10]. Cellulose nanofibrils (CNFs) or cellulose nanocrystals (CNCs) can be isolated from wood and other plant sources by partial disruption of their natural structures, which is usually achieved using chemical and/or mechanical treatments. Besides plants, some bacteria naturally produce cellulose microfibrils, which are referred to as bacterial nanocelluloses (BNCs) [11]. These three types of nanocelluloses (CNCs, CNFs, and BNCs) have different morphologies (sizes and shapes) depending on their biological origin and the processes used to isolate them [12,13]. Unlike the rigidity of the CNC, the CNF is flexible. This is mainly because the structure of CNF is an individual or aggregated soft and long chain, which is formed by alternately connecting crystalline regions and amorphous regions to each other [9–11].

The second most abundant natural biopolymer is chitin, the crucial structural biopolymer of crustaceans' exoskeletons, whereby its content varies not only between different sources but also between different species [9]. These types of polysaccharides have previously mostly been utilized and studied for biomedical applications [14]. However, in the search for new carbon-neutral renewable resources using the biorefinery approaches, turning cast-off shells into nitrogen-rich chemicals would benefit economies and the environment [15]. Other largely exploited sources for biopolymers are macroalgae, which are the rich source of indigestible polysaccharides that are commonly produced by and refined from various brown seaweed and can be developed into active food packaging materials [16,17]. In the recent review from Zhang et. al., the effect of the incorporation of CNC on the film's characteristics, including thickness, optical properties, barrier properties, water sensitivity, mechanical properties, antioxidant properties, and antimicrobial properties have been presented [18]. The main advantage of using cellulose nanoparticles as a reinforcing part in the film is most addressed by the "tortuous theory", where the cellulose nanoparticles, due to their size, form a denser microstructure, which mostly leads to an increase in the mechanical strength of the composite (bio)material. Moreover, cellulose

nanoparticles act as a physical barrier structure in the composite film materials leading to reducing the movement of gas molecules through the film. The films with a higher degree of nanocellulose fibrillation absorbed more water, and had the higher contact angles for glycerol and lower contact angles for water [19]. Recently, many studies have shown that the incorporation of cellulose nanomaterials as an additive could improve the performance of the food packaging films [20–22]. Further advances in nanocellulose research in biopolymers film are quite promising for active packaging applications, including the controlled release packaging and responsive packaging [22–25].

This study aimed to evaluate and compare the effect of the CNC, CNF, and BNC cellulose nanomaterial, where the first two were obtained from lignocellulosic biomass and the last one from bacterial origin. Altogether, 25 combinations of biopolymer films using chitosan, alginate, or nanocelluloses as a single component or in different combinations were prepared. Based on the determined mechanical properties in the first part of the study, the best film in terms of mechanical properties and physical appearance were selected and further characterized for density, contact angle, surface energy, water absorption, and morphological examination with SEM, oxygen, and water barrier properties. Finally, some suggestions and challenges of potential new sustainable packaging that need a further improvement/focus to commercially exploit this (nano) material renewable bioresource for packaging application.

2. Materials and Methods

2.1. Materials

High molecular weight (Mw = 310,000–375,000 Da) chitosan (<75% deacetylated), sodium alginate and 85 wt% lactic acid were purchased from Sigma Aldrich (Steinheim, Germany) and glycerol was purchased from Pharmacem Sušnik (Ljubljana, Slovenia). Nanocellulose materials were produced as presented in the sections below.

2.1.1. CNF Production

For CNF production, bleached hardwood Kraft pulp (kindly provided by Metsä Fibre, Ainekoski, Finland) was oxidized at 70 °C for 4 h in APS (ammonium persulfate) solution (APS: fibers amount ratio 5:1) with continuous stirring. Oxidation was stopped by cooling the mixture to 15 °C, treated fibres were washed until neutral and kept at 4 °C. Oxidized cellulose fibres were then suspended in water (1.5% *w/w*), sonicated (ultrasonic homogenizer SONIC-650W, MRC Ltd., Holon, Israel) for 15 min (90% power, 9 s on, 1 s off), and then processed in microfluidizer (LM20, Microfluidics, Quadro Engineering, Waterloo, ON, Canada); the first 3 times through 200 µm ceramic chamber H30Z, then through 100 µm diamond chamber H10Z at 300–600–900–1500 bar, three passes at each pressure, followed by 6 passes at 2000 bar. Sample was cooled in an ice bath during the treatment. Semi-transparent viscous 1.5% *w/w* solution was obtained and kept at 4 °C until used. The yield of CNF reached ~80% from the initial amount of pulp.

2.1.2. BNC Production

The raw material for BNC production was a cellulose-rich bio-film formed after acetic fermentation of apple juice [26] and was obtained from a local vinegar producer. Bio-film was thermo-mechanically treated as described in the article by Lavrič, Medveščeк, and Skočaj [27]. Treatment separated the individual nanofibrils, resulting in the formation of a homogeneous semi-transparent 0.5% *w/w* BNC gel. The yield of BNC from the initial solution (mother of vinegar) was ~87%. The rest were removed impurities (mainly brownish-colored particles of the apple pulp that had served as the raw material for the vinegar production).

2.1.3. CNC Production

CNC was prepared in accordance with the procedure described by Kunaver, Anžlovar, and Žagar in 2016 [28]. The liquefaction reaction, using glycols and mild acid catalysis

(methane sulphonic acid), was applied to eucalyptus wood. The process contains four steps: the milling, glycolysis reaction, centrifugation, and final rinsing with an organic solvent. The yield of CNC was 63 ± 8.5% and the final product was a stable, highly concentrated CNC suspension in water, which was diluted to 1.5% *w/w* before being used in film-forming solutions.

2.2. Films Preparation

Films were prepared with different polymer matrices: chitosan, alginate, and nanocellulose. Protocol commonly used in similar studies, e.g., [29], for dissolution, blending, and casting of alginate, chitosan, and nanocellulose was used. Chitosan and alginate film-forming solutions were prepared at concentrations 1.5% *w/w* by dissolving chitosan in 1 wt% aqueous solution of lactic acid and glycerol, and by dissolving sodium alginate in ultrapure water. Dissolution was realized for approximately 24 h under constant stirring with a magnetic stirrer (Ika, Staufen, Germany). The mixtures were then vacuum filtered through 4 layers of medical gauze to eliminate impurities. For chitosan and alginate films with nanocellulose additives, CNC, CNF, or BNC in amounts of 3 or 5 *w/w*% with respect to main biopolymer were added to prepared chitosan and alginate solutions and then homogenized with UltraTurrax (Ika, Staufen, Germany). To eliminate the air bubbles in the film, the mixtures were left overnight. For nanocellulose films, corresponding solutions BNC 0.5% *w/w*, CNF 1.5% *w/w* (or diluted to 0.5–1.0% *w/w* if viscosity was too high) and CNC 1.5% *w/w* were used. Glycerol was used as a plasticizer in some types of films and was added in the amount of 30 wt% with respect to the main biopolymer. The casting volumes of FFS were chosen in a range of 50–100 mL depending on dry mass of polymers in different solutions used and respecting the requisite final film casting weight, which was 47 ± 7 g m^{-2}. All films were casted into 12×12 cm^2 polyurethane petri dishes and dried under constant airflow in a laminar flow hood (Microbium d.o.o, Ljubljana, Slovenia) at room temperature and RH 40% for 48 h. In the case of nanocellulose films, a silicon pad was placed on the bottom of Petri dishes to prevent sticking.

2.3. Tensile Properties

Tensile properties of films were determined in accordance with ASTM D 882, using the tensile testing machine Zwick Roell Z010 equipped with 20 N measuring cell (Class 0.5, ISO 7500-1) and the testing software testXpert (Version II V3.2, Zwick GmbH & Co. KG, Ulm, Germany). Samples with a width of 15 mm were tested at 10 mm/min testing speed. The clamping length was set to 70 mm. Testing took place at 23 °C and 50% RH. Samples were exposed to these conditions 48 h before testing.

2.4. Water Contact Angle

Film was cut into pieces of approximately 2×3 cm^2 in size and placed onto the microscope glass. Contact angles were measured with water, employing the sessile drop method with Tensiometer Theta T200 (Biolin Scientific, Darmstadt, Germany). The measurements were done in triplicates.

2.5. Film Density

Films were cut into pieces of 3×3 cm^2 in size. The thickness was measured with ABS Digital Thickness Gauge (Mitutoyo, Japan) on three different parts of the film and then weighed on an analytical scale. The density was calculated through the Equation (1):

$$\text{Density} = \frac{\text{m}}{\text{d} \cdot \text{S}} \left(\text{g} \cdot \text{cm}^{-3} \right) \quad (1)$$

where m is the mass of the tested sample, d is the thickness of the film in cm, and S is the area of the sample. All measurements were done in triplicates.

2.6. Scanning Electron Microscope (SEM)

Film surfaces, as well as pure nanocellulose, were investigated under vacuum conditions by SEM SUPRA 35VP (Carl Zeiss, Jena, Germany). A small amount (approx. 50 mg) of CNC, BNC, and CNF were solvent exchanged to acetone through successive centrifugation steps and then placed onto a piece of microscope glass over a heating plate. This ensures quick evaporation of the solvent and prevents aggregation of nanocellulose. Before analysis, the samples were coated with 10 nm of gold. The size of nanocellulose particles was measured using ImageJ software (Version 1.52, LOCI, University of Wisconsin, Madison, WI, USA) on at least 10 different points. Films were placed on graphite tape before analysis. The magnification of all samples was 10,000×.

2.7. Water Vapour Transmission Rate (WVTR) and Water Vapor Permeability (WVP) Determination

Water vapor transmission rate was determined according to the principles of the ISO 2528:2018 standard at 23 °C and 50% RH. Since the hot wax could damage the films during the sample preparation (according to standard procedure), special vessels with a double-sided seal and a system of screws were used to perform the measurements.

$$\mathrm{WVTR} = \frac{\Delta m}{A \cdot t} \left(g \cdot \ cm^{-1} \cdot day^{-1} \right) \quad (2)$$

where A is tested area in cm^2, t time after 24 h of testing, and Δm the mass difference of tested sample.

Based on WVTR, WVP values were calculated. Calculations were done according to ASTM E96, described by Equation (3):

$$\mathrm{WVP} = \frac{\mathrm{WVTR}}{S\,(R_1 - R_2)} \left(g \cdot \ m^{-1} \cdot s^{-1}\, Pa^{-1} \right) \quad (3)$$

where WVTR is calculated through Equation (2), S is the saturation vapour pressure at test temperature (21.068 mmHg at 23 °C), R_1 is the relative humidity in the environment (50%), and R_2 is the relative humidity in the test tube (0%).

2.8. Oxygen Permeability (OTR)

Oxygen permeability of samples was determined in accordance with ISO-2:2003 at 23 °C and 50% RH using Labthink Perme OX2/230 device (Labthink, Boston, MA, USA).

2.9. Moisture Absorption

Moisture absorption was measured modifying the method proposed by Soni et al. [30]. Films were cut in pieces with dimensions 1 × 3 cm and conditioned at 0% RH (relative humidity) for 24 h. Film samples were then weighted and placed at 85% RH for 24 h. The relative humidity was created with a saturated solution of potassium chloride at room temperature. The samples were weighed, and the moisture absorption was calculated using the Equation (4):

$$\text{Moisture absorption } (\%) = \frac{W_{85} - W_0}{W_0} \times 100 \quad (4)$$

where W_{85} is the weight of the sample after 24 h at 85% RH and W_0 is the initial weight of the sample after conditioning at 0% RH. Four replicate measurements were taken for each film.

2.10. Statistical Analysis

Statistical analysis was done using the one-way ANOVA with the confidence level of 95% ($p < 0.05$) in conjunction with Tukey's honestly significant difference post-hoc test. All

experiments were done in a minimum of five parallels and the results were expressed as the mean ± standard deviation.

3. Results and Discussion

3.1. Tensile Properties

Altogether, 25 combinations of biopolymer films using chitosan, alginate, or nanocellulose (NC) as a single component or in different combinations were prepared; however, selection of samples for further investigation was made, based on preliminary evaluation, which was based on the appearance of dry films—integrity, surface properties, visual appearance of film homogeneity, presence of cracks, performance during film handling—the possibility of peeling of the casting dish, and appropriateness for testing (Table S1). Since tensile properties are one of the basic criteria for packaging materials, selection was based also on the results of measured tensile strength (TS) and strain at break (E) of all films, when it was technically possible to perform measurements. Different film compositions showed significantly different results (all the results are given as Supplementary Files), for instance, alginate-based films showed TS from 11.7 ± 0.7 to 42.6 ± 3.6 MPa and chitosan films showed TS from 14.0 ± 2.2 to 30.9 ± 2.2 MPa depending on the amount and type of NC added to the main biopolymer. In the case of chitosan, the addition of any NC type additive improved the mechanical strength of the film; however, in the case of alginate films, the impact depended on the type and amount of NC and was negative in most cases when CNF or BNC was added. As a result of preliminary evaluation, seven films were selected for further investigation: alginate, alginate +5% CNC, chitosan, chitosan +3% CNC, BNC with and without glycerol, and CNF with glycerol. Their properties are Table 1 and Figure 1.

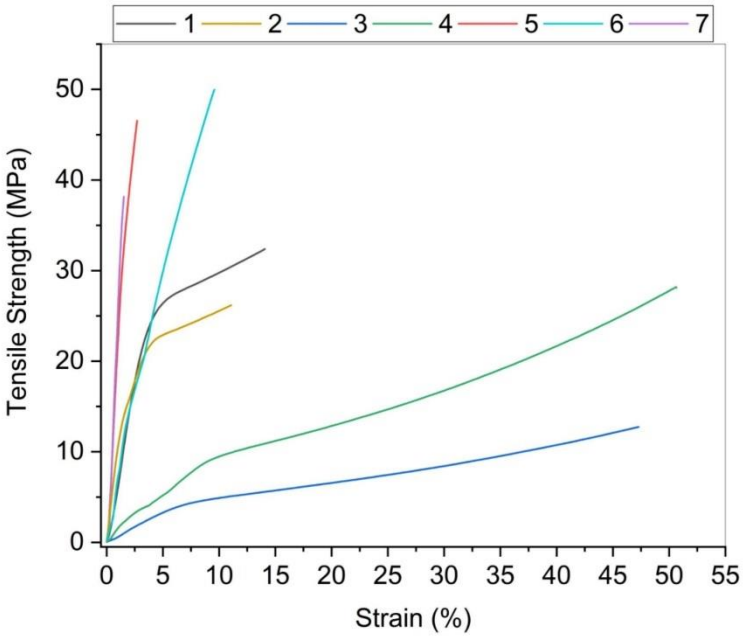

Figure 1. Tensile strength with the respective strain for nanocellulose, alginate, and chitosan nanocomposites. The composition of the films 1–7 are described in Table 1.

Table 1. Selected polysaccharide films are based on the specified properties and include the most promising candidate from each biopolymer. These films are also subjected to a full characterization of morphological and barrier properties (values are given as mean ± SD).

Sample Name	Film Composition	Thickness (μm)	Tensile Strength (MPa)	Strain at Break (%)	Water Contact Angle (°)
Film 1	Alginate	55 ± 3	40 ± 10	22 ± 6	39 ± 2
Film 2	Alginate + 5% CNC	50 ± 2	43 ± 4	28 ± 4	58 ± 3
Film 3	Chitosan	123 ± 3	14 ± 2	51 ± 4	75 ± 3
Film 4	Chitosan + 3% CNC	70 ± 1	31 ± 2	55 ± 6	108 ± 2
Film 5	BNC	66.4 ± 0.8	60 ± 11	4.2 ± 1	46 ± 3
Film 6	BNC + 30% glycerol	56 ± 2	53 ± 5	10 ± 0.4	65 ± 4
Film 7	CNF + 30% glycerol	31 ± 3	47 ± 3	2.4 ± 0.6	23 ± 1

As it was said above, tensile properties are one of the basic criteria for packaging materials. Namely, the mechanical behaviour of packaging films is a very important property of the film to maintain its authenticity and to withstand the environmental impact during the packaging application. The TS and E at break were determined for all film samples. The TS determines the maximum load that can be sustained per cross-sectional area of the film. Strain at break shows the extension of the film, e.g., the flexibility that can be stretched before the breaking point. These characteristics support the correlation of the mechanical properties of films with their compositions and chemical structures. Samples with chitosan and alginate, with the addition of CNC, showed an increase in both TS and E. The average tensile strength of pure CNC films is about 63 MPa, as reported in the literature [31,32]. As expected, the mechanical properties were influenced by the addition of CNC. Films based on alginate exhibited TS of 40 MPa, which increased by 12% upon the addition of 5% CNC. According to the measurement results, the alginate films of all samples showed the best TS/E ratio. Huq et al. [33] reported that the high TS of the alginate-based bio nanocomposite films is due to a good interfacial interaction between the nanofillers and the alginate-based matrix due to similar polysaccharide structures of cellulose and alginate, which was also confirmed on our samples [33]. The largest increase was found in chitosan film, where the addition of CNC improved strength by 120%. The same increase in E was found in both samples (alginate for 30% and chitosan for 6%). It is known from the literature that CNC has a large length/diameter ratio and very good tensile properties. Our analysis confirmed that there are interactions between CNC and chitosan molecules, such as electrostatic association and hydrogen bonding, which create an interactive network and improve overall tensile properties [34]. Cellulose based films have low flexibility, plasticizers should be added to improve this mechanical property and to facilitate the handling of these biopolymers' films. The most used plasticizer is glycerol due to its stability and compatibility with hydrophilic biopolymer chains [35]. The results have shown that bacterial nanocellulose films (BNC) have the highest TS (60.1 MPa) but a lower E (4.2%). The addition of glycerol changed the properties of the film made of BNC. Namely, the plasticization of BNC with glycerol, which reduced the strength of the hydrogen bonds between adjacent cellulose chains, changed the TS of the film. The TS decreased by 11.6%. At the same time the addition of glycerol increased the E values by about 145% (from 4.2 to 10.3%). According to the results obtained, it is predicted that the moisture absorbed into the matrix of the film had a plasticizing effect. As a result, the TS decreased and E increased by weakening the intermolecular forces, thus increasing the space between the polymers and reducing the crystallinity [36,37]. Overall, by improving the strain of rather rigid films, the glycerol improved their suitability for packaging materials.

CNF were produced from hardwood Kraft pulp by a mechanical process with previous chemical oxidation with APS, as described previously. The results showed that the fibrils were shorter and thinner compared to CNF produced by the TEMPO process [37], which is caused by the fibre cleaving effect of persulfate. Similar reinforcement properties for APS and TEMPO oxidized CNF have been proven [36]. However, in our research, CNF

apparently appears less cross-linked, resulting in a smaller surface area and pore volume. With the glycerol, the tensile properties decreased. As explained in many studies, the addition of plasticizer in biopolymers reduces crystallinity, which leads to a significant decrease in film strength and modulus [38–40]. In our case, the addition of glycerol also reduced the flexibility of the films, which is in contrast to previous investigations. The combination of decreasing tensile strength and strain at break is surprising, and the explanation could be the reduced density. The addition of glycerol lowered the density of the film (1.29 $g \cdot cm^{-3}$). In the CNF films described in the literature, the film density was about 1.52 $g \cdot cm^{-3}$ [37].

3.2. Water Contact Angle

The information about interactions between films and water is very important for packaging. Hydrophobic or hydrophilic character is frequently determined by surface free energy and surface morphology. The contact angle of the surface with water is important to characterize a material as such and can give an impression of absorption and adhesion as well. A lower contact angle with water is an indicator that films are hydrophilic and hygroscopic. The most wettable surfaces have low values (<20°) and the hydrophobic surfaces have high values of contact angle (>90°) [38]. In Table 1 and Figure 1, contact angles of polysaccharide films with water are recorded. Comparing films consisting of only one biopolymer, chitosan exhibited the highest contact angle (75°) and CNF with the addition of 30% glycerol the lowest (23°) (Figure 2). Alginate and nanocellulose films can be considered as hydrophilic. When combining chitosan and alginate with CNC, the contact angle with water increased by 44% and 49%, respectively. This trend was also confirmed by Mao et al. [34], where the hydrophobicity of chitosan/CNC film increased compared to only chitosan film. Although cellulose consists of β-D-glucopyranose units with three hydroxyl groups, which are responsible for the hydrophilic character of cellulose, electrostatic association and hydrogen bonding bids the CNC and chitosan molecules closely together, which improves the hydrophobicity [34,39–41]. The higher contact angle can also be a result of changed morphology, which interrupts water spreading. CNF + 30% glycerol films are the most hydrophilic. This behaviour is an indication of the high affinity of glycerol for water. Glycerol in cellulose films tends to migrate to the surface, as also confirmed by Spoljaric et al. [42]. However, this was not the case for BNC films, where the addition of glycerol led to an increase (by 141%) in the contact angle. It is possible that glycerol filled the pores between the fibres, reducing porosity, and thus decreased the surface free energy. In packaging, more hydrophobic materials are generally desired as they offer a wider range of applications [40].

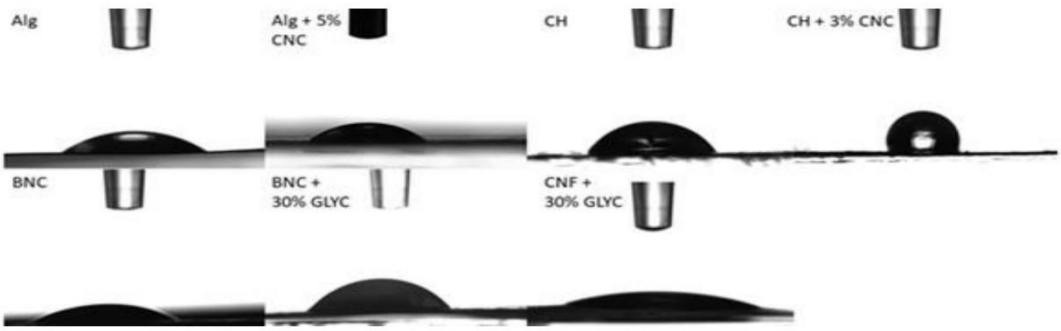

Figure 2. Visualization of the water contact angle for the selected films are shown in Table 1 (ALG—alginate; Alg + 5% CNC—alginate + 5% CNC; CH—chitosan; CH + 3% CNC—chitosan + 3% CNC; BNC—BNC; BNC + 30% GLYC—BNC + 30% glycerol; CNF + 30% GLYC—CNF + 30% glycerol).

3.3. Barrier Properties of the Films

The gas phase permeation through a non-porous material occurs by adsorption at the front interface, diffusion through the material, and desorption at the rear interface, and is often measured with transfer rate, permeance, and permeability. The transmission rate is the volume or weight of a permeating agent (e.g., oxygen or moisture) passing through a film per unit surface area and time in equilibrium with the test conditions.

The addition of CNC to alginate and chitosan reduced WVTR by 15% and 45%, respectively. OTR decreased by 45% for alginate and CNC and by 38% for chitosan and CNC, compared to pure film. It is obvious that the nanostructure of nanocomposites created a tortuous path for oxygen, which was also demonstrated by Enescu et al. [43].

As shown in the tensile properties of BNC with added glycerol, the water absorbed into the matrix of the films had a plasticizing effect, reducing tensile strength and increasing strain at break. In this area, adsorbed water molecules promoted the reorganization of the polymer chains, which was reflected in the change in water permeability in this area. The water barrier properties decreased enormously by 198%. The same trend was observed for oxygen permeability, which decreased for 77%.

For CNF film with added glycerol, it was impossible to measure the WVTR because the sample was too fragile and, therefore, this test was not performed. On the other hand, the OTR results of the sample showed that the oxygen permeability increased enormously, compared to pure CNF from the previous research [44]. This could be the reason for the microcracks that were present on the sample because the fibrils were very short, the film was fragile, and the oxygen could easily pass through.

In Figure 3, the results of WVTR and OTR of the films fabricated in this study as well as for other commercially polymer blends for comparison are presented. Pure polysaccharide films had higher WVTR compared to most commercial packaging films, except TOCN (TEMPO-oxidized cellulose nanofibers). When CNC was combined with alginate and chitosan, the OTR results showed higher OTR compared to cellophane but still lower OTR compared to bio-based polylactic acid films. Pure BNC and BNC with added glycerol showed similar oxygen and water vapor permeability to PLA and TOCN.

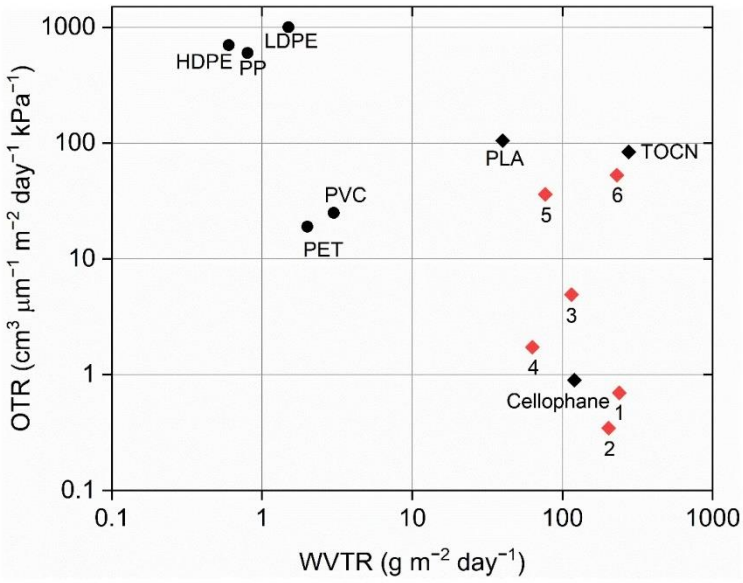

Figure 3. WVTR and Oxygen transmission rate (OTR) of some synthetic polymers compared to our nanocomposites packaging films. Adapted from [45] (Black circles—Petroleum-based Polymers, Black diamonds—commercial Biopolymers, red diamond—biopolymer nanocomposites tested in this study) (HDPE—high-density polyethylene; LDPE—low-density polyethylene; PP—polypropylene; PVC—polyvinyl chloride; PET—polyethylene terephthalate; PLA—polylactic acid; TOCN—TEMPO-oxidized cellulose nanofibers).

The addition of CNC reduced the WVP value of alginate films from 9.36 g/(m·s·Pa) to 7.32 g/(m·s·Pa) (Table 2). An even greater decrease in this value was observed with 3% CNC addition into the films made of chitosan. In this case, the value dropped from 10.1 g/(m·s·Pa) to 1.39 g/(m·s·Pa). The addition of glycerol drastically increased the WVP value of BNC films (from 3.62 g/(m·s·Pa) to 9.17 g/(m·s·Pa).

Table 2. Density, moisture absorption, water vapor transmission rate (WVTR), properties of films (values are presented as mean ± SD). Water vapor permeability results (WVP) are presented as a calculated mean value.

Sample Name	Film Composition	Film Density (g·cm^{-3})	Moisture Absorption (%)	WVTR (g·cm^{-1}·day^{-1})	WVP (g/(m·s·Pa))
Film 1	Alginate	1.87 ± 0.2	57.4 ± 1.6	239 ± 8	9.36
Film 2	Alginate + 5% CNC	1.34 ± 0.16	51.2 ± 1.9	203 ± 5	7.23
Film 3	Chitosan	2.00 ± 0.35	49.2 ± 1.5	115 ± 9	10.07
Film 4	Chitosan + 3% CNC	1.05 ± 0.10	36.5 ± 1.8	63 ± 2	1.39
Film 5	BNC	0.74 ± 0.05	9.7 ± 0.8	77 ± 4	3.62
Film 6	BNC + 30% glycerol	0.79 ± 0.10	21.3 ± 1.0	230 ± 11	9.17
Film 7	CNF + 30% glycerol	1.29 ± 0.20	20.4 ± 0.6	Not applicable	Not applicable

3.4. Visualization and Morphology of the Films

CNF films appeared as fully transparent materials with a glossy surface, CNC films were slightly whitish and pale semi-transparent material, while BNC films were slightly brownish semi-transparent material (Figure 4a). CNC additive in amounts of 3–5% *w/w* did not change the transparency or colour of chitosan or alginate films. CNC and CNF have been known for their application in optically transparent films [46]; however, CNC can be less transparent and haze depending on the size of crystals and thickness of film [47]. The

brownish colour of BNC films can be explained by the influence of fermentation medium, which was apple juice and culturing bacteria used for obtaining the initial material, since the growing conditions have a significant effect on the properties of bacterial cellulose [48].

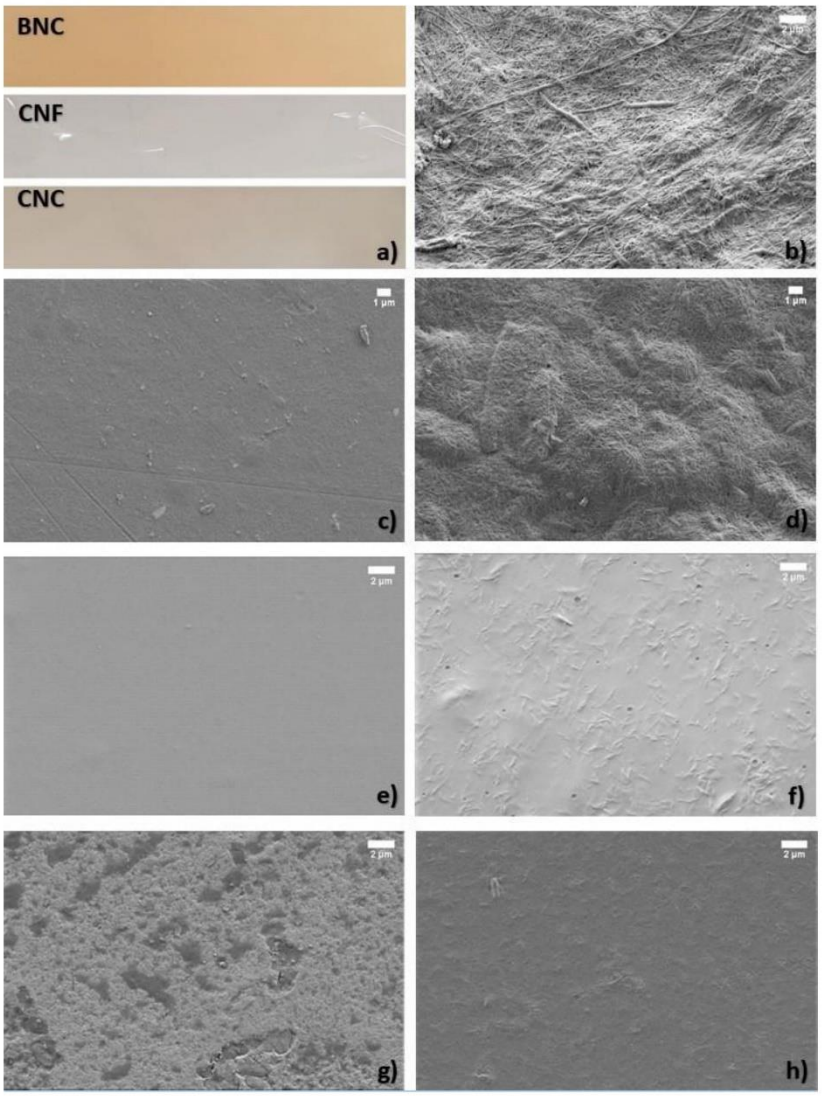

Figure 4. (**a**) Visualisation of BNC, CNF, and CNC films. SEM micrographs of (**b**) BNC, (**c**) CNF film with 30 wt% glycerol, (**d**) CNC film with 30 wt% glycerol, (**e**) chitosan film with 30 wt% glycerol, (**g**) alginate + 5% CNC, (**f**) chitosan + 3% CNC, and (**h**) alginate film with 30 wt% glycerol.

Inspection of the films with SEM revealed that BNC and CNF were in the shape of a long, fibrillary network (Figure 4b,c) with an average diameter of fibril of 69 ± 24.3 nm and 26 ± 6.5 nm, respectively. On the other hand, CNC were rod-like shaped particles with an average width of 83 ± 18.8 nm and length of 777 ± 112 nm (Figure 4d). Chitosan and alginate films have a smooth surface before being mixed with nanocellulose (Figure 4e,g, respectively). In alginate-CNC composite, clusters of CNCs are visible, indicating that

although both alginate and CNCs are hydrophilic, CNC tends to agglomerate when mixed into alginate matrix (Figure 4g), while in chitosan film, the CNCs are more homogeneously dispersed (Figure 4f).

3.5. Film Density and Moisture Adsorption

Alginate and chitosan films have the highest density, and it decreases with the addition of nanocellulose, which corresponds to observations on the films' morphology (Figure 4d,e). The mixing of CNC into the alginate or chitosan matrix creates porosity, which is responsible for the lower density. Wang et al. [44] described that CNC has a "rice-like" structure, which causes the changes in the microstructure of the films and consequently in the density.

Similarly, BNC and CNF have lower density compared to films with chitosan and alginate matrix but can be slightly increased with the addition of glycerol (Table 2).

As it was said earlier in section about contact angle measurements, interactions between films and water are significant for packaging and hydrophobicity or hydrophilicity properties of films can determine their application areas. Moisture absorption from air medium was tested and all biopolymer films, regardless of composition, demonstrated hygroscopic behaviour at high (85%) relative humidity, therefore showing their ability to absorb water vapour from ambient air. Such a high RH number was chosen in order to investigate the variation of absorption between films of different compositions. Although CNC film was not selected for detailed investigation because of cracks and breakage, the moisture absorption was measured and the comparison of nanocellulose films demonstrated moisture absorption of 13.3 ± 0.2% in the case of CNC and slightly higher in the cases of CNF (20.4 ± 0.6%) and BNC (21.3 ± 1.0%). Fibrillated forms of nanocellulose tend to absorb more water due to the fibrillar structure and bigger proportion of amorphous regions, where it is easier for water molecule to get into and to bond with hydroxyl groups of cellulose. After 24h in high humidity, nanocellulose films became more flexible on touch, especially BNC one; however, they retain their shape and part of their stiffness. Cellulosic fibres, being hydrophilic in nature, absorb moisture from their environment until equilibrium is reached [49]. Adding plasticizer to BNC increased moisture absorption by 120%, improving the highly hygroscopic behaviour of glycerol.

Chitosan and alginate films absorb more moisture than pure nanocellulose films. It is 49.2 ± 1.5% in the case of pure chitosan and 57.4 ± 1.6% in the case of pure alginate. It is worth noting that moisture changes the structure of chitosan and alginate films—they become sticky, loose, lose their shape and stiffness, and stick to the surfaces. However, the addition of 3–5% CNC decreased the moisture absorption of films. Moisture absorption values decreased to different extents depending on the amount of nanofillers. The addition of 3% CNC decreased the moisture absorption of chitosan films by 15.1%, however, in the case of alginate, the addition of 5% nanocellulose decreased the moisture absorption by 10.8%. Therefore, it can be concluded that nanocellulose additives help to preserve the structure of chitosan and alginate films in a humid environment and should be considered. Ability of NC to prevent the absorption of moisture of NC-reinforced chitosan films were investigated elsewhere [30].

4. Conclusions

In this research, 25 different formulations of 5 sustainable biopolymers were used to produce and characterize thin and flexible films with potential use for packaging purposes. Results of mechanical testing showed that the addition of 3–5% CNC, CNF, and BNC improved the tensile strength of chitosan films, however, for alginate films, the impact of NC depended on the type and amount of additive and was positive only when CNC was added. From the cellulose-based films, BNC had the highest tensile strength, 60 ± 11 MPa and 53 ± 5 MPa without and with glycerol accordingly, CNF (with glycerol) followed with a result of 47 ± 3 MPa. CNC films appeared as slightly whitish and pale semi-transparent material, while BNC films were slightly brownish semi-transparent material, and other formulations were fully transparent. Seven formulations—alginate, alginate +5% CNC,

chitosan, chitosan +3% CNC, BNC with and without glycerol, and CNF with glycerol—were selected as the most appropriate for packaging purposes based on visual/physical appearance and mechanical properties of films, and characterized in terms of morphological examination with SEM, density, contact angle, surface energy, water absorption, and oxygen and water barrier properties. SEM examination of cellulose-based films revealed typical morphology of crystalline and fibrillar forms of NC. Investigation of mixed formulations revealed more homogenous dispersing of CNC in chitosan than in alginate. Alginate and chitosan films had the highest density, which decreased with the addition of CNC because of greater porosity. Water contact angle differed among selected samples, the lowest was detected for CNF with glycerol (23 ± 1) and the highest for chitosan with 3% CNC (108 ± 2), the other films having results in the range from 39° to 75° and showing the increase of hydrophobicity of chitosan and alginate with the addition of CNC. This fact was approved also by moisture absorption results, which showed reduced moisture absorption for chitosan and alginate films after the addition of CNC for 15.1% and 8.8%, accordingly. Overall, chitosan and alginate films absorb more moisture than pure nanocellulose films, however, the addition of CNC can help to preserve the structure and function of chitosan and alginate packaging materials in humid environments. Therefore, materials with higher hydrophobicity would be more appropriate as they offer a wider range of applications. Results of barrier properties showed that the addition of CNC improved the WVTR of alginate by 15% and of chitosan films by 45%, while OTR decreased by 45% for alginate with CNC and by 38% for chitosan with CNC, compared to one component films. The addition of glycerol to BNC films decreased WVTR almost twice and OTR for 77%.

Based on the findings of this study, it was concluded that polysaccharide-based films with added CNC are the most suitable for packaging purposes. With good oxygen barrier, water barrier that is comparable to PLA, and good mechanical properties, we propose that such films would be a good alternative to conventional plastic packaging used for ready-to-eat foods with short storage time, such as sandwiches and solid, refrigerated vegetables (for instance cucumbers, cauliflower, broccoli).

Supplementary Materials: The following are available online at https://www.mdpi.com/article/10.3390/polym13152523/s1, Table S1: Overview of all the prepared biopolymers films and nanocomposites together with evaluated mechanical properties and moisture absorption.

Author Contributions: Conceptualization, G.L., U.N. and U.V.-B.; methodology, G.L., U.N. and A.O.; validation, G.L. and U.V.-B.; formal analysis, I.F.; investigation, G.L., A.O. and I.F.; data curation, G.L., A.O., U.N. and U.V.-B.; writing—original draft preparation, G.L., U.N., A.O., I.F., B.L. and U.V.-B.; writing—review and editing, G.L., U.N., A.O., I.F., B.L. and U.V.-B.; supervision, U.V.-B.; funding acquisition, B.L. All authors have read and agreed to the published version of the manuscript.

Funding: Author I.F. acknowledge the European Regional Development Fund, Contract No. 1.1.1.2/VIAA/1/16/211 (Agreement No. 1.1.1.2/16/I/001) "Study of novel method for nanocellulose isolation from biomass and its residues". This research was also funded by the PhD research grant (A.O.) and Slovenian Research Agency (Program P2-0152 and Program P2-0213 Textiles and Ecology).

Institutional Review Board Statement: Not applicable.

Informed Consent Statement: Not applicable.

Data Availability Statement: Data is contained within the article and Supplementary Material.

Acknowledgments: The authors acknowledge Anže Prašnikar for preparation of SEM images and Matej Skočaj for critical reading of the manuscript.

Conflicts of Interest: The authors declare no conflict of interest.

References

1. Rochman, C.M. Microplastics Research—From Sink to Source. *Science* **2018**, *360*, 28–29. [CrossRef]
2. Kawecki, D.; Nowack, B. Polymer-Specific Modeling of the Environmental Emissions of Seven Commodity Plastics as Macro- and Microplastics. *Environ. Sci. Technol.* **2019**, *53*, 9664–9676. [CrossRef] [PubMed]

3. Kunwar, B.; Cheng, H.; Chandrashekaran, S.R.; Sharma, B.K. Plastics to fuel: A review. *Renew. Sustain. Energy Rev.* **2016**, *54*, 421–428. [CrossRef]
4. Carus, M.; Dammer, L.; Raschka, A.; Skoczinski, P. Renewable Carbon: Key to a Sustainable and Future-oriented Chemical and Plastic Industry: Definition, Strategy, Measures and Potential. *Greenh. Gases Sci. Technol.* **2020**, *10*, 488–505. [CrossRef]
5. SusChem. Sustainable Plastics Strategy. 2020. Available online: http://suschem.org/files/library/Publications/Suschem_Sustainable_Plastics_Brochure-FINAL_2101.pdf (accessed on 29 May 2021).
6. Ghosh, K.; Jones, B.H. Roadmap to Biodegradable Plastics—Current State and Research Needs. *ACS Sustain. Chem. Eng.* **2021**, *9*, 6170–6187. [CrossRef]
7. Oberlintner, A.; Bajić, M.; Kalčíková, G.; Likozar, B.; Novak, U. Biodegradability study of active chitosan biopolymer films enriched with Quercus polyphenol extract in different soil types. *Environ. Technol. Innov.* **2021**, *21*, 101318. [CrossRef]
8. Simona, J.; Dani, D.; Petr, S.; Marcela, N.; Jakub, T.; Bohuslava, T. Edible Films from Carrageenan/Orange Essential Oil/Trehalose—Structure, Optical Properties, and Antimicrobial Activity. *Polymers* **2021**, *13*, 332. [CrossRef]
9. Novak, U.; Bajić, M.; Kõrge, K.; Oberlintner, A.; Murn, J.; Lokar, K.; Triler, K.V.; Likozar, B. From waste/residual marine biomass to active biopolymer-based packaging film materials for food industry applications—A review. *Phys. Sci. Rev.* **2019**, *5*, 5. [CrossRef]
10. Khalil, H.A.; Davoudpour, Y.; Islam, N.; Mustapha, A.; Sudesh, K.; Dungani, R.; Jawaid, M. Production and modification of nanofibrillated cellulose using various mechanical processes: A review. *Carbohydr. Polym.* **2014**, *99*, 649–665. [CrossRef]
11. Haghighi, H.; Gullo, M.; La China, S.; Pfeifer, F.; Siesler, H.W.; Licciardello, F.; Pulvirenti, A. Characterization of bio-nanocomposite films based on gelatin/polyvinyl alcohol blend reinforced with bacterial cellulose nanowhiskers for food packaging applications. *Food Hydrocoll.* **2021**, *113*, 106454. [CrossRef]
12. Bai, L.; Huan, S.; Zhu, Y.; Chu, G.; McClements, D.J.; Rojas, O.J. Recent Advances in Food Emulsions and Engineering Foodstuffs Using Plant-Based Nanocelluloses. *Annu. Rev. Food Sci. Technol.* **2021**, *12*, 383–406. [CrossRef]
13. Oberlintner, A.; Likozar, B.; Novak, U. Hydrophobic functionalization reactions of structured cellulose nanomaterials: Mechanisms, kinetics and in silico multi-scale models. *Carbohydr. Polym.* **2021**, *259*, 117742. [CrossRef]
14. Zhao, D.; Yu, S.; Sun, B.; Gao, S.; Guo, S.; Zhao, K. Biomedical Applications of Chitosan and Its Derivative Nanoparticles. *Polymers* **2018**, *10*, 462. [CrossRef]
15. Yan, N.; Chen, X. Sustainability: Don't waste seafood waste. *Nat. News* **2015**, *524*, 155–157. [CrossRef] [PubMed]
16. Carina, D.; Sharma, S.; Jaiswal, A.K.; Jaiswal, S. Seaweeds polysaccharides in active food packaging: A review of recent progress. *Trends Food Sci. Technol.* **2021**, *110*, 559–572. [CrossRef]
17. Khan, A.; Khan, R.A.; Salmieri, S.; Le Tien, C.; Riedl, B.; Bouchard, J.; Chauve, G.; Tan, V.; Kamal, M.R.; Lacroix, M. Mechanical and barrier properties of nanocrystalline cellulose reinforced chitosan based nanocomposite films. *Carbohydr. Polym.* **2012**, *90*, 1601–1608. [CrossRef] [PubMed]
18. Zhang, W.; Zhang, Y.; Cao, J.; Jiang, W. Improving the performance of edible food packaging films by using nanocellulose as an additive. *Int. J. Biol. Macromol.* **2021**, *166*, 288–296. [CrossRef] [PubMed]
19. Lengowski, E.C.; Júnior, E.A.B.; Simon, L.; De Muñiz, G.I.B.; De Andrade, A.S.; Nisgoski, S.; Klock, U. Different degree of fibrillation: Strategy to reduce permeability in nanocellulose-starch films. *Cellulose* **2020**, *27*, 10855–10872. [CrossRef]
20. Fang, Z.; Zhu, H.; Preston, C.; Hu, L. Development, application and commercialization of transparent paper. *Transl. Mater. Res.* **2014**, *1*, 015004. [CrossRef]
21. Shanmugam, K.; Doosthosseini, H.; Varanasi, S.; Garnier, G.; Batchelor, W. Nanocellulose films as air and water vapour barriers: A recyclable and biodegradable alternative to polyolefin packaging. *Sustain. Mater. Technol.* **2019**, *22*, e00115. [CrossRef]
22. Yu, Z.; Alsammarraie, F.K.; Nayigiziki, F.X.; Wang, W.; Vardhanabhuti, B.; Mustapha, A.; Lin, M. Effect and mechanism of cellulose nanofibrils on the active functions of biopolymer-based nanocomposite films. *Food Res. Int.* **2017**, *99*, 166–172. [CrossRef]
23. Atef, M.; Rezaei, M.; Behrooz, R. Characterization of physical, mechanical, and antibacterial properties of agar-cellulose bionanocomposite films incorporated with savory essential oil. *Food Hydrocoll.* **2015**, *45*, 150–157. [CrossRef]
24. Kõrge, K.; Šeme, H.; Bajić, M.; Likozar, B.; Novak, U. Reduction in Spoilage Microbiota and Cyclopiazonic Acid Mycotoxin with Chestnut Extract Enriched Chitosan Packaging: Stability of Inoculated Gouda Cheese. *Foods* **2020**, *9*, 1645. [CrossRef]
25. Lu, P.; Yang, Y.; Liu, R.; Liu, X.; Ma, J.; Wu, M.; Wang, S. Preparation of sugarcane bagasse nanocellulose hydrogel as a colourimetric freshness indicator for intelligent food packaging. *Carbohydr. Polym.* **2020**, *249*, 116831. [CrossRef]
26. Skočaj, M. Bacterial nanocellulose in papermaking. *Cellulose* **2019**, *26*, 6477–6488. [CrossRef]
27. Lavrič, G.; Medvešček, D.; Skočaj, M. Papermaking properties of bacterial nanocellulose produced from mother of vinegar, a waste product after classical vinegar production. *Tappi J.* **2020**, *19*, 197–203. [CrossRef]
28. Kunaver, M.; Anžlovar, A.; Žagar, E. The fast and effective isolation of nanocellulose from selected cellulosic feedstocks. *Carbohydr. Polym.* **2016**, *148*, 251–258. [CrossRef]
29. Zhao, K.; Wang, W.; Teng, A.; Zhang, K.; Ma, Y.; Duan, S.; Li, S.; Guo, Y. Using cellulose nanofibers to reinforce polysaccharide films: Blending vs. layer-by-layer casting. *Carbohydr. Polym.* **2020**, *227*, 115264. [CrossRef]
30. Soni, B.; Hassan, E.B.; Schilling, M.W.; Mahmoud, B. Transparent bionanocomposite films based on chitosan and TEMPO-oxidized cellulose nanofibers with enhanced mechanical and barrier properties. *Carbohydr. Polym.* **2016**, *151*, 779–789. [CrossRef] [PubMed]
31. Nan, F.; Nagarajan, S.; Chen, Y.; Liu, P.; Duan, Y.; Men, Y.; Zhang, J. Enhanced Toughness and Thermal Stability of Cellulose Nanocrystal Iridescent Films by Alkali Treatment. *ACS Sustain. Chem. Eng.* **2017**, *5*, 8951–8958. [CrossRef]

32. Wang, J.; Gardner, D.J.; Stark, N.M.; Bousfield, D.W.; Tajvidi, M.; Cai, Z. Moisture and Oxygen Barrier Properties of Cellulose Nanomaterial-Based Films. *ACS Sustain. Chem. Eng.* **2018**, *6*, 49–70. [CrossRef]
33. Huq, T.; Salmieri, S.; Khan, A.; Khan, R.A.; Le Tien, C.; Riedl, B.; Fraschini, C.; Bouchard, J.; Uribe-Calderon, J.; Kamal, M.R.; et al. Nanocrystalline cellulose (NCC) reinforced alginate based biodegradable nanocomposite film. *Carbohydr. Polym.* **2012**, *90*, 1757–1763. [CrossRef] [PubMed]
34. Mao, H.; Wei, C.; Gong, Y.; Wang, S.; Ding, W. Mechanical and Water-Resistant Properties of Eco-Friendly Chitosan Membrane Reinforced with Cellulose Nanocrystals. *Polymers* **2019**, *11*, 166. [CrossRef] [PubMed]
35. Cazón, P.; Velazquez, G.; Vázquez, M. UV-protecting films based on bacterial cellulose, glycerol and polyvinyl alcohol: Effect of water activity on barrier, mechanical and optical properties. *Cellulose* **2020**, *27*, 8199–8213. [CrossRef]
36. Faradilla, R.F.; Lee, G.; Roberts, J.; Martens, P.; Stenzel, M.; Arcot, J. Effect of glycerol, nanoclay and graphene oxide on physicochemical properties of biodegradable nanocellulose plastic sourced from banana pseudo-stem. *Cellulose* **2017**, *25*, 399–416. [CrossRef]
37. Filipova, I.; Serra, F.; Tarrés, Q.; Mutjé, P.; Delgado-Aguilar, M. Oxidative treatments for cellulose nanofibers production: A comparative study between TEMPO-mediated and ammonium persulfate oxidation. *Cellulose* **2020**, *27*, 10671–10688. [CrossRef]
38. Zhao, Y.; Moser, C.; Lindström, M.E.; Henriksson, G.; Li, J. Cellulose Nanofibers from Softwood, Hardwood, and Tunicate: Preparation–Structure–Film Performance Interrelation. *ACS Appl. Mater. Interfaces* **2017**, *9*, 13508–13519. [CrossRef]
39. Azeredo, H.M.; Mattoso, L.H.C.; Avena-Bustillos, R.J.; Filho, G.C.; Munford, M.L.; Wood, D.; McHugh, T.H. Nanocellulose Reinforced Chitosan Composite Films as Affected by Nanofiller Loading and Plasticizer Content. *J. Food Sci.* **2010**, *75*, N1–N7. [CrossRef]
40. Qing, Y.; Sabo, R.; Wu, Y.; Cai, Z. High-Performance Cellulose Nanofibril Composite Films. *BioResources* **2012**, *7*, 3064–3075.
41. Carneiro-Da-Cunha, M.G.; Cerqueira, M.; Souza, B.W.; Carvalho, S.; Quintas, M.A.; Teixeira, J.; Vicente, A.A. Physical and thermal properties of a chitosan/alginate nanolayered PET film. *Carbohydr. Polym.* **2010**, *82*, 153–159. [CrossRef]
42. Spoljaric, S.; Salminen, A.; Luong, N.D.; Seppälä, J. Ductile Nanocellulose-Based Films with High Stretchability and Tear Resistance. *Eur. Polym. J.* **2015**, *69*, 328–340. [CrossRef]
43. Enescu, D.; Gardrat, C.; Cramail, H.; Le Coz, C.; Sèbe, G.; Coma, V. Bio-Inspired Films Based on Chitosan, Nanoclays and Cellulose Nanocrystals: Structuring and Properties Improvement by Using Water-Evaporation-Induced Self-Assembly. *Cellulose* **2019**, *26*, 2389–2401. [CrossRef]
44. Wang, L.; Chen, C.; Wang, J.; Gardner, D.J.; Tajvidi, M. Cellulose nanofibrils versus cellulose nanocrystals: Comparison of performance in flexible multilayer films for packaging applications. *Food Packag. Shelf Life* **2020**, *23*, 100464. [CrossRef]
45. Ahankari, S.S.; Subhedar, A.R.; Bhadauria, S.S.; Dufresne, A. Nanocellulose in food packaging: A review. *Carbohydr. Polym.* **2021**, *255*, 117479. [CrossRef] [PubMed]
46. Sharma, A.; Thakur, M.; Bhattacharya, M.; Mandal, T.; Goswami, S. Commercial application of cellulose nano-composites—A review. *Biotechnol. Rep.* **2019**, *21*, e00316. [CrossRef]
47. Mascheroni, E.; Rampazzo, R.; Ortenzi, M.A.; Piva, G.; Bonetti, S.; Piergiovanni, L. Comparison of cellulose nanocrystals obtained by sulfuric acid hydrolysis and ammonium persulfate, to be used as coating on flexible food-packaging materials. *Cellulose* **2016**, *23*, 779–793. [CrossRef]
48. Gregory, D.A.; Tripathi, L.; Fricker, A.T.; Asare, E.; Orlando, I.; Raghavendran, V.; Roy, I. Bacterial cellulose: A smart biomaterial with diverse applications. *Mater. Sci. Eng. R Rep.* **2021**, *145*, 100623. [CrossRef]
49. Ali, A.; Shaker, K.; Nawab, Y.; Jabbar, M.; Hussain, T.; Militky, J.; Baheti, V. Hydrophobic treatment of natural fibers and their composites—A review. *J. Ind. Text.* **2018**, *47*, 2153–2183. [CrossRef]

Chapter 3

Hydrophobic Functionalization Reactions of Structured Cellulose Nanomaterials: Mechanisms, Kinetics and in silico Multi-Scale Models

In this chapter, possible routes to increase surface hydrophobicity of cellulose nanomaterials are comprehensively reviewed with an emphasis on mechanisms, kinetics and *in silico* multi-scale models. In general, three approaches for hydrophobic modifications are known: physical adsorption, conjugations of small molecules and grafting of polymers. The latter is then further divided into “grafting to” – coupling of pre-synthesized polymers to cellulose nanomaterials, and “grafting from”, where polymerization is induced on the surface of cellulose nanomaterials. Non-covalent adsorption of hydrophobic agents, such as quaternary ammonium salts, cationic surfactants, cetyltrimethylammonium bromide, zein nanoparticles, etc., to the surface of cellulose nanomaterials is usually applied to improve dispersion in hydrophobic solvents rather than increase the compatibility with matrices. Esterification is by far the most commonly used modification approach. However, it was observed that detailed studies of mechanisms and kinetics are lacking in the field. Furthermore, plasma was identified as an underutilized method for hydrophobic modification of cellulose nanomaterials. The findings of this chapter pinpointed the direction of further studies in the frame of this dissertation.

This chapter addresses Objective 2.

Regarding my contribution: I collected and reviewed the literature on the topic of cellulose nanomaterials hydrophobic modification with the emphasis on mechanistic and kinetic studies and wrote the initial version of the paper.

3.1 Hydrophobic Functionalization Reactions of Structured Cellulose Nanomaterials: Mechanisms, Kinetics and in silico Multi-scale Models

Carbohydrate Polymers 259 (2021) 117742

Contents lists available at ScienceDirect

Carbohydrate Polymers

journal homepage: www.elsevier.com/locate/carbpol

Review

Hydrophobic functionalization reactions of structured cellulose nanomaterials: Mechanisms, kinetics and *in silico* multi-scale models

Ana Oberlintner [a,b], Blaž Likozar [a,c,*], Uroš Novak [a,*]

[a] Department of Catalysis and Chemical Reaction Engineering, National Institute of Chemistry, Hajdrihova 19, 1000, Ljubljana, Slovenia
[b] Jožef Stefan International Postgraduate School, Jamova Cesta 39, 1000 Ljubljana, Slovenia
[c] Faculty of Chemistry and Chemical Technology, University of Ljubljana, Večna Pot 113, SI-1000, Ljubljana, Slovenia

ARTICLE INFO

Keywords:
Hydrophobic functionalization of cellulose nanomaterials
Mechanisms and kinetics insights
Cellulose nanocrystals and cellulose nanofibrils
Applications of hydrophobic cellulose nanomaterials
In-silico modeling

ABSTRACT

Nanoscale-interfaced cellulose nanomaterials are extracted from polysaccharides, which are widely available in nature, biocompatible and biodegradable. Moreover, the latter have a potential to be recycled, upcycled, and formulate therefore a great theoretical predisposition to be used in a number of applications. Nanocrystals, nanofibrils and nanofibers possess reactive functional groups that enable hydrophobic surface modifications. Analysed literature data, concerning mechanisms, pathways and kinetics, was screened, compared and assessed with regard to the demand of a catalyst, different measurement conditions and added molecule reactions. There is presently only a scarce technique description for carbonO—H bond functionalization, considering the elementary chemical steps, sequences and intermediates of these (non)catalytic transformations. The overview of the prevailing basic research together with *in silico* modelling approach methodology gives us a deeper physical understanding of processes. Finally, to further highlight the applicability of such raw materials, the review of the development in several multidisciplinary fields was presented.

1. Introduction

Cellulose is photosynthesized by green plants from carbon dioxide and water. Considering that forests cover 30 % of total Earth's land area (FAO, 2020), this makes cellulose the most abundant natural polymer on the planet and so it is naturally renewable, biodegradable, as well as cheap. Through disintegration of its hierarchical structure with acid hydrolysis, TEMPO-mediated oxidation or even mechanical treatment, it is possible to extract nanoparticles, which were shown to be a great reinforcement for various polymer-based nanocomposites for the first time already in the mid-1990s by Favier et al. (1995). Since then, cellulose nanomaterials and its applications have been extensively researched.

Surface of cellulose nanomaterials consists of hydroxyl groups (or $-OSO_3-$ groups, if processed with sulphuric acid), which give it a hydrophilic character and it is well dispersible only in aqueous solutions and organic solvents with high dielectric constant such as dimethyl sulfoxide (DMSO), dimethylformamide (DMF) and ethylene glycol. Mixing cellulose nanomaterials into other non-aqueous organic solvents or nonpolar polymer matrices results in unstable dispersion due to abundance of hydroxyl groups on the surface and hydrogen bonds between them. Moreover, hydrogen bonds that form between crystals induce aggregation (Lin et al., 2015). To expand applicability of cellulose nanomaterials, its surface has to be modified. Hydrophobicity can be reached either by lowering the surface energy or by roughening surface morphology so it hinders water spreading (Arslan et al., 2016; Cunha & Gandini, 2010; Yu, Zhang et al., 2019).

Various approaches to functionalization of cellulose nanomaterials have been extensively researched with goal to make cellulose nanomaterials more widely applicable. Reactions of functionalization of cellulose nanomaterials have to be aggressive enough to react with hydroxyl groups on the surface, but mild enough not to solubilize the top layer of cellulose nanomaterial or to react with underlying cellulose chains (Huang et al., 2014). In general, three approaches to modification are known: physical adsorption, small molecules conjugations (esterification, isocyanation and silylation), "grafting to" (or onto) and "grafting from". Non-covalent adsorption of molecules such as surfactants onto the cellulose nanomaterial's surface lacks the covalent bonding, and so this type of modification is more suitable for just improving cellulose dispersibility in organic solvents than with the goal to use cellulose nanomaterials in a polymer matrix (Kontturi et al., 2017; Lin et al., 2015). In the "grafting to" approach, pre-synthetized polymers are

* Corresponding author at: Department of Catalysis and Chemical Reaction Engineering, National Institute of Chemistry, Hajdrihova 19, 1000, Ljubljana, Slovenia.
E-mail addresses: ana.oberlintner@ki.si (A. Oberlintner), blaz.likozar@ki.si (B. Likozar), uros.novak@ki.si (U. Novak).

https://doi.org/10.1016/j.carbpol.2021.117742
Received 5 December 2020; Received in revised form 26 January 2021; Accepted 27 January 2021
Available online 2 February 2021

attached to the surface of cellulose nanomaterial, while in "grafting from" approach, cellulose nanomaterial is mixed with monomer molecules and initiator, which induce polymerization on its surface (Lin et al., 2015). "Graft to" reactions generally follow mechanisms of small molecule conjugation, however there is often a decrease in efficiency due to steric hindrance of larger polymer chains compared to small molecules (Espino-Pérez et al., 2016). There are previous literature reviews that cover various approaches to modification of cellulose nanomaterials (Abushammala & Mao, 2019; Cunha & Gandini, 2010; Eyley & Thielemans, 2014; Gericke et al., 2013), however to best of our knowledge there has been no focus yet on making an overview on cellulose nanomaterials hydrophobization mechanisms, kinetics and *in-silico* models including both cellulose nanocrystals and cellulose nanofibrils.

The aim of this review is to describe mechanisms and kinetics of hydrophobic cellulose nanoparticle modifications by collecting available data about used catalysts, conditions and added functional groups in such reactions. Although there are several possibilities of congregating modifications, here they are clustered according to the type of bond that is formed as this review is focusing on the chemistry with explanation of mechanism between surface of cellulose nanomaterial and compound in question. Moreover, the possible advantages for special applications emphasizing the hydrophobic cellulose nanomaterials are being presented.

2. Chemical structure of cellulose and its modification

To understand the mechanisms and kinetics of cellulose functionalization, it is important to describe structure of cellulose in-depth. Cellulose, unrelated to its source, consists of repeating β-D-anhydroglucopyranose units (AGUs), alternately turned for 180° around the axes and covalently linked by β-(1→4)-ether bonds, called glycosidic bonds (Fig. 1). The basic unit is a heterocycle that consists of five carbons, including anomeric carbon (labeled C-1) and an oxide. Inversions of basic units prevent cellulose from coiling and keep it in keep long, straight chain. Cellulose is a polymer formed by poly-condensation, so the two ends of the chain are chemically different. At one end, there is an unsubstituted hemiacetal group that may also adopt a form of open-chain aldehyde and acts as a reducing agent *i.e.* "reducing end", while the other end the "non-reducing end". Each anhydroglucose unit (AGU) has three hydroxyl groups: one primary at C-6 and two secondary units at C-2 and C-3. All AGUs adopt chair conformation.

Hydroxyl groups, attached directly to AGU, are placed in equatorial (ring) plane and hydrogen atoms are placed in axial plane. Position of C—6 attached hydroxyl group is determined by the placement of C—6—O—6 bond with respect to C—5—O—5 and C—4—C—5 bonds (French, 2017). The three possible conformations are labelled gauche-gauche, gauche-trans and trans-gauche, conditioned by torsion angle χ (χ = C—4—C—5—C—6—O—6) being 60°, 180° and 300°, respectively (Horii et al., 1983). In order to form a more stable molecule, cellulose chains tie through intra and intermolecular hydrogen and van der Waals bonds, which results in formation of cellulosic fibers. Various three-dimensional structures of cellulose chains form, which causes co-occurrence of crystalline and amorphous regions. Bonds within one chain of cellulose occur through the hydrogen of C-3 hydroxyl group in one anhydrous glucose unit and ether —O —in another AGU and between oxygen in hydroxyl group at C-6 and hydrogen at C-3. To form intermolecular bonding, hydrogen bonds between C-3 oxygen and C-6 hydrogen take place (Fig. 1) (Kamide et al., 1985; Rowland & Howley, 1988). Inspection of intra and intermolecular bonding can be done by ^{13}C NMR and IR and therefore obtain the idea of cellulose structure (Newman & Davidson, 2004).

Cellulose polymer, due to hydrogen and β-glycosidic bonds, exhibits higher rigidity, stiffness, viscosity and tendency to crystallize or form fibrillary structures, compared to other polysaccharides, that are linked through α-glycosidic bonds (Heinze, 2015). Seven different polymorphs of cellulose are known: cellulose I_α and I_β, II, III_I, III_{II}, IV_I and IV_{II} (Young & Rowell, 1986). Cellulose I is the native form and is further divided into two forms I_α and I_β, which differentiate in layer packing along c-plane. I_β form is obtained from higher plants. Cellulose II is formed from cellulose I by alkali treatment, mercerization or recrystallization from solution. The third polymorph, cellulose III_I, originates from cellulose I as well. It is formed by the treatment of cellulose I in supercritical ammonia or various amines. Cellulose IV cannot be obtained directly from cellulose I, but rather from cellulose II or III (Habibi & Lucia, 2012; Matthews et al., 2012).

Hydrogen bonds influence multiple properties, such as unequal reactivity of hydroxyl groups, high crystallinity and limited solubility in solvents. The latter proves to be an obstacle when incorporating cellulose nanoparticles in the matrices that have low polarity, which is why hydrophobic modification of cellulose nanoparticles is important. The improvement of dispersibility after modification is often demonstrated

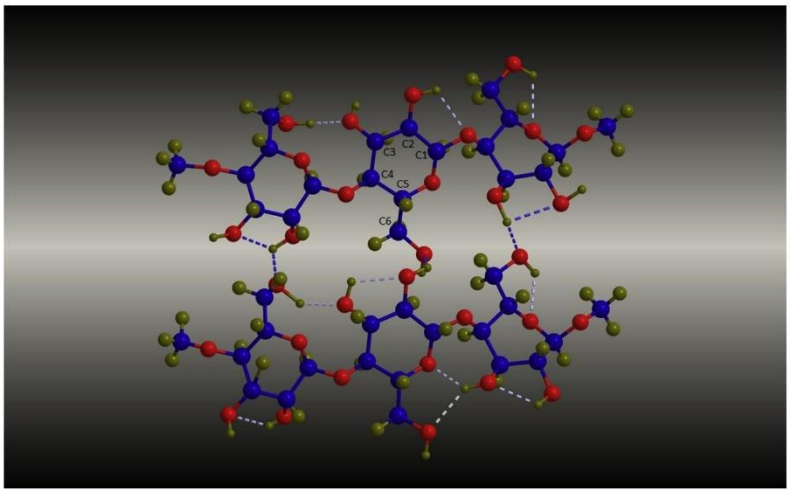

Fig. 1. Molecular model of two cellulose chains and their intra and intermolecular hydrogen bonds.

with use of common solvents with low dielectric constant such as ethyl acetate ($\varepsilon = 6.0$), chloroform ($\varepsilon = 4.8$), toluene ($\varepsilon = 2.4$), styrene ($\varepsilon = 2.4$), mineral oil ($\varepsilon = 2.1$), cyclohexane ($\varepsilon = 2.0$) and hexane (1.9). Different modifications result in different dispersibility. For example, acetylated cellulose nanocrystals (CNCs) cannot be dispersed in toluene or cyclohexane, but form a stable dispersion in both ethyl acetate and water, whereas higher acetyl content results in better dispersion (Sebe et al., 2013). On the other hand, alkenylated CNCs are well dispersible in chloroform, toluene, styrene and mineral oil (Miao & Hamad, 2016). Comparison of dispersibility of modified CNCs and pristine CNCs in a common used polymer matrix PLA was demonstrated by Spinella et al. (2016), where unmodified CNCs aggregated when incorporated into PLA. Morphology of grafted CNC/PLA nanocomposite appeared more homogeneous compared to pristine CNCs. It was further confirmed, through dynamic rheology, that grafting positively affects the dispersion in PLA matrix. In conclusion, hydrophobic modifications positively influence dispersibility in solvents and matrices in which cellulose nanomaterials are naturally not dispersible. Therefore its potential range can extend the current use of nanocellulose as fillers, in a composites manufacture, as coating or even in packaging achieving very interesting and promising properties, which are further amplified in Section 6.

3. The two types of cellulose nanomaterials: CNCs and CNFs

Cellulose nanoparticle is a form of cellulose, where at least one dimension is on nanoscale. It is an attractive material because of its wide availability, low price, renewability, biodegradability and overall sustainability. It can be present in three different forms: cellulose nanocrystals (CNC), cellulose nanofibrils (CNF) and bacterial cellulose (BC). However, it was proposed by USDA Forest Service, the Technical Association of the Pulp and Paper Industry and interested entities in Canada, to categorize cellulosic nanomaterials into only two groups: CNCs and CNFs as bacterial cellulose is in form of fibrils (Postek et al., 2013).

Production and characterization of CNCs and CNFs is well reviewed elsewhere (Habibi et al., 2010; Kumar et al., 2021; Mondal, 2016; Moon et al., 2011). However, for the better comprehension, the main information about cellulose nanomaterials will be described here as well. The main differences between the two types of cellulose nanomaterials, CNCs and CNFs, are in the amount of amorphous regions and their dimensions (Sacui et al., 2014) as visible in Fig. 2. CNFs, are long, flexible networks of fibrils with a diameter approximately 10–20 nm. They are obtained by fibrillation in which a cellulose fibril is separated from others. More than one procedure in known to obtain CNFs: high pressure homogenization (Li, Wang et al., 2020, TEMPO-mediated oxidation (Michel et al., 2020), enzymatic hydrolysis (Bian et al., 2019), mechanical fibrillation/grinding (Lee & Mani, 2017) possibly followed by high intensity ultrasonification (Tsalagkas et al., 2020), steam explosion (Tanpichai et al., 2019), and cryocrushing (Alemdar & Sain, 2008). The length of fibers is strongly dependent on the degree of fibrillation and pretreatment type (Gopakumar et al., 2016). CNCs are generally produced by strong acid hydrolysis (Gopakumar et al., 2016). Kunaver et al. (2015), patented the process of CNCs extraction in organic solvent with presence of small (2 wt% to 5 wt%) of acid catalyst. The most commonly used acids are HCl and H_2SO_4. Use of phosphoric and hydrobromic acid was reported as well (Camarero Espinosa et al., 2013; Sadeghifar et al., 2011). Strong acid destroys amorphous regions and yields a highly crystalline particles with needle or rod-like shape – CNCs (also known as cellulose nanowhiskers or nanocrystalline cellulose). They are 5–100 nm wide and several nanometers in long (Kargarzadeh et al., 2012; Kunaver et al., 2015).

Properties of cellulose nanomaterials are highly dependent on source and type of pretreatment. For instance, CNCs derived from wood and cotton are shorter than the ones obtained from tunicate and bacterial cellulose, as the latter possess higher degree of crystallinity. A higher degree of crystallinity also makes cellulose more resistant to hydrolysis, although higher concentrations and volumes of acid are required (Deepa et al., 2015; Sacui et al., 2014). CNFs, on the other hand, contain a lot more of amorphous regions and are overall less crystalline.

Furthermore, the type of pretreatment also effect the surface chemistry. Generally three functional groups can appear on surface of cellulose nanoparticles: —OH as a result of mechanical treatment, enzymatic hydrolysis or hydrolysis with HCl, $OSO3^{—}$ as result of pretreatment with H_2SO_4 or $COO^{—}$ as a result of TEMPO-mediated oxidation (Sacui et al., 2014).

4. Mechanisms and kinetics of hydrophobic functionalization of cellulose nanomaterial

High density of hydroxyl groups on the surface of cellulose nanomaterial leads to its inherent hydrophilicity. To improve its dispersion within nonpolar matrices, surface modifications seem to be the most promising solution. Reaction types, which were proven suitable for chemical modification of cellulose nanoparticles, are esterification, carbamation, etherification, silylation, cold argon plasma, oxygen plasma coupled with subsequent introduction of monomers and

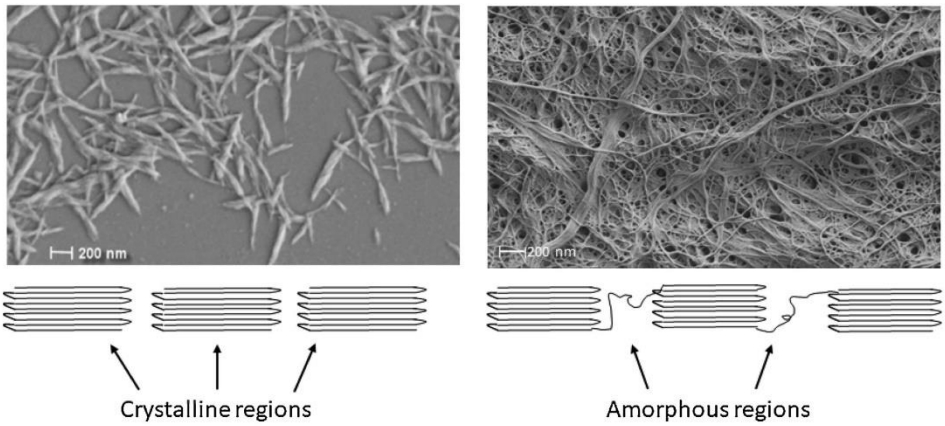

Fig. 2. SEM micrograph of CNC (left) (Kunaver et al., 2016) (reproduced by permission of Elsevier) and CNF (right) with belonging schematic representation of crystalline and amorphous structure.

fluorocarbon plasma treatment. Reactions primarily occur on the hydroxyl group at C-6 (see Fig. 1), which was reported to be ten times more reactive than other hydroxyl groups, followed by a hydroxyl group at C-2 is twice as reactive as hydroxyl group at C-3 (Rowland & Howley, 1988; Verlhac et al., 1990). Reactions that occur on the surface of cellulose nanofiber or nanocrystal are undergoing quite similar elemental steps as in the case with the single polymer forming building block. The main difference between molecule and (nano)cellulose is in effectiveness of modification and kinetics, which are strongly dependent on the form and state of cellulose nanoparticles, such as fibrillation, crystallinity, aggregation, pre-treatment, swelling, *etc*. Effectiveness of modification is measured by degree of substitution, with highest possible value of 3, which happens in case all hydroxyl groups on AGUs react. When considering only surface modifications, degree of surface substitution applies. In this case in cannot be higher than 1.5, because there are only three hydroxyl groups available on every two AGUs. However, due to low reactivity of C—3O—H, reaching full substitution is extremely unlikely (Eyley & Thielemans, 2014; Lin et al., 2015). Similarly, the reaction conditions, such as higher reactant concentration and prolonged reaction times can affect the structure of cellulose nanomaterial. Higher reactant concentrations and prolonged reaction times can disrupt the cellulose structure. As reaction proceeds from the surface into the bulk of cellulose nanoparticle and cause loss of crystallinity or size and consequently influence on the material physical properties (Ifuku et al., 2007; Lin et al., 2011). In the next subsections descriptions of reaction mechanisms to the formation of hydrophobic cellulose nanomaterial shown in Fig. 3 will be introduced and presented, together with the kinetic data if available.

4.1. Esterification

Commonly reported method for hydrophobic functionalization of cellulose nanoparticles is esterification. In Table 1 the literature overview of the CNC and CNF functionalization approach, agent, medium, conditions and catalyst employed is collected.

Most esterification techniques that are used on cellulose can be applied to cellulose nanoparticles as well, but the main challenge is to modify only surface hydroxyl groups while keeping the bulk intact in order to preserve crystallinity (Habibi et al., 2010). Generally, this depends on reaction conditions, which should be aggressive enough to initiate the reaction, but at the same time do not destroy the cellulose structure. Grafting of carbonyl moieties is most often confirmed with FTIR where the carbonyl peak at 1750 cm^{-1}, and adsorption band at 1240 cm^{-1} appear, elemental analysis and ^{13}C CP-MAS NMR spectroscopy (Brand et al., 2017). The possible effect of functionalization on crystallinity of cellulose nanoparticles is inspected with XRD, while possible morphological changes are observed with SEM and/or TEM. Hydrophobic character of cellulose nanomaterial is confirmed either by dispersing it in various organic solvents or by measuring contact angle with water.

Based on the type of reagents, esterification reactions can be categorized into five groups: esterification with acid anhydrides, acid halides, acid-catalyzed carboxylic acids, transesterification esters, and *in-situ* activated carboxylic acids (Peng et al., 2016).

Esterification of cellulose nanoparticles with acid anhydrides and acyl chlorides can be carried out in solvent systems such as LiCl/*N,N*-dimethylacetamide (DMAc) or tetraalkylammonium fluoride hydrate/DMSO and is catalysed by tertiary amines such as imidazole, pyridine or 4-dimethylaminopyridine (DMAP) (Guo et al., 2012; Nawaz et al., 2013). However, as these solvent systems can be quite expensive, esterification reaction are often done in anhydrous pyridine and/or excessive acetic anhydride. Acetylation with alkenyl succinic anhydride yielded highly hydrophobic CNCs, which was confirmed through their dispersion in medium and low polarity solvents (Yuan et al., 2006). Lin et al. (2011) studied acetylation of CNCs with acetic anhydride, with anhydrous pyridine as a catalyst. The mechanism of pyridine-catalyzed reaction between alcohol and anhydride (Clayden et al., 2012) is shown in Fig. 4A. Although the mechanism of CNCs functionalization with acetic anhydride is not completely known, observation of only minimal morphological changes of CNCs indicate that the functionalization happens exclusively on surface (Guo et al., 2012; Lin et al., 2011). Rod-like shape of CNCs was preserved after the acetylation, but they decreased in size. The outline of acetylated CNCs was blurry as seen on TEM. The authors propose this could be due to partial solubilization during the reaction. However, minimal change in crystallinity was confirmed through XRD, which points at preservation of original crystalline structure and functionalization of only surface hydroxyl groups. Improved dispersion in six common solvents, a decrease in surface polarity and higher decomposition temperature of PLA with incorporated acetylated CNCs were observed. Besides pyridine, citric acid was reported to be a suitable catalyst for this type of reaction as well (Ávila Ramírez et al., 2017). Alkynylated anhydride, with pyridine as a catalyst, was applied to prepare modified CNCs with decreased polar component and slightly increased nonpolar component of surface energy as calculated through Owens– Wendt approach as well as better dispersity in THF (Chen et al., 2015). Regarding kinetics, acylation of

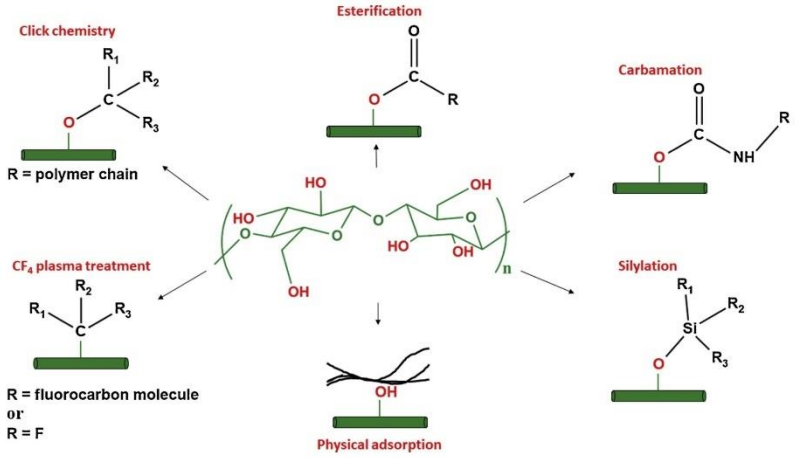

Fig. 3. Hydrophobic modifications of CNCs and CNFs that will be discussed within this review.

Table 1
Possible functionalization approaches with belonging conditions, medium and catalyst[1].

Form of cellulose nanomaterial	Functionalization approach	Agent	Medium	Conditions	Catalyst	Reference
CNC	esterification	acid anhydrides	pyridine	80 °C, 300 min	pyridine	(Peng et al., 2016)
CNC	esterification	acid chlorides	DMF	RT - 50 °C, 300 min	TEA	(Peng et al., 2016)
CNC	esterification	carboxylic acids	DMSO/water	80 °C, 24 h/20 h	CDI/HCl	(Peng et al., 2016)
CNC	esterification	acetic anhydride	pyridine	80 °C, 5h	pyridine	(Lin et al., 2011)
CNC	esterification	alkyenyl succinic anhydride	LiCl/DMAc	50 °C, 12 h	1-methylimidazole	(Yuan et al., 2006)
CNC	esterification	alkynylated anhydride	pyridine	80 °C, 5 h	DMAP	(Chen et al., 2015)
CNC	esterification	acetic anhydride	acetic anhydride	120 °C, 3 h	citric acid	(Ávila Ramírez et al., 2017)
MCC	esterification	long-chain acyl chlorides	DMAc/LiCl	60 °C, 3 h	pyridine	(Guo et al., 2012)
CNC	esterification	carboxylic acid	carboxylic acid	130 °C, 20 h	residual sulfate groups at the surface of CNC	(Espino-Pérez et al., 2014)
CNC	esterification	acetic acid	acetic anhydride	25 °C, 1 h	sulphuric acid	(Yokota et al., 2020)
CNC	esterification	11-mercaptoundecanoic acid	acetic anhydride	/	acidic catalyst	(Parambath Kanoth et al., 2015)
CNC	esterification	fatty acids, biodiesel, plant oils	aqueous lactic acid	190 °C, 100 mmHg, 30 min	zinc acetate dehydrate/ DBTL	(Yoo & Youngblood, 2016)
CNC	esterification	vinyl esters	DMF/DMSO	80 °C - 100 °C, 15–240 min, microwave radiation	K_2CO_3	(Brand et al., 2017)
CNC	esterification	pyridine-4-carbonyl chloride	DMF	80 °C, 24 h	triethylamine	(Li et al., 2015)
CNC	esterification by ROP	ε-caprolactone	ε-caprolactone	RT, 5 min, microwave radiation	$Sn(Oct)_2$	(Lin et al., 2009)
CNC	esterification by ROP	ε-caprolactone	ε-caprolactone	95 °C, 24 h	$Sn(Oct)_2$	(Goffin et al., 2011)
CNC	esterification by ROP	ε-caprolactone	ε-caprolactone	Ar, 120 °C, 24 h	/	(Labet & Thielemans, 2011)
CNC	esterification by ROP	ε-caprolactone	ε-caprolactone	Ar, 120 °C, 24 h	citric acid	(Labet & Thielemans, 2012)
CNC	esterification by ATRP	2-bromoisobutyryl bromide/styrene	DMF	Ar, 100 °C, 16–24 h	CuBr/PMDTA	(Morandi et al., 2009)
CNC	esterification by SET-LRP	CDI and methyl acrylate	DMSO	25 °C, 20–500 min	Cu(0)	(Wang et al., 2015)
CNC	esterification	organic acid	water	105 °C, 4–120 min	acidic catalyst	(Braun & Dorgan, 2009)
CNC	esterification by ROP	L-lactide	anhydrous toluene	90 °C, 68 h	$Sn(Oct)_2$	(Braun et al., 2012)
CNC	esterification	molten oxalic acid	oxalic acid	115 °C, 15–75 min, microwave and ultrasound	/	(Lu et al., 2019)
CNF	esterification	formic acid	formic acid	70–100 °C, 24 h	acidic catalyst	(Lv et al., 2019)
CNC	esterification	acetic anhydride	(TBAA)/DMAc	65 °Cm 1.5 h	/	(Miao et al., 2016)
CNF	esterification	alkyl ketene dimer	toluene	70–125 °C, 6 h	/	(Yuan & Wen, 2018)
CNF	esterification	varoius anhydrides	anhydride	60 °C, 3 h	/	(Sehaqui et al., 2014)
CNC	esterification	pentafluorobenzoyl chloride	anhydrous toluene	80 °C, 2 h	pyridine	(Salam et al., 2015)
CNC	carbamation	polycaprolactone	toluene	RT	/	(Habibi & Dufresne, 2008)
CNC	carbamation	low molecular weight PCL diol	anhydrous toluene	Ar, 75 °C,	/	(Zoppe et al., 2009)
CNC	carbamation by ATRP	polystyrene	THF	100 °C	Cu(I)Br/PMDTA	(Morandi & Thielemans, 2012)
CNC	carbamation by ATRP	methyl methacrylate and butylacrylate	DMF, THF, PMDTA	DMF, THF	Cu(0)	(Yu et al., 2016)

(continued on next page)

Table 1 (*continued*)

Form of cellulose nanomaterial	Functionalization approach	Agent	Medium	Conditions	Catalyst	Reference
CNC	carbamation	castor oil	toluene	N_2, 75 °C, 7 days	TEA	(Shang et al., 2013)
CNC/CNF	carbamation	n-octadecyl isocyanate	toluene	1–110 °C, 30 min	/	(Siqueira et al., 2009a, 2009b)
CNC	carbamation	1,6-hexamethylene diisocyanate	DMF	N_2, 80 °C, 24 h	/	(Rueda et al., 2011)
CNC	carbamation	3-isocyanatopropyl triethoxysilane	DMF	N_2, RT, 8.5 h	DBTDL	(de Oliveira Taipina et al., 2013)
CNC	carbamation	3-isocyanotepropyl triethoxysilane	THF	62–63 °C, 72 h	TEA	(Anžlovar et al., 2020)
CNC	carbamation	isophorone diisocyanate	DMSO	N_2, 60 °C, overnight	DBTDL	(Girouard et al., 2016)
CNC	silylation	3-aminopopyltriethoxysilane	water	pH = 4, RT, 120 min	/	(Khanjanzadeh et al., 2018)
MCC	silylation	3-glycidoxypropyltrimethoxysilane	water	70 °C, 24 h	/	(Pujiasih et al., 2018)
CNF	silylation	methylmetrimethoxysilane	water	pH = 0.4/4, RT, 120 min	/	(Deng et al., 2015)
CNF	silylation	(tridecafluoro-1,1,2,2-tetrahydrooctyl) trichlorosilane	/	chemical vapour deposition, 90 °C, 8 h	/	(Mertaniemi et al., 2012)
CNF	silylation	(tridecafluoro-1,1,2,2-tetrahydrooctyl) trichlorosilane	toluene	RT, 3 h	/	(Mertaniemi et al., 2012)
CNF	silylation	methyltrimethoxysilane	/	120 °C, 3 h	/	(Dilamian & Noroozi, 2021)
CNC	silyation	3-methacryloxypropyltrimethoxysilane	ethanol	70 °C, 24 h	/	(Yu, Yang et al., 2019)
CF	plasma	fluorocarbon plasma	/	RT, atm pressure	/	(Samanta et al., 2012)
CF	plasma	He/1,3-butadiene plasma	/	RT, atm pressure	/	(Samanta et al., 2012)
CF	plasma	oxygen plasma and Trisilanolisobutyl-polyhedral oligomeric silsesquioxane	/	RT, 25 Pa then 90 °C, 1 h	/	(Yao et al., 2021)
CNC	plasma	styrene, caprolactone, farnesene	/	strong electrical field	/	(Alanis et al., 2019)
CNC	click chemistry	polycarpolactone diol	DMF	ice-water bath - 30 °C, 48 h	DMAP	(Zhou et al., 2018)
CNC	click chemistry	3- mercaptopropyltrimethoxysilane	water/ $CHCl_2$	25 °C, 4 h / RT, UV light	acetophenone	(Huang et al., 2014)
CNF	click chemistry	carbic anhydride and thiol-ene	water	RT, pH = 9.5–10.5 and 37 °C, 3 h	/	(Fein et al., 2020a, 2020b)
CNC	adsorption	cetyltrimethylammonium bromide	cetyltrimethylammonium bromide	pH = 6.9, 49 °C, 30 min	/	(Qing et al., 2016)
CNC	adsorption	quaternary ammonium salts	NaOH aq solution	pH = 10, 60 °C- RT, 3 h + overnight	/	(Salajková et al., 2012)
CNF	adsorption	cationic surfactants	aqueous solutions of cationic surfactants	RT, 15 min	/	(Xhanari et al., 2011)
CNF	adsorption	cetyltrimethylammonium bromide	aqueous solutions of cationic surfactants	50 °C	/	(Syverud et al., 2011)
CNF	adsorption	galactoglucomannans	water	RT, 3.5 h	/	(Lozhechnikova et al., 2014)
CNF	adsorption	alkyl ketene dimer	$CHCl_3$, water, surfactant	RT	/	(Missoum et al., 2014)
CNF	adsorption	amino propyl trimethoxy silane	water	RT, 2 h	/	(Reverdy et al., 2018)
CNF	adsorption	functionalized zein nanoparticles	EtOH/water with sodium caseinate	RT, 30 min	/	(Li et al., 2020)
CNC	BlocBuilder with nitroxide-mediated polymerization	styrene	DMSO	NaOH, RT/90 °C/ 90–115 °C, 90 min	/	(Roeder et al., 2016)
CNC	nucleophilic substitution	various triaziniyls	dichloromethane	NaOH, RT, 24 h	K_2CO_3	(Fatona et al., 2018)
CNF aerogel	chemical vapor deposition	hexadecyltrimethoxylan	/	155 °C, 1 h	/	(Rafieian et al., 2018)
CNC	SI-ATRP	styrene	triethylamine, DMF	N_2, 100 °C, 12 h	Cu(I)Br	(Yin et al., 2016)
CNC	ozone-initiated free radical polymerization	polystyrene	sodium acetate buffer	ozone/77 °C, 36 h	/	(Espino-Pérez et al., 2016)
CNC	N-alkylation	alkylamines	water, $NaBH_3CN$ as reducing agent	45 °C, 3 h then RT, 21 h	/	(Nigmatullin et al., 2020)

[1] Cellulose nanocrystals (CNC), cellulose nanofibrils (CNF), cellulose fibers (CF) microcrystalline cellulose (MCC), triethylamine (TEA), 4-dimethylaminopyridine (DMAP), dibutyltin dilaurate (DBTL), pentamethyldiethylenetriamine (PMDTA), tert-butyl acetoacetate (TBAA).

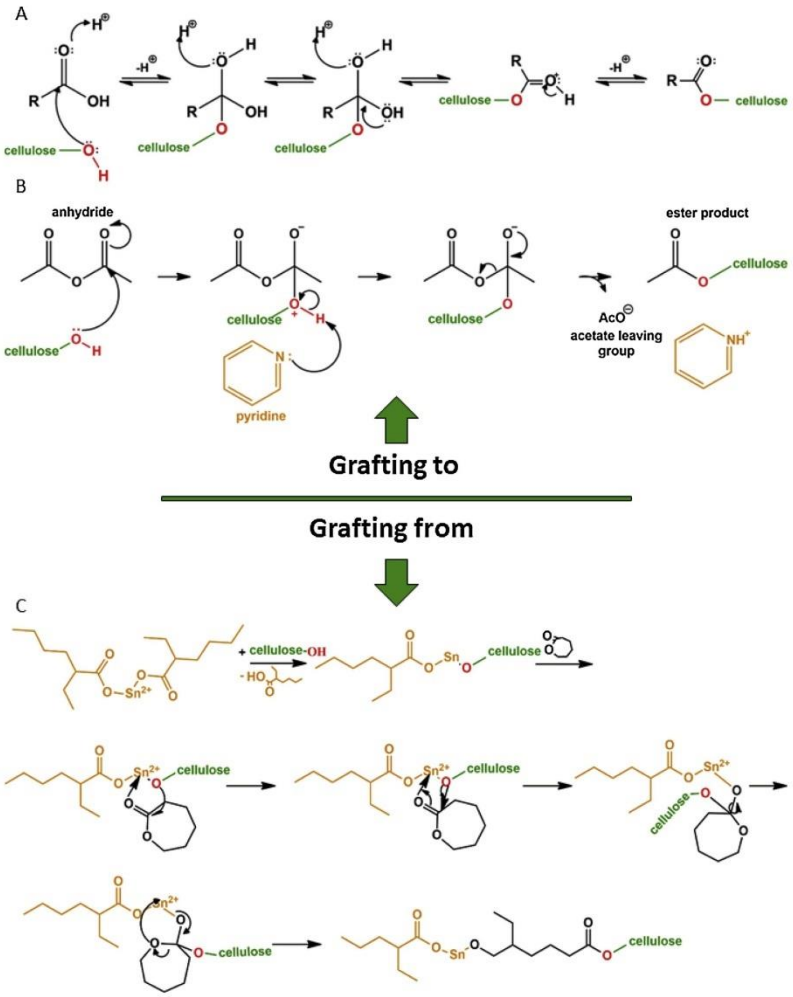

Fig. 4. Mechanism of A) pyridine-catalyzed esterification of cellulose nanoparticles with acetic anhydride, B) esterification of cellulose nanoparticles with carboxylic acid, and C) functionalization of cellulose nanoparticles *via* ROP of ε-caprolactone.

cellulose with acetic anhydride, catalyzed with H_2SO_4 follows first-order kinetics up to certain reaction time, which is conditioned with the concentration of catalyst (15 h for 0.4 vol % of H_2SO_4 or 50 h with 0.1 vol %). Extending reaction time can cause surface damage and structural modifications (Frisoni et al., 2001), however to our knowledge there are no systematic studies investigating such effects on cellulose nanomaterials. Kinetics of without catalyst and with imidazole-catalyzed esterification of cellulose with various anhydrides in LiCl/DMAc have been studied (Nawaz et al., 2012; Nawaz et al., 2013). Cyclohexylmethanol and trans-1,2-cyclohexanediol were used as model compounds for the hydroxyl groups of the anhydroglucose unit. It was found out, for the model compounds, that in uncatalyzed reaction $k_{(Prim\text{-}OH)}/k_{(Sec\text{-}OH)} > 1$. The reaction rate decreased with the increasing number of carbons in anhydrides from ethanoic to butanoic anhydride. However, it increased for pentanoic and hexanoic anhydride because of subtle changes in enthalpy and entropy and compensations thereof (Nawaz et al., 2012). A similar result was obtained for imidazole-catalyzed reaction: $k_{3,Prim\text{-}OH}/k_{3,Sec\text{-}OH} > 1$ (Nawaz et al., 2013).

Espino-Pérez et al. (2014) carried out hydrophobization of CNCs through esterification with two carboxylic acids: phenylacetic acid and hydrocinnamic acid. The reaction was carried out at the temperature above the carboxylic acid melting point; therefore, the carboxylic acid was acting as reaction media as well as a reactant (Fig. 4B) (Espino-Pérez et al., 2014). Change in width of CNCs was observed- possibly because of peeling-effect that is observed during acetylation and silylation or because of natural degradation of cellulose acidic conditions in reactions. Decrease in crystallinity of CNCs was observed, which could be

attributed to acidic conditions that cause break of crystalline contacts and substitute them with amorphous contacts (Ioelovich, 2012). Modified CNCs were well dispersable in chloroform and, compared to pristine CNCs, did not aggregate. Water contact angle measurement pointed to increased hydrophobicity as well.

Esterification of CNFs are significantly less described than CNCs. However, Kumagai & Endo (2020) researched functionalization of nanofibrils with butane-1,2,3,4-tetracarboxylic acid (BTCA) with aim to achieve immobilization of tannic acid. Higher protein absorbency in esterified CNFs was demonstrated which points to potential application as immobilization carrier. No significant change in morphology was detected. Moreover, when compared to CNFs with adsorbed tannic acid, the modified ones were smaller, with diameter is similar to TEMPO prepared CNF, compared to the adsorbed. It was concluded, that with esterification *via* BTCA not only the immobilization of tannic acid can be achieved, but also the nanofibrillation of cellulose materials (Kumagai & Endo, 2020).

Yoo and Youngblood (2016) aimed at reducing harmful reagents and solvents for hydrophobization of CNCs and therefore focused on modification in aqueous conditions. Reactions were carried out through two different reaction routes, using lactic acid as a solvent. Moreover, the byproduct polylactic acid (PLA) oligomers was then grafted onto the surface of CNCs. Higher hydrophobicity was then reached by grafting various side groups originating from fatty acids onto the surface of CNCs. In the first route, esterification was done in two steps: drafting of PLA oligomers to CNCs with zinc dehydrate catalyst and subsequent esterification with fatty acids, biodiesel or plant oil in the presence of dibutyl tin dilaurate (DBTDL) catalyst, while the second route was ''one-pot'', where fatty-acid was introduced directly into the PLA-CNCs reaction mixture. It was concluded, that this is a greener approach that can be used to graft free long-chain fatty acids (route 1) and triglycerides or fatty acid esters (route 2) and increase the CNCs dispersibility in common solvents. More recently, Le Gars et al. (2020) studied esterification of CNCs using fatty acids, but focused on the first part of reaction - role of solvent exchange and dispersion of CNCs. The optimal solvent exchange seems to be through ethanol to acetone, where particles remain in range 300 nm. Good dispersion is the basic for grafting: no peak for carbonyl bond was detected in badly dispersed CNCs. Higher values of DS obtained for stearic acid suggest better efficiency of the grafting using a longer fatty chain. Possible due to the difference in viscosity between lauric and stearic acids in the molten state or due to slight difference in acidity. Yokota et al. (2020) prepared amphiphilic CNFs *via* aqueous counter collision and acetylation with acetic anhydride in aqueous dispersion.

Peng et al. (2016) compared 4 different hydrophobization routes of CNCs *via* surface esterification. In order to comprehend the role of esterification type and tune hydrophobicity, chains with different hydrocarbon length (acetyl, hexanoyl, dodecanoyl, oleoyl and methacryloyl) were grafted using acid anhydride, acid chloride, acid catalyzed carboxylic acid, and 1,1-carbonyldiimidazole (CDI) activated carboxylic acid. Through FT-IR spectra, it was observed, that grafting anhydride, in presence of pyridine, is more efficient for low molecular moieties with shorter aliphatic chains, such as acetyl. Pyridine has a double role in this reaction: on one hand, it acts as a catalyst and on the other as a solvent that causes reduction in hydrogen bonding between CNCs, which could promote the reaction. However this approach was not as efficient for grafting longer chains (dodecanoyl), where grafting with CDI reached higher degree of substitution due to higher availability of grafting moieties in carboxylic acid form. Willberg-Keyriläinen & Ropponen (2019) showed that for grafting long chain carboxylic acids such as dodecanoicoc or octadecanoic, acyl chloride is the most efficient method. It was demonstrated, that both anhydride and CDI are suitable for grafting unsaturated moieties such as methacryloyl and oleyl. Grafting acid chloride or carboxylic acids was shown to be less efficient than previously mentioned approaches, however Trinh and Mekonnen (2018) achieved higher degrees of substitution (0.2 compared to previously reported 0.07) without disturbing the crystalline structure. Crystallinity of CNCs slightly changed but there was no clear trend that would correlate degree of substitution with crystallinity change. Hydrophobicity, tested by dispersing modified CNCs in water, ethanol, acetone, THF and toluene, highly depends on degree of substitution as well as on length of the grafted aliphatic chain – with longer chain the dispersibility is better even at low degree of substitution (Peng et al., 2016).

Another approach to hydrophobization of CNCs and CNFs is with transesterification. Brand et al. (2017) studied kinetics of transesterification reactions with vinyl acetate that were carried out under microwave for activation and with K_2CO_3 acting as a catalyst. It was observed that DMSO is a more suitable solvent than DMF and that chemical reactivity is greatly impacted by the degree of CNCs dispersion in the solvent. A higher concentration of reagent increases rate of reaction, however after initially fast reaction, a slower conversion rate follows although there are still unreacted hydroxyl groups on the surface. This phenomenon was explained with two possibilities: either the reaction rate starts to be controlled by diffusion of reactant and catalyst through aggregates of CNCs or the reaction rate slows down due to different reactivity of hydroxyl groups on the surface. Despite high reactivity of the reagent, a significant amount of surface hydroxyl groups was left unreacted even after 4 h of reaction, which was assigned to the low reactivity of C—3O—H (Brand et al., 2017).

In ''grafting from'' approach, a commonly used reaction is transesterification of ε-caprolactone *via* ring-opening polymerization (ROP) (Goffin et al., 2011; Habibi et al., 2008; Labet & Thielemans, 2011, 2012; Lin et al., 2009). This reaction is frequently carried out using metal-based catalysts, especially tin(II) octoate [$Sn(Oct)_2$] (Goffin et al., 2011; Habibi et al., 2008; Lin et al., 2009). Tin-based catalyst, in combination with alcohol (-OH), initiates the reactions shown in Fig. 4C. (Kowalski et al., 1998; Labet & Thielemans, 2009, 2011). High temperatures, that are needed for the reaction catalyzed by tin (II) octoate, can lead to intra and intermolecular transesterification, which causes an unwanted formation of a network (Penczek & Duda, 1996).

The drawback is that metal catalysts often stay incorporated into the polymer and additional separation is needed for some applications. With this in mind, Labet and Thielemans (2012), studied utilization of citric acid as a catalyst in ROP of ε-caprolactone. In the initiation step, acid activates the monomer, which is then attacked by a nucleophile (—OH). Propagation follows similarly, with the alcohol at the end of the chain acting as a nucleophile (Labet & Thielemans, 2011). Generally, no change on the surface of nanocrystals or in crystallinity was observed. The surface was confirmed to be hydrophobic, through water contact angle measurement and utilization of modified CNCs by incorporating them into high molecular weight PCL matrix (Goffin et al., 2011; Habibi et al., 2008).

In ''grafting from'' approach, cellulose nanomaterial is first grafted with macro initiator that usually contains bromide (Morandi et al., 2009; Wang et al., 2015). For example, Morandi et al. (2009) carried out grafting of polystyrene (PS) chains through surface-initiated transfer radical polymerization (SI-ATRP), where 2-bromoisobutyryl bromide was first esterified onto CNCs surface with TEA acting as a catalyst and prepared initiating sites for ATRP by a CuBr/PMDETA (*N,N,N'*,*N''*, *N''*-pentamethyldiethylenetriamine)-catalyzed of styrene. After the first step, the substitution of surface hydroxyl groups was varying from 21 % to 70 % as confirmed with elemental analysis. Higher temperature, reactant concentration and longer reaction time led to higher grafting efficiency. For identical reaction time and temperature, a linear dependence between reactant concentration and grafting efficiency was observed and so the density of grafted initiating sites can be easily controlled. Moreover, length of grafted polymer chains can be controlled by concentration of monomer and sacrificial initiator in the second step. Water contact angle increased significantly after the modifications while morphology and crystallinity of nanocrystals did not change (Morandi et al., 2009). Wang et al. (2015) first grafted CNCs with bromoisobutyric

acid in presence 1,1'-carbonyldiimidazole which then induced Cu (0)-catalyzed living radical polymerization of poly(methyl acrylate). The kinetics of the second step in functionalization were shown to be fast, grafting six times the mass of poly(methyl acrylate) with respect to CNCs in 30 min of reaction.

To avoid multiple reaction steps and decrease time and cost needed for functionalization, several research groups explored the possibility to perform hydrolysis of cellulose and then functionalization of nanocrystals in one step. Braun and Dorgan (2009) performed single step hydrolysis and esterification of cellulose, called Fischer esterification, resulting in hydrophobicity of CNCs, demonstrated by dispersing them in toluene and ethyl acetate. Two different acids have two different roles in this reaction. HCl is responsible for hydrolysis and acts as a catalyst for the esterification reaction between cellulose and carboxylic acid that is grafted to surface. With simultaneous hydrolysis and esterification, degree of substitution as determined through FT—IR is lower than reported by Trinh & Mekonnen (2018). The same research group upgraded this reaction by introducing lactide after Fischer esterification (Braun et al., 2012). Polymerization reactions were carried out both in solution and in bulk. However, polymerization of lactide was carried out in a separate step, with additional solvent. Similarly, Miao et al. (2016) hydrolyzed and subsequent esterified CNCs in tetrabutylammonium acetate with dimethylacetamide.

More recently, Lv et al. (2019) obtained CNCs an CNFs by performing formic acid hydrolysis, whereas hydrolysis mechanisms and kinetics were studied as well. Results showed that conditions with formic acid concentration 84–92 wt%, reaction temperature of 80–100 °C and hydrolysis time of 4–14 h were suitable to achieve the highest yields of hydrophobic CNCs and CNFs. Ionic liquids were shown to dissolve cellulose when co-solvent such as DMAc is applied.

To conclude this subchapter, functionalization of cellulose nanomaterials through esterification offers a wide variety of reactions. However, there is no universal rule as to which is the best esterification approach and has to be selected according to a desired result, but also to eliminate use of solvents because of the health and environmental risk, high price, and disposal and make it as sustainable as possible. For example, acetylation is a widely researched reaction, but is sensitive to water so it requires freeze drying of the cellulose nanomaterial or use of solvent through additional solvent exchange steps. One pot reactions in aqueous solution are good alternative, and should be preferred because of elimination of the solvent, as well as additional step of solvent exchange or drying, but are limited to grafting of lactide or several carboxylic acids that are well miscible with water and have high boiling point. Similarly, esterification with carboxylic acids can possibly cause a peel-off effect and affect crystallinity of cellulose nanoparticle. It was shown that generally, with grafting of shorter chains, higher degree of substitution can be reached and grafting through anhydrides is the optimal option for this approach. However, as anhydrides can be quite expensive, CDI seems to be a good alternative that can also deal with terminal double and triple bonds, but is less efficient with shorter chains. Grafting through acid chloride is less efficient than the previous ones. Moreover, higher concentrations of acid chloride and pyridine can disturb crystalline structure. Degree of substitution strongly depend on the state of starting material and the solvent. Freeze-drying, for example can disturb the structure of cellulose nanomaterial, cause agglomeration and restrict it from re-dispersion. Yet, it is easier to carry out a water-sensitive reaction with freeze-dried CNCs. Solvent exchange to acetone through ethanol keeps particles sufficiently small, but requires extra steps and chemicals. As noticed, the approaches to hydrophobic modifications are well researched, but the descriptions of kinetics of this reactions are rare and should be in the focus in the future, as this data is needed for optimization of the reactions with regards to greener production.

4.2. Carbamation

Term carbamation generally represent of two types of reactions, both involving isocyanates: grafting of functional polymers onto the surface using isocyanates as linkers or use of nonpolar isocyanates modify cellulose surface. Grafting of polymers proceeds in three steps. Firstly, a reaction between polymer and isocyanate with one isocyanate functionality, such as phenylisocyanate is carried out to protect one end of polymer. The second step attaches isocyanate with two isocyanate functionalities such as toluene 2,4-diisocyanate (TDI) to the other end of the polymer and in the last step, the unreacted isocyanate group is reacted with hydroxyl groups on the surface of cellulose nanomaterial (Habibi & Dufresne, 2008; Paquet et al., 2010). Tertiary amines, commonly triethylamine (TEA), were shown to be suitable catalysts. Simplified reaction mechanism between isocyanate and cellulose catalyzed by tertiary amine (Eyley & Thielemans, 2014) is shown in Fig. 5. However, these same catalysts could catalyze undesirable self-polymerization of isocyanates as well (Guo et al., 2015).

One of the first studies focusing on application of isocyanate as an assisting in grafting of polycaprolactone on surface of polysaccharides (starch and cellulose) was published by Habibi and Dufresne (2008). Two different molecular weights (10.000 g mol^{-1} and 42.500 g mol^{-1}) of polycaprolactone were grafted to the CNCs according to the three steps described above and shown in Fig. 6. It was confirmed that with lower molecular weight of polymer, higher degree of substitution was reached. Water contact angle increased in both cases, with 10.000 g mol^{-1} being slightly higher. Crystallinity of CNCs did not change, however additional diffraction peak that corresponds to crystalline structure of PCL was observed. Similarly was TDI as a linker used to graft a natural vegetable oil (castor oil) on CNCs surface in the presence of TEA acting as a catalyst (Shang et al., 2013). Two out of three hydroxyl groups on castor oil were terminated with phenyl isocyanate before functionalization in order to leave only one hydroxyl group available to modify CNC surface. With this step, inter- and intramolecular bonding was prevented (Shang et al., 2013).

An even further step forward was the synthesis of CNCs modified with photocleavable polymers that could expand the use of cellulose nanoparticles to smart delivery vehicles and smart materials (Morandi & Thielemans, 2012). Firstly, a photosensitive *o*-nitrobenzyl ester derivative that holds one initiation site for surface initiated atomic transfer radical polymerization (SI-ATRP) and one hydroxyl functionality was grafted onto the surface of CNCs through TDI. SI-ATRP initiating sites on modified CNCs were now readily available to initiate the graft polymerization of polystyrene (PS) onto the surface of CNCs. When compared to direct esterification, a lower degree of substitution was reached in the first step of reaction. 17 % of primary hydroxyl groups were substituted, significantly less than compared with direct esterification where all primary and one secondary hydroxyl group of all surface glucose units were modified. It has to be taken in account that photocleavable linker is bulkier than initiator, which decreases the degree of substitution. Regarding the polymerization step, the molecular weight of degrafted PS chains was similar to PS homopolymer molecular weight, demonstrating that with a sacrificial initiator it is possible to efficiently control the length of the grafted chains (Morandi & Thielemans, 2012).

In order to be able to carry out the above mentioned carbamation functionalization, the two isocyanate groups on the linker (for example TDI) should have different reactivity. Methyl group causes a steric hindrance onto ortho isocyanates, which makes them 5–10 times less reactive as the para ones (Belgacem et al., 1993). However, ortho isocyanate group is not entirely unreactive in the first step, which can cause lower grafting efficiency. In regard to this, Abushammala (2019) studied para/ortho reactivity of isocyanate groups of TDI with respect to temperature, TDI/CNCs molar ratio, and volumes of catalyst and solvent. It was observed that the optimal conditions to obtain maximum p-NCO selectivity were shown to be 35 °C and molar ratio of 3, whereas higher

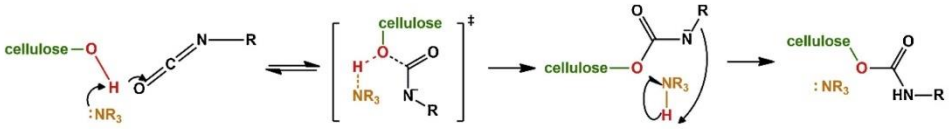

Fig. 5. Simplified reaction mechanism between isocyanate and cellulose, catalyzed by tertiary amine.

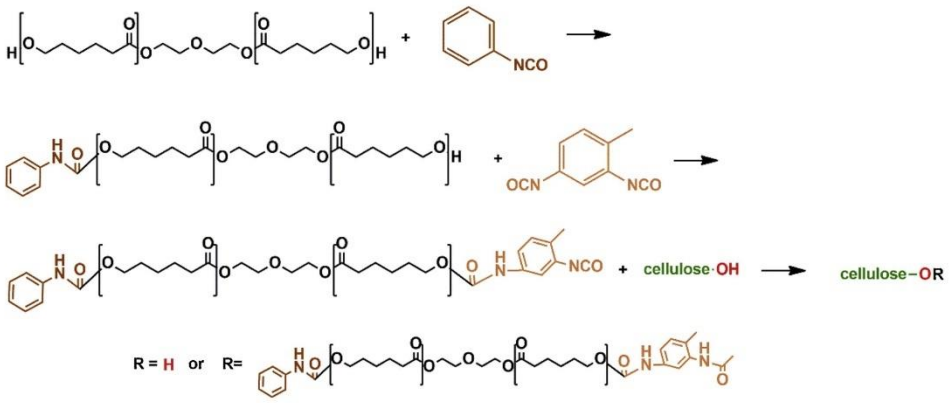

Fig. 6. Schematic presentation of three steps in carbamation of cellulose nanoparticles.

temperature s and molar ratios cause substitution of not only surface hydroxyl groups but of amorphous as well (Abushammala, 2019).

The second approach involving isocyanates is grafting nonpolar isocyanates *i.e. n*-octadecyl isonyanate (Espino-Pérez et al., 2013; Guo et al., 2017; Siqueira et al., 2009a, 2009b) directly onto surface of cellulose nanomaterial. The advantage of this process is that it excludes toxic reagents or catalyst. However, a change in crystallinity was observed pointing to possible peel-off effect and damage of nanocrystals at higher temperatures and longer reaction times. At the same time, smaller increase in water contact was observed in these samples, confirming the peeling off (Siqueira et al., 2009b). De Oliveira Taipina et al. (2013) and more recently Anžlovar et al. (2020) as well, reduced hydrophilicity of CNCs by reacting them with isocyanatepropyltriethoxysilane and exploiting silane hydrophobic character. Girouard et al. (2016) carried out modification of CNCs with isophane diisocyanate, which has unequal reactivity on isocyanate groups to create CNCs surface with both isocyanate and urethane functionality. The selectivity of catalyst DBTL for secondary isocyanate group was proven by ^{13}C NMR.

With carbamation, lower degree of substitution can be reached compared to direct esterification, however for direct esterification, generally a high excess of the reactant needed. By using di-isocyanate as a linker and providing sacrificial initiator a controlled polymerization can be achieved (Morandi & Thielemans, 2012). Considering mono-isocyanates, a relatively high grafting of available hydroxyl groups was reached. Even so, it is worth noting that n-octadecyl isocyanate as well as the solvents used in reaction represent a health hazard. In our opinion, in order to make this type of modification more sustainable and easier to implement at industrial level, optimization of reaction parameters through a kinetic studies, which are currently lacking, should be performed. Furthermore elimination or recycle of the used solvents should be examined.

4.3. Silylation

Silylation, also called silane grafting, is a form of etherification and was shown to be a successful way to functionalize cellulose nanomaterial to enhance adhesion between polymeric matrices and cellulose nanoparticles (Brochier Salon et al., 2005; Eyley & Thielemans, 2014; Khanjanzadeh et al., 2018). Various functional trialkoxysilanes, which possess two types of reactive groups e.g. γ –methacryloxypropyltrimethoxysilane (MPS) (Brochier Salon et al., 2005; Yu, Yang et al., 2019; Zhang et al., 2015), γ –aminopropyltriethoxysilane (APS) (Brochier Salon et al., 2005; Khanjanzadeh et al., 2018), γ-diethylenetriaminopropyltrimethoxysilane (TAS) (Brochier Salon et al., 2005), 3-glycidoxypropyltrimethoxysilane (Pujiasih et al., 2018) and methyltrimethoxysilane (Dilamian & Noroozi, 2021; Kim et al., 2019). The most commonly used APS, due to its low cost and simple structure (Khanjanzadeh et al., 2018). The latter will be presented here as a model compound for the mechanism of reaction as well. The reactions of silylation have to be carried out in water or water/alcohol mixture under slightly acidic pH (the slowest rate is at neutral pH) (Osterholtz & Pohl, 1992). Silylation occurs in three steps, as indicated in Fig. 7: i) in the presence of water, hydrolysis of alkoxy groups on silane takes place, resulting in formation of silanol, ii) through hydrogen bonding of —OH on silanol and O—H groups on the cellulose nanomaterial, silanol is adsorbed onto OH rich the surface of cellulose nanoparticles, iii) chemical condensation, occurs after thermal activation, causes grafting of silanol on the surface of cellulose nanoparticles through Si—OC— bond (Brochier Salon et al., 2005; Khanjanzadeh et al., 2018). In the last step, siloxane bridges Si—O—Si form as a result of self-condensation and contributes to the construction of polysiloxane network on the surface of cellulose nanoparticles (Brochier Salon et al., 2005; Khanjanzadeh et al., 2018).

It is also possible for the cellulose —O—Si—O— linkage to undergo reverse hydrolysis, which would strip silane off the the cellulose nanoparticle's surface. With this in mind, it is important to make sure that silane is linked to more sites on the surface and that adsorbed silanols are close enough to each other to undergo self-condensation (Brochier Salon et al., 2005).

All three steps of silylation were studied in terms of kinetics of adsorption on cellulose fibers (Brochier Salon et al., 2005). Hydrolysis of

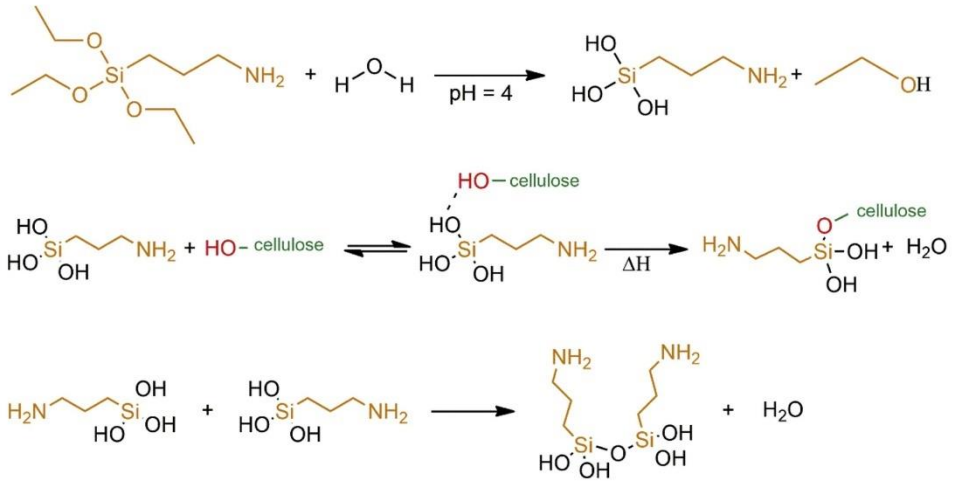

Fig. 7. Reactions cellulose silylation with APS and its self-condensation.

three different alkoxysilane agents was carried out in an ethanol/water (80/20) solution. Inspection by ^{1}H, $^{13}C$and ^{29}Si NMR spectroscopy showed that rate increased in order MPS > APS > TAS. Followed by a study of adsorption isotherms, it was discovered that adsorption increased with an increasing initial concentration of alkoxysilane until reaching a plateau at 0.24×10^{-3}, 0.91 and 0.6 mmol of adsorbed silane per g of cellulose for pre-hydrolyzed MPS, APS and TAS respectively. With further increase of initial concentration, adsorption increased again, which could be an indicator that adsorption continued through monolayer formation (Brochier Salon et al., 2005, 2007). Khanjanzadeh et al. (2018) confirmed that this mechanism is accurate for CNCs functionalization as well. Minimal change in crystallinity (1 %) was observed. Mertaniemi et al. (2012) described another two approaches of silylation: chemical vapour deposition and secondly, dispersion in trichlorosilane containing a fluorinated alkyl chain, to produce superhydrophobic CNFs microparticles with low contact angle hysteresis. Structure of layers of CNF microparticles e.g. density and uniformity of layers, micron-scale roughness has a great impact on hydrophobicity as well (Mertaniemi et al., 2012).

Silylation is more sustainable that some carbamation and esterification methods since it eliminates use of solvents, however reagents containing silane can be expensive and silane stays incorporated in cellulose nanomaterial after modification, which could be of concern for some applications.

4.4. Plasma treatment

In the last two decades, an interest in functionalization of cellulosic fibers with plasma has raised. In this chapter, the overview is broadened, including cellulosic materials as well. Relatively little research has been done on cellulose nanomaterial specifically, but we believe it is a promising way for hydrophobic functionalization. Plasma treatment is greener in terms of the elimination of strong acids or discarded solvents. For hydrophobization of cellulose nanomaterial, several different techniques were used: low pressure plasma, atmospheric pressure and submerged liquid plasma (Alanis et al., 2019; Castelvetro et al., 2006; Ihara & Iriyama, 2011; Samanta et al., 2012, 2016). One of the first plasma-induced modifications of cellulose was done with continuous cold argon plasma, which activated cellulose fibers towards surface initiated graft polymerization of glycidyl methacrylate, 2-hydroxyethyl methacrylate and 1,1,2,2-tetrahydroperfluorodecyl methacrylate (Castelvetro et al., 2006). The result of Ar plasma is limited to physical etching, which causes the higher surface density of free radicals activated for grafting. One (impregnation with a monomer before plasma treatment) or two-step (exposure to monomer after plasma treatment) grafting was applied, depending on the monomer. Ihara and Iriyama (2011) prepared liquid marbles by the processing of cellulosic powders with different diameters by O_2 plasma, following with adsorption of tetramethylcyclotetrasiloxane in order to make them hydrophobic.

Samanta et al. (2012) hydrophobized cellulose fibers using He/1, 3-butadiene plasma at atmospheric conditions. The same research group modified cellulose using fluorocarbon plasma under atmospheric pressure (Samanta et al., 2016) and He/TFE plasma (Samanta et al., 2021). Alanis et al. (2019) described strategy to functionalize CNCs by delivering monomer gas (styrene, caprolactone or farnesene) in reaction chamber to which strong electrical field was applied. Ionized and excited molecules and radicals than attack CNCs surface and induce growth of polymer chain *via* plasma deposition. More recently, Yao et al. (2021) prepared a super-hydrophobic cellulose material *via* two-step modification: firstly, the surface of cellulose was etched with oxygen plasma on which trisilanolisobutyl-polyhedral oligomeric silsesquioxane was then deposited.

Plasma seems to be a fast and sustainable alternative that eliminates solvents and strong acids. However, commonly used for hydrophobization is fluorocarbon gases (CF_4) gas that is one of the most persistent greenhouse gasses and should be avoided to be releases to the atmosphere. This type of the cellulose nanomaterial hydrophobization is explored as much as other approaches. Furthermore the exact mechanisms and kinetics of the reactions that happen on the surface of cellulose nanomaterials are yet to be researched. Despite this, in our opinion, plasma has a potential for sustainable functionalization of cellulose nanomaterials.

4.5. Adsorption

Adsorption is a simple and fast modification that generally, in advantage to some other techniques, does not require organic solvents. Adsorption can be divided into two categories: adsorption of polyelectrolytes, which bind mostly through electrostatic interactions and adsorption of other components as defined by Hatton Malmström, & Carlmark (2015), who review in details the adsorption of tailor made copolymers on cellulosic surfaces. The second group binds through Van der Waals interactions and hydrogen bonds and is primarily researched for hydrophobization of cellulose nanomaterials. The disadvantage of

adsorption is the weakness of bonds, which can cause loss or migration of adsorbate. In contrast to other techniques, adsorption is better researched on CNFs compared to CNCs, which is probably due to different final application as CNFs modified through adsorption are often used as a coating or films, and much less used in other polymer matrices as reinforcement. Furthermore, there are numerous studies on adsorption kinetics available.

Syverud et al. (2011), and Salajková et al. (2012), Xhanari et al. (2011) describe the adsorption of cationic surfactants onto the surface of CNFs. Xhanari et al. (2011) compared surfactants with different chain lengths and different solubility in water in regards to adsorption isotherms. It was revealed that adsorption is significantly better when CNFs are first TEMPO-oxidized, which increases the anionic charge on the surface of CNFs. The study of adsorption isotherm revealed three mechanisms of adsorption: at low surfactant concentration, the driving force of adsorption are the electrostatic interactions between negatively charged carboxyl groups on the surface of TEMPO-oxidized CNFs and positively charged cationic surfactant. Then, admicelles are formed and adsorption abruptly rises. Further increasing of surfactant concentration results formation of a double layer, where hydrophilic headgroups face CNFs surface and outer environment. This causes the increase in hydrophilicity. In conclusion, to reduce water-wettability, adsorption at lower concentrations of surfactant is suitable (Xhanari et al., 2011). The same group studied adsorption of cetyltrimethylammonium bromide (CTMAB) on film made of CNFs, in contrast to adsorption on CNFs, where it was further found that higher concentration of CTMAB reduces the decrease of tensile strength upon adsorption (Syverud et al., 2011). Qing et al. (2016) studied the adsorption of CTMAB on CNCs and its kinetics. The results showed that adsorption followed pseudo-second-order kinetics. Adsorption isotherm can be described with the Freundlich equation, demonstrating multi-layer adsorption of CTMAB on CNCs surface (Qing et al., 2016). Inspired by silica-modified CNCs, a modification *via* adsorption using quaternary ammonium salts was carried out on TEMPO-oxidized CNFs.

Reverdy et al. (2018) compared hydrophobic properties of CNFs coating with adsorbed amino propyl trimethoxy silane (AMPS) or with adsorbed alkyl ketene dimer (AKD). Coating with adsorbed AKD gave a slightly higher water contact angle than CNFs with adsorbed AMPS. However, the procedure of AKD adsorption on CNFs involves chloroform (Missoum et al., 2014), which is undesirable in terms of sustainability.

4.6. Click chemistry

Click chemistry, as defined by Sharpless and his colleagues (Kolb et al., 2001), represents a series of rapid reactions, characterized by the mild reaction conditions, high yields, high efficiency and harmless by-products. Moreover, such modification can be carried out in water, which eliminates organic solvents (Tingaut et al., 2011) Recently, click chemistry has become of interest for hydrophobization of cellulose nanomaterials as it enables attachment of alkyl and azide groups (Chen et al., 2015; Fein et al., 2020a, 2020b; Huang et al., 2014; Zhou et al., 2018). Huang et al. (2014) prepared hydrophobic CNCs by combining alkoxysilane chemistry and photochemical thiol-ene click reaction with the assistance of UV-light. Alkyne-azide Huisgen cycloaddition has been used to functionalize cellulose as well, but the complete mechanism is yet unknown (Danese et al., 2019). For example, Zhou et al. (2018) grafted PCL onto CNCs with the three-step procedure, including click-reaction. Firstly, CNC—N_3 and PCL diolCC—≡H were synthesized, followed by a copper-catalyzed cycloaddition click reaction between them. A similar principle that led to the highly alkynl-functionalization of CNCs reinforced nanocomposites was implemented by Chen et al. (2015). Recently, Fein et al. (2020a) modified CNFs with various thiols in a two-step reaction: firstly, the norbornene groups were attached to the surface through a reaction of CNFs with *cis*-5-norbornene-*endo*-2, 3-dicarboxylic anhydride (carbic anhydride), followed by thiol-norbornene reaction. Modification affected the viscosity and drainage rate when forming a film. Attachment of non-polar groups reduces flocculation and viscosity. On the contrary, modification with polar groups increases the flocculation and viscosity as well as drainage rate. Furthermore, the same group investigated water-based compatibilization between carbic-modified CNFs and natural rubber (NR) through thiol-ene reaction (Fein et al., 2020b). CNF-NR hybrid particles that drained faster and provided homogeneous distribution of NR all through the coating were formed. However, the hydrophobicity was dependant only on the concentration of NR, regardless of modification (Fein et al., 2020b).

Currently, there are no kinetic data available for modification thorough click-reactions, but the kinetics of each step should be evaluated in the future in order to optimize the process.

4.7. Other strategies to hydrophobization of cellulose nanomaterials

Along with atom transfer radical polymerization, mentioned in Sections 4.1 and 4.2, nitroxide-mediated polymerization was shown to be a prospective method for functionalizing cellulose nanoparticles (Roeder et al., 2016).

In nucleophilic substitution, hydroxyl group is substituted. Various triazinyl derivatives, consisting of nonpolar aliphatic chains, aromatic rings and alkyne functionalities, had been grafted onto CNCs. This reaction can be used to obtain either standalone product or a building block for further reactions (Fatona et al., 2018).

Nigmatullin et al. (2020) modified CNCs with alkylamines of different alkyl chain lengths in aqueous suspension and studied the gelation of such materials. It was revealed that hydrophobization of CNCs leads to more robust gels because hydrophobic effects induce sol-gel transformation at lower concentrations.

CNCs were surface-modified using immobilized lipase to form laurate ester groups. Reaction was carried out in tert-butanol followed by addition of dodecanoic acid. The modified CNCs were then integrated into PLA matrix and showed decreased hydrophilicity and enhanced mechanical properties (Yin et al., 2020).

5. *In-silico* approaches to surface modifications of cellulose nanomaterials

Theoretical chemistry approaches such as density functional theory (DFT) and molecular dynamics (MD) can be used to determine the arrangement of cellulose chains inside CNC or CNF. Information about conformation of cellulose chains can help in explaining the kinetics of functionalization reactions. Currently, DFT has been applied to provide information about hydroxide bonds strengths (Watts et al., 2014), mechanism of reaction between TDI and cellulose (Cao et al., 2016), and adsorption of various metals and dyes onto functionalized cellulose nanomaterials (Kim et al., 2016; Zhu et al., 2020). MD simulations showed that ω dihedral angle (O—5—C—5—C—6—O—6), which corresponds to a hydroxyl-methyl group, Kulasinski et al. (2014) studied crystalline, amorphous and paracrystalline states of cellulose by MD. It was demonstrated that amorphous regions hold a lower amount of the total number of hydrogen bonds per unit of glucose. Moreover, the biggest difference between crystalline and amorphous cellulose is in the intermolecular bonding system, which creates larger spaces between chains in amorphous cellulose and the result is a porous structure of amorphous cellulose (Kulasinski et al., 2014). Because CNFs consist of both crystalline and amorphous regions, this has to be taken into account when designing modification reactions. More recently, MD simulations were used to study the effects of topochemical surface modifications, using acetylation of cellulose nanomaterial in aqueous environment as a model system, on specific particle-particle interactions and on interactions between nanoparticle and liquid medium. It was revealed that the work of adhesion between cellulose nanomaterial with modified C-6 position is decreased and is therefore induces hydrophobization of cellulose nanomaterial. Moreover, it was found that the

net effect of modification is the reduction of cellulose nanomaterial's tendency to aggregate in water through the disruption of near crystalline structure between two aggregated cellulose nanoparticles, which decreases hydrogen and van der Waal's bonding (P. Chen et al., 2020). Sáenz Ezquerro et al. (2019) developed models of cellulose fibril surface using steered MD to observe forces between cellulose fibril surfaces and the effect of adsorption of polyelectrolyte. Similarly, Ren et al. (2020) studied the interfacial structure and adhesion between crystalline cellulose planes and PLA through MD simulations.

Although the *in-silico* approaches are helpful in determination of thermodynamic properties, structural parameters, bond strengths or kinetic parameters, they are not yet widely described in the literature. However, their potential to be exploited as an important tool in the cellulose nanomaterials research is big. The future approaches involving green chemistry principles can be evaluated on the molecular level bridging the gaps in the experimental observation and modelling the (micro)kinetics.

6. Applications and future prospects of hydrophobic functionalized cellulose nanomaterials

Hydrophobic cellulose nanoparticles were found to have a great potential in multiple fields due to its non-toxicity, biocompatibility, biodegradability, good mechanical properties, high surface area and versatile surface chemistry (Fig. 8). However, there are some limitations that prevent the commercial use of these materials. While CNFs can be extracted at room temperature and neutral conditions, CNCs require low pH and high temperatures. Moreover, many of the discussed modifications require organic solvents and expensive reactants, which further limits the practical use of cellulose nanomaterials. Nevertheless, high value applications of cellulose nanomaterials, preferably modified through a sustainable method, should be the focus.

Most frequently, it is used as reinforcement in nonpolar matrices in polymer composites. For instance, carbamated CNCs were incorporated in thermoplastic polyurethane (Girouard et al., 2016) with intent to produce flame retardant composite foam (Kim et al., 2019), poly (ethylene-cobutylene) (Biyani et al., 2013), silylated CNCs into polydimethylsiloxane (Zhang et al., 2014), esterified into poly(lactic acid) (Shojaeiarani et al., 2018), modified *via* SI-ATRP to poly(methyl methacrylate) (Yin et al., 2016), and so on. Better dispersion and therefore better adhesion between grafted CNCs and PLA matrix increases thermal stability of the nanocomposite (Spinella et al., 2015). Compared to incorporation of unmodified cellulose nanomaterial, the storage modulus at temperature below and above PLAs glass transition temperature increased when incorporating modified CNCs, compared to PLA and unmodified/PLA nanocomposite. It is worth noting, that the greatest improvement of properties was observed when incorporating lactate grafted CNCs into PLA (Spinella et al., 2015). With use of modified CNCs, smart polymers can be formed. For instance, CNCs modified *via* thiol-ene reaction, were blended with poly(ethylene glycol)−poly(ε-caprolactone)-based polyurethane (PECU) and pH-responsive shape-memory nanocomposite was obtained (Li et al., 2015). For instance, pH-responsive CNCs was assembled by grafting pyridine moieties. Pyridine-4-carbonyl chloride was synthesized from isonicotinic acid and $SOCl_2$. When adding a base to a water solution of $CNC–C_6H_4NO_2$, H^- is neutralized with OH^- and nitrogen is deprotonated. This causes change to hydrophobicity and precipitation from water solution (Li et al., 2015). CNCs modified *via* nitroxide-mediated

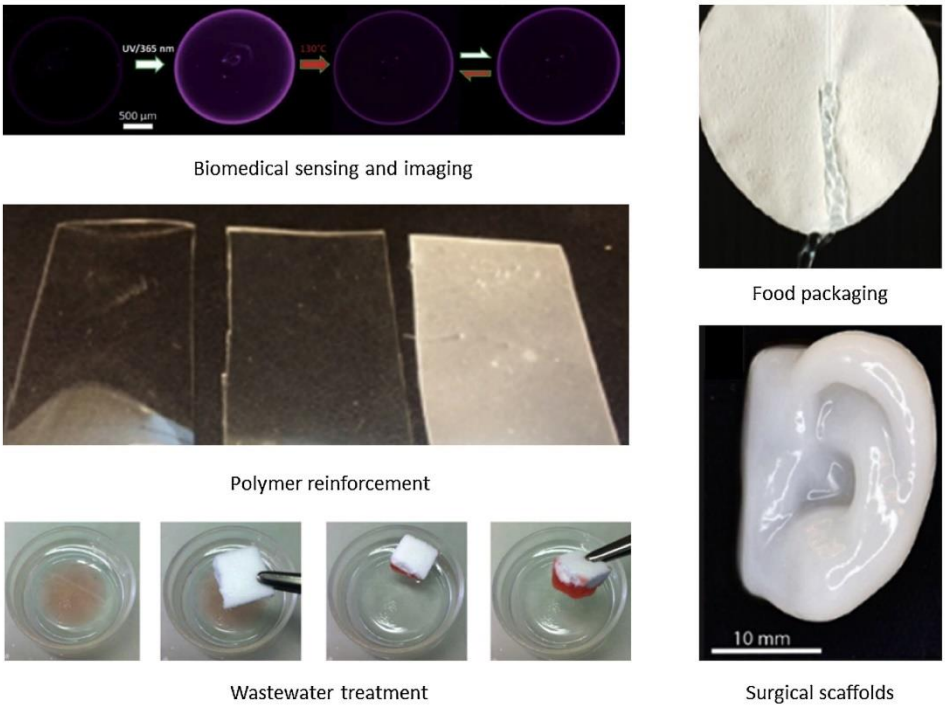

Fig. 8. Applications of hydrophobic cellullose nanomaterials: biomedical sensing and imaging (Li et al. 2014) (Published by The Royal Society of Chemistry); in surgical scaffolds (Markstedt et al. 2015) (reproduced by permission of American Chemical Society), food packaging (Le et al. 2016) (reproduced by permission of Elsavier), polymer reinforcement (Girouard et al., 2016) (reproduced by permission of American Chemical Society,) and wastewater treatment (Zhang et al. 2014)) (reproduced by permission of American Chemical Society).

polymerization were shown to be a universal nanofiller, as they can be either hydrophilic or hydrophobic and are regulated with CO_2 (Farnia et al., 2019; Glasing et al., 2017).

Although many studies cover polymer reinforcement with cellulose nanomaterials, there are very few that would systematically research the effect of modification on reinforcement or economical and ecological justification for the modifying cellulose nanomaterials in order to mix them into polymer matrix.

Cellulose nanomaterials are prospective in biomedical applications as well. pH-responsive CNCs obtained through adsorption of surfactant have the potential to be used as carriers for controlled drug release (Qing et al., 2016). Cellulose nanomaterial has become interesting for the construction of biocompatible and biodegradable scaffolds, with the final application as surgical implants (Guo et al., 2012; Markstedt et al., 2015; Zoppe et al., 2009). Poly(ε-caprolactone) nanofibers reinforced with CNCs carbamated with poly(ε-caprolactone) diol were shown to have good mechanical properties and satisfying morphological homogeneity for such application (Zoppe et al., 2009). Fluorescently esterified cellulose nanoparticles show potential in bio-imaging and labelling in biomedicine (Li et al., 2014; Sîrbu et al., 2016).

High surface area, versatile surface chemistry chemical inertness make membranes and filters based on cellulose nanomaterials great water pollutants adsorbents (Voisin et al., 2017; Wang, 2019; Wang et al., 2014). Several researchers proposed use of hydrophobic CNF aerogel as oil absorbents and furthermore showed that the aerogels are highly absorbent as well as reusable (Chin et al., 2014; Dilamian & Noroozi, 2021; Jiang & Hsieh, 2017; Korhonen et al., 2011; Rafieian et al., 2018; Zhang et al., 2014).

As cellulose nanoparticles can improve water and oxygen barrier, it has a potential application in food packaging. They can be added as a reinforcement to a polymer or used as an independent matrix. A sustainably prepared bacterial CNFs-zein nanocomposite was shown to be hydrophobic and antibacterial (Li, Gao et al., 2020). Spinella et al. (2016) showed that modified CNCs provided lower gas permeability compared to unmodified CNCs. Acetylated CNCs were incorporated into polycaprolactone together with acetylated hemicellulose in active food packaging films (Mugwagwa & Chimphango, 2020). On the other hand, hydrophobic and oleophobic CNCs were obtained by introducing fluorine moieties to the surface and could be used in the packaging of foods such as bakery items, pet foods and fast foods (Salam et al., 2015). CNFs-silica films were shown to be durable and flexible and, therefore, suitable for food packaging, however, they were extremely oleophilic (Le et al., 2016). Similarly, poly (3-hydroxybutyrate) modified bacterial nanocellulose, additionally treated with plasma to introduce antibacterial ZnO coating, was shown to be suitable as an alternative to conventional food packaging (Panaitescu et al., 2018). For readers seeking for more information, an extensive review covering cellulose nanomaterials in food packaging was published recently by Ahankari, Subhedar, Bhadauria, & Dufresne (2021).

7. Conclusions

The review describes hydrophobic modifications of cellulose nanomaterials, where esterification, carbamation, silylation, plasma, adsorption and click chemistry have been presented. Future research on modifications of cellulose nanomaterials should take into account greener principles, such as recycling or complete elimination of solvents and acids and avoidance of harmful side products to enable broader usage and acceptance of hydrophobic cellulose nanomaterials. Considering this, modifications that are carried out in aqueous solutions are much more desirable. Moreover, it was shown that plasma treatment and adsorption have a great potential for modifications of cellulose nanomaterials because they are relatively simple and more sustainable compared to some other methods, as there is no need of solvents. However, this type of modification is not yet well described in the literature and often not mentioned in literature reviews. Through the literature review, it was also observed that CNFs are considerably less researched in terms of functionalizations and applications compared to CNCs, in our opinion this is possibly due to their higher sensitivity to harsher conditions and difficulty in reaching homogeneous dispersion. However, modified CNFs have a great potential as a low cost material in applications such as coatings, food packaging and water/oil separation. The current overview of the hydrophobic CNFs and CNCs functionalization further shows scarce kinetic studies, where the reason for this could be that majority of studies are focusing on the new chemical options rather than the reaction optimizations. The stronger emphasis on determination of kinetic parameters, which are important in optimization of processes towards greener production, should be included more in the future experiments. In conclusion, a stronger emphasis on a deeper understanding of the presented chemical approaches toward obtaining hydrophobic cellulose nanomaterials is needed and *in-silico* and (micro)kinetics studies should be an added value in future process engineering studies. The latter is needed to further push the utilization of these highly useful and abundant materials towards the more sustainable industrial-based applications. Considering final applications of modified cellulose nanomaterials, it was found that such materials have a high practicality, but there is a limited number of studies considering contribution of the modification to the final product.

Funding

This research was funded by the PhD research grant (Ana Oberlintner) and Slovenian Research Agency (Program P2-0152).

Declaration of Competing Interest

Authors declare no conflict of interest.

References

Abushammala, H. (2019). On the para/ortho reactivity of isocyanate groups during the carbamation of cellulose nanocrystals using 2,4-toluene diisocyanate. *Polymers, 11*(7), 1–12. https://doi.org/10.3390/polym11071164

Abushammala, H., & Mao, J. (2019). A review of the surface modification of cellulose and nanocellulose using aliphatic and aromatic mono- and di-isocyanates. *Molecules, 24*(15), 2782. https://doi.org/10.3390/molecules24152782

Ahankari, S. S., Subhedar, A. R., Bhadauria, S. S., & Dufresne, A. (2021). Nanocellulose in food packaging: A review. *Carbohydrate Polymers, 255*, Article 117479. https://doi.org/10.1016/j.carbpol.2020.117479

Alanis, A., Valdés, J. H., María Guadalupe, N.-V., Lopez, R., Mendoza, R., Mathew, A. P., Díaz De León, R., & Valencia, L. (2019). Plasma surface-modification of cellulose nanocrystals: A green alternative towards mechanical reinforcement of ABS. *RSC Advances, 9*(30), 17417–17424. https://doi.org/10.1039/c9ra02451d

Alemdar, A., & Sain, M. (2008). Isolation and characterization of nanofibers from agricultural residues – Wheat straw and soy hulls. *Bioresource Technology, 99*(6), 1664–1671. https://doi.org/10.1016/j.biortech.2007.04.029

Anžlovar, A., Krajnc, A., & Žagar, E. (2020). Silane modified cellulose nanocrystals and nanocomposites with LLDPE prepared by melt processing. *Cellulose, 27*(10), 5785–5800. https://doi.org/10.1007/s10570-020-03181-y

Arslan, O., Aytac, Z., & Uyar, T. (2016). Superhydrophobic, hybrid, electrospun cellulose acetate nanofibrous mats for Oil/Water separation by tailored surface modification. *ACS Applied Materials & Interfaces, 8*(30), 19747–19754. https://doi.org/10.1021/acsami.6b05429

Ávila Ramírez, J. A., Fortunati, E., Kenny, J. M., Torre, L., & Foresti, M. L. (2017). Simple citric acid-catalyzed surface esterification of cellulose nanocrystals. *Carbohydrate Polymers, 157*, 1358–1364. https://doi.org/10.1016/j.carbpol.2016.11.008

Belgacem, M. N., Quillerou, J., & Gandini, A. (1993). Urethanes and polyurethanes bearing furan moieties—3. Synthesis, characterization and comparative kinetics of the formation of diurethanes. *European Polymer Journal, 29*(9), 1217–1224. https://doi.org/10.1016/0014-3057(93)90151-5

Bian, H., Dong, M., Chen, L., Zhou, X., Ni, S., Fang, G., & Dai, H. (2019). Comparison of mixed enzymatic pretreatment and post-treatment for enhancing the cellulose nanofibrillation efficiency. *Bioresource Technology, 293*, Article 122171. https://doi.org/10.1016/j.biortech.2019.122171

Biyani, M. V., Foster, E. J., & Weder, C. (2013). Light-healable supramolecular nanocomposites based on modified cellulose nanocrystals. *ACS Macro Letters, 2*(3), 236–240. https://doi.org/10.1021/mz400059w

Brand, J., Pecastaings, G., & Sèbe, G. (2017). A versatile method for the surface tailoring of cellulose nanocrystal building blocks by acylation with functional vinyl esters. *Carbohydrate Polymers, 169*, 189–197. https://doi.org/10.1016/j.carbpol.2017.03.077

Braun, B., & Dorgan, J. R. (2009). Single-step method for the isolation and surface functionalization of cellulosic nanowhiskers. *Biomacromolecules, 10*(2), 334–341. https://doi.org/10.1021/bm8011117

Braun, B., Dorgan, J. R., & Hollingsworth, L. O. (2012). Supra-molecular ecobionanocomposites based on polylactide and cellulosic nanowhiskers: Synthesis and properties. *Biomacromolecules, 13*(7), 2013–2019. https://doi.org/10.1021/bm300149w

Brochier Salon, M. C., Abdelmouleh, M., Boufi, S., Belgacem, M. N., & Gandini, A. (2005). Silane adsorption onto cellulose fibers: Hydrolysis and condensation reactions. *Journal of Colloid and Interface Science, 289*(1), 249–261. https://doi.org/10.1016/j.jcis.2005.03.070

Brochier Salon, M. C., Gerbaud, G., Abdelmouleh, M., Bruzzese, C., Boufi, S., & Belgacem, M. N. (2007). Studies of interactions between silane coupling agents and cellulose fibers with liquid and solid-state NMR. *Magnetic Resonance in Chemistry, 45* (April), 473–483. https://doi.org/10.1002/mrc

Camarero Espinosa, S., Kuhnt, T., Foster, E. J., Weder, C., Espinosa, S. C., Kuhnt, T., … Weder, C. (2013). Isolation of thermally stable cellulose nanocrystals by phosphoric acid hydrolysis. *Biomacromolecules, 14*(4), 1223–1230. https://doi.org/10.1021/bm400219u

Cao, J., Liu, Y., Shi, A., Yuan, Y., & Wang, M. (2016). A DFT study on the mechanism of reaction between 2, 4-diisocyanatotolune and cellulose. *Journal of Theoretical & Computational Chemistry, 15*(2), 1–14. https://doi.org/10.1142/S0219633616500127

Castelvetro, V., Fatarella, E., Corsi, L., Giaiacopi, S., & Ciardelli, G. (2006). Graft polymerisation of functional acrylic monomers onto cotton fibres activated by continuous Ar plasma. *Plasma Processes and Polymers, 3*(1), 48–57. https://doi.org/10.1002/ppap.200500066

Chen, J., Lin, N., Huang, J., & Dufresne, A. (2015). Highly alkynyl-functionalization of cellulose nanocrystals and advanced nanocomposites thereof via click chemistry. *Polymer Chemistry, 6*(24), 4385–4395. https://doi.org/10.1039/c5py00367a

Chen, P., Lo Re, G., Berglund, L. A., & Wohlert, J. (2020). Surface modification effects on nanocellulose-molecular dynamics simulations using umbrella sampling and computational alchemy. *Journal of Materials Chemistry A, 8*(44), 23617–23627. https://doi.org/10.1039/d0ta09105g

Chin, S. F., Binti Romainor, A. N., & Pang, S. C. (2014). Fabrication of hydrophobic and magnetic cellulose aerogel with high oil absorption capacity. *Materials Letters, 115*, 241–243. https://doi.org/10.1016/j.matlet.2013.10.061

Clayden, J., Greeves, N., & Warren, S. (2012). *Organic chemistry organic chemistry* (2nd edition). Oxford University Press Inc.

Cunha, A. G., & Gandini, A. (2010). Turning polysaccharides into hydrophobic materials: A critical review. Part 1. Cellulose. *Cellulose, 17*(5), 875–889. https://doi.org/10.1007/s10570-010-9434-6

Danese, M., Bon, M., Piccini, G., & Passerone, D. (2019). The reaction mechanism of the azide-alkyne Huisgen cycloaddition. *Journal of the Chemical Society Faraday Transactions, 21*(35), 19281–19287. https://doi.org/10.1039/c9cp02386k

de Oliveira Taipina, M., Ferrarezi, M. M. F., Yoshida, I. V. P., & Gonçalves, M. C. (2013). Surface modification of cotton nanocrystals with a silane agent. *Cellulose, 20*(1), 217–226. https://doi.org/10.1007/s10570-012-9820-3

Deepa, B., Abraham, E., Cordeiro, N., Mozetic, M., Mathew, A. P., Oksman, K., … Pothan, L. A. (2015). Utilization of various lignocellulosic biomass for the production of nanocellulose: A comparative study. *Cellulose, 22*(2), 1075–1090. https://doi.org/10.1007/s10570-015-0554-x

Deng, F., Ge, X., Zhang, Y., Li, M. C., & Cho, U. R. (2015). Synthesis and characterization of microcrystalline cellulose-graft-poly(methyl methacrylate) copolymers and their application as rubber reinforcements. *Journal of Applied Polymer Science, 132*(41), 1–10. https://doi.org/10.1002/app.42666

Dilamian, M., & Noroozi, B. (2021). Rice straw agri-waste for water pollutant adsorption: Relevant mesoporous super hydrophobic cellulose aerogel. *Carbohydrate Polymers, 251*, Article 117016. https://doi.org/10.1016/j.carbpol.2020.117016

Espino-Pérez, E., Bras, J., Ducruet, V., Guinault, A., Dufresne, A., & Domenek, S. (2013). Influence of chemical surface modification of cellulose nanowhiskers on thermal, mechanical, and barrier properties of poly(lactide) based bionanocomposites. *European Polymer Journal, 49*(10), 3144–3154. https://doi.org/10.1016/j.eurpolymj.2013.07.017

Espino-Pérez, E., Domenek, S., Belgacem, N., Sillard, C., & Bras, J. (2014). Green process for chemical functionalization of nanocellulose with carboxylic acids. *Biomacromolecules, 15*(12), 4551–4560. https://doi.org/10.1021/bm5013458

Espino-Pérez, E., Gilbert, R. G., Domenek, S., Brochier-Salon, M. C., Belgacem, M. N., & Bras, J. (2016). Nanocomposites with functionalised polysaccharide nanocrystals through aqueous free radical polymerisation promoted by ozonolysis. *Carbohydrate Polymers, 135*, 256–266. https://doi.org/10.1016/j.carbpol.2015.09.005

Eyley, S., & Thielemans, W. (2014). Surface modification of cellulose nanocrystals. *Nanoscale, 6*(14), 7764–7779. https://doi.org/10.1039/c4nr01756k

FAO. (2020). *Global forest resources assessment 2020: Main report*. https://doi.org/10.4060/ca9825en

Farnia, F., Fan, W., Dory, Y., & Zhao, Y. (2019). Making nanocomposites of hydrophilic and hydrophobic polymers using gas-responsive cellulose nanocrystals. *Macromolecular Rapid Communications, 40*(12), 1–7. https://doi.org/10.1002/marc.201900114

Fatona, A., Berry, R. M., Brook, M. A., & Moran-Mirabal, J. M. (2018). Versatile surface modification of cellulose fibers and cellulose nanocrystals through modular triazinyl chemistry. *Chemistry of Materials, 30*(7), 2424–2435. https://doi.org/10.1021/acs.chemmater.8b00511

Favier, V., Canova, G. R., Cavaillé, J. Y., Chanzy, H., Dufresne, A., & Gauthier, C. (1995). Nanocomposite materials from latex and cellulose whiskers. *Polymers for Advanced Technologies, 6*(5), 351–355. https://doi.org/10.1002/pat.1995.220060514

Fein, K., Bousfield, D. W., & Gramlich, W. M. (2020a). The influence of versatile thiol-norbornene modifications to cellulose nanofibers on rheology and film properties. *Carbohydrate Polymers, 230*, Article 115672. https://doi.org/10.1016/j.carbpol.2019.115672

Fein, K., Bousfield, D. W., & Gramlich, W. M. (2020b). Thiol-norbornene reactions to improve natural rubber dispersion in cellulose nanofiber coatings. *Carbohydrate Polymers, 250*, Article 117001. https://doi.org/10.1016/j.carbpol.2020.117001

French, A. D. (2017). Glucose, not cellobiose, is the repeating unit of cellulose and why that is important. *Cellulose, 24*(11), 4605–4609. https://doi.org/10.1007/s10570-017-1450-3

Frisoni, G., Baiardo, M., Scandola, M., Lednická, D., Cnockaert, M. C., Mergaert, J., & Swings, J. (2001). Natural cellulose fibers: Heterogeneous acetylation kinetics and biodegradation behavior. *Biomacromolecules, 2*(2), 476–482. https://doi.org/10.1021/bm0056409

Gericke, M., Trygg, J., & Fardim, P. (2013). Functional cellulose beads: Preparation, characterization, and applications. *Chemical Reviews, 113*(7), 4812–4836. https://doi.org/10.1021/cr300242j

Girouard, N. M., Xu, S., Schueneman, G. T., Shofner, M. L., & Meredith, J. C. (2016). Site-selective modification of cellulose nanocrystals with isophorone diisocyanate and formation of Polyurethane-CNC composites. *ACS Applied Materials & Interfaces, 8*(2), 1458–1467. https://doi.org/10.1021/acsami.5b10723

Glasing, J., Bouchard, J., Jessop, P. G., Champagne, P., & Cunningham, M. F. (2017). Grafting well-defined CO2-responsive polymers to cellulose nanocrystals via nitroxide-mediated polymerisation: Effect of graft density and molecular weight on dispersion behaviour. *Polymer Chemistry, 8*(38), 6000–6012. https://doi.org/10.1039/C7PY01258F

Goffin, A. L., Raquez, J. M., Duquesne, E., Siqueira, G., Habibi, Y., Dufresne, A., & Dubois, P. (2011). Poly(ε-caprolactone) based nanocomposites reinforced by surface-grafted cellulose nanowhiskers via extrusion processing: Morphology, rheology, and thermo-mechanical properties. *Polymer, 52*(7), 1532–1538. https://doi.org/10.1016/j.polymer.2011.02.004

Gopakumar, D. A., Thomas, S., & Grohens, Y. (2016). Nanocelluloses as innovative polymers for membrane applications. *Multifunctional polymeric nanocomposites based on cellulosic reinforcements* (pp. 253–275). https://doi.org/10.1016/B978-0-323-44248-0.00008-0. Issue 1.

Guo, J., He, Y., Xie, D., & Zhang, X. (2015). Process investigating and modelling for the self-polymerization of toluene diisocyanate (TDI)-based polyurethane prepolymer. *Journal of Materials Science, 50*(17), 5844–5855. https://doi.org/10.1007/s10853-015-9134-6

Guo, J., Du, W., Gao, Y., Cao, Y., & Yin, Y. (2017). Cellulose nanocrystals as water-in-oil Pickering emulsifiers via intercalative modification. *Colloids and Surfaces A, Physicochemical and Engineering Aspects* (Vol. 529,, 634–642. https://doi.org/10.1016/j.colsurfa.2017.06.056

Guo, Y., Wang, X., Li, D., Du, H., Wang, X., & Sun, R. (2012). Synthesis and characterization of hydrophobic long-chain fatty acylated cellulose and its self-assembled nanoparticles. *Polymer Bulletin, 69*(4), 389–403. https://doi.org/10.1007/s00289-012-0729-7

Habibi, Y., & Dufresne, A. (2008). Highly filled bionanocomposites from functionalized polysaccharide nanocrystals. *Biomacromolecules, 9*(7), 1974–1980. https://doi.org/10.1021/bm8001717

Habibi, Y., & Lucia, L. A. (2012). Nanocelluloses: Emerging building blocks for renewable materials. *Polysaccharide building blocks: A sustainable approach to the development of renewable biomaterials* (pp. 105–125). https://doi.org/10.1002/9781118229484.ch3

Habibi, Y., Goffin, A. L., Schiltz, N., Duquesne, E., Dubois, P., & Dufresne, A. (2008). Bionanocomposites based on poly(ε-caprolactone)-grafted cellulose nanocrystals by ring-opening polymerization. *Journal of Materials Chemistry, 18*(41), 5002–5010. https://doi.org/10.1039/b809212e

Habibi, Y., Lucia, L. A., & Rojas, O. J. (2010). Cellulose nanocrystals: Chemistry, self-assembly, and applications. *Chemical Reviews, 110*(6), 3479–3500. https://doi.org/10.1021/cr900339w

Hatton, F. L., Malmström, E., & Carlmark, A. (2015). Tailor-made copolymers for the adsorption to cellulosic surfaces. *European Polymer Journal, 65*(57), 325–339. https://doi.org/10.1016/j.eurpolymj.2015.01.026

Heinze, T. (2015). Applications of chitosan and chitosan derivatives in drug delivery. *Advances in Polymer Science = Fortschritte Der Hochpolymeren-Forschung* (Vol. 5,(Issue 1), 28–37. https://doi.org/10.1007/12

Horii, F., Hirai, A., & Kitamaru, R. (1983). Solid-state 13C-NMR study of conformations of oligosaccharides and cellulose. *Polymer Bulletin, 10*(7), 357–361. https://doi.org/10.1007/BF00281948

Huang, J. L., Li, C. J., & Gray, D. G. (2014). Functionalization of cellulose nanocrystal films via "thiol-ene" click reaction. *RSC Advances, 4*(14), 6965–6969. https://doi.org/10.1039/c3ra47041e

Ifuku, S., Nogi, M., Abe, K., Handa, K., Nakatsubo, F., & Yano, H. (2007). Surface modification of bacterial cellulose nanofibers for property enhancement of optically transparent composites: Dependence on acetyl-group DS. *Biomacromolecules, 8*(6), 1973–1978. https://doi.org/10.1021/bm070113b

Ihara, T., & Iriyama, Y. (2011). Characteristics of liquid marbles formed with plasma-treated hydrophobic cellulose powder. *Journal of Photopolymer Science and Technology, 24*(4), 435–440. https://doi.org/10.1017/CBO9781107415324.004

Ioelovich, M. (2012). Study of cellulose interaction with concentrated solutions of sulfuric acid. *ISRN Chemical Engineering, 2012*, Article 428974. https://doi.org/10.5402/2012/428974

Jiang, F., & Hsieh, Y. L. (2017). Cellulose nanofibril aerogels: Synergistic improvement of hydrophobicity, strength, and thermal stability via cross-linking with diisocyanate. *ACS Applied Materials & Interfaces, 9*(3), 2825–2834. https://doi.org/10.1021/acsami.6b13577

Kamide, K., Okajima, K., Kowsaka, K., & Matsui, T. (1985). CP/MASS 13C NMR spectra of cellulose solids: An explanation by the intramolecular hydrogen bond concept. *Polymer Journal, 17*(5), 701–706. https://doi.org/10.1295/polymj.17.701

Kargarzadeh, H., Ahmad, I., Abdullah, I., Dufresne, A., Zainudin, S. Y., & Sheltami, R. M. (2012). Effects of hydrolysis conditions on the morphology, crystallinity, and thermal stability of cellulose nanocrystals extracted from kenaf bast fibers. *Cellulose, 19*(3), 855–866. https://doi.org/10.1007/s10570-012-9684-6

Khanjanzadeh, H., Behrooz, R., Bahramifar, N., Gindl-Altmutter, W., Bacher, M., Edler, M., & Griesser, T. (2018). Surface chemical functionalization of cellulose nanocrystals by 3-aminopropyltriethoxysilane. *International Journal of Biological Macromolecules, 106*, 1288–1296. https://doi.org/10.1016/j.ijbiomac.2017.08.136

Kim, H., Park, J., Minn, K. S., Pak, S. Y., Lee, D., Youn, J. R., & Song, Y. S. (2019). Flame retardant composite foam modified by silylated nanocellulose and tris(2-chloropropyl) phosphate. *Fibers and Polymers, 20*(11), 2280–2288. https://doi.org/10.1007/s12221-019-9491-x

Kim, J. H., Gu, M., Lee, D. H., Kim, J. H., Oh, Y. S., Min, S. H., … Lee, S. Y. (2016). Functionalized nanocellulose-integrated heterolayered nanomats toward smart battery separators. *Nano Letters, 16*(9), 5533–5541. https://doi.org/10.1021/acs.nanolett.6b02069

Kolb, H. C., Finn, M. G., & Sharpless, K. B. (2001). Click chemistry: Diverse chemical function from a few good reactions. *Angewandte Chemie - International Edition, 40*(11), 2004–2021. https://doi.org/10.1002/1521-3773(20010601)40:11<2004::AID-ANIE2004>3.0.CO;2-5

Kontturi, K. S., Biegaj, K., Mautner, A., Woodward, R. T., Wilson, B. P., Johansson, L. S., Lee, K. Y., Heng, J. Y. Y., Bismarck, A., & Kontturi, E. (2017). Noncovalent surface modification of cellulose nanopapers by adsorption of polymers from aprotic solvents. *Langmuir, 33*(23), 5707–5712. https://doi.org/10.1021/acs.langmuir.7b01236

Korhonen, J. T., Kettunen, M., Ras, R. H. A. A., & Ikkala, O. (2011). Hydrophobic nanocellulose aerogels as floating, sustainable, reusable, and recyclable oil absorbents. *ACS Applied Materials & Interfaces, 3*(6), 1813–1816. https://doi.org/10.1021/am200475b

Kowalski, A., Duda, A., & Penczek, S. (1998). Kinetics and mechanism of cyclic esters polymerization initiated with tin(II) octoate. 3. Polymerization of L,L-dilactide. *Macromolecules, 33*(20), 7359–7370. https://doi.org/10.1021/ma000125o

Kulasinski, K., Keten, S., Churakov, S. V., Derome, D., & Carmeliet, J. (2014). A comparative molecular dynamics study of crystalline, paracrystalline and amorphous states of cellulose. *Cellulose, 21*(3), 1103–1116. https://doi.org/10.1007/s10570-014-0213-7

Kumagai, A., & Endo, T. (2020). Tannic acid-immobilized cellulose nanofiber prepared by esterification using polycarboxylic acid. *Cellulose Chemistry and Technology, 54*(5–6), 415–419. https://doi.org/10.35812/CelluloseChemTechnol.2020.54.42

Kumar, R., Rai, B., Gahlyan, S., & Kumar, G. (2021). A comprehensive review on production, surface modificationand characterization of nanocellulose derived from biomassand its commercial applications.pdf. *Express Polymer Letters, 15*(2), 104–120. https://doi.org/10.3144/expresspolymlett.2021.11

Kunaver, M., Anžlovar, A., & Žagar, E. (2016). The fast and effective isolation of nanocellulose from selected cellulosic feedstocks. *Carbohydrate Polymers* (Vol. 148,, 251–258. https://doi.org/10.1016/j.carbpol.2016.04.076

Kunaver, M., Kos, T., Anžlovar, A., Žagar, E., & Huskić, M. (2015). *Method for the production of nanocrystalline cellulose (Patent No. WO 2015/137888 A1)*. World Intellectual Property Organization, International Bureau.

Labet, M., & Thielemans, W. (2009). Synthesis of polycaprolactone: A review. *Chemical Society Reviews, 38*(12), 3484–3504. https://doi.org/10.1039/b820162p

Labet, M., & Thielemans, W. (2011). Improving the reproducibility of chemical reactions on the surface of cellulose nanocrystals: ROP of ε-caprolactone as a case study. *Cellulose, 18*(3), 607–617. https://doi.org/10.1007/s10570-011-9527-x

Labet, M., & Thielemans, W. (2012). Citric acid as a benign alternative to metal catalysts for the production of cellulose-grafted-polycaprolactone copolymers. *Polymer Chemistry, 3*(3), 679–684. https://doi.org/10.1039/c2py00493c

Le, D., Kongparakul, S., Samart, C., Phanthong, P., Karnjanakom, S., Abudula, A., & Guan, G. (2016). Preparing hydrophobic nanocellulose-silica film by a facile one-pot method. *Carbohydrate Polymers* (Vol. 153,, 266–274. https://doi.org/10.1016/j.carbpol.2016.07.112

Le Gars, M., Roger, P., Belgacem, N., & Bras, J. (2020). Role of solvent exchange in dispersion of cellulose nanocrystals and their esterification using fatty acids as solvents. *Cellulose, 27*(8), 4319–4336. https://doi.org/10.1007/s10570-020-03101-0

Lee, H., & Mani, S. (2017). Mechanical pretreatment of cellulose pulp to produce cellulose nanofibrils using a dry grinding method. *Industrial Crops and Products, 104*, 179–187. https://doi.org/10.1016/j.indcrop.2017.04.044

Li, W., Wang, W., Yang, Y., & Zhang, K. (2014). Redox-responsive, reversibly fluorescent nanoparticles from sustainable cellulose derivatives. *Journal of Materials Chemistry A, 2*(33), 13675–13681. https://doi.org/10.1039/c4ta02126f

Li, Y., Chen, H., Liu, D., Wang, W., Liu, Y., & Zhou, S. (2015). PH-responsive shape memory poly(ethylene glycol)-Poly(ε-caprolactone)-based polyurethane/cellulose nanocrystals nanocomposite. *ACS Applied Materials & Interfaces, 7*(23), 12988–12999. https://doi.org/10.1021/acsami.5b02940

Li, Q., Gao, R., Wang, L., Xu, M., Yuan, Y., Ma, L., … Yang, X. (2020). Nanocomposites of bacterial cellulose nanofibrils and zein nanoparticles for food packaging. *ACS Applied Nano Materials, 3*(3), 2899–2910. https://doi.org/10.1021/acsanm.0c00159

Li, P., Wang, Y., Hou, Q., Liu, H., Lei, H., Jian, B., & Li, X. (2020). Preparation of cellulose nanofibrils from okara by high pressure homogenization method using deep eutectic solvents. *Cellulose, 27*(5), 2511–2520. https://doi.org/10.1007/s10570-019-02929-5

Lin, N., Chen, G., Huang, J., Dufresne, A., & Chang, P. R. (2009). Effects of polymer-grafted natural nanocrystals on the structure and mechanical properties of poly (lactic acid): A case of cellulose whisker-graft-polycaprolactone. *Journal of Applied Polymer Science, 113*(5), 3417–3425. https://doi.org/10.1002/app

Lin, N., Huang, J., Chang, P. R., Feng, J., & Yu, J. (2011). Surface acetylation of cellulose nanocrystal and its reinforcing function in poly(lactic acid). *Carbohydrate Polymers, 83*(4), 1834–1842. https://doi.org/10.1016/j.carbpol.2010.10.047

Lin, N., Huang, J., & Dufresne, A. (2015). Polysaccharide nanocrystals-based materials for advanced applications. In J. Huang, P. R. Chang, N. Lin, & A. Dufresne (Eds.), *Polysaccharide-based nanocrystals: Chemistry and applications* (pp. 63–108). Chemical Industry Press. https://doi.org/10.1002/9783527689378.ch3.

Lozhechnikova, A., Dax, D., Vartiainen, J., Willför, S., Xu, C., & Österberg, M. (2014). Modification of nanofibrillated cellulose using amphiphilic block-structured galactoglucomannans. *Carbohydrate Polymers, 110*, 163–172. https://doi.org/10.1016/j.carbpol.2014.03.087

Lu, Q., Lu, L., Li, Y., Yan, Y., Fang, Z., Chen, X., & Huang, B. (2019). High-yield synthesis of functionalized cellulose nanocrystals for nano-biocomposites. *ACS Applied Nano Materials, 2*(4), 2036–2043. https://doi.org/10.1021/acsanm.9b00048

Lv, D., Du, H., Che, X., Wu, M., Zhang, Y., Liu, C., … Li, B. (2019). Tailored and integrated production of functional cellulose nanocrystals and cellulose nanofibrils via sustainable formic acid hydrolysis: Kinetic study and characterization. *ACS Sustainable Chemistry & Engineering, 7*(10), 9449–9463. https://doi.org/10.1021/acssuschemeng.9b00714

Markstedt, K., Mantas, A., Tournier, I., Martínez Ávila, H., Hägg, D., & Gatenholm, P. (2015). 3D bioprinting human chondrocytes with nanocellulose-alginate bioink for cartilage tissue engineering applications. *Biomacromolecules, 16*(5), 1489–1496. https://doi.org/10.1021/acs.biomac.5b00188

Matthews, J. F., Himmel, M. E., & Crowley, M. F. (2012). Conversion of cellulose Iα to Iβ via a high temperature intermediate (I-HT) and other cellulose phase transformations. *Cellulose, 19*(1), 297–306. https://doi.org/10.1007/s10570-011-9608-x

Mertaniemi, H., Laukkanen, A., Teirfolk, J. E., Ikkala, O., & Ras, R. H. A. (2012). Functionalized porous microparticles of nanofibrillated cellulose for biomimetic hierarchically structured superhydrophobic surfaces. *RSC Advances, 2*(7), 2882–2886. https://doi.org/10.1039/c2ra00020b

Miao, C., & Hamad, W. Y. (2016). Alkenylation of cellulose nanocrystals (CNC) and their applications. *Polymer* (Vol. 101,, 338–346. https://doi.org/10.1016/j.polymer.2016.08.099

Miao, J., Yu, Y., Jiang, Z., & Zhang, L. (2016). One-pot preparation of hydrophobic cellulose nanocrystals in an ionic liquid. *Cellulose, 23*(2), 1209–1219. https://doi.org/10.1007/s10570-016-0864-7

Michel, B., Bras, J., Dufresne, A., Heggset, E. B., & Syverud, K. (2020). Production and mechanical characterisation of TEMPO-oxidised cellulose nanofibrils/β-cyclodextrin films and cryogels. *Molecules, 25*(10), 1–18. https://doi.org/10.3390/molecules25102381

Missoum, K., Bras, J., & Belgacem, N. (2014). *Method for forming a hydrophobic layer (Patent No. EP3024978B1)*. European Patent Office. https://register.epo.org/application?number=EP14790133.

Mondal, S. (2016). Preparation, properties and applications of nanocellulosic materials. *Carbohydrate Polymers* (Vol. 163,, 301–316. https://doi.org/10.1016/j.carbpol.2016.12.050

Moon, R. J., Martini, A., Nairn, J., Simonsen, J., Youngblood, J., Martini, A., & Nairn, J. (2011). Cellulose nanomaterials review: Structure, properties and nanocomposites. *Chemical Society Reviews, 40*(7), 3941–3994. https://doi.org/10.1039/C0CS00108B

Morandi, G., & Thielemans, W. (2012). Synthesis of cellulose nanocrystals bearing photocleavable grafts by ATRP. *Polymer Chemistry, 3*(6), 1402–1407. https://doi.org/10.1039/c2py20069d

Morandi, G., Heath, L., & Thielemans, W. (2009). Cellulose nanocrystals grafted with polystyrene chains through surface-initiated atom transfer radical polymerization (SI-ATRP). *Langmuir, 25*(14), 8280–8286. https://doi.org/10.1021/la900452a

Mugwagwa, L. R., & Chimphango, A. F. A. (2020). Enhancing the functional properties of acetylated hemicellulose films for active food packaging using acetylated nanocellulose reinforcement and polycaprolactone coating. *Food Packaging and Shelf Life* (Vol. 24). https://doi.org/10.1016/j.fpsl.2020.100481

Nawaz, H., Casarano, R., & El Seoud, O. A. (2012). First report on the kinetics of the uncatalyzed esterification of cellulose under homogeneous reaction conditions: A rationale for the effect of carboxylic acid anhydride chain-length on the degree of biopolymer substitution. *Cellulose, 19*(1), 199–207. https://doi.org/10.1007/s10570-011-9622-z

Nawaz, H., Pires, P. A. R., & Seoud, O. A. E. (2013). Kinetics and mechanism of imidazole-catalyzed acylation of cellulose in LiCl/N,N-dimethylacetamide. *Carbohydrate Polymers* (Vol. 92,, 997–1005.

Newman, R. H., & Davidson, T. C. (2004). Molecular conformations at the cellulose-water interface. *Cellulose, 11*(1), 23–32. https://doi.org/10.1023/B:CELL.0000014778.49291.c6

Nigmatullin, R., Johns, M. A., Muñoz-García, J. C., Gabrielli, V., Schmitt, J., Angulo, J., … Eichhorn, S. J. (2020). Hydrophobization of cellulose nanocrystals for aqueous colloidal suspensions and gels. *Biomacromolecules, 21*(5), 1812–1823. https://doi.org/10.1021/acs.biomac.9b01721

Osterholtz, F. D., & Pohl, E. R. (1992). Kinetics of the hydrolysis and condensation of organofunctional alkoxysilanes: A review. *Journal of Adhesion Science and Technology, 6*(1), 127–149. https://doi.org/10.1163/156856192X00106

Panaitescu, D. M., Ionita, E. R., Nicolae, C. A., Gabor, A. R., Ionita, M. D., Trusca, R., Lixandru, B. E., Codita, I., & Dinescu, G. (2018). Poly(3-hydroxybutyrate) modified by nanocellulose and plasma treatment for packaging applications. *Polymers, 10*(11), 1–24. https://doi.org/10.3390/polym10111249

Paquet, O., Krouit, M., Bras, J., Thielemans, W., & Belgacem, M. N. (2010). Surface modification of cellulose by PCL grafts. *Acta Materialia* (Vol. 58,(Issue 3), 792–801. https://doi.org/10.1016/j.actamat.2009.09.057

Parambath Kanoth, B., Claudino, M., Johansson, M., Berglund, L. A., & Zhou, Q. (2015). Biocomposites from natural rubber: Synergistic effects of functionalized cellulose nanocrystals as both reinforcing and cross-linking agents via free-radical thiol-ene chemistry. *ACS Applied Materials & Interfaces, 7*(30), 16303–16310. https://doi.org/10.1021/acsami.5b03115

Penczek, S., & Duda, A. (1996). Selectivity as a measure of "livingness" of the polymerization of cyclic esters. *Macromolecular Symposia, 107*(1), 1–15. https://doi.org/10.1002/masy.19961070103

Peng, S. X., Chang, H., Kumar, S., Moon, R. J., & Youngblood, J. P. (2016). A comparative guide to controlled hydrophobization of cellulose nanocrystals via surface esterification. *Cellulose, 23*(3), 1825–1846. https://doi.org/10.1007/s10570-016-0912-3

Postek, M. T., Moon, R. J., Rudie, A. W., & Bilodeau, M. A. (2013). Foreword. In M. T. Postek, R. J. Moon, A. W. Rudie, & M. A. Bilodeau (Eds.), *Production and applications of cellulose nanomaterials* (p. 1). Tappi Press.

Pujiasih, S., Kurnia, Masykur, A., Kusumaningsih, T., & Saputra, O. A. (2018). Silylation and characterization of microcrystalline cellulose isolated from Indonesian native oil palm empty fruit bunch. *Carbohydrate Polymers, 184*(December 2017), 74–81. https://doi.org/10.1016/j.carbpol.2017.12.060

Qing, W., Wang, Y. Y. Y., Wang, Y. Y. Y., Zhao, D., Liu, X., & Zhu, J. (2016). The modified nanocrystalline cellulose for hydrophobic drug delivery. *Applied Surface Science, 366*, 404–409. https://doi.org/10.1016/j.apsusc.2016.01.133

Rafieian, F., Hosseini, M., Jonoobi, M., & Yu, Q. (2018). Development of hydrophobic nanocellulose-based aerogel via chemical vapor deposition for oil separation for water treatment. *Cellulose, 25*(8), 4695–4710. https://doi.org/10.1007/s10570-018-1867-3

Ren, Z., Guo, R., Bi, H., Jia, X., Xu, M., & Cai, L. (2020). Interfacial adhesion of polylactic acid on cellulose surface: A molecular dynamics study. *ACS Applied Materials & Interfaces, 12*(2), 3236–3244. https://doi.org/10.1021/acsami.9b20101

Reverdy, C., Belgacem, N., Moghaddam, M. S., Sundin, M., Swerin, A., & Bras, J. (2018). One-step superhydrophobic coating using hydrophobized cellulose nanofibrils. *Colloids and Surfaces A, Physicochemical and Engineering Aspects* (Vol. 544,, 152–158. https://doi.org/10.1016/j.colsurfa.2017.12.059

Roeder, R. D., Garcia-Valdez, O., Whitney, R. A., Champagne, P., & Cunningham, M. F. (2016). Graft modification of cellulose nanocrystals: Via nitroxide-mediated polymerisation. *Polymer Chemistry, 7*(41), 6383–6390. https://doi.org/10.1039/c6py01515h

Rowland, S. P., & Howley, P. S. (1988). Hydrogen bonding on accessible surfaces of cellulose from various sources and relationship to order within crystalline regions. *Journal of Polymer Science Part A: Polymer Chemistry, 26*(7), 1769–1778. https://doi.org/10.1002/pola.1988.080260708

Rueda, L., Fernández d'Arlas, B., Zhou, Q., Berglund, L. A., Corcuera, M. A., Mondragon, I., & Eceiza, A. (2011). Isocyanate-rich cellulose nanocrystals and their selective insertion in elastomeric polyurethane. *Composites Science and Technology* (Vol. 71,(Issue 16), 1953–1960. https://doi.org/10.1016/j.compscitech.2011.09.014

Sacui, I. A., Nieuwendaal, R. C., Burnett, D. J., Stranick, S. J., Jorfi, M., Weder, C., … Gilman, J. W. (2014). Comparison of the properties of cellulose nanocrystals and cellulose nanofibrils isolated from bacteria, tunicate, and wood processed using acid, enzymatic, mechanical, and oxidative methods. *ACS Applied Materials & Interfaces, 6*(9), 6127–6138. https://doi.org/10.1021/am500359f

Sadeghifar, H., Filpponen, I., Clarke, S. P., Brougham, D. F., & Argyropoulos, D. S. (2011). Production of cellulose nanocrystals using hydrobromic acid and click reactions on their surface. *Journal of Materials Science, 46*(22), 7344–7355. https://doi.org/10.1007/s10853-011-5696-0

Sáenz Ezquerro, C., Crespo Miñana, C., Izquierdo, S., & Laspalas, M. (2019). A molecular dynamics model to measure forces between cellulose fibril surfaces: On the effect of non-covalent polyelectrolyte adsorption. *Cellulose, 26*(3), 1449–1466. https://doi.org/10.1007/s10570-018-2166-8

Salajková, M., Berglund, L. A., & Zhou, Q. (2012). Hydrophobic cellulose nanocrystals modified with quaternary ammonium salts. *Journal of Materials Chemistry, 22*(37), 19798–19805. https://doi.org/10.1039/c2jm34355j

Salam, A., Lucia, L. A., & Jameel, H. (2015). Fluorine-based surface decorated cellulose nanocrystals as potential hydrophobic and oleophobic materials. *Cellulose, 22*(1), 397–406. https://doi.org/10.1007/s10570-014-0507-9

Samanta, K. K., Amish, G. J., Manjeet, J., & Aswini, K. A. (2012). Study of hydrophobic finishing of cellulosic substrate using He_1,3-butadiene plasma at atmospheric pressure _ Elsevier Enhanced Reader.pdf. *Surface & Coatings Technology, 213*, 65–76.

Samanta, K. K., Gayatri, T. N., Basak, S., Chattopadhay, S. K., Arputharaj, A., & Prasad, V. (2016). Hydrophobic functionalization of cellulosic substrates using atmospheric pressure plasma. *Cellulose Chemistry and Technology, 50*(March 2017), 745–754.

Samanta, K. K., Joshi, A. G., Jassal, M., & Agrawal, A. K. (2021). Hydrophobic functionalization of cellulosic substrate by tetrafluoroethane dielectric barrier discharge plasma at atmospheric pressure. *Carbohydrate Polymers, 253*, Article 117272. https://doi.org/10.1016/j.carbpol.2020.117272

Sebe, G., Ham-Pichavant, F., & Pecastaings, G. (2013). Dispersibility and emulsion-stabilizing effect of cellulose nanowhiskers esterified by vinyl acetate and vinyl cinnamate. *Biomacromolecules, 14*(8), 2937–2944. https://doi.org/10.1021/bm400854n

Sehaqui, H., Zimmermann, T., & Tingaut, P. (2014). Hydrophobic cellulose nanopaper through a mild esterification procedure. *Cellulose, 21*(1), 367–382. https://doi.org/10.1007/s10570-013-0110-5

Shang, W., Huang, J., Luo, H., Chang, P. R., Feng, J., & Xie, G. (2013). Hydrophobic modification of cellulose nanocrystal via covalently grafting of castor oil. *Cellulose, 20*(1), 179–190. https://doi.org/10.1007/s10570-012-9795-0

Shojaeiarani, J., Bajwa, D. S., & Stark, N. M. (2018). Green esterification: A new approach to improve thermal and mechanical properties of poly(lactic acid) composites reinforced by cellulose nanocrystals. *Journal of Applied Polymer Science, 135*(27), 1–8. https://doi.org/10.1002/app.46468

Siqueira, G., Bras, J., & Dufresne, A. (2009a). Cellulose whiskers versus microfibrils: Influence of the nature of the nanoparticle and its surface functionalization on the thermal and mechanical properties of nanocomposites. *Biomacromolecules, 10*(2), 425–432. https://doi.org/10.1021/bm801193d

Siqueira, G., Bras, J., & Dufresne, A. (2009b). New process of chemical grafting of cellulose nanoparticles with a long chain isocyanate. *Langmuir, 26*(1), 402–411. https://doi.org/10.1021/la9028595

Sîrbu, E., Eyley, S., & Thielemans, W. (2016). Coumarin and carbazole fluorescently modified cellulose nanocrystals using a one-step esterification procedure. *The Canadian Journal of Chemical Engineering, 94*(11), 2186–2194. https://doi.org/10.1002/cjce.22624

Spinella, S., Lo Re, G., Liu, B., Dorgan, J., Habibi, Y., Leclère, P., Raquez, J. M., Dubois, P., & Gross, R. A. (2015). Polylactide/cellulose nanocrystal nanocomposites: Efficient routes for nanofiber modification and effects of nanofiber chemistry on PLA reinforcement. *Polymer, 65*, 9–17. https://doi.org/10.1016/j.polymer.2015.02.048

Spinella, S., Samuel, C., Raquez, J.-M., McCallum, S. A., Gross, R., & Dubois, P. (2016). Green and efficient synthesis of dispersible cellulose nanocrystals inBiobased polyesters for engineering applications. *ACS Sustainable Chemistry & Engineering, 4*, 2517–2527. https://doi.org/10.1021/acssuschemeng.5b01611

Syverud, K., Xhanari, K., Chinga-Carrasco, G., Yu, Y., & Stenius, P. (2011). Films made of cellulose nanofibrils: Surface modification by adsorption of a cationic surfactant and characterization by computer-assisted electron microscopy. *Journal of Nanoparticle Research, 13*(2), 773–782. https://doi.org/10.1007/s11051-010-0077-1

Tanpichai, S., Witayakran, S., Srimarut, Y., Woraprayote, W., & Malila, Y. (2019). Porosity, density and mechanical properties of the paper of steam exploded bamboo microfibers controlled by nanofibrillated cellulose. *Journal of Materials Research and Technology, 8*(4), 3612–3622. https://doi.org/10.1016/j.jmrt.2019.05.024

Tingaut, P., Hauert, R., & Zimmermann, T. (2011). Highly efficient and straightforward functionalization of cellulose films with thiol-ene click chemistry. *Journal of Materials Chemistry, 21*(40), 16066–16076. https://doi.org/10.1039/C1JM11620G

Trinh, B. M., & Mekonnen, T. (2018). Hydrophobic esterification of cellulose nanocrystals for epoxy reinforcement. *Polymer* (Vol. 155,, 64–74. https://doi.org/10.1016/j.polymer.2018.08.076

Tsalagkas, D., Zhai, L., Kafy, A., Kim, J. W., Kim, H. C., & Kim, J. (2020). Production of Micro- and nanofibrillated cellulose through an aqueous counter collision system followed by ultrasound: Effect of mechanical pretreatments. *Journal of Natural Fibers, 17*(8), 1099–1110. https://doi.org/10.1080/15440478.2018.1558144

Verlhac, C., Dedier, J., & Chanzy, H. (1990). Availability of surface hydroxyl groups in valonia and bacterial cellulose. *Journal of Polymer Science Part A: Polymer Chemistry, 28*(5), 1171–1177. https://doi.org/10.1002/pola.1990.080280517

Voisin, H., Bergström, L., Liu, P., & Mathew, A. P. (2017). Nanocellulose-based materials for water purification. *Nanomaterials, 7*(3). https://doi.org/10.3390/nano7030057

Wang, D. (2019). A critical review of cellulose-based nanomaterials for water purification in industrial processes. *Cellulose, 26*(2), 687–701. https://doi.org/10.1007/s10570-018-2143-2

Wang, H. D., Roeder, R. D., Whitney, R. A., Champagne, P., & Cunningham, M. F. (2015). Graft modification of crystalline nanocellulose by Cu(0)-mediated SET living radical polymerization. *Journal of Polymer Science Part A: Polymer Chemistry, 53*(24), 2800–2808. https://doi.org/10.1002/pola.27754

Wang, X., Yeh, T.-M., Wang, Z., Yang, R., Wang, R., Ma, H., Hsiao, B. S., & Chu, B. (2014). Nanofiltration membranes prepared by interfacial polymerization on thin-film nanofibrous composite scaffold. *Polymer, 55*(6), 1358–1366. https://doi.org/10.1016/j.polymer.2013.12.007

Watts, H. D., Mohamed, M. N. A., & Kubicki, J. D. (2014). A DFT study of vibrational frequencies and 13C NMR chemical shifts of model cellulosic fragments as a function of size. *Cellulose, 21*(1), 53–70. https://doi.org/10.1007/s10570-013-0128-8

Willberg-Keyriläinen, P., & Ropponen, J. (2019). Evaluation of esterification routes for long chain cellulose esters. *Heliyon* (Vol. 5)(Issue 11). https://doi.org/10.1016/j.heliyon.2019.e02898

Xhanari, K., Syverud, K., Chinga-Carrasco, G., Paso, K., & Stenius, P. (2011). Reduction of water wettability of nanofibrillated cellulose by adsorption of cationic surfactants. *Cellulose, 18*(2), 257–270. https://doi.org/10.1007/s10570-010-9482-y

Yao, M. Z., Liu, Y., Qin, C. N., Meng, X. J., Cheng, B. X., Zhao, H., Wang, S. F., & Huang, Z. Q. (2021). Facile fabrication of hydrophobic cellulose-based organic/inorganic nanomaterial modified with POSS by plasma treatment. *Carbohydrate Polymers, 253*, Article 117193. https://doi.org/10.1016/j.carbpol.2020.117193

Yin, Y., Lucia, L. A., Pal, L., Jiang, X., & Hubbe, M. A. (2020). Lipase-catalyzed laurate esterification of cellulose nanocrystals and their use as reinforcement in PLA composites. *Cellulose, 27*(11), 6263–6273. https://doi.org/10.1007/s10570-020-03225-3

Yin, Y., Tian, X., Jiang, X., Wang, H., & Gao, W. (2016). Modification of cellulose nanocrystal via SI-ATRP of styrene and the mechanism of its reinforcement of polymethylmethacrylate. *Carbohydrate Polymers, 142*, 206–212. https://doi.org/10.1016/j.carbpol.2016.01.014

Yokota, S., Tagawa, S., & Kondo, T. (2020). Facile surface modification of amphiphilic cellulose nanofibrils prepared by aqueous counter collision. *Carbohydrate Polymers*, 117342. https://doi.org/10.1016/j.carbpol.2020.117342

Yoo, Y., & Youngblood, J. P. (2016). Green one-pot synthesis of surface hydrophobized cellulose nanocrystals in aqueous medium. *ACS Sustainable Chemistry & Engineering, 4*(7), 3927–3938. https://doi.org/10.1021/acssuschemeng.6b00781

Yu, J., Wang, C., Wang, J., & Chu, F. (2016). In situ development of self-reinforced cellulose nanocrystals based thermoplastic elastomers by atom transfer radical polymerization. *Carbohydrate Polymers, 141*, 143–150. https://doi.org/10.1016/j.carbpol.2016.01.006

Yu, Q., Yang, W., Wang, Q., Dong, W., Du, M., & Ma, P. (2019). Functionalization of cellulose nanocrystals with γ-MPS and its effect on the adhesive behavior of acrylic pressure sensitive adhesives. *Carbohydrate Polymers* (Vol. 217,, 168–177. https://doi.org/10.1016/j.carbpol.2019.04.049

Yu, L., Zhang, Z., Tang, H., & Zhou, J. (2019). Fabrication of hydrophobic cellulosic materials via gas–solid silylation reaction for oil/water separation. *Cellulose, 26*(6), 4021–4037. https://doi.org/10.1007/s10570-019-02355-7

Yuan, Z., & Wen, Y. (2018). Enhancement of hydrophobicity of nanofibrillated cellulose through grafting of alkyl ketene dimer. *Cellulose, 25*(12), 6863–6871. https://doi.org/10.1007/s10570-018-2048-0

Yuan, H., Nishiyama, Y., Wada, M., & Kuga, S. (2006). Surface acylation of cellulose whiskers by drying aqueous emulsion. *Biomacromolecules, 7*(3), 696–700. https://doi.org/10.1021/bm050828j

Zhang, Z., Sèbe, G., Rentsch, D., Zimmermann, T., & Tingaut, P. (2014). Ultralightweight and flexible silylated nanocellulose sponges for the selective removal of oil from water. *Chemistry of Materials, 26*(8), 2659–2668. https://doi.org/10.1021/cm5004164

Zhang, Z., Tingaut, P., Rentsch, D., Zimmermann, T., & Sèbe, G. (2015). Controlled silylation of nanofibrillated cellulose in water: Reinforcement of a model polydimethylsiloxane network. *ChemSusChem, 8*(16), 2681–2690. https://doi.org/10.1002/cssc.201500525

Zhou, L., He, H., Li, M. C., Huang, S., Mei, C., & Wu, Q. (2018). Grafting polycaprolactone diol onto cellulose nanocrystals via click chemistry: Enhancing thermal stability and hydrophobic property. *Carbohydrate Polymers, 189*(February), 331–341. https://doi.org/10.1016/j.carbpol.2018.02.039

Zhu, C., Monti, S., & Mathew, A. P. (2020). Evaluation of nanocellulose interaction with water pollutants using nanocellulose colloidal probes and molecular dynamic simulations. *Carbohydrate Polymers, 229*(July 2019), 115510. https://doi.org/10.1016/j.carbpol.2019.115510

Zoppe, J. O., Peresin, M. S., Habibi, Y., Venditti, R. A., & Rojas, O. J. (2009). Reinforcing poly(ε-caprolactone) nanofibers with cellulose nanocrystals. *ACS Applied Materials & Interfaces, 1*(9), 1996–2004. https://doi.org/10.1021/am9003705

Young, Raymond, & Rowell, Roger (1986). In Raymond Young, & Roger Rowell (Eds.), *Cellulose: Structure, Modification, and Hydrolysis*. New York: Wiley-Interscience.

Chapter 4

Acetylation of Cellulose Nanomaterials

In this chapter, acetylation of cellulose nanomaterials, as well as the use of acetylated CNCs in biopolymer matrices is studied. Esterification reactions were shown to be among the most widely researched in terms of agents, solvents and conditions, however, detailed mechanism and kinetic studies that are needed to push cellulose nanomaterials to industrial scale are still lacking. Furthermore, there is little literature demonstrating the effect of incorporation of acetylated materials into other biopolymer matrices and biodegradation of such biocomposite films. Cellulose nanomaterials acetylated with acetic anhydride in the presence of pyridine that acts as a catalyst have previously been incorporated into (poly)lactic acid and have shown to improve its mechanical properties (Jamaluddin et al. 2019; Lin et al. 2011). However, taking into consideration that (poly)lactic acid has several drawbacks (interference with food supply chain and poor degradability requiring high temperatures), we propose the use of chitosan and alginate as biopolymer matrices that are further improved by incorporating pristine or acetylated CNCs.

The chapter is divided into three subsections (4.1 Multiscale Study of Functional Acetylation of Cellulose Nanomaterials by Design: *ab initio* Mechanisms and Chemical Reaction Microkinetics, 4.2 Effect of Environment on Acetylated Cellulose Nanocrystal-Reinforced Biopolymers Films, 4.3 Biodegradation of Polysaccharide-Based Biocomposites with Acetylated Cellulose Nanocrystals, Alginate and Chitosan in Aqueous Environment), each focusing on the distinct aspect of acetylation of cellulose nanomaterials with acetic anhydride in the presence of pyridine.

The chapter addresses Objectives 3 and 4.

4.1 Multiscale Study of Functional Acetylation of Cellulose Nanomaterials by Design: *ab initio* Mechanisms and Chemical Reaction Microkinetics

In this section, a joint experimental-computational approach to propose acetylation reaction mechanism and develop a microkinetic model through which kinetic parameters were developed is presented. CNCs and CNFs were analyzed by the means of SEM, TEM to observe morphology and ^{31}P NMR to determine surface-accessible hydroxyl groups prior to functionalization with acetic anhydride in pyridine medium under various temperatures and reactant ratios. The acetylated materials were analyzed with solid-state NMR and ATR-FTIR to confirm successful modification and determine acetyl content, respectively. Additionally, XRD analysis was carried out to follow any change in crystallinity. First principles calculations on cellotriose as a model, carried out independently of experimental data, offered an insight into the mechanism of the studied reaction. It was proposed that the reaction occurs through two competitive mechanisms: i) direct conversion to cellulose acetate and ii) through active intermediate acetylpyridinium. Based on these findings, a microkinetic model was developed to which experimental values were fitted, yielding kinetic parameters.

Regarding my contribution: I carried out the experimental part of the study, developed a microkinetic model and co-wrote the manuscript.

ACS Sustainable Chemistry & Engineering

pubs.acs.org/journal/ascecg

Research Article

Multiscale Study of Functional Acetylation of Cellulose Nanomaterials by Design: *Ab Initio* Mechanisms and Chemical Reaction Microkinetics

Ana Oberlintner, Matej Huš, Blaž Likozar, and Uroš Novak*

Cite This: *ACS Sustainable Chem. Eng.* 2022, 10, 15480−15489

Read Online

ACCESS | Metrics & More | Article Recommendations | Supporting Information

ABSTRACT: Cellulose nanomaterials, namely cellulose nanocrystals (CNCs) and cellulose nanofibrils (CNFs), present a class of multipurpose, renewable, biodegradable, and nontoxic materials, paving the way into the future of biobased materials. The abundance of hydroxyl groups on the surface allows modification of the materials properties according to application; however, to fully exploit their potential, better compatibility on the molecular level with the hydrophobic matrixes has to be explored beyond lab scale. One of the main missing pieces in functionalization of nanomaterials is a lack of studies focusing on mechanisms and kinetics, which are prerequisite for further optimization of conditions leading to optimal process in terms of both sustainable processing and optimal performance. In this study, the "by design" based approach to tailor biomaterial properties has been simulated multiscale-wise, thus providing a greatly needed input for commercialization. The microkinetic parameters of the elementary reaction steps for acetylation of two distinct types of cellulose nanomaterials were determined and refined by regression analysis. *Ab initio* part utilizes the density functional theory (DFT) for cellotriose as a model, which suggested that products were obtained through a mechanism consisting of active intermediate formation/subsequent competing one- or two-step (through binding/decomposition of complex) reactions. Quantum chemical simulations were used to pinpoint the most probable sequence through calculated activation barriers that served as a foundation for the development of a thorough regression analysis on experimental data sets. The yield of reaction, through formed acetyl groups was determined through Fourier transform infrared spectroscopy, leading to acquisition of critical elementary characteristics.

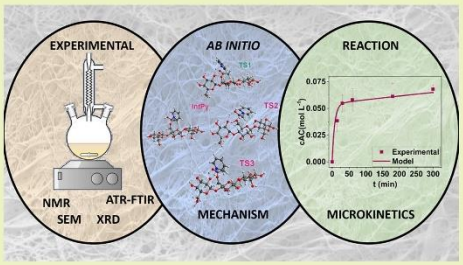

KEYWORDS: *cellulose, esterification, hydrophobicity, chemical reaction mechanism, density functional theory, multiscale microkinetic modeling*

INTRODUCTION

Produced by plants through the process of photosynthesis, cellulose takes the place as the most abundant polymer in nature, and is as such readily available worldwide to be used in various applications. Besides economic feasibility, its further advantages are biodegradability, nontoxicity, biocompatibility, and the possibility to extract particles of nanoscale.[1] Cellulose nanocrystals (CNCs) are, as defined by The American Paper & Pulp Association (TAPPI WI 3021), nanoparticles with pure crystalline structure measuring up to 3−10 nm in width and with an aspect ratio larger than 5, however usually less than 50.[2] 2,2,6,6-Tetramethylpiperidine-1-oxyl radical(TEMPO)-mediated oxidation of cellulose biomass coupled with mechanical treatment yields cellulose nanofibrils (CNFs), which are in the form of long fibrilous networks with a diameter of individual fibril up to 100 nm and length up to a few micrometers.[3] The backbone of cellulose nanomaterials consists of anhydroglucose units (AGUs) alternately rotated around their axis for 180° and linked by β-glycosidic bonds which are, along with hydrogen bonds, the reason behind cellulose's rigidity, stiffness, high mechanical strength, and crystalline character.[4] There are two proposed models defining the distribution of ordered (crystalline) and disordered (amorphous) regions in cellulose: (a) it can be described as an alternation of the crystalline and amorphous domains along the biopolymer fiber, where the amorphous domains are placed between the crystalline regions as a result of internal strain causing the fiber to tilt and twist,[5] or (b) such defects are not

Received: August 5, 2022
Revised: October 25, 2022
Published: November 9, 2022

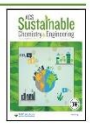

https://doi.org/10.1021/acssuschemeng.2c04686
ACS Sustainable Chem. Eng. 2022, 10, 15480−15489

fully amorphous; however, at the twists and sharp bends of the fiber, its core remains crystalline and the disordered regions are present only on the surface.[6,7]

Along with other nanofibers, cellulose nanomaterials are heavily investigated as a filler for polymers or biopolymers, especially by researchers in the wood and paper industry as well as groups dealing with biomaterials.[8] Potential applications of cellulose/polymer nanocomposite are rising due to its truly sustainable character and abundance, and it has achieved a status of a "new" class of materials for use in various fields including thermosets used for packaging, automobile, electronics, textile, construction, medical devices, and many more. In terms of processing cellulose nanocomposites, almost half of the published research reports the use of solvent casting method, which is not easily industrially scalable.[9] In a conventional industrial setting, fibers and thermoplastics are melt mixed to generate compounds, followed by profile extrusion, compression molding, or injection molding processes to yield composite products at high production rates. There are several processing challenges and sustainability issues involved in applying cellulose nanomaterials into conventional and biobased thermoplastic processing systems.[10] The latter is related to the greener chemistry of cellulose functionalization and diminishing the environmental footprint of the chemicals but also to improving the economic feasibility.[11] To overcome the dispersion of cellulose nanomaterials in thermoplastic (bio)polymers solution, both a nanocellulose treatment chemically or physical surface treatments have been demonstrated as an efficient option, thus potentially boosting the industrial applications.[12] Hydroxyl groups on the surface allow a vast range of surface modifications[13] that can overcome the weakness posed by hydrogen bonding causing limited compatibility with polymer matrices,[14] but it has to be taken into account that among the three hydroxyl groups on the surface of a monomeric unit, not all of them are equally reactive and susceptible to functionalization. The hydroxyl group on the C6 position (using conventional numbering with C1 being the anomeric carbon) is much more reactive than C2- or C3-bound hydroxyl groups. Additionally, modification of only the C6-bound group does not interfere with the mechanical strength of cellulose fibers, leading to recent efforts of regioselective acetylation.[15,16] An overview of hydrophobization methods on cellulose nanomaterials shows esterification is the favored way of minimizing the hydrophilic effect,[15,17] with acetylation being one of the most widely used cellulose modifications that has also been commercially utilized in a number of applications and can be translated to the nanoscale, as well. Commercial cellulose acetylation is carried out with sulfuric acid as a catalyst, but the process is environmentally problematic and presents a health hazard, prompting research in better substitutes. Alternatively, acetylation of CNCs using acetic anhydride in various media, such as citric acid and pyridine, has been described by several authors.[17,18] Acetylation of cellulose nanomaterials was shown to improve dispersibility in common solvents as well as polymer matrices. In practical applications, the result of modification was an increase in mechanical strength of PLA-based polymers with integrated acetylated cellulose nanomaterials, due to better compatibility as a result of surface hydrophobicity.[18,19] Furthermore, acetylated CNCs were demonstrated to improve the toughness of a vitrimer upon their incorporation.[20] Due to their fibrilous structure, acetylated CNFs were successfully (as opposed to pristine CNFs) utilized as Pickering emulsion stabilizers.[21] Despite their huge potential, cellulose nanomaterials are not utilized on the industrial scale yet, due to several limitations that are well described by Wang et al.[12] The industrialization of these materials depends on solving problems regarding both processing techniques and surface modification.

While a number of studies inspected possible routes to esterification of cellulose nanomaterials and their practical applications, only a limited number of them focused on the reaction mechanisms and kinetics.[22] Several authors have investigated the kinetic of wood acetylation with acetic anhydride, assuming either a one-step (direct acetylation of hydroxyl groups) or a two-step mechanism (including dissolution of sulfated chains), with reaction kinetics following a pseudo-first-order expression.[23−26] To be able to evaluate the economic feasibility and sustainability of acetylated nanomaterials and promote their wider use in commercial applications, this precise knowledge is needed as demonstrated by Kanematsu et al.[27]

With this in mind, the present study revisits the investigation of pyridine-mediated acetylation with acetic anhydride mechanisms and kinetics on two types of cellulose nanomaterials (CNCs and CNFs). A revised mechanism of cellulose nanomaterials acetylation consisting of several routes is hypothesized. *Ab initio* calculations should provide an insight into the atomistic mechanism through the determination of activation barriers. The subsequent microkinetic modeling, supported by experiments under various conditions (temperatures in the range from 60 to 90 °C and varying reactant ratios), can confirm the preliminary hypothesis. Additionally, in the frame of experimental investigation, the chemical and morphological characterization of the cellulose derivatives was carried out using ATR-FTIR, phosphorus-31 NMR, solid-state NMR, XRD, and SEM. The final hypothesis aims to confirm that the developed microkinetic model can describe the acetylation reaction for CNCs as well as CNFs.

EXPERIMENTAL SECTION

Materials. CNFs (Valida S, 3% wt. suspension) was supplied by Sappi (Maastricht, Netherlands), and CNCs were purchased from Navitas (Stari trg pri Ložu, Slovenia). For acetylation of cellulose nanomaterials, the following chemicals were used: toluene (Honeywell), pyridine (Merck), acetic anhydride and acetone (Sigma-Aldrich). For NMR analyses, deuterated chloroform, chromium(III) acetylacetonate (relaxation agent), and 2-chloro-4,4,5,5- tetramethyl-1,2,3-dioxophospholane (TMDP) were all purchased from Sigma-Aldrich, while the internal standard *N*-hydroxy-5-norbornene-2,3-dicarboxylic acid imide (NHND, > 99%) was purchased from Tokyo Chemical Industry.

Methods. *Characterization Pristine and Modified Cellulose Nanomaterials.* To ascertain the morphology, approximately 100 mg of cellulose nanomaterial dispersion in water (approximately 3 wt %) was diluted in 5 mL of acetone. A few drops of cellulose nanomaterial−acetone solution were added onto the surface of a heated sample holder, which was previously smoothed with sand paper, to quickly evaporate the solvent. The sample was then inspected as is with scanning electron microscope SUPRA 35VP (Carl Zeiss, Jena, Germany) at near-vacuum conditions. For TEM analysis, 10 mg of cellulose nanomaterial was dispersed in 20 mL of acetone and analyzed using JEOL ARM 200F electron microscope (JEOL, Akishima, Japan). The size of the nanoparticles was determined from the TEM micrograph from at least 25 points with ImageJ software, and the average is reported.

The amount of accessible hydroxyl groups on the surface of pristine nanocellulose was assessed by measuring ^{31}P with Bruker Avance Neo 600 MHz NMR spectrometer (Bruker, Germany). TMDP was

https://doi.org/10.1021/acssuschemeng.2c04686
ACS Sustainable Chem. Eng. 2022, 10, 15480−15489

reacted with freeze-dried and vacuumed CNCs and CNFs for 30 min in the presence of the internal standard (NHND), following the protocol proposed by Brand et al.[28] The amount of accessible groups was calculated from the peak integrals of the unreacted TMDP, internal standard NHND, and water. The amount of surface hydroxyl groups was also calculated theoretically through the crystallite size.

^{13}C cross-polarization/magic-angle spinning (^{13}C CP/MAS) solid state NMR spectra were recorded on Bruker Avance Neo 400 MHz NMR spectrometer (Bruker, Germany) equipped with a 4 mm HX MAS probe. The analysis was done at a spinning rate of 15 kHz.

To evaluate the crystallinity, the freeze-dried samples of CNCs were analyzed directly, while CNFs had to be flattened by pressure once dry as described by Peng et al.[29] to be suitable for analysis. Before the analysis they were fixed on modeling clay. The XRD spectra were recorded with the PANanalytical X'Pert PRO (Malvern Panalytical, UK) high-resolution diffractometer using Cu Kα radiation (1.5406 Å) in a 2θ range from 5° to 59° (100 s per step 0.034°). The crystallinity index CrI was calculated by the Segal method:[30]

$$\mathrm{CrI} = \frac{I_{200} - I_{\mathrm{am}}}{I_{200}} 100 \quad (1)$$

where I_{200} is the maximum intensity of the diffraction from the crystalline (200) plane at $2\theta = 22.8°$ and I_{am} is the minimum intensity of the amorphous region measured at $2\theta = 18°$. Crystallite size (C_A) was calculated based on the obtained XRD spectra following eq 2.

$$C_A = \frac{K\lambda}{\beta \cos 2\theta} \quad (2)$$

where K is 1 (the Scherrer constant for needle-like crystallites) and λ is the used wavelength (0.15406 nm). β is the width of half-maximum of the diffraction peak angle of the (002) crystal plane. β is expressed in radians, while 2θ is in degrees.[31] The amount of surface chains (R) proportional to total amount of chains was calculated using lattice plane d-spacings of the cellulose I monoclinic unit cell.[28]

The freeze-dried samples were measured with FT-IR Spectrum Two (PerkinElmer, Waltham, USA) instrument in a range of wavelengths of 4000−400 cm^{-1} with 64 scans with increments (resolution) of 4 cm^{-1}. The spectra were adjusted to the same baseline and normalized to the C−O peak at 1056 cm^{-1} that is a characteristic peak for a cellulose backbone and is not altered by the reaction. The acetyl content is calculated through the $I_{C=O}$ and I_{C-O} ratio as stated in the literature.[32] The accuracy of the method was assessed through titration (Supporting Information).

Acetylation of Cellulose Nanomaterials. CNCs and CNFs were acetylated according to a modified protocol by Lin et al.[18] The detailed description of the procedure can be found in the Supporting Information. The reaction conditions are summarized in Table 1, with additionally tested parameters in Table S1.

Quantum Chemical Simulations. DFT calculations served to study the reaction mechanism. Electronic structures were calculated with NWChem 6.8.[33] Within the linear combination of atomic orbitals method, we used a hybrid functional (M06-2X)[34] with Pople's basis set 6-31+G(d) for optimization and TS search[35−38] and 6-311++G(d,p) for single-point energy calculations, which is known to reproduce the main group thermochemistry sufficiently well.[39] Solvation was modeled implicitly with the solvation model based on density (SMD)[40] with the default values for pyridine (dielectric constant: 12.978). Benchmark calculations were also done using toluene (dielectric constant: 2.4) to evaluate the effect of adding toluene, which was necessary for CNFs.

Structural optimization was performed until the forces dropped below 1.5×10^{-5} hartree/bohr. The structures were characterized with vibrational analysis to differentiate between stable and saddle points. The transition states were identified using the climbing image nudged elastic band method[41] and confirmed by IRC.

Modeling. *The Quantum Model.* Cellulose is a prohibitively large system to be described by contemporary quantum chemistry methods. Ponnuchamy et al.[42] have already shown that cellobiose can be used as a model compound for studying wood modification with acetic anhydride. Due to the computational power available, we use cellotriose (an oligomer of three *D*-glucose units) in the most stable tg configuration[43] as a model, as shown in Figure S1. This structure is large enough to allow for the cooperation of neighboring monomeric units (see the mechanism below) and reproduces the steric hindrance brought about by a chain of monomeric units, yet small enough to be computationally tractable. Acetic anhydride was modeled as the acetylating agent.

Table 1. Tested Experimental Conditions

Experiment No.	T (°C)	AGU:Pyridine:Acetic Anhydride (mol)
	CNC	
1.1	60	1:10:8.56
1.2	60	1:30:8.56
1.3	60	1:50:8.56
1.4	70	1:10:8.56
1.5	70	1:30:8.56
1.6	70	1:50:8.56
1.7	80	1:20:8.56
1.8	80	1:30:8.56
1.9	80	1:40:8.56
1.10	80	1:50:8.56
1.11	90	1:8.6:8.6
1.12	90	1:10:8.56
1.13	90	1:30:6.00
1.14	90	1:30:8.56
1.15	90	1:40:8.56
1.16	90	1:50:8.56
	CNF	
2.1	60	1:10:8.56
2.2	60	1:30:8.56
2.3	70	1:30:8.56
2.4	70	1:40:8.56
2.5	80	1:10:8.56
2.6	80	1:30:4.82
2.7	80	1:30:8.56
2.8	80	1:40:8.56
2.9	80	1:50:8.56
2.10	90	1:10:8.56
2.11	90	1:30:8.56
2.12	90	1:40:8.56

With large molecules, several local minima exist. To find the lowest-lying initial structure, several different relative positions were tested. Upon structural relaxation, each geometry was slightly perturbed and subjected to first-principles molecular dynamics to locate any adjacent lower minima. Moreover, after any transition state was located, a full IRC descent to the reactants was performed and further optimized. Herein, we present only global minima for the reactants, intermediates, and products.

The Microkinetic Model. The DFT-obtained reaction parameters for the reaction mechanism were cast in the microkinetic model, which assumed the following:

- negligible side reactions
- homogeneously stirred reaction mixture
- a fraction of equally reactive surface hydroxyl groups available for reaction (determined experimentally)
- batch mode operation of the ideal reactor
- no mass transfer limitations

A system of differential equations (dc/dt) describing the concentration profiles of each reaction step was solved as described in the Supporting Information, using the DFT-obtained parameters for the Arrhenius-like kinetics.

https://doi.org/10.1021/acssuschemeng.2c04686
ACS Sustainable Chem. Eng. 2022, 10, 15480−15489

ACS Sustainable Chemistry & Engineering pubs.acs.org/journal/ascecg Research Article

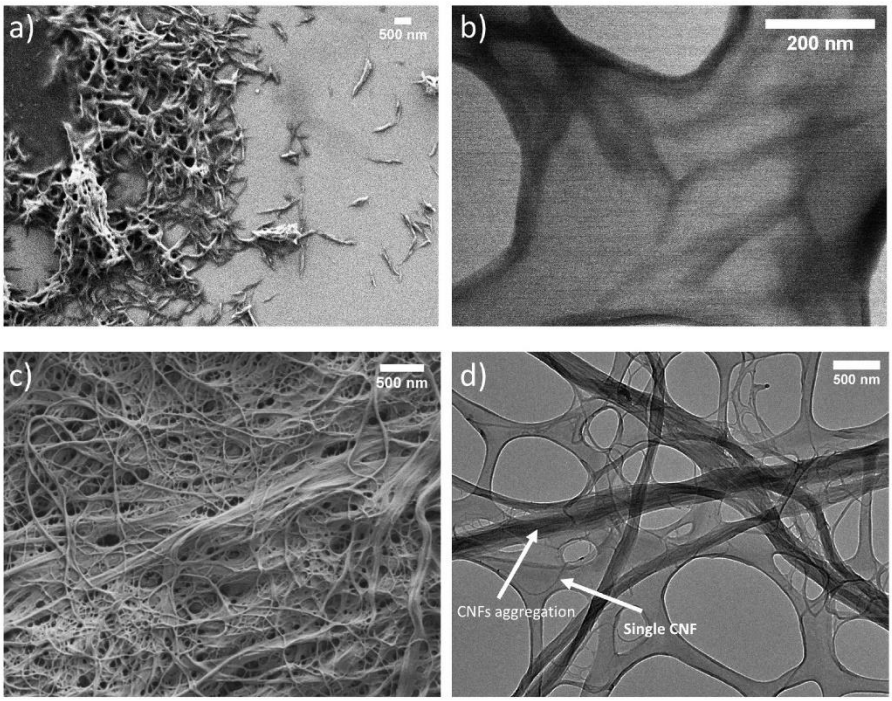

Figure 1. SEM and TEM micrographs of CNCs (a and b, respectively), SEM and TEM micrographs of CNFs (c and d, respectively).

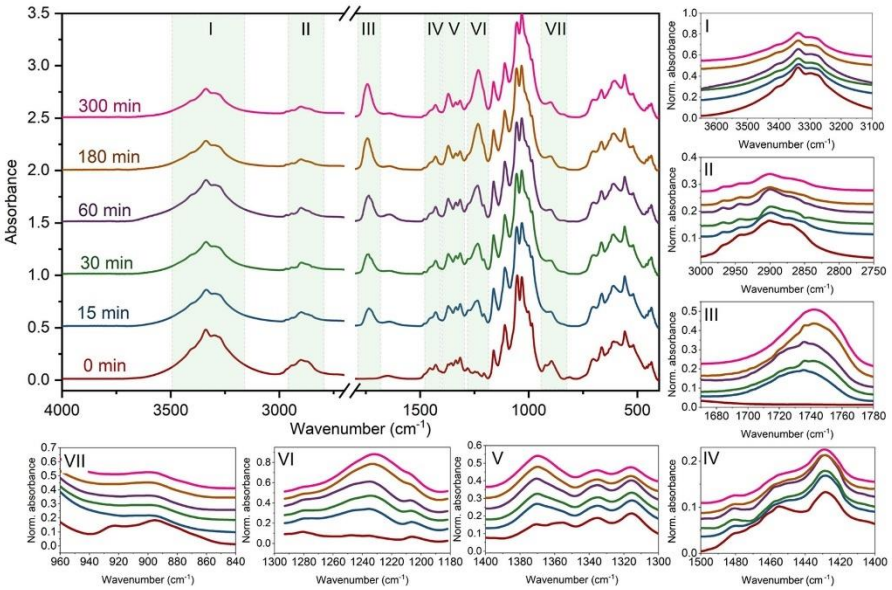

Figure 2. FT-IR spectra of unmodified and modified CNCs, with marked regions (I–VII) where change upon acetylation is observed. The peak at 1744 cm^{-1} is characteristic for acetyl bond and is proportional to acetyl content.

RESULTS AND DISCUSSION

Characterization Cellulose Nanomaterials. The morphological differences between the two tested materials were visible under SEM and TEM. The CNCs are in the form of rod-shaped particles that tend to aggregate, as visible in Figure 1a, with an average length of 294 ± 84 nm and width 11 nm ±5 nm (Figure 1b), which is in agreement with the literature.[31] On the other hand, CNFs are shaped as a long, fibrilous

https://doi.org/10.1021/acssuschemeng.2c04686
ACS Sustainable Chem. Eng. 2022, 10, 15480–15489

network with an average diameter of a single fibril being 17 nm ± 6 nm and length of more than 100 μm (Figure 1c,d). Additional TEM images with lower magnification can be found in the Supporting Information (Figure S2).

On the surface of cellulose nanomaterials, not all hydroxyl groups are accessible for reaction because of different nucleophilicity of the surface hydroxyl groups and aggregation of cellulose nanomaterials. For acetylation, the hydroxyl group on C_6 is the most reactive, followed by C_2 and C_3[44,45] (in our model, we study C_6 with cooperating adjacent C_2). The amount of accessible hydroxyl groups was determined indirectly by integrating the signals obtained by ^{31}P NMR for unreacted TMDP, internal standard NHND and water (Figure S3). The results point to higher availability of hydroxyl groups in CNCs (3.05 ± 0.075 $mmol_{OH}\ g^{-1}_{CNCs}$) than CNFs (2.7 ± 0.22 $mmol_{OH}\ g^{-1}_{CNFs}$), revealing that 16.4% of all hydroxyl groups in CNCs and 14.7% in CNFs are reactive and hence potentially available for modification, which is in agreement with the literature.[28] It has to be taken into account that the limitation of this method regarding CNFs applies as the material was freeze-dried before analysis, which could impact the hydrogen bonding and hydroxyl groups accessibility. The theoretically calculated hydroxyl groups on the surface of CNCs (calculated 17.8% of all hydroxyl groups) was in agreement with experimentally obtained values, while it was higher for CNFs (the obtained value was 28.2% of all OH groups). For the experimentally obtained value to match the theoretically calculated one, the crystallite size would have to be 8 nm. However, as previously described by Brand et al.,[28] the difference could be attributed to the agglomeration and entanglement of the fibrils, also visible in Figure 1, causing not all surface hydroxyl groups to be available for the reaction. The difference in availability of surface hydroxyl groups between the two materials can be reasoned according to differences in the morphology as CNFs are more entangled.[46]

To evaluate the structural changes upon functionalization, the treated samples were inspected with FTIR-ATR. All FTIR spectra contain the characteristic peak for cellulose, located at 1056 cm^{-1}, which remains unchanged throughout the modification. The absence of the peak positioned between 1810 and 1785 cm^{-1} corresponding to C═O stretching in acetic anhydride[47,48] points to successful elimination of reactant residues. Since there are no major differences between the materials, in Figure 2 only the time evolution of CNCs spectra is shown (see Figure S4 for ATR-FTIR spectra of CNFs).

Functionalization affects seven regions, marked with I–VII. In region I, a decline in the intensity of a broad peak between 3500 and 3150 cm^{-1}, corresponding to stretching of O–H bonds in alcohols, is observed, which indicates a substitution of hydroxyl groups. Similarly, acetylation decreases the peak around 2900 cm^{-1} (region II), which corresponds to a C–H alkane stretching, which was previously noted in the literature.[49] Regions III and VI are associated with the carbonyl C═O stretching and C–O stretching of the acetyl group, respectively, all implying an increase in the acetyl content. Furthermore, in region IV, the nonmodified sample exhibits two peaks related to H–C–H and O–C–H in-plane bending (at 1430 cm^{-1})[50] and C–H bending in the methylene group (1465 cm^{-1}), while in the modified sampled a new adjacent peak, corresponding to C–H bending in methylene group arises in-between (at 1450 cm^{-1}). C–H bending vibrations of the newly formed methyl group are also responsible for changes in spectra in region V.[49] Lastly, the peak between 940 and 860 cm^{-1} (region VII) belong to the alkane C–H bending.

A CP-MAS ^{13}C NMR analysis of pristine and functionalized CNCs (Figure 3a) and CNFs (Figure 3b) was carried out and

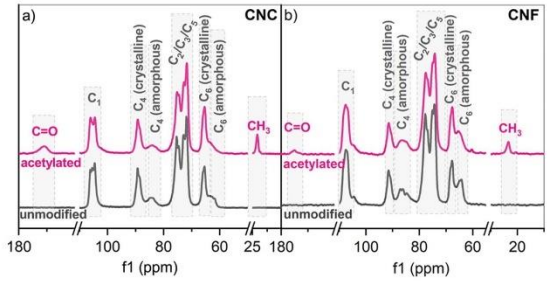

Figure 3. Representative CP MAS solid-state ^{13}C NMR spectra of (a) unmodified and acetylated CNCs (experiment 1.14); (b) unmodified and acetylated CNFs (experiment 2.7).

further confirmed successful grafting. All of the obtained spectra are characteristic for cellulose materials with well-defined peaks, corresponding to C1, C4, and C6 located at 105.7, 89.19, and 65.3 ppm for CNCs and 107.0, 91.5, and 67.6 ppm for CNFs, respectively, and overlapping signals for C2, C3, and C5 between 80–70 ppm. For CNFs, the C4 crystalline peak exhibits a lower intensity than for CNCs, pointing to lower crystallinity of CNFs, which is consistent with intrinsic properties of the materials. After the acetylation, new peaks centered at 175 and 23 ppm develop, corresponding to the C═O and CH_3 bonds, respectively, of the acetyl group. The peaks for C1 in CNCs additionally form a shoulder. No broadening of the peak for the C4 crystalline plane shows that the crystallinity does not change during the reaction.

The crystallinity of the samples was further inspected with XRD, revealing an initial 80% crystallinity in CNCs and a maximum loss of 4%, and a 77% crystallinity in CNFs with a maximum loss of 11% (Table S3 and Figures S5 & S6). Although it is reported in the literature that formation of allomorphs is possible,[51] the peak at 11.5° pointing to their existence is not present in this study.

Mechanism from First-Principles. Acetylation is generally described as a nucleophilic attack of the hydroxylic oxygen atom on the carbonylic carbon. A Lewis base, which can be pyridine, acetic anion or even water, abstracts the hydroxylic proton. The ensuing negatively charged intermediate loses an acetylic group, yielding the acetylated product. Since it is experimentally well-known that the C6 site is the most reactive for the nucleophilic attack,[44,45] we limit our theoretical investigations to the mechanism of 6OH acetylation. Electronic properties calculations (Fukui functions) showed that 2OH and 3OH are indeed less active (see Supporting Information).

This simplistic depiction is useful in predicting the reactivity of organic compounds but must be refined using quantum methods. First, we deal with the uncatalyzed reaction since no catalyst is present in our experimental setup.

During acetylation, a new C–O bond between the alcohol and acetyl forms, and a C–O bond in the acetic anhydride disintegrates. In a one-step mechanism, the rearrangements happen in a concerted fashion, while in the two-step

https://doi.org/10.1021/acssuschemeng.2c04686
ACS Sustainable Chem. Eng. 2022, 10, 15480–15489

mechanism a new bond form first and then the formed intermediate quickly decomposes. Both cases are accompanied by proton migration to any of the three oxygen atoms in the anhydride (see Figure 6).

We must also consider the involvement of the (sterically) adjacent hydroxyl groups. When the hydroxylic proton migrates, it can attach to the anhydride molecule directly or it can migrate to the neighboring hydroxylic group, whose proton moves to the anhydride. The latter transition state is lower in energy because the six- or eight-ring transition state is more stable than a four-ring transition state (*cf.* benzene and cyclobutadiene).[52] The 2-OH group from the adjacent monomeric unit is closest to the 6-OH group of the active monomeric unit (see Supporting Information). Since the energy difference between the gg, tg, and gt conformers is less than 1 kcal mol^{-1},[53] tg can transform to gg, which is sterically more accessible for the reaction with bulky nucleophiles.

Using pyridine to facilitate acetylation with acetic anhydride is analogous to the Steglich esterification,[54] where 4-(dimethylamino)pyridine[55] or imidazole[15] is used for acetylation of alcohols. We show the postulated mechanism in Figure 6. First (step 0), the acetylpyridinium (**AcPy**) ion as an active intermediate is formed in a reaction between the acetic anhydride (**AAn**) and pyridine (**Py**).[56] We calculate the activation barrier for this reaction at 34 kJ mol^{-1} acetate (**AA**) forming in the process.

The active intermediate (**AcPy**) then reacts with an accessible cellulose hydroxyl group. If its proton is transferred to the pyridinium nitrogen, the acetylation proceeds in one step (step 1) and yields acetylcellulose (**AC**) and a pyridinium ion (**PyH**). The proton is not directly transferred to the nitrogen atom, which would entail a barrier of >100 kJ mol^{-1} (not shown). Instead, the hydroxyl group from the adjacent monomeric unit chaperons the reaction, as depicted in Figure 4 in an exothermic reaction (ΔE = −78 kJ mol^{-1}) with an activation barrier of 56 kJ mol^{-1}.

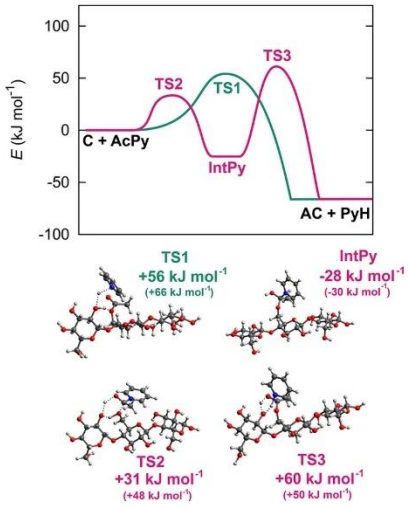

Figure 4. (top) Potential energy surface for acetylpyridinium-mediated acetylation of cellulose, and (bottom) intermediate and transition states with energies and Gibbs free energies (in parentheses) written. Note that the values are relative to **C** + **AcPy**.

This is expected since a direct proton transfer would occur in a four-member ring transition state, which is sterically strained. When an adjacent OH group participates, the transition state assumes a single-member ring structure, which is energetically more favorable. A similar effect was observed by Lawal et al.[52]

Alternatively, the hydroxylic proton atom can first bind to the carbonylic oxygen atom of the acetylpyridinium. This reaction step has a lower barrier (31 kJ mol^{-1}), producing an intermediate (**IntPy**) (step 2), which decomposes into acetylcellulose (**AC**) and a pyridinium ion (**PyH**) (step 3) after overcoming a barrier of 88 kJ mol^{-1}. Both proton transfers are mediated by a hydroxyl group from the adjacent monomeric unit (Figure 4).

Since **Py** and **PyH** quickly interconvert with acetic acid **AAH**/**AA** in a acid−base proton exchange, they are not differentiated in the model.

The activation barrier of the first step in the two-step mechanism is lower than that of the one-step mechanism, which is not true for the second step. Hence, both mechanisms must be accounted for in a microkinetic model. The calculated thermodynamic and kinetic parameters are summarized in Table 2 and used in the microkinetic model.

Table 2. Kinetic Parameters of the Elementary Reaction Steps as Labeled in Figure 6 as Determined by DFT and Refined by Regression Analysis of the Microkinetic Model

	DFT		Regression analysis	
Reaction step	ΔE(kJ mol^{-1})	E_a(kJ mol^{-1})	E_a(kJ mol^{-1})	A (s^{-1})
0	+32	34	33.5	1.56×10^{07}
1	−78	56	50.4	1.55×10^{04}
2	−28	31	34.1	6.06×10^{01}
3	−50	88	79.2	6.28×10^{06}

The reported values are from simulations using pyridine as the solvent in the SMD model. Additionally, the most probable reaction pathway was modeled using toluene as the solvent to ascertain if there is a noticeable difference in a pyridine/toluene mixture, which was used for CNFs. The toluene-calculated values were negligibly different (≤5%), which is expected because both solvents are rather apolar. This difference is smaller than the subsequent refinement of the DFT values in the regression analysis of the kinetic model and can thus be ignored.

Kinetics and Modeling. The acetyl content in the cellulose nanomaterials, from the ATR-FTIR spectra, was evaluated for varying reaction time and temperature, and reactants ratio. To eliminate the effect of transport on the acetylation, three mixing rates and different durations of CNCs pretreatment were tested. The obtained results are presented and discussed in Figures S7−S9.

CNCs generally allowed for a higher degree of acetylation under the same conditions compared to CNFs, as seen in Figure 5, which is consistent with a higher availability of hydroxyl groups for the reaction on the surface; however, dilution due to the presence of a solvent (toluene) in CNFs acetylation has to be taken into account. The grafting efficiency increases with the reaction temperature in CNCs modification, and the highest acetyl content was obtained at 90 °C (94% of the hydroxyl groups accessible for reaction, experiment 1.12). To the contrary, 70 °C was shown to be optimal for the acetylation of CNFs, reaching 72% of accessible hydroxyl

https://doi.org/10.1021/acssuschemeng.2c04686
ACS Sustainable Chem. Eng. 2022, 10, 15480−15489

ACS Sustainable Chemistry & Engineering pubs.acs.org/journal/ascecg Research Article

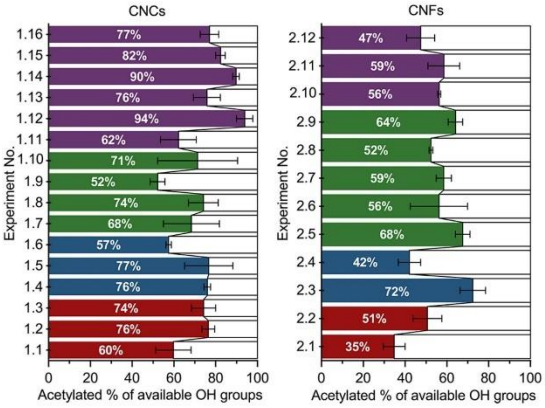

Figure 5. Proportion of acetylated groups relative to accessible hydroxyl groups on the surface, as determined in this study. The experiment numbers refer to Table 1. For clarity, bars are color-coded: red (60 °C), blue (70 °C), green (80 °C), violet (90 °C).

groups (experiment 2.3), while the acetyl content began to decrease with higher temperature (2.5−2.12), which could be attributed to the temperature approaching the boiling point of the solvent toluene (110.6 °C). As the role of toluene is to prevent aggregation of fibers, its shift to gaseous phase might cause lower availability of hydroxyl groups on the surface. Further testing of different reactant ratios (between concentrations of acetic anhydride and pyridine relative to cellulose nanomaterial) revealed the negative influence of higher pyridine concentration for the acetylation of CNCs, due to the dilution of the reaction media and consequent shift of the dependency of the reaction rate onto the reactant transfer to the surface of cellulose nanomaterials (experiments 1.5, 1.6, 1.8, 1.9, 1.14, 1.15, 1.16). On the other hand, an increase in the relative concentration of acetic anhydride improves esterification (1.13, 1.14, 2.6, 2.7).

Using microkinetic modeling with DFT input, reaction kinetic constants and activation energies for the individual functionalization steps on the cellulose nanomaterials surface were obtained. The microkinetic model was constructed as a system of differential equations (see Supporting Information), describing the reactions from the mechanism, shown in Figure 6.

The reaction rate is the highest in the first 60 min and then plateaus, regardless of the cellulose nanomaterial or the conditions used (Figure 7). An increase in the amount of pyridine added to the reaction mixture adversely affects the initial reaction rate for CNCs surface modification, indicating that the kinetics is controlled by the acetic anhydride concentration. However, this effect is not as noticeable during CNFs functionalization. At longer reaction times, a slight decrease in the acetyl content in CNFs was observed in experiments with AGU:pyridine ratio 1:30 (experiments 2.1, 2.6, and 2.11), indicating that the overall reaction might be reversible in the presence of the solvent, which has been proposed by Chunilall et al.[57]

While DFT-derived data were used as an initial guess for the microkinetic model, the inherent approximations in the model mean that they should be further refined for a problem at hand. Using regression analysis, as described in a previous section, we obtained the optimized values which are listed in Table 2. Additionally, the temperature-independent pre-exponential factors (A_i) were back-calculated from the determined (temperature-dependent) reaction rates and (temperature-independent) activation barriers. The values for a single-step reaction reported in the literature are slightly lower (41.6 and 39 kJ mol^{-1}); however, the acetylation was carried out on wood blocks.[24,58]

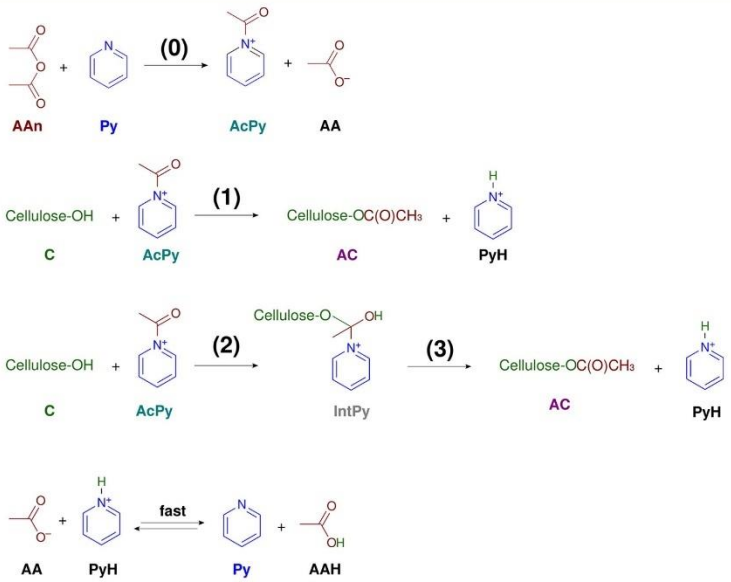

Figure 6. Mechanism of pyridine-mediated acetylation with acetic anhydride with labeled relevant reaction steps (0−3) and fast interconversion of **PyH** and **Py** that is not differentiated in the model.

https://doi.org/10.1021/acssuschemeng.2c04686
ACS Sustainable Chem. Eng. 2022, 10, 15480−15489

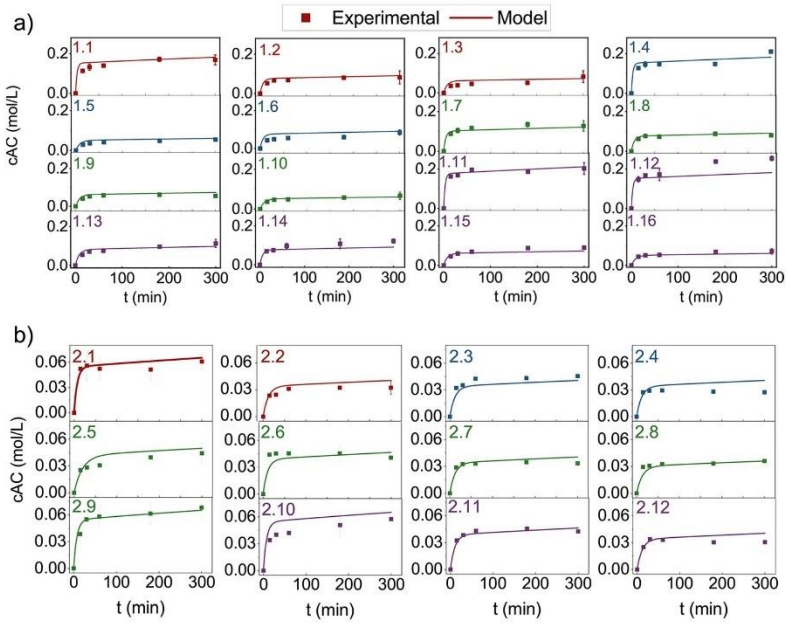

Figure 7. Experimental and model values of (a) CNCs acetylation and (b) CNFs acetylation. The plots are color-coded by temperature: red (60 °C), blue (70 °C), green (80 °C), violet (90 °C).

CONCLUSIONS

In this work, the hypothesis of a revised mechanism for acetylation of two cellulose nanomaterials (CNCs and CNFs) with acetic anhydride in the presence of pyridine was confirmed. Computation suggested that the reactions proceeds via two competitive mechanisms. The active species (acetylpyridinium ion) must first form, which then reacts with accessible cellulose hydroxyl groups. The calculated kinetic parameters (activation barriers) served as a skeleton for the developed microkinetic model, which described the experimental results and, through regression analysis, honed in on the true kinetic parameters.

ASSOCIATED CONTENT

Supporting Information

The Supporting Information is available free of charge at https://pubs.acs.org/doi/10.1021/acssuschemeng.2c04686.

Additional experimental methods, characterization (^{31}P NMR, FTIR, XRD, degrees of substitution, surface free energy) and detailed explanation of the kinetic model (PDF)

AUTHOR INFORMATION

Corresponding Author

Uroš Novak − *Department of Catalysis, Chemical Reaction Engineering, SI-1000 Ljubljana, Slovenia;* orcid.org/0000-0003-0561-8427; Phone: +386 (0)1 4760 283; Email: uros.novak@ki.si

Authors

Ana Oberlintner − *Department of Catalysis, Chemical Reaction Engineering, SI-1000 Ljubljana, Slovenia; Jožef Stefan International Postgraduate School, SI-1000 Ljubljana, Slovenia*

Matej Huš − *Department of Catalysis, Chemical Reaction Engineering, SI-1000 Ljubljana, Slovenia; Association for Technical Culture of Slovenia (ZOTKS), SI-1000 Ljubljana, Slovenia; University of Nova Gorica, SI-5000 Nova Gorica, Slovenia;* orcid.org/0000-0002-8318-5121

Blaž Likozar − *Department of Catalysis, Chemical Reaction Engineering, SI-1000 Ljubljana, Slovenia;* orcid.org/0000-0001-7226-4302

Complete contact information is available at: https://pubs.acs.org/10.1021/acssuschemeng.2c04686

Notes

The authors declare no competing financial interest.

ACKNOWLEDGMENTS

Sappi is acknowledged for the generous donation of Valida S. The authors are grateful to Dr. Anže Prašnikar for SEM imaging, Dr. Goran Dražić for TEM imaging, and Žan Lavrič for help with the microkinetic model development. This research was funded by a Ph.D. grant from the Slovenian Research Agency (Ana Oberlintner). M.H. thanks the Slovenian Research Agency (project funding J1-3020, core funding P2-0421, infrastructure funding I0-0039). The authors also acknowledge the financial support from the Slovenian Research Agency (research core funding No. P2-0152).

REFERENCES

(1) Lv, D.; Du, H.; Che, X.; Wu, M.; Zhang, Y.; Liu, C.; Nie, S.; Zhang, X.; Li, B. Tailored and Integrated Production of Functional Cellulose Nanocrystals and Cellulose Nanofibrils via Sustainable Formic Acid Hydrolysis: Kinetic Study and Characterization. *ACS Sustainable Chem. Eng.* **2019**, *7*, 9449−9463.

(2) *Sandard Terms and Their Definition for Cellulose Nanomaterial*; TAPPI, 2022; https://www.tappi.org/content/hide/draft3.pdf.
(3) Gamelas, J. A.; Pedrosa, J.; Lourenço, A. F.; Mutjé, P.; González, I.; Chinga-Carrasco, G.; Singh, G.; Ferreira, P. J. On the morphology of cellulose nanofibrils obtained by TEMPO-mediated oxidation and mechanical treatment. *Micron* **2015**, *72*, 28−33.
(4) Heinze, T. Cellulose: Structure and Properties. *Cellulose Chemistry and Properties: Fibers, Nanocelluloses and Advanced Materials. Advances in Polymer Science* **2016**, *271*, 1−52.
(5) Habibi, Y.; Lucia, L. A.; Rojas, O. J. Cellulose Nanocrystals: Chemistry, Self-Assembly, and Applications. *Chem. Rev.* **2010**, *110*, 3479−3500.
(6) Tardy, B. L.; Mattos, B. D.; Otoni, C. G.; Beaumont, M.; Majoinen, J.; Kämäräinen, T.; Rojas, O. J. Deconstruction and Reassembly of Renewable Polymers and Biocolloids into Next Generation Structured Materials. *Chem. Rev.* **2021**, *121*, 14088−14188.
(7) Wickholm, K.; Larsson, P. T.; Iversen, T. Assignment of non-crystalline forms in cellulose I by CP/MAS 13C NMR spectroscopy. *Carbohydr. Res.* **1998**, *312*, 123−129.
(8) Miao, C.; Hamad, W. Y. Cellulose reinforced polymer composites and nanocomposites: a critical review. *Cellulose* **2013**, *20*, 2221−2262.
(9) Oksman, K.; Aitomäki, Y.; Mathew, A. P.; Siqueira, G.; Zhou, Q.; Butylina, S.; Tanpichai, S.; Zhou, X.; Hooshmand, S. Review of the recent developments in cellulose nanocomposite processing. *Composites Part A: Applied Science and Manufacturing* **2016**, *83*, 2−18. Special Issue on Biocomposites
(10) Shojaeiarani, J.; Bajwa, D. S.; Stark, N. M. Green esterification: A new approach to improve thermal and mechanical properties of poly(lactic acid) composites reinforced by cellulose nanocrystals. *J. Appl. Polym. Sci.* **2018**, *135*, 46468.
(11) Espino-Pérez, E.; Domenek, S.; Belgacem, N.; Sillard, C.; Bras, J. Green process for chemical functionalization of nanocellulose with carboxylic acids. *Biomacromolecules* **2014**, *15*, 4551−4560.
(12) Wang, L.; Gardner, D. J.; Wang, J.; Yang, Y.; Tekinalp, H. L.; Tajvidi, M.; Li, K.; Zhao, X.; Neivandt, D. J.; Han, Y.; Ozcan, S.; Anderson, J. Towards industrial-scale production of cellulose nanocomposites using melt processing: A critical review on structure-processing-property relationships. *Composites Part B: Engineering* **2020**, *201*, 108297.
(13) Eyley, S.; Thielemans, W. Imidazolium grafted cellulose nanocrystals for ion exchange applications. *Chem. Commun.* **2011**, *47*, 4177−4179.
(14) Sèbe, G.; Ham-Pichavant, F.; Pecastaings, G. Dispersibility and Emulsion-Stabilizing Effect of Cellulose Nanowhiskers Esterified by Vinyl Acetate and Vinyl Cinnamate. *Biomacromolecules* **2013**, *14*, 2937−2944.
(15) Beaumont, M.; Jusner, P.; Gierlinger, N.; King, A. W. T.; Potthast, A.; Rojas, O. J.; Rosenau, T. Unique reactivity of nanoporous cellulosic materials mediated by surface-confined water. *Nat. Commun.* **2021**, *12*, 2513.
(16) Beaumont, M.; Tardy, B. L.; Reyes, G.; Koso, T. V.; Schaubmayr, E.; Jusner, P.; King, A. W. T.; Dagastine, R. R.; Potthast, A.; Rojas, O. J.; Rosenau, T. Assembling Native Elementary Cellulose Nanofibrils via a Reversible and Regioselective Surface Functionalization. *J. Am. Chem. Soc.* **2021**, *143*, 17040−17046.
(17) Ávila Ramírez, J. A.; Fortunati, E.; Kenny, J. M.; Torre, L.; Foresti, M. L. Simple citric acid-catalyzed surface esterification of cellulose nanocrystals. *Carbohydr. Polym.* **2017**, *157*, 1358−1364.
(18) Lin, N.; Huang, J.; Chang, P. R.; Feng, J.; Yu, J. Surface acetylation of cellulose nanocrystal and its reinforcing function in poly(lactic acid). *Carbohydr. Polym.* **2011**, *83*, 1834−1842.
(19) Jamaluddin, N.; Kanno, T.; Asoh, T.-A.; Uyama, H. Surface modification of cellulose nanofiber using acid anhydride for poly(lactic acid) reinforcement. *Materials Today Communications* **2019**, *21*, 100587.
(20) Swartz, J. L.; Li, R. L.; Dichtel, W. R. Incorporating Functionalized Cellulose to Increase the Toughness of Covalent Adaptable Networks. *ACS Appl. Mater. Interfaces* **2020**, *12*, 44110−44116.
(21) Sulbarán-Rangel, B.; Diaz, A. J. H.; Guzmán, A. C. G.; Rojas, O. J. Partially acetylated cellulose nanofibrils from Agave tequilana bagasse and Pickering stabilization. *J. Dispersion Sci. Technol.* **2022**, 1−9.
(22) Oberlintner, A.; Likozar, B.; Novak, U. Hydrophobic functionalization reactions of structured cellulose nanomaterials: Mechanisms, kinetics and in silico multi-scale models. *Carbohydr. Polym.* **2021**, *259*, 117742.
(23) Chen, M.; Li, R.-M.; Runge, T.; Feng, J.; Feng, J.; Hu, S.; Shi, Q.-S. Solvent-Free Acetylation of Cellulose by 1-Ethyl-3-methylimidazolium Acetate-Catalyzed Transesterification. *ACS Sustainable Chem. Eng.* **2019**, *7*, 16971−16978.
(24) Minato, K.; Ito, Y. Analysis of the factors influencing the acetylation rate of wood. *Journal of Wood Science* **2004**, *50*, 519−523.
(25) Luo, P.; Cao, C.; Liang, Y.; Ma, X.; Xin, C.; Jiao, Z.; Cao, J.; Zhang, J. Kinetic Study of the Acetylation of Cotton Linter Pulp. *BioResources* **2013**, *8*, 2708−2718.
(26) Ramsden, M. J.; Blake, F. S. R.; Fey, N. J. The effect of acetylation on the mechanical properties, hydrophobicity, and dimensional stability ofPinus sylvestris. *Wood Science and Technology* **1997**, *31*, 97−104.
(27) Kanematsu, Y.; Kikuchi, Y.; Yano, H. Life Cycle Greenhouse Gas Emissions of Acetylated Cellulose Nanofiber-Reinforced Polylactic Acid Based on Scale-Up from Lab-Scale Experiments. *ACS Sustainable Chem. Eng.* **2021**, *9*, 10444−10452.
(28) Brand, J.; Pecastaings, G.; Sèbe, G. A versatile method for the surface tailoring of cellulose nanocrystal building blocks by acylation with functional vinyl esters. *Carbohydr. Polym.* **2017**, *169*, 189−197.
(29) Peng, Y.; Gardner, D. J.; Han, Y.; Kiziltas, A.; Cai, Z.; Tshabalala, M. A. Influence of drying method on the material properties of nanocellulose I: thermostability and crystallinity. *Cellulose* **2013**, *20*, 2379−2392.
(30) Segal, L.; Creely, J. J.; Martin, J. A.; Conrad, C. M. An Empirical Method for Estimating the Degree of Crystallinity of Native Cellulose Using the X-Ray Diffractometer. *Text. Res. J.* **1959**, *29*, 786−794.
(31) Kunaver, M.; Anžlovar, A.; Žagar, E. The fast and effective isolation of nanocellulose from selected cellulosic feedstocks. *Carbohydr. Polym.* **2016**, *148*, 251−258.
(32) Tingaut, P.; Zimmermann, T.; Lopez-Suevos, F. Synthesis and characterization of bionanocomposites with tunable properties from poly(lactic acid) and acetylated microfibrillated cellulose. *Biomacromolecules* **2010**, *11*, 454−464.
(33) Valiev, M.; Bylaska, E.J.; Govind, N.; Kowalski, K.; Straatsma, T.P.; Van Dam, H.J.J.; Wang, D.; Nieplocha, J.; Apra, E.; Windus, T.L.; de Jong, W.A. NWChem: A comprehensive and scalable open-source solution for large scale molecular simulations. *Comput. Phys. Commun.* **2010**, *181*, 1477−1489.
(34) Zhao, Y.; Truhlar, D. G. The M06 suite of density functionals for main group thermochemistry, thermochemical kinetics, noncovalent interactions, excited states, and transition elements: two new functionals and systematic testing of four M06-class functionals and 12 other function. *Theor. Chem. Acc.* **2008**, *120*, 215−241.
(35) Krishnan, R.; Binkley, J. S.; Seeger, R.; Pople, J. A. Self-consistent molecular orbital methods. XX. A basis set for correlated wave functions. *J. Chem. Phys.* **1980**, *72*, 650−654.
(36) Clark, T.; Chandrasekhar, J.; Spitznagel, G. W.; Schleyer, P. V. R. Efficient diffuse function-augmented basis sets for anion calculations. III. The 3-21+G basis set for first-row elements, Li−F. *J. Comput. Chem.* **1983**, *4*, 294−301.
(37) Frisch, M. J.; Pople, J. A.; Binkley, J. S. Self-consistent molecular orbital methods 25. Supplementary functions for Gaussian basis sets. *J. Chem. Phys.* **1984**, *80*, 3265−3269.
(38) McLean, A. D.; Chandler, G. S. Contracted Gaussian basis sets for molecular calculations. I. Second row atoms, Z = 11−18. *J. Chem. Phys.* **1980**, *72*, 5639−5648.

https://doi.org/10.1021/acssuschemeng.2c04686
ACS Sustainable Chem. Eng. 2022, 10, 15480−15489

(39) Walker, M.; Harvey, A. J. A.; Sen, A.; Dessent, C. E. H. Performance of M06, M06-2X, and M06-HF Density Functionals for Conformationally Flexible Anionic Clusters: M06 Functionals Perform Better than B3LYP for a Model System with Dispersion and Ionic Hydrogen-Bonding Interactions. *J. Phys. Chem. A* **2013**, *117*, 12590−12600.
(40) Marenich, A. V.; Cramer, C. J.; Truhlar, D. G. Universal Solvation Model Based on Solute Electron Density and on a Continuum Model of the Solvent Defined by the Bulk Dielectric Constant and Atomic Surface Tensions. *J. Phys. Chem. B* **2009**, *113*, 6378−6396.
(41) Zarkevich, N. A.; Johnson, D. D. Nudged-elastic band method with two climbing images: Finding transition states in complex energy landscapes. *J. Chem. Phys.* **2015**, *142*, 24106.
(42) Ponnuchamy, V.; Sandak, A.; Sandak, J. Multiscale modelling investigation of wood modification with acetic anhydride. *Phys. Chem. Chem. Phys.* **2020**, *22*, 28448−28458.
(43) Paajanen, A.; Ceccherini, S.; Maloney, T.; Ketoja, J. A. Chirality and bound water in the hierarchical cellulose structure. *Cellulose* **2019**, *26*, 5877−5892.
(44) Goodlett, V. W.; Dougherty, J. T.; Patton, H. W. Characterization of cellulose acetates by nuclear magnetic resonance. *Journal of Polymer Science Part A-1: Polymer Chemistry* **1971**, *9*, 155−161.
(45) Miyamoto, T.; Sato, Y.; Shibata, T.; Tanahashi, M.; Inagaki, H. 13C-NMR spectral studies on the distribution of substituents in water-soluble cellulose acetate. *Journal of Polymer Science: Polymer Chemistry Edition* **1985**, *23*, 1373−1381.
(46) Doyle, S.; Pethrick, R. A.; Harris, R. K.; Lane, J. M.; Packer, K. J.; Heatley, F. 13C nuclear magnetic resonance studies of cellulose acetate in the solution and solid states. *Polymer* **1986**, *27*, 19−24.
(47) Wallace, E. W. Infrared Spectra by NIST Mass Spectrometry Data Center. https://www.nist.gov/mml/biomolecular-measurement/mass-spectrometry-data-center, 2022.
(48) Muhammad Djuned, F.; Asad, M.; Mohamad Ibrahim, M. N.; Wan Daud, W. R. Synthesis and Characterization of Cellulose Acetate from TCF Oil Palm Empty Fruit Bunch Pulp. *BioResources* **2014**, *9*, 4710−4721.
(49) Fei, P.; Liao, L.; Cheng, B.; Song, J. Quantitative analysis of cellulose acetate with a high degree of substitution by FTIR and its application. *Analytical Methods* **2017**, *9*, 6194−6201.
(50) Proniewicz, L. M.; Paluszkiewicz, C.; Wesełucha-Birczyńska, A.; Majcherczyk, H.; Barański, A.; Konieczna, A. FT-IR and FT-Raman study of hydrothermally degradated cellulose. *J. Mol. Struct.* **2001**, *596*, 163−169.
(51) Operamolla, A.; Casalini, S.; Console, D.; Capodieci, L.; Di Benedetto, F.; Bianco, G. V.; Babudri, F. Tailoring water stability of cellulose nanopaper by surface functionalization. *Soft Matter* **2018**, *14*, 7390−7400.
(52) Lawal, M. M.; Govender, T.; Maguire, G. E. M.; Honarparvar, B.; Kruger, H. G. Mechanistic investigation of the uncatalyzed esterification reaction of acetic acid and acid halides with methanol: a DFT study. *J. Mol. Model.* **2016**, *22*, 235.
(53) Klewinghaus, P.; van Eijck, B. P.; Kouwijzer, M. L. C. E.; Kroon, J. Molecular dynamics study of conformational equilibria in aqueous d-glucose and d-galactose. *Journal of Molecular Structure: THEOCHEM* **1997**, *395*−*396*, 289−295.
(54) Neises, B.; Steglich, W. Simple Method for the Esterification of Carboxylic Acids. *Angewandte Chemie International Edition in English* **1978**, *17*, 522−524.
(55) Xu, S.; Held, I.; Kempf, B.; Mayr, H.; Steglich, W.; Zipse, H. The DMAP-Catalyzed Acetylation of Alcohols—A Mechanistic Study (DMAP = 4-(Dimethylamino)pyridine). *Chem. Eur. J.* **2005**, *11*, 4751−4757.
(56) Fersht, A. R.; Jencks, W. P. Acetylpyridinium ion intermediate in pyridine-catalyzed acyl transfer. *J. Am. Chem. Soc.* **1969**, *91*, 2125−2126.
(57) Chunilall, V.; Bush, T.; Larsson, P. T.; Iversen, T.; Kindness, A. A CP/MAS 13C-NMR study of cellulose fibril aggregation in eucalyptus dissolving pulps during drying and the correlation between aggregate dimensions and chemical reactivity. *Holzforschung* **2010**, *64*, 693−698.
(58) Hill, C. A. S.; Jones, D.; Strickland, G.; Cetin, N. S. Kinetic and Mechanistic Aspects of the Acetylation of Wood with Acetic Anhydride. *Holzforschung* **1998**, *52*, 623−629.

https://doi.org/10.1021/acssuschemeng.2c04686
ACS Sustainable Chem. Eng. 2022, 10, 15480−15489

Supporting Information

Multiscale Study of Functional Acetylation of Cellulose Nanomaterials by Design: *Ab Initio* Mechanisms and Chemical Reaction Microkinetics

Ana Oberlintner[a,b], Matej Huš[a,c,d], Blaž Likozar[a], Uroš Novak[a,*]

[a]Department of Catalysis and Reaction Engineering, National Institue of Chemistry, Hajdrihova 19, SI-1000 Ljubljana, Slovenia
[b]International Postgraduate School Jožef Stefan, Jamova cesta 39, SI-1000 Ljubljana, Slovenia
[c]Assosiation or Techical Culture of Slovenia (ZOTKS), Zaloška 64, SI-1000 Ljubljana, Slovenia
[d]University of Nova Gorica, Vipavska 13, SI-5000 Nova Gorica, Slovenia
*Corresponding author: uros.novak@ki.si

Number of pages: 12
Number of figures: 9
Number of tables: 5

1 Additional experimental information

1.1 Additionally tested parameters

Table S1: Additionally tested parameters, varying mixing rate, pretreatment duration (CNCs only) and absence of pyridine.

Material	Experiment No.	AGU:Pyridine: Acetic anhydride	Comments
CNC	3.1	1.00 : 0.00 : 17.12	350 rpm, T = 90 °C
CNC	3.2	1.00 : 40.00 : 8.56	350 rpm, 3 min pretreatment
CNC	3.3	1.00 : 40.00 : 8.56	550 rpm, 3 min pretreatment
CNC	3.4	1.00 : 40.00 : 8.56	550 rpm, 5 min pretreatment
CNF	3.5	1.00 : 0.00 : 17.12	350 rpm, T = 80 °C
CNF	3.6	1.00: 40.00 : 8.56	350 rpm
CNF	3.7	1.00: 40.00 : 8.56	500 rpm

1.2 Acetylation of cellulose nanomaterials

For CNCs acetylation 0.5 g of freeze dried CNCs were crushed in a mortar for 3 min to homogeneous powder, transferred into a round-bottom reactor equipped with a magnetic stirrer and water-cooled reflux. After adding an appropriate amount of pyridine and performing sonication for 15 minutes, the mixture was heated to the desired temperature under a nitrogen flow while stirred at 350 rpm. Some adjustments regarding mixing (500 rpm and 550 rpm for CNCs and CNFs, respectively) and CNC particle size (5 min crushing in a mortar) size were performed to observe the impact of these parameters on the reaction kinetics).

To acetylate CNFs, the appropriate amount of 3 wt % water dispersed CNFs to reach the final amount of biopolymer mass of 0.5 g was solvent exchanged to acetone in three successive centrifugation cycles (10 min, 4500 rpm) and then finally to toluene through last centrifugation cycle (10 min, 4500 rpm). The CNFs were transferred to the reactor with 5 mL of toluene. The required volume of pyridine was added and the mixture was heated to the desired temperature under nitrogen flow while stirred at 300 rpm. The acetic anhydride was added drop-wise when functionalizing all materials. After the reaction, the samples were washed in three consequent washing steps with water and finally with a water/acetone solution. The samples were then freeze-dried and kept at 4 °C for further analyses. All experiments were carried out in parallels.

1.3 Determination of acetyl content through titration method

The accuracy of the method was confirmed by determination of acetyl content through a standard saponification method [1]. Briefly, approximately 0.1 g of the sample was analytically weighted into an Erlenmeyer flask, 4 mL of 75 wt % ethanol was added and stirred on a magnetic stirrer in an oil bath at 60 °C. After 30 min, 4 mL of 0.5 M NaOH was added and further stirred at 60 °C for 15 min. The flasks were left on the counter to rest for 72 hours and then titrated with 9.5 M HCl after addition of phenolphthalein indicator. Another 0.1 mL of HCl (0.5 M) was added and the flasks were again left on the counter to rest for another 24 hours. Lastly, they were titrated with NaOH (0.5 M). Acetyl content was evaluated through Equation S1:

$$\%\,Acetyl = [(B_{HCl} - V_{HCl})\,x\,N_{HCl} + (V_{NaOH} - B_{NaOH})\,x\,N_{NaOH}]\,x\,\frac{4.305}{m} \qquad \textit{Equation S1}$$

B_{HCl} and B_{NaOH} present volume of the titrated HCl and NaOH in blank sample in mL, V_{HCl} and V_{NaOH} present volume of the titrated HCl and NaOH in the tested sample in mL, while N_{HCl} and N_{NaOH} stand for molarity of the HCl and NaOH solution, respectively. m denotes mass of the weighted sample in grams.

1.4 Determination of surface free energy

To evaluate the surface free energy, samples from three different experiments (1.1, 1.10, 1.15) with various DS (0, 0.29, 0.35 and 0.40, respectively) were pressed into the tablets with force of 100 kN. Contact angles with water, diiodomethane and formamide were measured with Tensiometer Theta T200 (Biolin Scientific, Germany), the size of a droplet was 2 µL. Surface free energy was calculated according to the van Oss model [2].

1.5 The quantum model

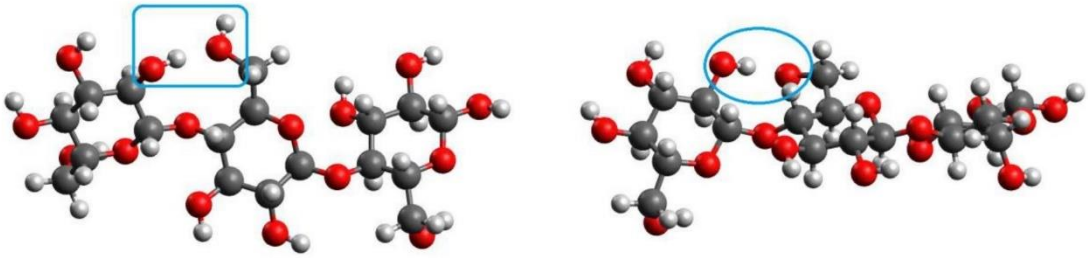

Figure S1: The top and side view of cellotriose used in quantum calculations as a model of cellulose. The cooperating hydroxyl group (C2-OH) from the adjacent monomeric unit is delineated in blue.

1.6 Reactivity of OH groups in the cellotriose model

It is experimentally known that C6 is most reactive[3,4]. To make sure that the model reproduces this fact, considering that the reaction mechanism is complex and several elementary steps can produce the same product (C2-, C3-, and C6-acetylated cellotriose), Fukui functions and Mulliken atomic charges were used as proxies for the reactivity of different sites (O2, O3, O6).

Table S2: Reactivity of different OH groups in cellotriose, as determined by Mulliken charge and Fukui functions for electrophilic and nucleophilic attack (calculated on the hydroxyl oxygen atom).

Acetylation site	Mulliken charge	f+	f-
C2	-0.63	-0.0029	0.0004
C3	-0.63	-0.0101	0.0014
C6	**-0.65**	**-0.0168**	**0.0024**

2 Supplementary results

2.1 Morphology of the cellulose nanomaterials

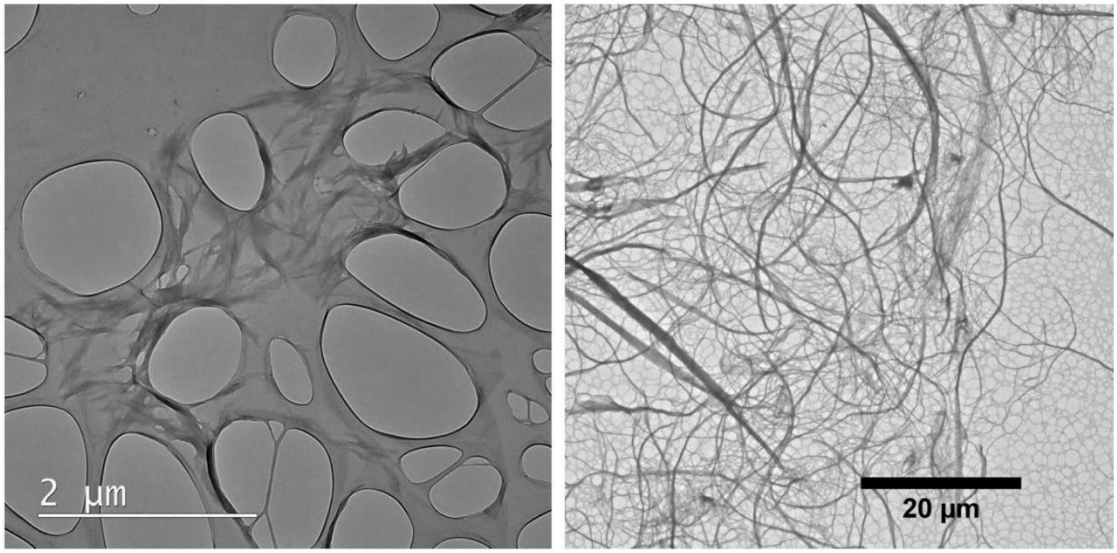

Figure S2: TEM images of CNCs (left) and CNFs (right).

2.2 Experimental determination of surface hydroxyl groups availability

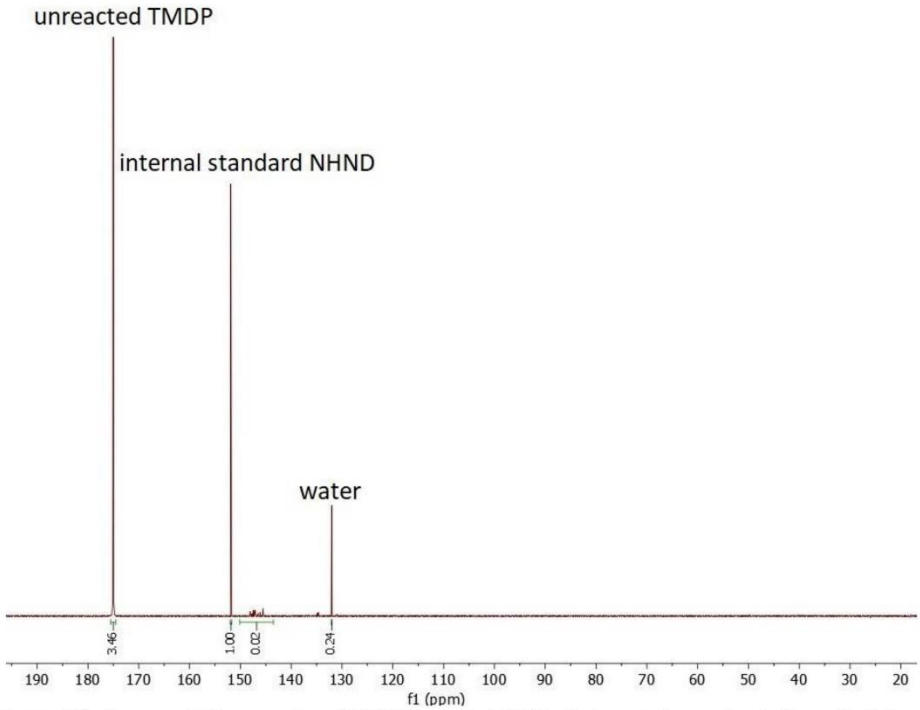

Figure S3: Representative spectra of TMDP-reacted CNFs that served as a basis for calculation of surface hydroxyl groups' availability

2.2 Fourier Transformation Infrared Spectroscopy of cellulose nanofibrils

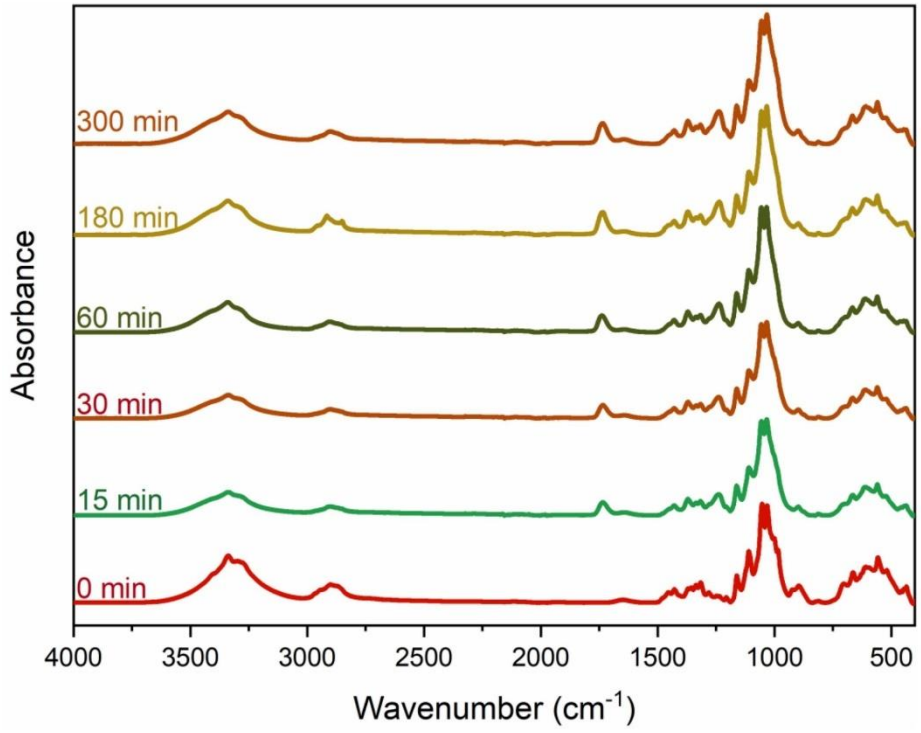

Figure S4: Representative spectra of acetylation time-evolution of CNFs.

Accuracy of ATR-FTIR method was confirmed to be suitable through titration method. The obtained value was in accordance to the acetyl content obtained through FT-IR calculations with discrepancy of 0.78 %.

2.3 X-Ray Powder Diffraction

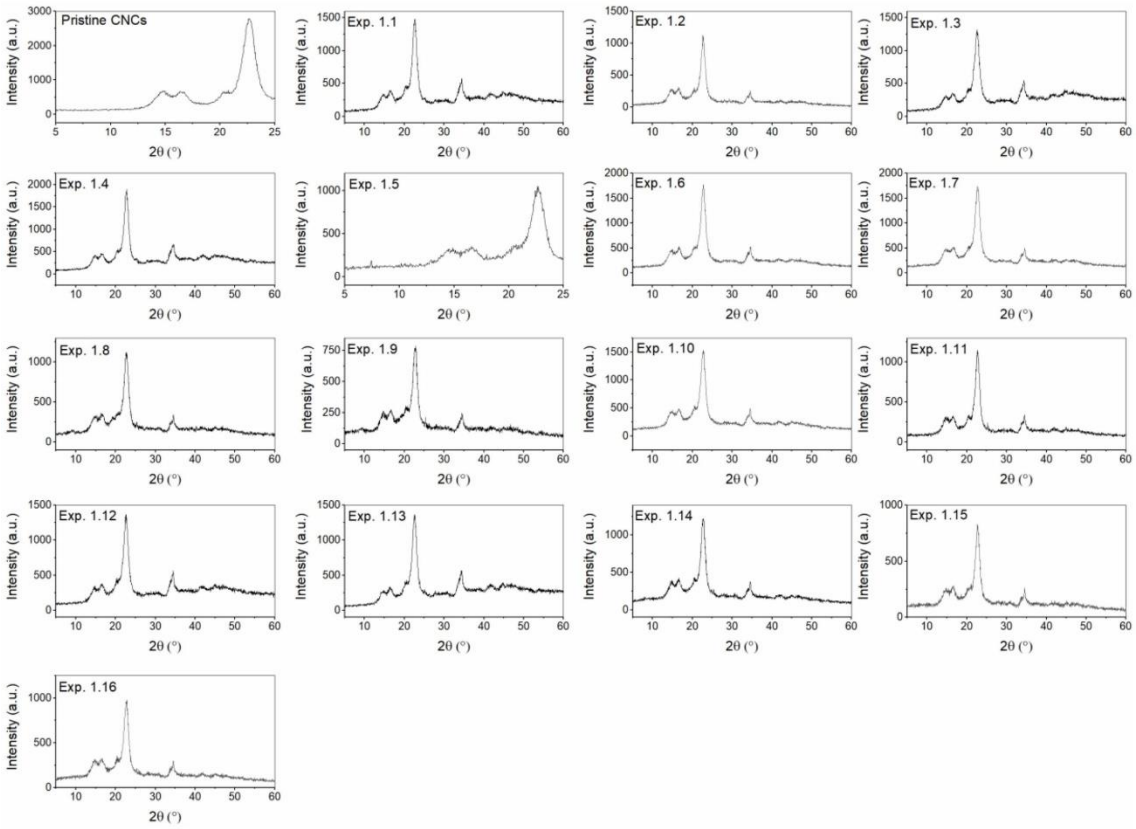

Figure S5: XRD spectra of pristine and modified CNCs for all performed experiments.

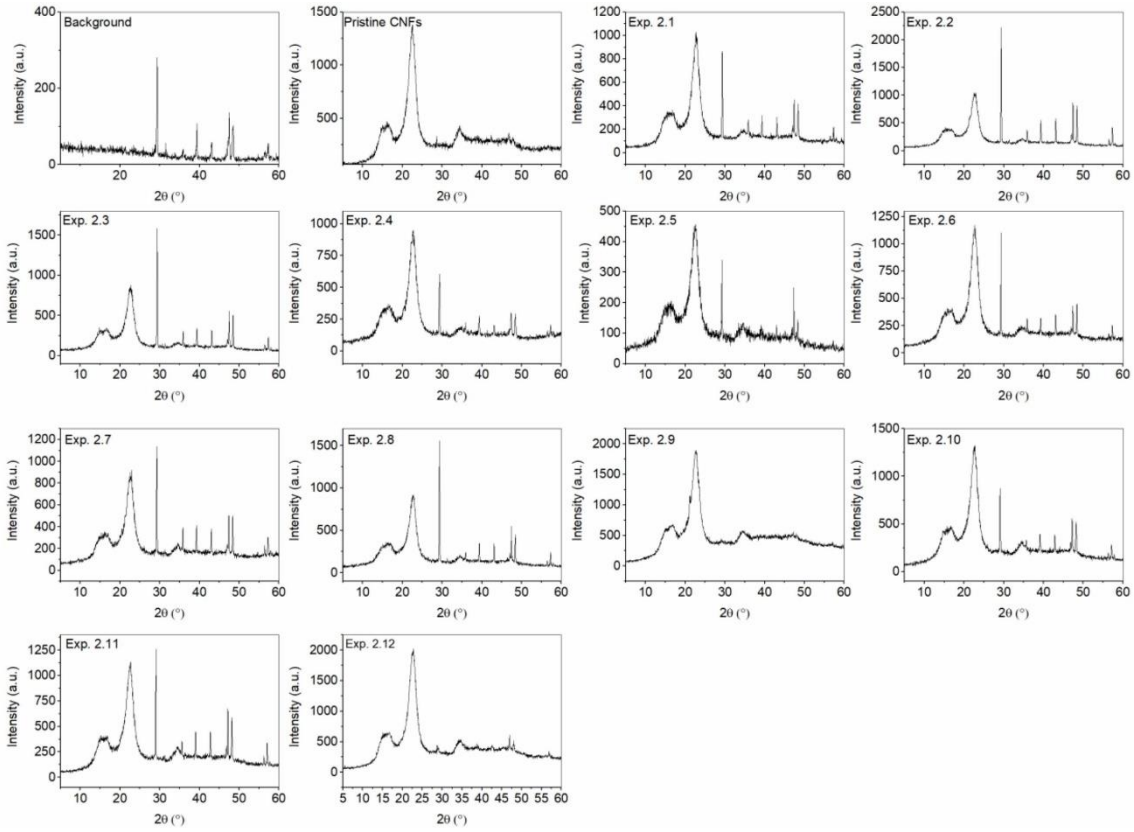

Figure S6: XRD spectra of pristine and modified CNFs for all performed experiments. The background (modelling clay) spectrum is also presented, however it does not interfere with CNFs peaks.

Table S3: Calculated crystallinity indices of pristine and acetylated cellulose nanomaterials.

Experiment No.	Crystallinity (%)
Pristine CNCs	89
1.1	83
1.2	80
1.3	84
1.4	86
1.5	80
1.6	83
1.7	82
1.8	79
1.9	77
1.10	79
1.11	86
1.12	82
1.13	84
1.14	79
1.15	78
1.16	79
Pristine CNFs	77
2.1	75
2.2	73
2.3	74
2.4	72

2.5	69
2.6	75
2.7	72
2.8	72
2.9	74
2.10	74
2.11	74
2.12	77
3.3	76
3.4	79

2.4 Free surface energy of acetylated cellulose nanomaterials

Introduction of acetyl groups to the surface of cellulose nanomaterials decreases hydrophilicity and thus increases contact angle with water by lowering the surface free energy of the material (Table S3).

Table S4: Surface free energy for selected samples with various degrees of acetylation, calculated through van Oss model.

Experiment No.	Contact angle with water (°)	Contact angle with formamide (°)	Contact angle with diiodomethane ()	Surface free energy (mJ/m^2)
Pristine	27 ± 5	28 ± 3	38 ± 1	87
1.1	59 ± 1	52 ± 3	40 ± 3	61
1.10	60 ± 3	50 ± 4	36 ± 2	60
1.15	64 ± 3	48 ± 4	40 ± 4	53

2.5 Kinetics of cellulose nanomaterials acetylation – absence of pyridine, effect of mixing and pretreatment duration

Acetylation can be carried out in the absence of pyridine, as well. In this case, the active species is acetic anhydride, which reacts more slowly than acetylpyridinium. Moreover, since pyridine also acts as a solvent, the required volume of acetic anhydride is higher to ensure homogeneous mixing (17.12 mol_{AA} mol_{AGU}. For this reason and lower efficiency of the reaction (60 ± 0.2 % and 55 ± 13.1 % for CNCs and CNFs, respectively), we further studied only pyridine-mediated acetylation (Si Figure 6).

To determine the effect of mixing rate and ensure that mass transfer poses no limitations, the mixing speed was increased from 350 rpm to 500 rpm in CNFs and to 550 rpm in CNCs. In CNF there is no notable difference in DS with respect to time (SI Figure 7). In CNCs minor variance between samples was detected. However, taking in account that the difference was in range of standard deviance, it can be assumed that mixing rate above 350 rpm and pretreatment duration longer than 3 min do not further affect reaction rate. With a longer pretreatment of CNCs (5 min of particles crushing), the initial reaction rate did not change (SI Figure 8). Nevertheless, the final acetyl content reached 18 % relative to all hydroxyl groups, which is higher than the determined amount of available hydroxyl groups, indicating a disturbance in the original structure. The suspected loss of crystallinity was then confirmed with XRD analysis (SI Table 2).

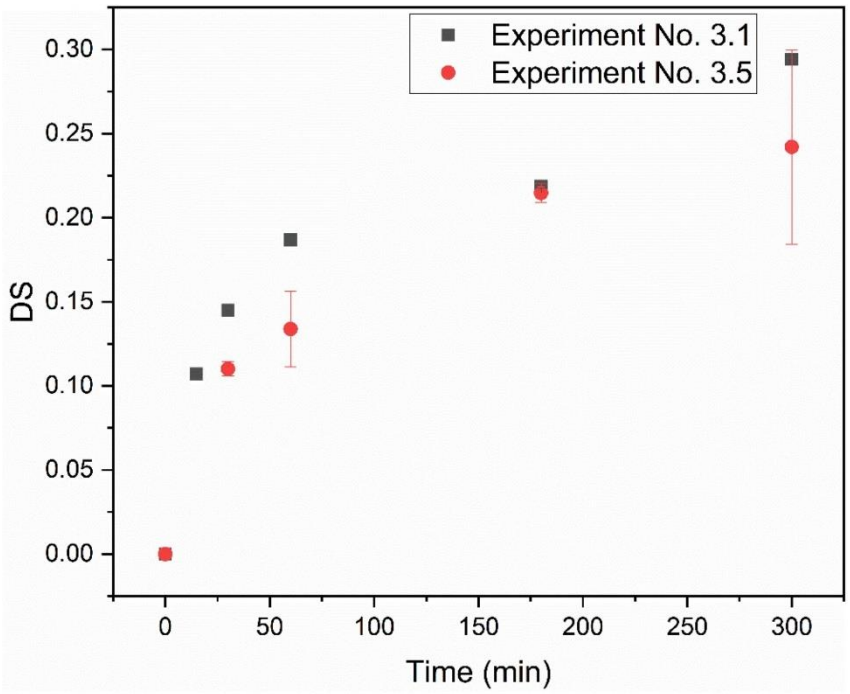

Figure S7: Increase of DS (degree of substitution) with respect to time in lack of pyridine presence.

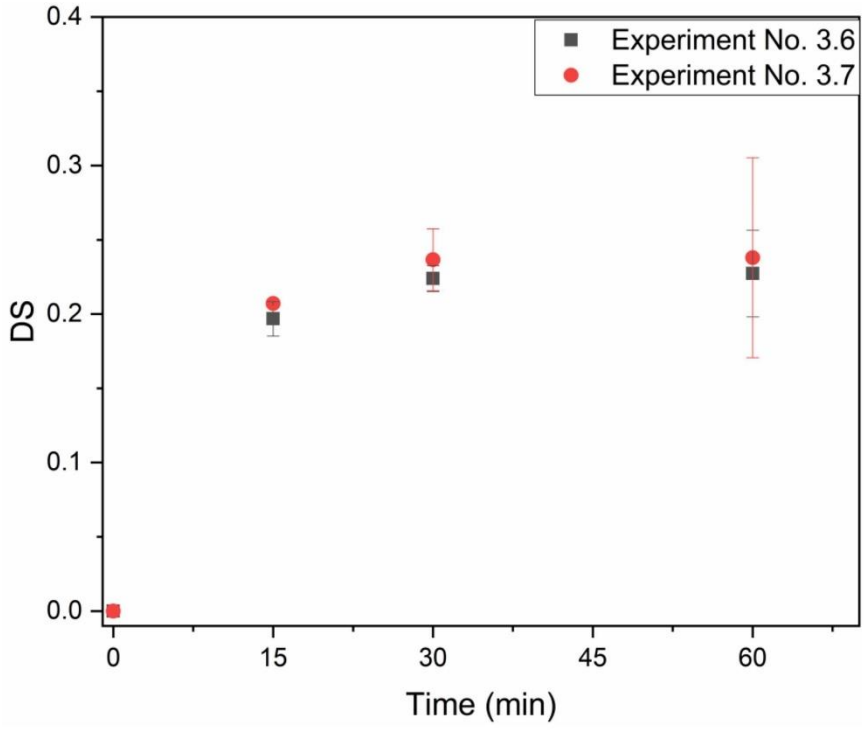

Figure S8: The effect of mixing rate (350 rpm and 500 rpm) on DS (degree of substitution) in CNFs with respect to time.

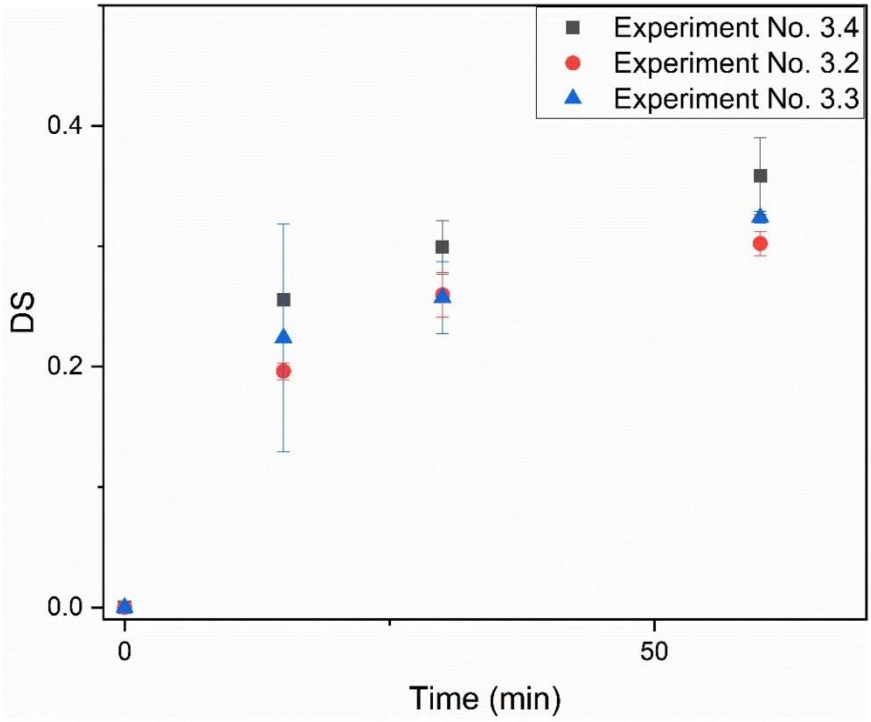

Figure S9: The effect of mixing rate (350 rpm and 550 rpm) and pretreatment duration (3 min and 5 min) on DS (degree of substitution) in CNCs with respect to time.

2.5 Kinetics of cellulose nanomaterials acetylation – Degree of substitution

Table S5: Acetyl content and DS in modified cellulose nanomaterials

Experiment	Ac wt %	DS
1.1	7.2 ± 1.1	0.29 ± 0.042
1.2	9.1 ± 0.4	0.38 ± 0.015
1.3	8.8 ± 3.2	0.36 ± 0.127
1.4	9.0 ± 0.2	0.37 ± 0.008
1.5	9.1 ± 1.5	0.38 ± 0.002
1.6	7.0 ± 0.2	0.28 ±0.006
1.7	8.2 ± 1.7	0.36 ± 0.066
1.8	8.8 ± 0.9	0.36 ± 0.035
1.9	6.4 ± 0.5	0.26 ± 0.175
1.10	8.5 ± 2.4	0.35 ± 0.094
1.11	7.5 ± 1.1	0.31 ± 0.042
1.12	10.9 ± 0.5	0.46 ± 0.019
1.13	9.0 ± 0.8	0.37 ± 0.032
1.14	10.5 ± 0.2	0.44 ± 0.008
1.15	9.7 ± 0.3	0.40 ± 0.011
1.16	9.17 ± 1.8	0.38 ± 0.068
2.1	3.9 ± 0.60	0.15 ± 0.023
2.2	5.6 ± 0.81	0.22 ± 0.307
2.3	7.8 ± 0.71	0.32 ± 0.027
2.4	4.7 ± 0.62	0.18 ± 0.023
2.5	7.3 ± 0.41	0.30 ± 0.015
2.6	6.2 ± 1.58	0.25 ± 0.060
2.7	6.4 ± 0.43	0.26 ± 0.016

2.8	5.7 ± 0.10	0.23 ± 0.004
2.9	7.0 ± 0.4	0.28 ± 0.015
2.10	6.2 ± 0.1	0.25 ± 0.003
2.11	6.4 ± 0.9	0.26 ± 0.036
2.12	5.3 ± 0.8	0.21 ± 0.030

2.6 The kinetic model

A system of differential equations was solved using the ODEINT solver from 0 to 300 min. The reaction rate was described as $r_i = k_i[A][B]$ where [*A*] and [*B*] represent concentrations of the components, presuming the Arrhenius kinetics ($k_i(T) = A\exp(-E_A/RT)$).

Regression of the parameters to the experimental data was carried out using the Nelder-Mead method. First, the experimental points collected at T = 80 °C were fitted to the model values, yielding initial rate constants, k_i. These were used as the initial approximation in the subsequent global fitting at all temperatures, providing the activation energy parameters, $E_{a,i}$, according to:

$$k_{T,i} = k_{80,i}\left(-\frac{E_{a,i}}{R}\left(\frac{1}{T}-\frac{1}{T_0}\right)\right)$$

The lower bound for the rate constant was set to zero. Initial approximations for $E_{a,i}$ were obtained from the DFT calculations and were constrained to 90 % and 110 % of these values during the fitting of the microkinetic model. Ultimately, all experimental points were used in a global of the model to the experimental data, yielding final k_i and $E_{a,i}$.

The following differential equations constitute the model:

$$\frac{d[Py]}{dt} = -k_0[Py][AAn] + k_1[C][AcPy] + k_3[IntPy] \quad \textit{Equation S2}$$

$$\frac{d[AAn]}{dt} = -k_0[Py][AAn] \quad \textit{Equation S3}$$

$$\frac{d[AcPy]}{dt} = k_0[Py][AAn] - k_1[C][AcPy] - k_2[C][AcPy] \quad \textit{Equation S4}$$

$$\frac{d[C]}{dt} = -k_1[C][AcPy] + k_2[C][AcPy] \quad \textit{Equation S5}$$

$$\frac{d[AA]}{dt} = k_0[Py][AAn] \quad \textit{Equation S6}$$

$$\frac{d[AC]}{dt} = k_1[C][AcPy] + k_3[IntPy] \quad \textit{Equation S7}$$

$$\frac{d[IntPy]}{dt} = k_2[C][AcPy] - k_3[IntPy] \quad \textit{Equation S8}$$

Supplementary References

(1) Brand, J.; Pecastaings, G.; Sèbe, G. A Versatile Method for the Surface Tailoring of Cellulose Nanocrystal Building Blocks by Acylation with Functional Vinyl Esters. *Carbohydr Polym* **2017**, *169*, 189–197. https://doi.org/10.1016/j.carbpol.2017.03.077.

(2) Good, R. J.; van Oss, C. J. The Modern Theory of Contact Angles and the Hydrogen Bond Components of Surface Energies. In *Modern Approaches to Wettability*; Loeb, G. I., Schrader, M. E., Eds.; Springer US: New York, 1992; pp 1–27.

(3) Miyamoto, T., Sato, Y., Shibata, T., Tanahashi, M. and Inagaki, H. (1985), 13C-NMR spectral studies on the distribution of substituents in water-soluble cellulose acetate. J. Polym. Sci. Polym. Chem. Ed., 23: 1373-1381. https://doi.org/10.1002/pol.1985.170230511

(4) Goodlett, V.W., Dougherty, J.T. and Patton, H.W. (1971), Characterization of cellulose acetates by nuclear magnetic resonance. J. Polym. Sci. A-1 Polym. Chem., 9: 155-161. https://doi.org/10.1002/pol.1971.150090114

4.2 Effect of Environment on Acetylated Cellulose Nanocrystal-Reinforced Biopolymers Films

This section continues research on acetylation of CNCs with acetic anhydride in pyridine media, and examines the use of acetylated CNCs in alginate and chitosan matrices. Incorporation of CNCs with various degrees of substitution (determined by ATR-FTIR) was evaluated in terms of morphology (through SEM analysis), structure (ATR-FTIR analysis), barrier properties, WCA and thermal stability (TGA). Furthermore, as real-world conditions in which such packaging could be used include environments with different relative humidity, the mechanical properties were evaluated after conditioning of films in a controlled environment (RH 33 %, 53 % and 75 %). The results have shown that acetylation of CNC prior to incorporation into chitosan matrix enhances compatibility, reduces aggregation, improves barrier and mechanical properties as well as WCA. Furthermore, slight increase in thermal stability was detected. Higher degree of substitution was shown to have more impact on the measured properties. On the other hand, alginate matrix is more compatible with pristine CNCs, seeing a decrease in mechanical strength upon acetylation and no change in water barrier properties. Additionally, it was observed that both alginate and chitosan-based films perform the best in an environment with lower relative humidity.

Regarding my contribution: I carried out the experimental work, analyses and wrote the manuscript.

polymers

MDPI

Article

Effect of Environment on Acetylated Cellulose Nanocrystal-Reinforced Biopolymers Films

Ana Oberlintner [1,2], Blaž Likozar [2] and Uroš Novak [1,*]

[1] Department of Catalysis and Chemical Reaction Engineering, National Institute of Chemistry, SI-1000 Ljubljana, Slovenia; ana.oberlintner@ki.si
[2] International Postgraduate School Jožef Stefan, SI-1000 Ljubljana, Slovenia; blaz.likozar@ki.si
* Correspondence: uros.novak@ki.si

Abstract: Cellulose nanocrystals (CNCs) were acetylated to the various parametrised degrees of substitution (DS), determined through attenuated total reflection Fourier transform infrared spectroscopy (ATR–FTIR) and incorporated into alginate (ALG) and chitosan (CH) film-forming solutions. An investigation of morphology with scanning electron microscopy (SEM) revealed increased chemical compatibility with the CH matrix after acetylation, producing a smooth surface layer, while ALG mixed better with pristine CNCs. The ATR–FTIR analysis of films demonstrated inter-diffusional structural changes upon the integration of pristine/modified CNCs. Films were evaluated in terms of water contact angle (WCA), which decreased upon CNC addition in either of the biocomposite types. The H_2O barrier assessed through applicative vapour transmission (WVT) rate increased with the CNC esterification in CH, but was not influenced in ALG. To evaluate the relationship between environmental humidity and mechanical properties, conditioning was applied for 48 h under controlled relative humidity (33%, 54% and 75%) prior to the evaluation of the mechanical properties and moisture content. It was observed that tensile strength was highest upon specimens being dry (25 ± 3 MPa for ALG, reinforced with neat CNCs, or 16 ± 2 MPa in the CH with CNCs, reacting to the highest DS), lowering with dewing, and the elongation at break exhibited the opposite. It is worth noting that the modification of CNCs improved the best base benchmark stress–strain performance. Lastly, (thermal) stability was assessed by means of the thermogravimetric analysis (TGA) technique, suggesting a slight improvement.

Keywords: functionalisation; acetylation; reinforcing cellulose nanocrystal; bionanocomposites; biopolymer-based composite films; bio-based flexible packaging

Citation: Oberlintner, A.; Likozar, B.; Novak, U. Effect of Environment on Acetylated Cellulose Nanocrystal-Reinforced Biopolymers Films. *Polymers* **2023**, *15*, 1663. https://doi.org/10.3390/polym15071663

Academic Editor: Luminita Marin

Received: 25 February 2023
Revised: 21 March 2023
Accepted: 23 March 2023
Published: 27 March 2023

1. Introduction

In light of recent efforts to find a suitable alternative that would be indispensable in the fight against plastic pollution, marine biomass has become an attractive raw-material source of biopolymers [1]. Considering that the packaging sector uses a noteworthy amount of all produced plastics (44% in the EU market in 2021 [2]), along with the fact that these materials also have the shortest lifetime, as it is limited to the lifetime of its contents (e.g., fresh produce), bio-based and biodegradable packaging materials are urgently needed to ensure a cleaner future. One of the solutions is offered by chitosan, a derivate of chitin—the second most abundant polymer on the planet. Chitin is found in the shells of crustaceans, a waste product of the food-processing industry, the use of which is in line with circular-economy guidelines. The disadvantage of marine waste biomass as a raw material is tropomyosin, a known allergen found in the muscles of crustaceans, leading to the popularization of fungal biomass as a source of chitin [3]. Chitosan is obtained from chitin using (partial) deacetylation, and therefore consists of β-D-1,4-glucosamine and N-acetyl-D-glucosamine units linked by glycosidic bonds. Chitosan is, contrary to chitin, soluble in acidic aqueous media and exhibits antimicrobial activity. These properties

are beneficial for a wide range of already commercial applications such as drug delivery, wound dressings, and skin-tissue engineering, as a coagulant, flocculant or adsorbent in wastewater treatment, and as a food additive and dietary fibre [4–6]. Its ability to form films and its biocompatibility and biodegradability promotes the use of chitosan as a single-use packaging material [1,7], which is the focus of this study.

Also perceived to be suitable for such applications is alginate, which consists of linear co-polymers of (1-4)-linked β-D mannuronic acid and α-L-guluronic acid [8]. It can be isolated from brown algae such as *Laminaria digitata, Laminaria japonica, Laminaria hyperborea, Macrocystis pyrifera* and *Ascophyllum nodosum*. Alginate is used commercially in the food and pharmaceutical industry as a thickening, gel-forming and stabilization agent; however, its versatility has not yet been fully exploited. Recent studies suggest the use of alginate in biomedical applications (drug delivery, wound dressing, tissue regeneration), the food industry (encapsulation, functional food) and as film packaging [9,10].

Cellulose nanocrystals (CNCs), commonly extracted by acidic hydrolysis of cellulose, have been applied as a reinforcement agent to biopolymer-based films to improve mechanical and barrier properties, bringing such materials closer to achieving protection and user experience comparable to commercial plastic foils and wrappings [11–13]. The advantage of CNCs lies in the worldwide availability of the raw material, economical accessibility, high mechanical strength, high specific surface, biocompatibility, and biodegradability. Several studies have reported the increase of tensile strength upon the addition of CNCs into the chitosan matrix [14–16]; however, the uniform dispersion of CNCs in the matrix is crucial for the production of a large matrix/nanofiller interfacial area that is responsible for changing molecular mobility and consequently improving mechanical properties [17]. Although CNCs have shown good compatibility with alginate-based films [18,19], significantly improving mechanical strength, their numerous hydroxyl groups on the surface are the reason for their hydrophilic character that induces lower compatibility with non-polar or positively charged polymer matrices, such as chitosan. The authors in Dong et al. [14] and Rubentheren et al. [20] observed the improvement of mechanical strength in chitosan-based films upon CNC integration that increased gradually with the concentration of incorporated CNCs; however, the water barrier of such films was not evaluated in these studies. The homogeneous dispersion of CNCs in the chitosan matrix can be inflicted mechanically by homogenization [21] and microfluidization [22] or by the surface modification of CNCs. The latter is frequently implemented in polymer chemistry, e.g., the authors in Grunert and Winter [23] functionalised the surface of CNCs through silylation and incorporated them into cellulose acetate butyrate matrix; the authors in Lin et al. [24] acetylated CNCs, which improves their compatibility with poly(lactic) acid; and the authors in Vasconcelos et al. [25] applied carboxymethylation, which improved the solubility of CNCs in polar media. However, the use of modified CNCs is not as widespread in biopolymer applications. Regarding chitosan-based films, the incorporation of CNCs was ensured either mechanically or by surface modification such as functionalisation with methyl adipolychloride [26] and treatment with O_2/laccase/TEMPO [13], which were shown to be successful.

The main advantage of such biocomposites is their renewable origin, non-toxicity, and biodegradability. However, currently, the commercial use of alginate, chitosan and CNC biocomposites is not yet viable due to a lack of technology for cost-effective industrial production as well as insufficient knowledge of their behaviour in real-life applications such as in environments with high or low humidity [27,28]. To push such biocomposites closer to commercial use as biodegradable packaging, understanding the impact of environmental conditions (such as environmental humidity) on the performance of the film is essential, as it affects moisture content and thus mechanical properties. The structure of chitosan that is abundant in hydroxyl and amino functional groups, as well as glycosidic linkages, giving chitosan-based films a high affinity to water [29,30]. The presence of moisture in the film induces a plasticizing effect by interrupting hydrogen bonding between the oxygen in the remaining acetyl group and hydrogen in the hydroxyl group in chitosan chains, causing

Polymers **2023**, *15*, 1663

an alteration in mechanical properties [31,32]. Although da Silva et al. [33] investigated the relationship between drying technique, moisture content and mechanical properties in alginate-based films and Giz et al. [34] observed that the extent of stress relaxation increases with the increase of humidity, so far, there has been no systematic study of the mechanical, barrier and thermal properties of both chitosan- and alginate-based films reinforced with pristine and acetylated CNCs. Furthermore, to the best of our knowledge, there has been no research depicting the relationship between environment humidity and the mechanical properties of such biocomposites.

With this in mind, chitosan- and alginate-based films with incorporated pristine and modified CNCs were investigated in terms of their suitability as single-use biodegradable packaging by evaluation of WVT rate, WCA, TGA, mechanical properties, ATR–FTIR and morphology. As acetylation is the most commonly used modification that is already carried out on an industrial scale for cellulose materials, this type of functionalisation was chosen for CNCs that were acetylated to three different degrees of substitution (determined by ATR–FTIR analysis) and then incorporated into chitosan and alginate film-forming solutions. The morphology of the fabricated films was observed with SEM, the chemical structure was inspected with ATR–FTIR, and the performance of the films for packaging purposes was assessed through the evaluation of moisture content (MC), tensile strength (TS) and elongation at break (ϵ) in dependency to environmental relative humidity (RH), as well as water contact angle (WCA), thermal stability and the ability to reduce water vapour transmission rate (WVT) as demonstrated in Figure 1.

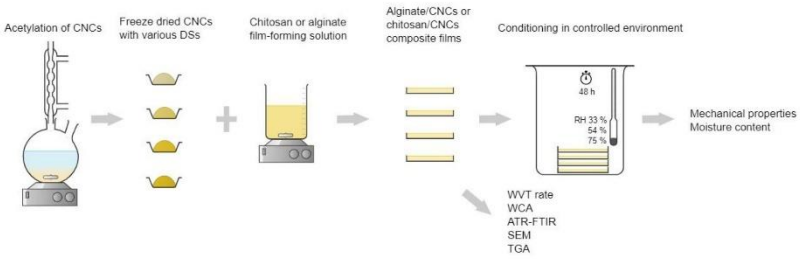

Figure 1. Schematic representation of the study.

2. Materials and Methods

2.1. Materials

Chitosan (high molecular weight, >85% deacetylated), lactic acid (85% aqueous solution) and sodium alginate were purchased from Sigma–Aldrich (Darmstadt, Germany). Glycerol, used as plasticizer, and cellulose nanocrystals (in 3 wt.% suspension) were bought from Pharmachem d.o.o (Ljubljana, Slovenia) and Navitas (Stari trg pri Ložu, Slovenia), respectively. $CaCl_2$ (99.0–103.0%) and NaCl (≥99.5%, analytical grade), used in water-barrier studies and conditioning of the films, were acquired from Merck (Darmstadt, Germany), while $MgNO_3 \times 6H_2O$ (≥98.0%) was purchased from Honeywell (Charlotte, NC, USA). For the acetylation of CNCs, pyridine (Merck, Darmstadt, Germany), acetic anhydride (Sigma–Aldrich, Darmstadt, Germany) and acetone (Honeywell, Charlotte, North Carolina, USA) were used. Deionized water was used throughout the experiments unless stated otherwise.

2.2. Methods

2.3. Cellulose Nanocrystal Acetylation

A total of 1 g of lyophilized and crushed CNC powder was weighed into a round-bottom reactor. After the addition of 5 mL of pyridine, the mixture was sonicated for 15 min and heated to 90 °C. As the temperature stabilized, the reaction was started by the dropwise addition of 5 mL of acetic anhydride. CNCs were subjected to the reaction for 60 min, 180 min and 300 min, and then washed in three consecutive cycles with water and with

50% acetone in water solution to remove any unreacted acetic anhydride. CNCs were then low-pressure freeze-dried prior to analysis and incorporation into the chitosan-based films.

2.4. Fabrication of Biopolymer/Acetylated CNCs Biocomposite Films

The films were fabricated according to the protocol described by Lavrič et al. [15]. Briefly, chitosan in the amount of 1.5 wt.% was dissolved in 1 *v/v*% lactic acid (prepared from ultrapure water, 18.2 MΩ cm) and stirred overnight on a magnetic stirrer (300 rpm) at room temperature together with 30% glycerol (based on biopolymer mass) to form a film-forming solution (FFS). The solution was vacuum-filtered through medical gauze to remove impurities. For chitosan/cellulose biocomposites, pristine CNCs and CNCs with different acetyl content were added in an amount to reach 3 wt.% with respect to chitosan. The mixture was homogenized at 6000 rpm for 3 min with an UltraTurrax homogenizer (IKA, Straufen, Germany). FFS was left on the laboratory counter overnight covered with para-film to eliminate air bubbles in the form of foam on the surface, which was collected with a spatula. A total of 50 g of FFS was carefully poured into a 12 × 12 cm petri dish. For alginate-based films, sodium alginate in an amount to reach 1.5 wt.% and glycerol (30 wt.% with respect to biomass) were dissolved in ultrapure water (18.2 MΩ cm) on the magnetic stirrer. Both pristine and modified CNCs were added in an amount to reach 5 wt.% based on the mass of alginate, as previously described in Lavrič et al. [15] and Huq et al. [35]. Again, 50 g of FFS was poured into a 12 × 12 cm petri dish. All samples were dried in the ventilated oven (Kambic, Slovenija) at 40 °C for 48 h and conditioned for 48 h in an airtight glass box at room temperature with RH controlled by $CaCl_2$ (for RH 33%), saturated solution of $MgNO_3 \times 6H_2O$ (for RH 53%) and a saturated solution of NaCl (for RH 75%).

2.5. Physico-Chemical Properties

To determine the acetyl content in CNCs, ATR–FTIR analysis using Spectrum Two 135 (Perkin Elmer, Rodgau, Germany) was carried out in a wavenumber range from 400 cm^{-1} to 4000 cm^{-1} with a step of 4 cm^{-1} (accumulation of 32 scans for each step). The spectra were adjusted to the same baseline and normalized. The acetylation degree was calculated according to a ratio of $I_{C=O}/I_{C-O}$. The intensity $I_{C=O}$ was correlated with the stretching of the acetyl group at 1740 cm^{-1}, normalized to I_{C-O} at 1060 cm^{-1} which is unaffected by the reaction [36].

To observe pristine and modified CNCs under SEM, lyophilized CNCs powders were dispersed in water (approximately 0.05 wt.%) and sonicated for 10 min. A drop of the dispersion was placed on an aluminium holder that was previously polished with abrasive paper to smooth the surface and was left to dry. The samples were sputtered with a 2 nm layer of gold and inspected with a SUPRA 35V scanning electron microscope (Carl Zeiss, Jena, Germany) under near-vacuum conditions and with an accelerating voltage of 1 kV. For insight into the morphology of the fabricated films, they were cut to approximately 1 × 1 cm pieces, placed onto carbon tape and inspected under the same conditions as CNCs. Images were captured under magnification 10,000× and 20,000×.

The structure of the films was evaluated through ATR–FTIR with Spectrum Two 135 (Perkin Elmer, Germany) with wavenumber ranging from 400 to 4000 cm^{-1} with a step of 4 cm^{-1} (32 scans for each step).

Moisture content was determined using a Moisture Analyzer HE53 (Mettler Toledo, Columbus, OH, USA). Approx. 5 g of the sample was heated to 105 °C until constant mass. The difference between the initial and the final mass was accounted for by the moisture of the sample.

Film thickness was measured using an ABS Digital Thickness Gauge (Mitutoyo, Aurora, IL, USA).

For the determination of mechanical properties, samples were cut into pieces of length 6 cm and width 2 cm. Tensile strength (TS) and elongation at break ϵ were determined with an XLW Auto Tensile Tester (Labthink® Instruments, Jinan, China) equipped with

a 100 N loading cell. The gauge length segment was set to 4 cm and crosshead speed to 25 mm min^{-1}. TS represents the ratio between maximal load and average initial cross-sectional area in the sample gauge segment, while ϵ is calculated by dividing the increase in length after the break-point with the initial gauge length.

For the evaluation of WVT, a film was fixed over a 15 mL glass flask filled with $CaCl_2$ (previously activated at 105 °C for 2 h) with diameter 5 cm, with a top that had a carved circular area of 2.1 cm. These flasks were then subjected to the environment with 70% RH provided by saturated NaCl. For five consecutive days, the flask containing $CaCl_2$ was weighed and *WVT*,expressed in g m^2 24 h^{-1} was calculated by Equation (1).

$$WVT = \frac{\Delta m}{St} \quad (1)$$

where Δm stands for an increase in mass (g), S represents the area of the film exposed to water vapour ($1.84 \times 10^{-4} m^2$) and t is time in hours.

The evaluation of hydrophilicity/hydrophobicity was carried out through static WCA analysis, employing sessile drop measurement with a Tensiometer Theta T200 (Biolin Scientific, Darmstadt, Germany). The samples were cut into smaller pieces (approx. 2×3 cm^{-1}) and fixed on a microscope slide. Ultrapure water (18.2 MΩ) with drop volume of 4 µL was used. The measurements were repeated at least five times per sample.

2.6. Thermal Stability

Thermogravimetric analysis was carried out in EGA 4000 (Perkin Elmer, Germany). Approximately 15 mg of the sample was subjected to thermal degradation under nitrogen atmosphere (flow rate was 30 mL min^{-1}) in temperatures ranging from 50 °C to 700 °C with a rate of 10 °C min^{-1}. The measurements were performed in duplicate.

2.7. Statistical Analysis

All results are reported as the mean value. A two-way analysis of variance (ANOVA) followed by Tukey's test was applied using Origin 2018 (version b9.5.0.193) software to the data relating to mechanical properties to evaluate the impact of CNC acetylation and environmental humidity.

3. Results and Discussion

3.1. Acetylated Cellulose Nanomaterials

The ATR–FTIR analysis (Figure 2) of non-modified CNCs (labelled as C0) exhibits a characteristic peak for cellulose at 1070 cm^{-1} that is related to C-O stretching in the glucopyranose ring. The successful esterification of samples C1, C2 and C3 (denoting different reaction times and DS as presented in Table 1) was proven through the appearance of peaks centred at 1750 cm^{-1}, 1370 cm^{-1} and 1250 cm^{-1} that are associated with C=O stretching, C-H bending and C-O stretching, respectively. The intensity of all of the newly formed peaks increases with reaction time. The FTIR spectra served as a basis for the calculation of DS indicated in Table 1. Pristine CNCs and samples modified to the highest DS were analysed under SEM (the lower part of Figure 2). In both samples, the particles are approximately 100 nm long and 14 nm wide; however, pristine CNCs tend to connect on their edges, forming a spider's-web-like shape, which is not as pronounced in C3. This could be a consequence of surface modification that affects interparticle interactions.

Table 1. Labelling of the CNC samples according to reaction time and their corresponding calculated DS.

Sample	Reaction Time [min]	DS
C0	0	0
C1	60	0.299
C2	180	0.334
C3	300	0.399

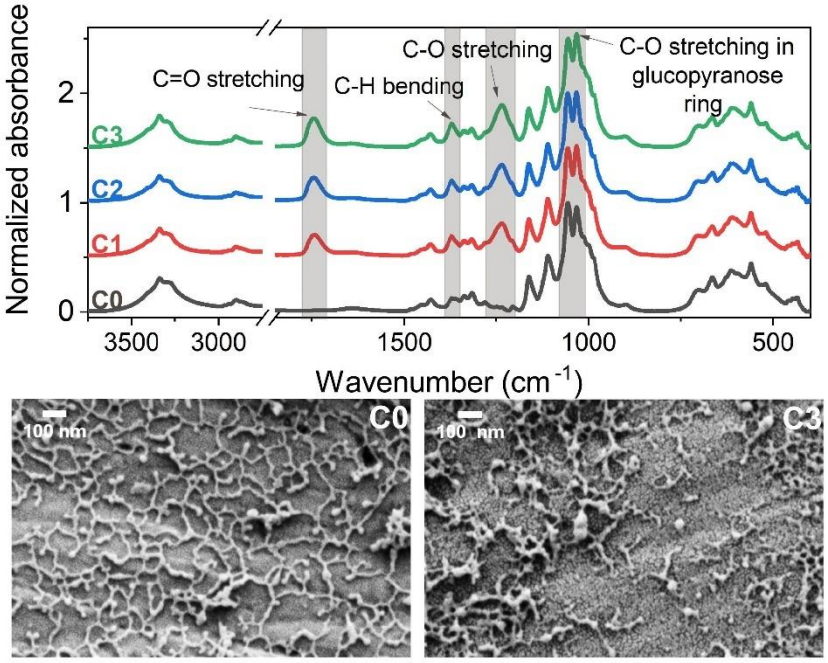

Figure 2. FTIR–ATR spectra of acetylated CNCs with C0 denoting the pristine material, C1, C2 and C3 representing samples with reaction time 1 h, 3 h and 5 h, respectively (upper part) and SEM micrographs of pristine (C0) and modified (C3) CNCs (lower part).

3.2. Morphology of the Fabricated Polysaccharide-Based Films

The fabricated films were first inspected under SEM to obtain an insight into the morphology (Figures 3 and S1). For clarity, the following labels apply for the films throughout the manuscript: CH, CH+C0, CH+C1, CH+C2 and CH+C3 for chitosan film; chitosan film with incorporated pristine CNCs; chitosan film with incorporated C1, C2 and C3, respectively; and ALG, ALG+C0, ALG+C1, ALG+C2 and ALG+C3 alginate-based films; the film consisting only of alginate was labelled ALG; alginate film with pristine CNCs was labelled ALG+C0; and films with incorporated C1, C2 and C3 were labelled ALG+C1, ALG+C2 and ALG+C3, respectively. The addition of CNCs into initially smooth CH film resulted in aggregates with an average length of 700 ± 200 nm and width of 80 ± 30 nm. It has to be noted that the size of an individual CNC is up to 6 nm in width and no more than 20 nm in length [37]. After incorporation of C3, no aggregates were visible on the surface of the film, pointing to the homogeneous incorporation of acetylated CNCs into the chitosan matrix. On the other hand, the surface of ALG appears rougher

Polymers **2023**, *15*, 1663 7 of 14

and more granulated, which does not change upon the addition of C0. However, the surface of ALG+C3 increases even further in roughness, indicating that the modified CNCs do not mix as well into the alginate matrix as pristine CNCs.

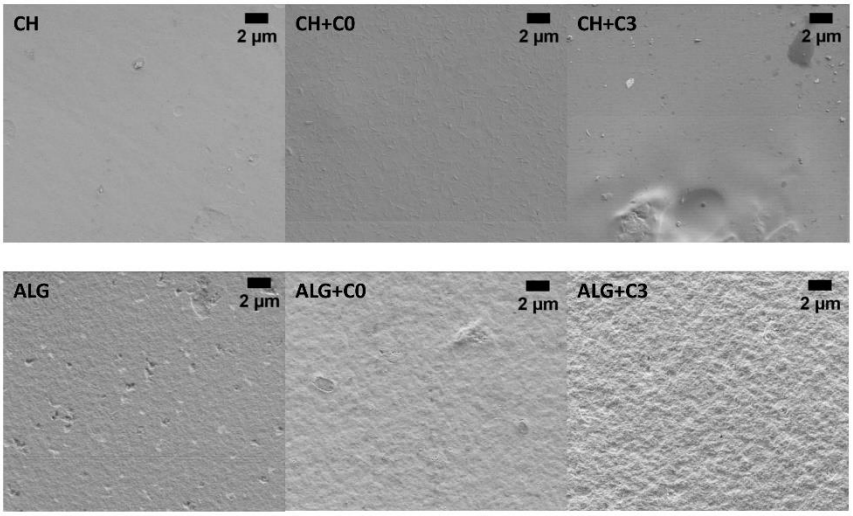

Figure 3. SEM micrographs of chitosan-based film (CH), chitosan films with pristine CNCs (CH+C0), chitosan films with acetylated CNCs (CH+C3) in the upper part and alginate-based film (ALG), alginate films with pristine CNCs (ALG+C0), alginate films with acetylated CNCs (ALG+C3).

3.3. FTIR–ATR Analysis of the Fabricated Polysaccharide-Based Films

Chitosan is a linear co-polymer consisting of D-glucosamine and N-acetyl-D-glucosamine, which is mirrored in its FTIR spectrum (the blue line in Figure 4) and exhibits a broad peak between 3500 cm^{-1} and 3000 cm^{-1} corresponding to N-H and O-H stretching and the peak between 3000 cm^{-1} and 2800 cm^{-1} associated with C-H bond stretching. The peaks appearing between 1750 cm^{-1} and 1500 cm^{-1} are correlated with -C=O- stretching (amide I, 1723 cm^{-1}), -NH- bending (amide II, 1570 cm^{-1})) and -CN- stretching vibrations (amide III, 1377 cm^{-1}) [32,38]. Upon the addition of CNCs (pristine as well as modified), only relatively minor changes in the spectra are observed. A peak located at 1068 cm^{-1}, corresponding to -C-O-C- stretching, increased due to -C-O-C- bridge vibrations of the glucopyranose ring. For better visibility, the regions between 1590 cm^{-1} and 1550 cm^{-1} in which slight changes occurred are magnified in Figure 4. The peak at 1580 cm^{-1}, related to N-H bending in amines is slightly more pronounced in CH+C0 and CH+C1, and it decreases again with higher DS. Similarly, the peak centred at 1550 cm^{-1} correlated with -N-O- stretching is increased in samples CH+C0, CH+C1 and starts to decrease again with CH+C2 and CH+C3. These observations could point to repulsive intra-molecular interactions between chitosan and CNCs that decrease with higher DS.

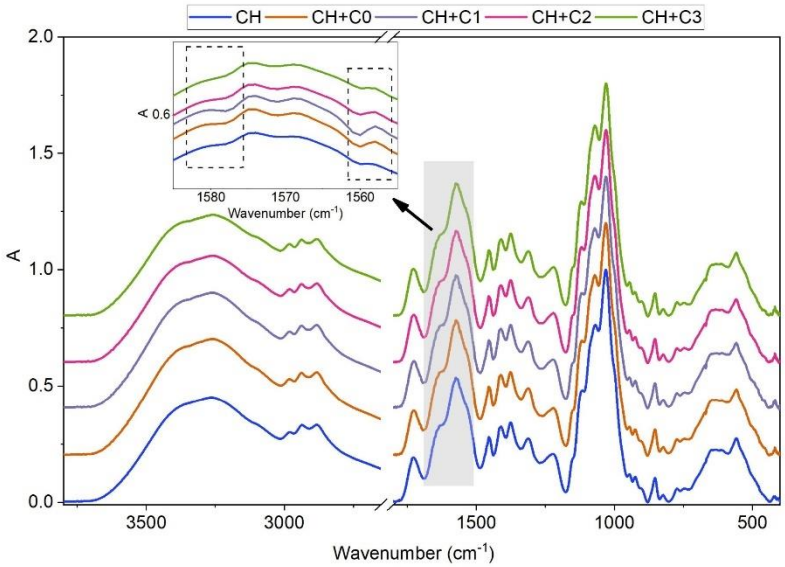

Figure 4. FTIR–ATR analysis of chitosan-based films with and without integrated CNCs of various DS.

Alginate, also a linear co-polymer, is made of β-D-mannuronate and α-L-guluronate, which are linked by β-1,4 and α-1,4 glycosidic bonds. In Figure 5a, full spectra of the samples are presented, and Figure 5b–f exhibit the fragments of the spectra where changes upon integration of pristine and modified CNCs occur. The blue line denotes the characteristic spectrum of ALG. A broad peak between 3700 cm^{-1} and 2980 cm^{-1}, correlated to -O-H stretching, decreases in intensity, first slightly upon the incorporation of C0, and then further with the acetylation of CNCs. The peaks located between 2980 cm^{-1} and 2880 cm^{-1} are related to the asymmetric and symmetric stretching modes of -CH_2- [39], and the wear peak centred at 2938 cm^{-1} is related to -CH- stretching (Figure 5b). Although the shape of the peak remained the same when incorporating pristine CNCs, the original bonds were disturbed by acetylated CNCs, whereas the peaks for -CH_2- stretching shifted to lower wavenumbers, which points to a weakening of the bond [39], and the peak correlated with -CH- stretching disappeared. In the region between 1770 cm^{-1} and 1710 cm^{-1}, Figure 5c, a peak corresponding to -C=O- stretching vibrations in acetylated CNCs emerges in samples ALG+C1, ALG+C2 and ALG+C3. Its intensity, however, is inversely proportional to the DS of CNCs. This could be attributed to the better integration of CNCs with lower DS in the alginate matrix, while a higher degree of acetylation leads to the aggregation of CNCs. Indicating the presence of cellulose, the peaks at 1335 cm^{-1} (related to -OH- bending) and 1160^{-1} (related to -C-O- stretching) can be observed in Figure 5d,e in samples with incorporated CNCs but not in ALG. Lastly, the peaks centred at 1123 cm^{-1} and 1086 cm^{-1} (Figure 5f) ascribed to -C-C- and -C-O- stretching vibrations, respectively, became less pronounced upon the reinforcement of alginate-based films with CNCs.

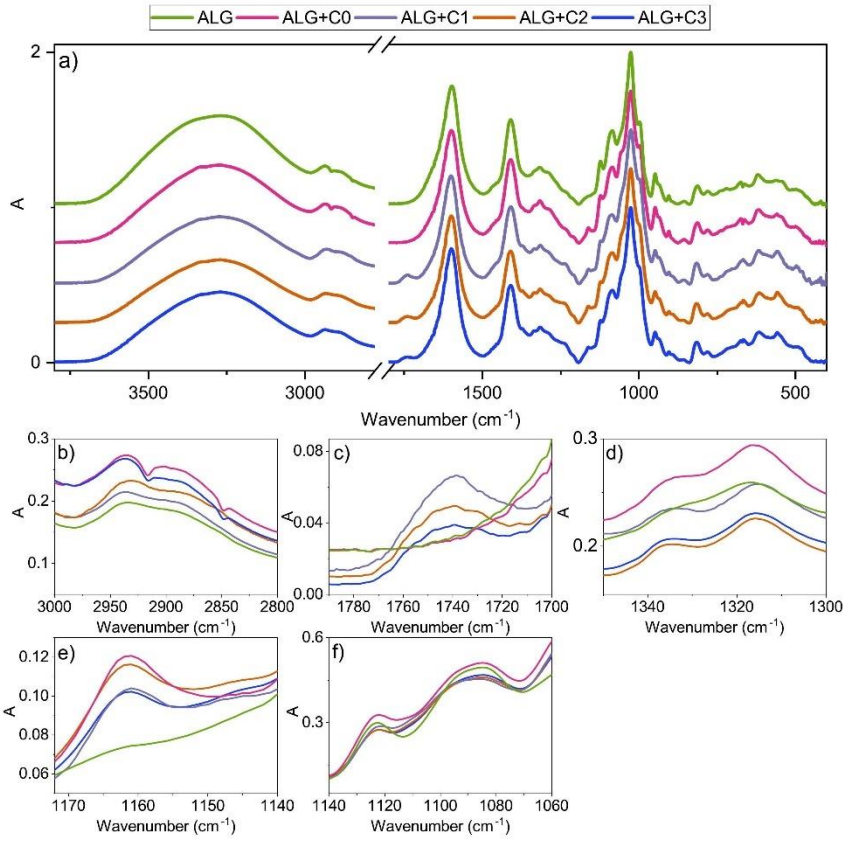

Figure 5. (**a**) FTIR–ATR analysis of alginate-based films with and without integrated CNCs of various DS, with subfigures (**b**–**f**) exhibiting regions where change upon addition of pristine or modified CNCs is observed.

3.4. Physiochemical Properties of the Fabricated Polysaccharide-Based Films

Water-related properties, such as WCA and WVT rate, are important properties in packaging materials for the protection of the product from external impact. In chitosan-based films, the addition of non-modified CNCs already caused an increase in WCA from the initial 57° to 64° (Figure 6a), which agrees with the literature [15]. This could be attributed to the change in morphology and formation of aggregates on the surface. Furthermore, acetylation decreases the surface free energy and thus hydrophilicity through the introduction of acetyl groups to the surface of CNCs, the WCA in samples CH+C1, CH+C2, and CH+C3 further increases (up to 81°). WVT rate decreases slightly upon the inclusion of pristine CNCs (from an initial 33 g m^{-2} h^{-1} ± 4 g m^{-2} h^{-1} to 30 g $m^{-2}h^{-1}$ ± 1 g m^{-2} h^{-1}). Sample CH+C3 exhibits a notable improvement in water vapour barrier—the WVT rate decreased as much as 77% from the initial value that was observed with the functionalisation of CNCs (Figure 6b).

The mechanical properties of biocomposite films are strongly dependent on environmental moisture, as they influence the MC. To simulate various environments, the films were conditioned in three different relative humidities (RH 33%, 50%, 75%). Regardless of the humidity, the samples with the modified CNCs exhibited the highest mechanical resistance compared to CH and CH+CNCs, which increased with DS (Figure 6c)—the highest TS was observed in sample CH+C3. The addition of pristine CNCs to the chitosan matrix resulted in a slight decrease of TS in comparison to CH films, which was attributed to the fact that pristine CNCs did not mix as homogeneously into the chitosan matrix as modified CNCS, and formed aggregates, as seen in Figure 3. At RH 54%, it slightly increased, but remained in the range of standard deviation. It was observed that the films exhibit higher TS in drier environments (RH 33%) and therefore lower MC in the film. However, the MC in the films seems to be independent of dopant as, in all samples conditioned at the same RH, the values are in the range of standard deviation (around 2.5% in RH 33%, 3.0% in RH 50% and 3.6% in RH 75%). Contrary to TS, elongation at break (ϵ) is not as closely related to the DS of modified CNCs and is higher in more humid environments. This is reasoned by the fact that moisture in the film (which increases along with RH) acts as a plasticizer and induces the stretchiness of the film by promoting the movement of biopolymer chains [32].

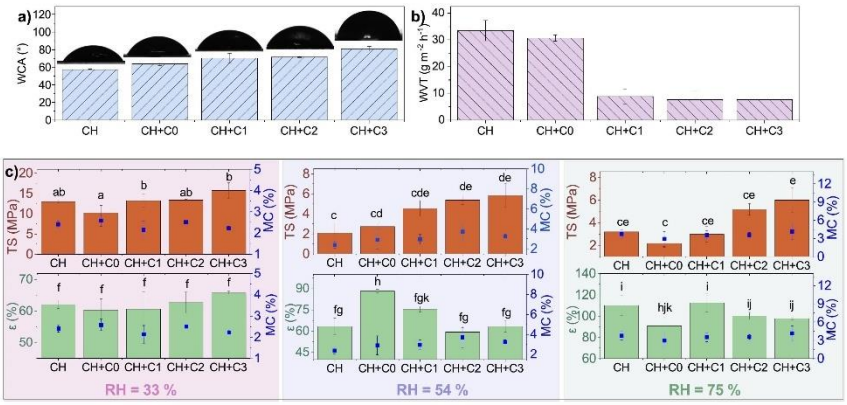

Figure 6. (**a**) Water contact angle (WCA), (**b**) water vapour transmission (WVT) and (**c**) mechanical properties with respect to environmental RH of chitosan-based films, where different letters denote samples with significantly different mean value ($p < 0.05$).

Both alginate-based films and CNCs are very hydrophilic in nature. The initial alginate film (ALG) exhibits WCA of 35 ± 0.4 °, and the addition of pristine and modified CNCs into the matrix slightly decreases hydrophilicity (up to 60 ± 3.6 ° in sample ALG+C3). Only minor differences in WCA are observed between samples ALG+C0, ALG+C1, ALG+C2 and ALG+C3, indicating that the change in water repellency is due to morphology rather than a change in free surface energy. The incorporation of CNCs into the alginate matrix does not alter the barrier properties. WVT through alginate-based films was measured to be about 40 g m^{-2} h^{-1} (from 39 g m^{-2} h^{-1} to 42 g m^{-2} h^{-1} with the difference in range of standard deviation) as shown in Figure 7b.

Contrary to chitosan-based films, mixing pristine CNCs into the alginate matrix slightly improves the TS of films, while it is significantly decreased by the incorporation of surface acetylated nanoparticles. This could be attributed to the fact that modified CNCs do not mix homogeneously into the alginate FFS and therefore form aggregates and cause the uneven surface of the film (seen in Figure 3). The trend of decreasing mechanical strength was observed in all three tested RHs. Again, the TS of the films is greatly influenced by environmental humidity and drops with an increase in RH. The films perform best in

Polymers **2023**, *15*, 1663 11 of 14

drier environments as the maximum TS was measured with sample ALG+C0, reaching 25 ± 3 MP in RH 33%. It was observed that MC remains rather stable in ALG+C1, ALG+C2 and ALG+C3, which could be explained by the formation of aggregates that induce pores in the film that hold the moisture in the film. The largest fluctuation in samples containing modified CNCs is 1% (in sample ALG+C1), while the MC in ALG samples is highly affected by environmental humidity and ranges from 1.6 ± 0.1% to 5.8 ± 0.6%. The trend is reversed in the environment with the highest humidity, where the samples doped with pristine or modified CNCs exhibit lower MC. This phenomenon could be attributed to the hydrophilic nature of alginate, binding water from the environment. ϵ shows less distinct trends among neat and reinforced alginate films. In RH 33% and RH 50%, sample ALG+C1 exhibits the highest elongation (36 ± 6% and 40 ± 5%, respectively), while in humid environments (RH 75%), the highest ϵ is observed in film doped with C1 (34 ± 3%).

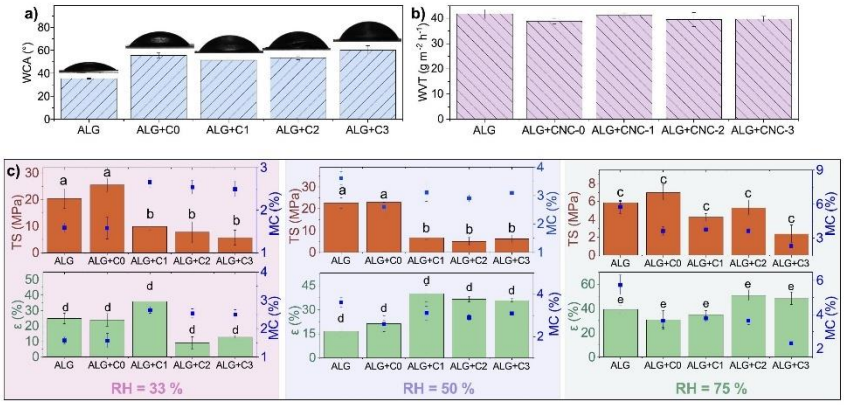

Figure 7. (**a**) Water contact angle (WCA), (**b**) water vapour transmission (WVT) and (**c**) mechanical properties with respect to environmental RH of alginate-based films, where different letters denote samples with significantly different mean value ($p < 0.05$).

3.5. Thermal Stability

The thermal stability of biocomposite films was determined through the observation of the change in sample weight. The degradation of CNCs (both pristine and modified) occurs in a single stage that begins at 260 °C, as shown in Figure 8a,c and results in a loss of 80% of the initial mass. Chitosan-based films show degradation in three stages (Figure 8b,c), with the first one featuring a loss of free bound water, occurring between 60 °C and 140 °C. The second stage of degradation starts at around 140 °C and represents a loss of bound water in the films as well as degradation of shorter chains [40]. Here, a slight shift in the CH+C3 curve is observed, as it reaches maximum degradation 10 °C later than CH and CH+C0, pointing to the fact that the water is well bound into the matrix and a higher temperature is needed for it to evaporate. The last stage takes place after 250 °C and is related to the decomposition of chitosan polymer chains, with the residues accounting for 23% of initial mass in CH+C0 and CH+C3 and 21% in CH. The degradation of alginate-based films occurs in two stages. As with chitosan-based films, the loss of mass up to 120 °C accounts for the loss of free water (Figure 8c,f). The second stage starts at 160 ° C and is responsible for the loss of bound water, as well as the decomposition of polymer chains. In samples ALG+C0 and ALG+C3, degradation to the final 28% of initial mass is slightly delayed compared to ALG, indicating the better thermal stability of films doped with CNCs.

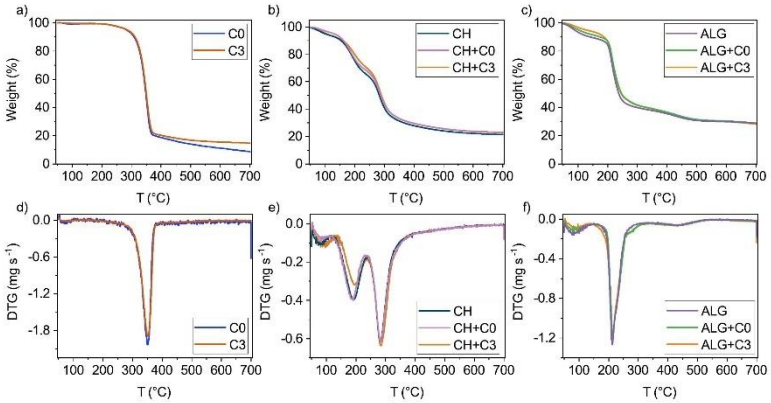

Figure 8. Thermal stability of (**a**) pristine and modified CNCs, (**b**) chitosan-based films (samples CH, CH+C0, CH+C3), and (**c**) alginate-based films (samples ALG, ALG+C0, ALG+C3) and derivates of their weight loss (**d**–**f**), respectively.

4. Conclusions

Pristine and acetylated CNCs with various DSs (0.299, 0.334 and 0.399) were incorporated into chitosan and alginate matrices to fabricate biocomposite films. Properties relevant to single-use packaging applications, such as WVT rate, wettability, thermal stability, moisture content and mechanical properties, were thoroughly investigated. Furthermore, the effect of environmental humidity on the latter was evaluated to obtain insight into the applicability of such materials in the real world. SEM investigation indicated that the incorporation of pristine CNCs induced the formation of aggregates in chitosan-based films due to their hydrophilic nature, while their acetylated counterparts mixed homogeneously into the film. On the other hand, in alginate-based films, the modification of CNCs produced a more structured surface that was not observed upon the incorporation of pristine CNCs. ATR–FTIR analysis of fabricated biocomposites revealed a slight change in the peak corresponding to -C-O-C- vibrations in chitosan-based films, while spectra of alginate-based films were altered in five different regions. In chitosan-based films, the modification of CNCs prior to their integration positively influenced WCA, WVT rate and mechanical properties, which was especially noticeable in environments with high humidity (RH 75%). On the contrary, in the alginate matrix, the best performance was observed in films with incorporated pristine CNCs, as they mix homogeneously into the matrix without the need for modification. Overall, films exhibited the highest mechanical strength in dryer environments, whereas elongation was higher in more humid environments, which is in line with the published literature [41,42]. The results of this study show that a higher degree of acetylation of CNCs (DS = 0.399) prior to incorporation into the chitosan matrix improves properties relevant for packaging applications, and this pretreatment is not needed in alginate-based biocomposites. Such materials could be suitable for packing dry products.

Supplementary Materials: The following supporting information can be downloaded at: www.mdpi.com/10.3390/polym15071663/s1, Figure S1. SEM micrographs of alginate films with pristine CNCs (ALG+C0), alginate films with acetylated CNCs (ALG+C3), chitosan films with pristine CNCs (CH+C0), chitosan films with acetylated CNCs (CH+C3) in the upper part.

Author Contributions: Conceptualization: A.O. and U.N.; Data curation: A.O.; Formal analysis: A.O.; Investigation: A.O.; Visualization: A.O.; Writing—original draft: A.O.; Funding acquisition: U.N. and B.L.; Supervision: U.N. and B.L.; Writing—review & editing: U.N. and B.L. All authors have read and agreed to the published version of the manuscript.

Funding: This study was funded by Slovenian Research Agency research core funding No. P2-0152 and PhD Grant (Ana Oberlintner). As well as Horizon Europe projects ESTELLA (GA 101058371), REMEDIES (GA 101093964) and RURALITIES (GA 101060876).

Institutional Review Board Statement: Not applicable.

Data Availability Statement: The data that support the findings of this study and materials are available from the corresponding author upon reasonable request.

Acknowledgments: Anže Prašnikar is acknowledged for capturing of SEM images. A.O. is thankful for "For Women in Science 2023" Fellowship granted by L'Oreal-UNESCO.

Conflicts of Interest: The authors declare no conflict of interest.

References

1. Cazón, P.; Velazquez, G.; Ramírez, J.A.; Vázquez, M. Polysaccharide-based films and coatings for food packaging: A review. *Food Hydrocoll.* **2017**, *68*, 136–148. [CrossRef]
2. PlasticsEurope. Plastics-the Facts 2022: An Analysis of European Plastics Production, Demand and Waste Data. Available online: https://plasticseurope.org/knowledge-hub/plastics-the-facts-2022/ (accessed on 7 January 2022).
3. Huq, T.; Khan, A.; Brown, D.; Dhayagude, N.; He, Z.; Ni, Y. Sources, production and commercial applications of fungal chitosan: A review. *J. Bioresour. Bioprod.* **2022**, *7*, 85–98. [CrossRef]
4. Madni, A.; Kousar, R.; Naeem, N.; Wahid, F. Recent advancements in applications of chitosan-based biomaterials for skin tissue engineering. *J. Bioresour. Bioprod.* **2021**, *6*, 11–25. [CrossRef]
5. Morin-Crini, N.; Lichtfouse, E.; Torri, G.; Crini, G. Applications of chitosan in food, pharmaceuticals, medicine, cosmetics, agriculture, textiles, pulp and paper, biotechnology, and environmental chemistry. *Environ. Chem. Lett.* **2019**, *17*, 1667–1692. [CrossRef]
6. Zhao, D.; Yu, S.; Sun, B.; Gao, S.; Guo, S.; Zhao, K. Biomedical Applications of Chitosan and Its Derivative Nanoparticles. *Polymers* **2018**, *10*, 462. [CrossRef] [PubMed]
7. Oberlintner, A.; Bajić, M.; Kalčikova, G.; Likozar, B.; Novak, U. Biodegradability study of active chitosan biopolymer films enriched with Quercus polyphenol extract in different soil types. *Environ. Technol. Innov.* **2020**, *21*, 101318. [CrossRef]
8. Novak, U.; Bajić, M.; Körge, K.; Oberlintner, A.; Murn, J.; Lokar, K.; Triler, K.V.; Likozar, B. From waste/residual marine biomass to active biopolymer-based packaging film materials for food industry applications—A review. *Phys. Sci. Rev.* **2020**, *5*, 20190099. [CrossRef]
9. Lee, K.; Jeon, Y.; Kim, D.; Kwon, G.; Kim, U.J.; Hong, C.; Choung, J.W.; You, J. Double-crosslinked cellulose nanofiber based bioplastic films for practical applications. *Carbohydr. Polym.* **2021**, *260*, 117817. [CrossRef]
10. Bi, D.; Yang, X.; Yao, L.; Hu, Z.; Li, H.; Xu, X.; Lu, J. Potential Food and Nutraceutical Applications of Alginate: A Review. *Mar. Drugs* **2022**, *20*, 564. [CrossRef]
11. Pritchard, C.Q.; Funk, G.; Owens, J.; Stutz, S.; Gooneie, A.; Sapkota, J.; Foster, E.J.; Bortner, M.J. Adjustable film properties of cellulose nanofiber and cellulose nanocrystal composites. *Carbohydr. Polym.* **2022**, *286*, 119283. [CrossRef]
12. Ma, L.; Wang, L.; Wu, L.; Zhuo, D.; Weng, Z.; Ren, R. Cellulosic nanocomposite membranes from hydroxypropyl cellulose reinforced by cellulose nanocrystals. *Cellulose* **2014**, *21*, 4443–4454. [CrossRef]
13. Liu, Y.; Yu, Y.; Wang, Q.; Xu, J.; Fan, X.; Wang, P.; Yuan, J. Biological–chemical modification of cellulose nanocrystal to prepare highly compatible chitosan-based nanocomposites. *Cellulose* **2019**, *26*, 5267–5279. [CrossRef]
14. Dong, F.; Li, S.J.; Yan, M.L.; Li, C.J. Preparation and Properties of Chitosan/Nanocrystalline Cellulose Composite Films for Food Packaging. *Asian J. Chem.* **2014**, *26*, 5895–5898. [CrossRef]
15. Lavrič, G.; Oberlintner, A.; Filipova, I.; Novak, U.; Likozar, B.; Vrabič-Brodnjak, U. Functional Nanocellulose, Alginate and Chitosan Nanocomposites Designed as Active Film Packaging Materials. *Polymers* **2021**, *13*, 2523. [CrossRef] [PubMed]
16. Adel, A.M.; El-Shafei, A.M.; Ibrahim, A.A.; Al-Shemy, M.T. Chitosan/Nanocrystalline Cellulose Biocomposites Based on Date Palm (Phoenix Dactylifera L.) Sheath Fibers. *J. Renew. Mater.* **2019**, *7*, 567–582. [CrossRef]
17. Azeredo, H.M.; Mattoso, L.H.C.; Avena-Bustillos, R.J.; Filho, G.C.; Munford, M.L.; Wood, D.; McHugh, T.H. Nanocellulose reinforced chitosan composite films as affected by nanofiller loading and plasticizer content. *J. Food Sci.* **2010**, *75*, 1–7. [CrossRef]
18. Sirviö, J.A.; Kolehmainen, A.; Liimatainen, H.; Niinimäki, J.; Hormi, O.E.O. Biocomposite cellulose-alginate films: Promising packaging materials. *Food Chem.* **2014**, *151*, 343–351. [CrossRef]
19. Wang, L.F.; Shankar, S.; Rhim, J.W. Properties of alginate-based films reinforced with cellulose fibers and cellulose nanowhiskers isolated from mulberry pulp. *Food Hydrocoll.* **2017**, *63*, 201–208. [CrossRef]
20. Rubentheren, V.; Ward, T.A.; Chee, C.Y.; Nair, P. Physical and chemical reinforcement of chitosan film using nanocrystalline cellulose and tannic acid. *Cellulose* **2015**, *22*, 2529–2541. [CrossRef]
21. Mujtaba, M.; Salaberria, A.M.; Andres, M.A.; Kaya, M.; Gunyakti, A.; Labidi, J. Utilization of flax (Linum usitatissimum) cellulose nanocrystals as reinforcing material for chitosan films. *Int. J. Biol. Macromol.* **2017**, *104*, 944–952. [CrossRef] [PubMed]
22. Celebi, H.; Kurt, A. Effects of processing on the properties of chitosan/cellulose nanocrystal films. *Carbohydr. Polym.* **2015**, *133*, 284–293. [CrossRef]

23. Grunert, M.; Winter, W.T. Nanocomposites of Cellulose Acetate Butyrate Reinforced with Cellulose Nanocrystals. *J. Polym. Environ.* **2002**, *10*, 27–30. [CrossRef]
24. Lin, N.; Huang, J.; Chang, P.R.; Feng, J.; Yu, J. Surface acetylation of cellulose nanocrystal and its reinforcing function in poly(lactic acid). *Carbohydr. Polym.* **2011**, *83*, 1834–1842. [CrossRef]
25. Vasconcelos, N.F.; Feitosa, J.P.A.; Andrade, F.K.; Miranda, M.A.R.; Sasaki, J.M.; Morais, J.P.S.; e Silva, L.M.A.; Canuto, K.M.; de Freitas Rosa, M. Chemically modified cellulose nanocrystals as polyanion for preparation of polyelectrolyte complex. *Cellulose* **2019**, *26*, 1725–1746. [CrossRef]
26. de Mesquita, J.P.; Donnici, C.L.; Teixeira, I.F.; Pereira, F.V. Bio-based nanocomposites obtained through covalent linkage between chitosan and cellulose nanocrystals. *Carbohydr. Polym.* **2012**, *90*, 210–217. [CrossRef]
27. Souza, V.G.L.; Pires, J.R.A.; Rodrigues, C.; Coelhoso, I.M.; Fernando, A.L. Chitosan Composites in Packaging Industry—Current Trends and Future Challenges. *Polymers* **2020**, *12*, 417. [CrossRef]
28. Tyuftin, A.A.; Kerry, J.P. Gelatin films: Study review of barrier properties and implications for future studies employing biopolymer films. *Food Packag. Shelf Life* **2021**, *29*, 100688. [CrossRef]
29. Madeleine-Perdrillat, C.; Karbowiak, T.; Debeaufort, F.; Delmotte, L.; Vaulot, C.; Champion, D. Effect of hydration on molecular dynamics and structure in chitosan films. *Food Hydrocoll.* **2016**, *61*, 57–65. [CrossRef]
30. Gocho, H.; Shimizu, H.; Tanioka, A.; Chou, T.J.; Nakajima, T. Effect of polymer chain end on sorption isotherm of water by chitosan. *Carbohydr. Polym.* **2000**, *41*, 87–90. [CrossRef]
31. Madeleine-perdrillat, C.; Karbowiak, T.; Raya, J.; Gougeon, R.; Bodart, P.R.; Debeaufort, F. Water-induced local ordering of chitosan polymer chains in thin layer films. *Carbohydr. Polym.* **2015**, *118*, 107–114. [CrossRef]
32. Bajić, M.; Ročnik, T.; Oberlintner, A.; Scognamiglio, F.; Novak, U.; Likozar, B. Natural plant extracts as active components in chitosan-based films: A comparative study. *Food Packag. Shelf Life* **2019**, *21*, 100365. [CrossRef]
33. da Silva, M.A.; Bierhalz, A.C.K.; Kieckbusch, T.G. Influence of Drying Conditions on Physical Properties of Alginate Films. *Dry. Technol.* **2012**, *30*, 72–79. [CrossRef]
34. Giz, A.S.; Aydelik-Ayazoglu, S.; Catalgil-Giz, H.; Bayraktar, H.; Alaca, B.E. Stress relaxation and humidity dependence in sodium alginate-glycerol films. *J. Mech. Behav. Biomed. Mater.* **2019**, *100*, 103374. [CrossRef] [PubMed]
35. Huq, T.; Salmieri, S.; Khan, A.; Khan, R.A.; Tien, C.L.; Riedl, B.; Fraschini, C.; Bouchard, J.; Uribe-Calderon, J.; Kamal, M.R.; et al. Nanocrystalline cellulose (NCC) reinforced alginate based biodegradable nanocomposite film. *Carbohydr. Polym.* **2012**, *90*, 1757–1763. [CrossRef]
36. Brand, J.; Pecastaings, G.; Sèbe, G. A versatile method for the surface tailoring of cellulose nanocrystal building blocks by acylation with functional vinyl esters. *Carbohydr. Polym.* **2017**, *169*, 189–197. [CrossRef]
37. Oberlintner, A.; Huš, M.; Likozar, B.; Novak, U. Multiscale Study of Functional Acetylation of Cellulose Nanomaterials by Design: Ab Initio Mech. Chem. React. Microkinetics. *ACS Sustain. Chem. Eng.* **2022**, *10*, 15480–15489. [CrossRef]
38. Bajić, M.; Jalšovec, H.; Travan, A.; Novak, U.; Likozar, B. Chitosan-based films with incorporated supercritical CO2 hop extract: Structural, physicochemical, and antibacterial properties. *Carbohydr. Polym.* **2019**, *219*, 261–268. [CrossRef]
39. Sartori, C.; Finch, D.S.; Ralph, B.; Gilding, K. Determination of the cation content of alginate thin films by FTi.r. spectroscopy. *Polymer* **1997**, *38*, 43–51. [CrossRef]
40. Song, J.; Zhang, C.; Kong, S.; Liu, F.; Hu, W.; Su, F.; Li, S. Novel chitosan based metal-organic polyhedrons/enzyme hybrid hydrogel with antibacterial activity to promote wound healing. *Carbohydr. Polym.* **2022**, *291*, 119522. [CrossRef] [PubMed]
41. Rachtanapun, P.; Wongchaiya, P. Effect of Relative Humidity on Mechanical Properties of Blended Chitosan-Methylcellulose Film. *Chiang Mai J. Sci.* **2012**, *39*, 133–137.
42. Olivas, G.I.; Barbosa-Cánovas, G.V. Alginate–calcium films: Water vapor permeability and mechanical properties as affected by plasticizer and relative humidity. *LWT—Food Sci. Technol.* **2008**, *41*, 359–366. [CrossRef]

Supplementary

Effect of Environment on Acetylated Cellulose Nanocrystal-Reinforced Biopolymers Films

Ana Oberlintner 1,2, Blaž Likozar 2 and Uroš Novak 1,*

1 Department of Catalysis and Chemical Reaction Engineering, National Institute of Chemistry, SI-1000 Ljubljana, Slovenia

2 International Postgraduate School Jožef Stefan, SI-1000 Ljubljana, Slovenia

* Correspondence: uros.novak@ki.si

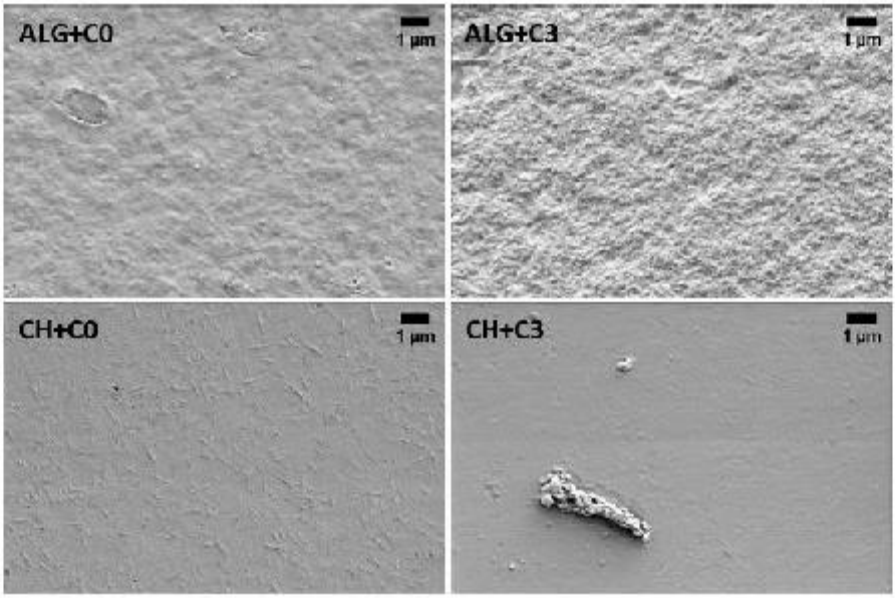

Figure S1. SEM micrographs of alginate films with pristine CNCs (ALG+C0), alginate films with acetylated CNCs (ALG+C3), chitosan films with pristine CNCs (CH+C0), chitosan films with acetylated CNCs (CH+C3) in the upper part.

4.3 Biodegradation of Polysaccharide-Based Biocomposites with Acetylated Cellulose Nanocrystals, Alginate and Chitosan in Aqueous Environment

The last section of this chapter is dedicated to the analysis of biopolymer-based packaging end-of-life, which is crucial in designing truly sustainable materials. Chitosan and alginate-based composites with (acetylated) CNCs were evaluated in terms of morphology (SEM), structure (ATR-FTIR) water content and water solubility, mechanical properties, thermal degradation (TGA coupled with FTIR) and crystallinity (XRD) and exposed to activated sludge biodegradation medium with known physicochemical parameters, elemental composition and morphology. Biodegradation was followed *via* respirometry with OxiTop system over the course of 120 h. Additionally, *in situ* FTIR was performed to propose a biodegradation mechanism of the films. The results showed initial faster degradation of chitosan-based films compared to alginate-based ones. Furthermore, chitosan-based films with incorporated pristine and modified CNCs degraded at faster rate and to higher degradation percentage. Still, pure chitosan films, with added pristine CNCs and with incorporated acetylated CNCs degraded to 76 %, 89 % and 92 %, respectively, where the degradation rate plateaued until the end of the experiment. On the other hand, all alginate-based films degraded completely over a maximum of 112 hours. Furthermore, advanced statistical analysis revealed that biodegradation of biocomposite films is mostly dependent on biopolymer type, followed by thermal stability and water solubility. While this study has several limitations (controlled environment that is not present in real-world treatment facilities and analysis of activated sludge medium with *in situ* FTIR instead of films), this study presents a good starting insight into the biodegradation process of biopolymer-based films.

Regarding my contribution: I was involved in the conceptualization of the study, film preparation and their physicochemical analyses, interpreted *in situ* FTIR results and co-wrote the manuscript.

Biodegradation of polysaccharide-based biocomposites with acetylated cellulose nanocrystals, alginate and chitosan in aqueous environment

Beti Vidmar[a, †], Ana Oberlintner[a, b, †], Blaž Stres[a, c, d, e], Blaž Likozar[a], Uroš Novak[a, *]

[a] National Institute of Chemistry, Department of Catalysis and Chemical Reaction Engineering, Hajdrihova 19, SI-1000 Ljubljana, Slovenia

[b] Jožef Stefan International Postgraduate School, Jamova cesta 39, SI-1000 Ljubljana, Slovenia

[c] Jožef Stefan Institute, Department of Automation, Biocybernetics and Robotics, Jamova cesta 39, SI-1000 Ljubljana, Slovenia

[d] Faculty of Civil and Geodetic Engineering, Institute of Sanitary Engineering, Jamova 2, SI-1000 Ljubljana, Slovenia

[e] University of Ljubljana, Biotechnical Faculty, Jamnikarjeva 101, SI-1000 Ljubljana, Slovenia

[†] The authors contributed equally to this work and share first authorship

Abstract

Biocomposite films from renewable sources are seen to be viable candidates as sustainable, zero-waste packaging materials. In this study, biocomposites films using chitosan and alginate as matrices, and pristine or acetylated cellulose nanocrystals (CNCs) as reinforcement agents, were fabricated, thoroughly characterized in terms of structure (with ATR-FTIR and XRD), morphology (SEM), thermal stability (TGA coupled with FTIR), water content and solubility and mechanical properties and subjected to controlled biological degradation in aqueous environment with added activated sludge. Biodegradation activity was followed through respirometry by measurement of change in partial O_2 pressure using OxiTop® system. While the initial rate of biodegradation is higher in

*Corresponding author.

E-mail address: uros.novak@ki.si (U. Novak)

chitosan-based films with incorporated CNCs (both pristine and modified) compared to any other tested biocomposites, it was observed that chitosan-based films are not completely degradable in activated sludge medium, whereas alginate-based films reached complete biodegradation in 107 h to 112 h. Additional study of the aqueous medium with in situ FTIR during biodegradation offered an insight into biodegradation mechanisms. Use of advanced statistical methods indicated that selection of material (ALG vs CH) has the highest influence on biodegradability, followed by solubility of the material and its thermal stability.

Keywords: polysaccharide-based films, cellulose nanocrystals acetylation, activated sludge characterization, biodegradation activity, biochemical oxygen demand, OxiTop®;

1. Introduction

Plastic based on fossil fuels is one of the most abundant materials due to its good mechanical properties, versatility and low price [1]. The global production of plastics is > 380 million tons per year and is further increasing annually by 4 %. Since 1950, a total of 6.3 billion tons of plastic waste has been produced [2]. Approximately 50 % of plastics is used to make disposable, single use packaging materials with one of the main pollutants being polyethylene (PE) based food wrappings that persist in the environment long after their use [3,4]. Due to chemical inertness, stable carbon-hydrogen bond, very large complex polymeric structure and hydrophobicity, microorganisms do not possess an adequately efficient mechanism for its rapid digestion causing physical and chemical contamination of soils and oceans around the world [5][6], highlighting the urgency for action on reducing plastic pollution.

Given the enormous amount of plastic waste around the world, efforts have spurred to create innovative strategies for managing plastic waste [7], educate on proper disposal, expose the challenges on waste management [8] and to develop new class of biodegradable materials [9]. Such bio-based

alternatives have been developed mostly over the last decade, with the main goal of enabling a safe return of carbon back to terrestrial and aquatic ecosystems, where decomposed products would act as source of food for microorganisms, and thus aligning with concept of zero-waste circular economy [6].

Polysaccharides from various renewable sources, such as cellulose (in native as well as nanostructured form), starch, chitosan, agar, alginate, etc. have been used to eco-design packaging materials [10–13]. The increasing interest in nanosized materials is due to the fact that by reducing the size of cellulose fibers, a more consistent material with high mechanical strength, despite being lightweight, can be obtained [14]. Regardless of the positive impact that wider use of biopolymers based materials would have on the environment, their applicability is currently limited due to their weaker mechanical properties compared to petrol-based polymers, especially brittleness of material, strong hydrophilic behavior and therefore poor solubility for some polysaccharides (for example amylopectin), which causes agglomeration, thermal instability etc. [15,16]. It remains a challenge to create a material that exhibits sufficient mechanical strength, while still being biodegradable as it requires a unique balance between biodegradability and durability [1]. It is also of paramount importance to learn and explore the biotic and abiotic factors that facilitate their decomposition. Even though biopolymer-based materials are still in their developing phase they are highly useful in various applications such as food packaging, composting bags, technical applications, construction, engineering, cosmetics, catering, agriculture and horticulture, pharmaceutical and medical industry [17,18].

The drawbacks of using natural biopolymers can be improved by making biocomposites where nanosized materials based on cellulose are incorporated into a biopolymer matrix. For clarity, throughout this paper 'biomaterials' is a general term that is used for all biopolymers and biopolymer-based films (chitosan, alginate, CNCs as well as chitosan and alginate with incorporated CNCs), while 'biocomposites' contain at least two of the biomaterials (e.g. chitosan with incorporated CNCs).

Incorporation of these materials shows an increment in the mechanical and barrier properties [19]. Nanocellulose is used as a reinforcing filler to alter the viscosity and enhance mechanical properties, while also enabling the acceleration of the biodegradation rate [20,21]. However, cellulose and its nanoscaled counterparts exhibit low compatibility with numerous polymer matrices due to their inherent hydrophilicity. As a solution, surface modifications are carried out, with one of the most commonly used reactions being esterification [22]. Acetylation of CNCs was previously already carried out to enhance mechanical strength in polymer matrices such as polylactic acid and poly(ε-caprolactone) [23–25]**.** For that reason, CNCs and their modified forms are actively used in the preparation of polymer films, composites, hydrogels, and various other prospectuses [26]. While several studies are conducted to indicate the biodegradability of the cellulose nanomaterials, chitosan and alginate films [12,27], it is important to study biodegradability of biocomposites as well [19].

With this is mind, the aim of this study is to fabricate biocomposite films based on alginate, chitosan and (modified) CNCs, characterize them in terms of structure, morphology, mechanical properties, thermal stability, crystallinity and water-related properties (moisture content and water solubility) and finally to evaluate their biodegradation in activated sludge, that was analyzed beforehand in terms of its physicochemical properties. Biological degradation in controlled environment using OxiTop® system following standard BOD involved six different combinations of biodegradable biomaterials or the biocomposites with cellulose nanomaterials, furthermore determining biodegradation mechanism on chemical level using in situ FTIR. Use of advanced statistical analysis shed a light onto dependence of biodegradation process on physicochemical parameters of the films and therefore allowed the final comparison between the various biocomposites.

2. Materials and methods

2.1. Materials

Chitosan (high molecular weight, 310000-375000 Da, >85 % deacetylated), sodium alginate and lactic acid (85 wt % aqueous solution) were purchased from Sigma-Aldrich (Darmstadt, Germany). Glycerol and cellulose nanocrystals (CNCs, 3 wt % suspension in water) were obtained from Pharmachem (Ljubljana, Slovenia) and Navitas (Stari trg pri Ložu, Slovenia), respectively. For chemical modification pyridine (Merck, Darmstadt, Germany), acetic anhydride (Sigma Aldrich, Darmstadt, Germany) and acetone (Sigma Aldrich, Darmstadt, Germany) were used. All other reagents used in this work were purchased from Sigma Aldrich (Darmstadt, Germany).

2.2. Preparation of polysaccharide biocomposites and their characterization

2.2.1. Fabrication of polysaccharide films

CNCs surface modification was carried out on Radleys Carousel 6 Plus Reaction Station™ under reflux and constant nitrogen flow. 1 g of previously freeze-dried CNCs was grinded in mortar to uniform powder and dispersed in 10 mL of pyridine. Upon reaching the reaction temperature (90 °C), 5 mL of acetic anhydride was added dropwise. After 300 min, the modified CNCs were washed with water four times and finally with mixture of acetone and water. The samples were again freeze dried under vacuum and stored in refrigerator at 4 °C until further use.

For chitosan and alginate-based films 1.5 wt % of biopolymer was dissolved on a magnetic stirrer at 300 rpm in 1 v/v % lactic acid (chitosan) or water (alginate) and 30 wt % glycerol with respect to the biopolymer. Lactic acid is often utilized in the development of chitosan films for packaging purposes because of its ability to act as a plasticizer. This results in a reduction of stiffness and an increase in the percentage of elongation in the films [28]. To remove the impurities, the chitosan solution was vacuum filtered over four layers of medical gauze. For films reinforced with nanosized cellulose, CNCs in either form (pristine or acetylated) were added in amount to reach 3 wt % based on the mass of chitosan or 5 wt % based on the mass of alginate, as previously described in literature as the optimal concentration [11,27], and homogenized by circular stirring for 1 to 2 min using

UltraTurrax homogenizer (Ika, Straufen, Germany). The solutions were left on the counter overnight to eliminate the bubbles and then casted onto the petri dishes (12x12 cm) with the final amount of biopolymer being 52 g m^{-2}. The films were dried in a ventilated dehydrator (Hendi, Germany) at 40 °C for 24 h. Before further analysis, they were conditioned at relative humidity 50 % for 48 h.

For clarity, alginate-based films without CNCs, with incorporated pristine CNCs and with incorporated modified CNCs were labeled throughout the manuscript as ALG, ALG+CNCs and ALG+modCNCs, respectively. Similar applies to chitosan-based films without added CNCs (CH), with pristine CNCs (CH+CNCs) and with incorporated modified CNCs (CH+modCNCs).

2.2.2. Physicochemical analysis of the fabricated films

The structure of the produced films was analyzed with ATR-FTIR Omega 2 (Perkin Elmer, USA) with wavenumber in the range of 500 cm^{-1} to 4000 cm^{-1}, with a resolution of 4 cm^{-1} and accumulation of 16 scans. The measurements were carried out in parallel and the mean value is reported.

Tensile strength (σ) and elongation at beak (ε) were measured with XLW Auto Tensile Rester (Labthink® Instruments, Jinan, China) that is equipped with 100 N loading cell. The samples were cut to pieces sized 10 x 2 cm and fixed between the gauge segment (8 cm in length) and the cross-head speed during the analysis was 25 mm min^{-1}. For each biocomposite three samples were measured, with the average being reported. Thickness, used for calculation of σ, was evaluated with digital micrometer ABS Digital Thickness Gauge (Mitutoyo, Aurora, USA), where each sample was measured on 6 points.

To evaluate the moisture content (*MC*), the film samples were cut to pieces with approximate weight of 30 mg and dried at 105 °C for at least 12 h to ensure constant mass. The loss in weight was accounted to *MC*, which was expressed as percentage of initial sample mass. To determine solubility of biocomposites in water (*WS*), the samples were dried to eliminate water, cut to pieces of approximate 20 mg, and were immersed in 50 mL of water. After 24 h, the solution was filtered using previously

dried and weighted Whatman no. 1 filter papers, dried at 105 °C for 12 hours and weighted. The loss of mass was accounted to *WS*.

For SEM analysis of morphology, the samples were placed onto the carbon tape, sputtered with 2 nm of gold and inspected with SEM Supra 35V (Carl Zeiss, Jena, Germany) under near-vacuum conditions and accelerating voltage 1 kV.

Thermal stability was assessed through thermogravimetric analysis (TGA) with EGA 4000 (Perkin Elmer, USA), equipped with FTIR Spectrum 3 (Perkin Elmer, USA). Thermal degradation was carried out in nitrogen (50 ml min^{-1}) from 40 °C to 700 °C with a step of 10 °C min^{-1}. The FTIR spectra of exhaust in the cell were continuously acquired between 4000 cm^{-1} and 500 cm^{-1} with accumulation of 4 scans.

XRD spectra were recorded with high resolution X-ray diffractometer PANalytical X'Pert PRO (Malvern Panalytical, United Kingdom) between recorded between 5 and 50 ° using Cu K-alpha radiation source.

2.3. Determination of physicochemical parameters of activated sludge

2.3.1. Activated sludge for biodegradation

Activated sludge was collected from aerated pool of wastewater treatment facility in Ljubljana, Slovenia that treats mainly municipal wastewater. The sludge was preconditioned to reduce endogenous respiration rate by storing at 4 °C for 5-7 days, in which time physicochemical parameters of the sludge were determined as described in Supplementary material (Determination of physicochemical parameters of activated sludge).

2.3.2. Determination of total COD, soluble COD, total nitrogen and soluble nitrogen

The total COD analyses were achieved with a COD cell test (14555, Merck, Germany) designed for water samples under the working conditions of the specified procedure [29]. This method determines

the oxygen equivalent of materials by oxidizing them in the presence of sulfuric acid and a known excess of potassium dichromate. Samples of polysaccharide films and fresh activated sludge were dried and homogenized prior testing and were later on mixed with water and added inside of the tilted reaction cell onto the reagent. The contents of the cell were vigorously mixed. The reaction took place at 148 °C in the preheated reactor for 120 min. Absorbance was measured at 605 nm using Synergy™ 2 Multi-Detection Microplate Reader (BioTek, Winooski, USA). Results were expressed as g/L COD (=g/L O_2).

For all other analyses only activated sludge was used. To get the soluble fraction of wastewater sludge, the samples were centrifuged at 15000 rpm for 20 minutes, after which supernatant represented the soluble fraction. Soluble COD was measured using LCK 114 cuvette tests, nitrogen (soluble) and total nitrogen were measured using LCK 338 cuvette test (Hach, USA). Organic carbon (soluble) was measured using LCK 386 cuvette test (Hach, USA). When necessary, samples were appropriately diluted with deionized water (Milipore) as described before [30].

2.3.3. SEM micrographs of activated sludge

The activated sludge samples were prepared for SEM by centrifugation of the liquid suspension from the aerated pool. The pellet was resuspended in 5 % glutaraldehyde prepared in 0.1 M phosphate buffer and has been further processed as described before [31]. To observe the morphological properties of the activated sludge the dried cells were mounted on to a SEM sample stub with a double-sided carbon tape. Surface morphology was observed by scanning electron microscope SUPRA 35VP (Carl Zeiss, Jena, Germany) under near-vacuum conditions.

2.4. Biodegradation studies

The biodegradation of alginate- and chitosan-based biocomposites was monitored using the OxiTop® Control system (WTW) which measures automatic respirometric pressure in closed bottles at a constant temperature. The test is based on measuring biochemical oxygen demand (BOD) as microorganisms break down organic matter, consuming oxygen and producing carbon dioxide that is absorbed by sodium hydroxide (NaOH) pellets, thus not affecting the measured pressure. Pressure decrease is solely due to oxygen consumption in the bottle. The instrument calculates the BOD in mg/L according to the Eq. (1):

$$\mathrm{BOD}\left(\frac{\mathrm{mg}}{\mathrm{L}}\right) = \frac{M(O_2)}{R*T_m} * \left[\frac{V_{tot} - V_1}{V_1} + \frac{\alpha\, T_m}{T_0}\right] * \Delta p\,(O_2) \quad (1)$$

where M (O_2) is molecular weight of oxygen, R is the gas constant (8.314 kPa mol^{-1} K^{-1}), T_m is the temperature of measurement, T_0 is 273.15 K, V_{tot} is the volume of the bottle, V_1 is the volume of the solution, α is the Bunsen absorption coefficient (0.03103) and Δp (O_2) is the change in partial oxygen pressure [32,33].

The biodegradability measurements were carried out in an aqueous medium and according to the protocol of the international standard ISO 9408 [34]. The medium in which biocomposite films were degraded contained deionized water and nutrients as followed – 1 % solution A (8.5 g/L KH_2PO_4; 21.75 g/L K_2HPO_4; 33.4 g/L $Na_2HPO_4 \cdot 2H_2O$ and 0.5 g/L NH_4Cl), 0.1 % solution B (22.5 g/L $MgSO_4 \cdot 7H_2O$), solution C (27.5 g/L $CaCl_2$) and solution D (0.25 g/L $FeCl_3 \cdot 6H_2O$). The nitrification inhibitor *n*-allylthiourea (c=10 mg/L) as well as activated sludge (concentration of dissolved organic carbon was 80 mg/L) as the source of microorganisms were added to the nutrient medium. The latter was divided into OxiTop® bottles of 365 mL each and films of biocomposites were added in different weights, according to their COD (final amount being 274 mg/L). As seen in Fig. 1, negative control contained no biocomposite films and for positive control 125 mg/L sodium acetate was added, which

is easily degradable substrate that allowed us to evaluate the activity of the used activated sludge and present microorganisms. The measurements were carried in closed bottles under constant temperature (23 ± 1 °C) for 5 days. After the incubation period, the degrading capability of the activated sludge was analyzed and interpreted using various parameters as mentioned below in the section 3.3.

The aquatic biodegradation percentage was calculated based on measured oxygen consumption during testing according to Eq. (2):

$$\text{Biodegradability (\%)} = \frac{(BOD_S - BOD_B) * 2}{COD} * 100 \quad (2)$$

where BOD_S is the biochemical oxygen consumption of the sample, BOD_B is the biochemical oxygen consumption of the negative control (blank) and COD of the sample The oxygen consumption values of the sample and negative control had to be multiplied by appropriate factors based on the medium volume used (e.g., 365 mL, multiplied by a factor of 2) [34]. The schematic representation of experimental setup for biodegradation studies can be found in SI Fig 1.

2.4.1. In situ Fourier-transform infrared spectroscopy

Activated sludge medium was followed with in situ Fourier-transform infrared spectroscopy (in situ FTIR) throughout the biodegradation process. The spectra were recorded for maximum of 88 h with analyzing changes every 5 minutes to determine the newly present species in medium as a result of biopolymers degradation. The analysis was performed at a room temperature (23 ± 1 °C) at a wavelength of 4000 cm^{-1} to 650 cm^{-1} with a resolution of 1 cm^{-1} with a ReactIR 45P in situ process FTIR (Mettler Toledo, Ohio, USA). Biodegradability evaluation was conducted in an aqueous medium (Section 2.4) with 10 times more substrate added based on the COD of biocomposite films (2.74 g/L). The probe was initially placed in the medium until the baseline stabilized (approximately 2 hours), followed by addition of the biocomposite films and sealing the bottle with parafilm.

2.4.2. Multivariate statistical analysis

The data derived from measurements within OxiTop®, in situ FTIR, ATR-FTIR, XRD, TGA, mechanical characteristics (σ, ε, thickness, moisture content, solubility) were organized into matrices. For the datasets represented by thousands of datapoints (e.g. in situ FTIR, ATR-FTIR, XRD) dimensionality was reduced utilizing NonMetric Multidimensional Scaling (nmMDS) using Euclidean, Hotelling and Ochiai distance with 500 random starts with real and randomized data and Principal Cooordinate analysis (PCoA) to balance the contribution of information by each of the techniques and to reduce the inflation of information by the differences in the number of internal datapoints (e.g. FTIR, XRD and mechanical properties contained > 3500, > 200 and 4 datapoints per sample). The Monte-Carlo (MC) technique was used to assess the significance of correlations, stress decomposition (MC Scree plot) and the number of dimension axes to retain. The resulting coordinates derived of complex multivariate were included as explanatory variables describing the contributions of each technique to scatter in biodegradation data (described by OxiTop®) in multivariate redundancy analyses. A linear-constrained ordination, redundancy analysis (RDA) with forward selection was used to create a model of parameters explaining the variability in biological variables. The MC permutation test (500 permutations), with chemical and mechanical characteristics used as predictors, was applied to compute the significance of hypothetical relations using multivariate data analysis software Canoco for Windows V4.5, as described before [35–37].

3. Results and discussion

3.1. Analysis of activated sludge

The results of physicochemical characterization of activated sludge are presented in Table S1 and Table S2.

Direct investigation using SEM revealed that the activated sludge obtained from the wastewater treatment plant exhibited a complex environment with a diverse microbial consortium. The microorganisms appeared to connect with each other predominantly through numerous thread-like shapes, as shown in Fig. 1 b. Additionally, the activated sludge had a flocculent appearance, as seen in Fig. 1 a, with colonies of bacteria cells surrounded by mucous (Fig. 1 c). Furthermore, apart from rod-shaped bacteria, some spirillum-shaped bacteria were also observed (Fig. 1 d). These SEM images provided some insights into the morphology and composition of the activated sludge, highlighting the complexity of the microbial community present in the wastewater treatment plant.

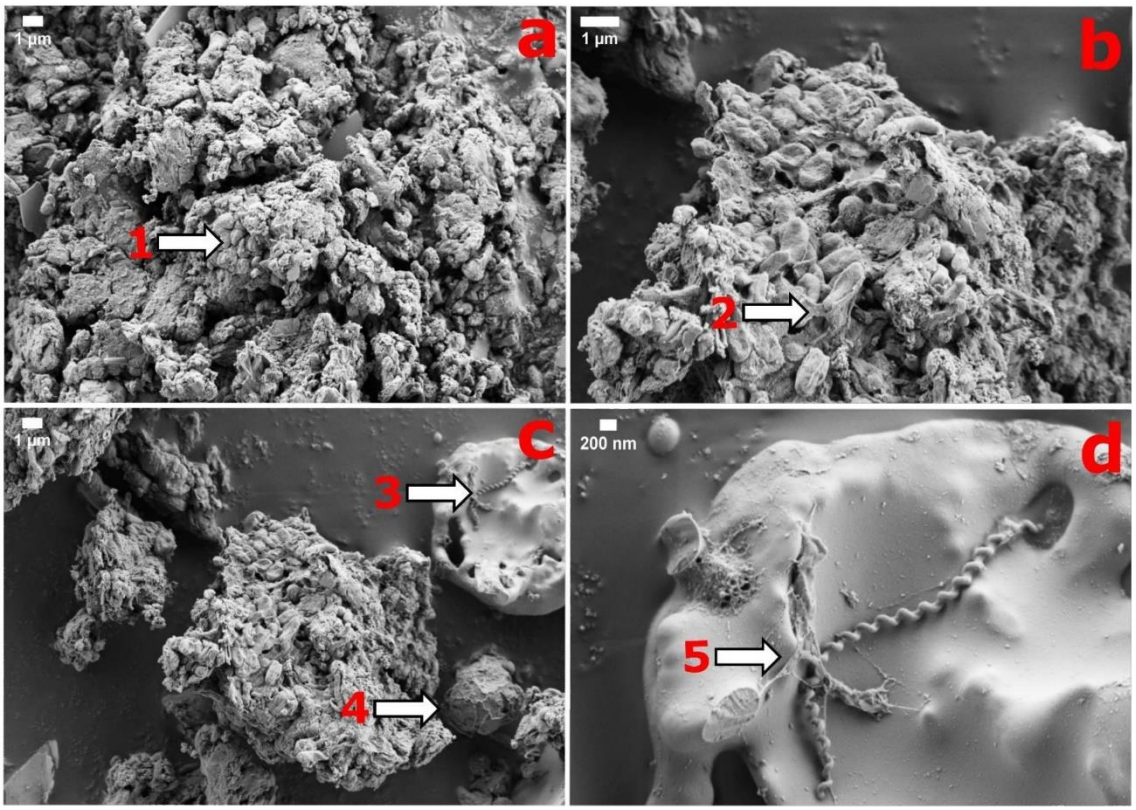

Fig. 1. SEM micrographs of the wastewater activated sludge. (a) Flocculent appearance of activated sludge (arrow 1, magnification 10000x); (b) microbe associations interconnected with threads (arrow

2, magnification 20000x); (c) spirillum-shaped bacteria (arrow 3) and colony of bacteria cells surrounded by mucous (arrow 4, magnification 10000x); (d) spirillum-shaped bacteria attached by mucous threads to a fragment (arrow 5, magnification 40980x).

3.2 Physicochemical and structural properties of the fabricated alginate-based films

As demonstrated in Fig. 2 a, the fabricated alginate-based films appeared uniform, transparent, colorless and shiny. Upon addition of CNCs and modified CNCs they gained cloudy milky-like appearance. Detailed inspection of the samples with SEM revealed that upon addition of both pristine and modified CNCs, the roughness of previously smooth and even surface is slightly increased. However, even at higher magnifications, there are no CNCs visible, indicating homogeneous incorporation into the matrix. Structural changes related to incorporation of CNCs were investigated through ATR-FTIR analysis. Spectrum of the films consisting of alginate biopolymer only (blue line in Fig. 2 b) exhibits characteristic peaks for alginate: a broad peak between 3500 cm^{-1} and 3000 cm^{-1} corresponding to O-H stretching vibrations, peaks between 3000 cm^{-1} and 2810 cm^{-1} correlated to symmetric C-H_2 and asymmetric C-H_2 stretching vibrations [35], -COO- asymmetric and symmetric stretching related peaks centered at 1598 cm^{-1} and 1411 cm^{-1}, respectively, with the latter overlapping with O-H bonding modes, and a sharp peak at 1024 cm^{-1} corresponding to C-O-C stretching vibrations in alginate backbone [36,37]. With incorporation of modified CNCs a new peak centered at 1744 cm^{-1}, related to C=O stretching in acetylated CNCs. The shape of XRD spectra (Fig. 2 c) indicated that alginate-based films exhibit a mostly amorphous structure. In ALG the crystalline peak centered at 20.8 ° is broad, while in samples ALG+CNCs and ALG+modCNCs the peak is narrowed, shifted to 22.6 ° and of higher intensity, indicating increase of crystallinity due to incorporation of crystalline CNCs, the XRD spectra of which are presented alongside for comparison. There are no additional CNCs peaks that would suggest phase separation.

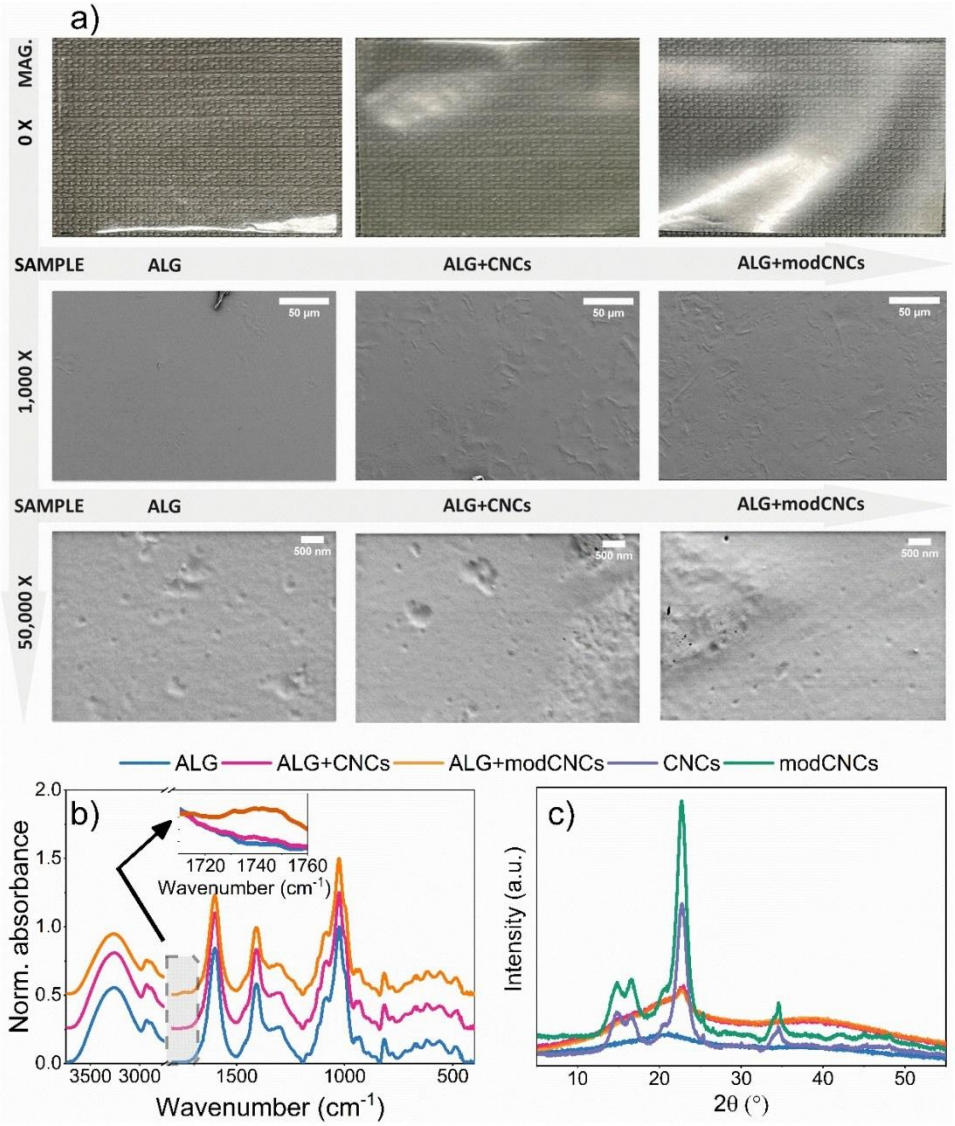

Fig. 2. (a) Photographs and SEM micrographs films as seen with naked eye and at two different magnifications (1000x and 50000x); (b) ATR-FTIR spectra of alginate-based films; (c) XRD analysis of alginate-based films alongside with pristine and modified CNCs.

To have a better insight into biological degradation, thermal stability of the fabricated biocomposites up to 700 °C was studied accompanied with FTIR analysis of the exhaust (Fig. 3). In Fig. 3 a, all spectra

collected during the degradation are presented, indicating occurrence of water (O-H stretching related peak at 3736 cm^{-1}), carbohydrate species (peaks at 2937 cm^{-1}, 1166 cm^{-1}, 1061 cm^{-1} that are correlated to C-H stretching, C-O stretching in tertiary alcohol and C-O stretching in primary alcohol, respectively), CO_2 (peak centered at 2360 cm^{-1}) and carboxylic acid (C=O stretching related peak at 1751 cm^{-1}). TGA demonstrated that degradation of alginate-based samples occurs in three temperature ranges: i) 50 – 140 °C, where the weight loss is accounted to loss of water, ii) 140 – 315 °C with maximum rate at 206 °C, and iii) 380 – 515 °C (Fig. 3 b). Following the individual peaks from FTIR analysis through full temperature range enables understanding of degradation stages. Profiles of previously detected species, presented in Fig. 3 c, confirm presence of water in first stage of degradation. In the second stage, breakage of glycosidic bonds, dehydration and decarboxylation processes occur, resulting in detection of CO_2, carboxylic acid (most likely acetic acid), C-H and C-O stretching vibrations [27,41]. Additionally, at this stage (up to 250 °C) decomposition of glycerol occurs as well [42]. The third stage of degradation is associated with the release of CH_4 [43].

As such biocomposites are designed for packaging applications, mechanical and water-related properties are important for their functioning (Table 1). It was observed that addition of pristine CNCs into alginate film forming solution slightly decreased σ of the film (25 ± 3.0 MPa) compared to ALG (29 ± 0.5 MPa), while acetylation had a positive impact onto σ (36 ± 4.4 MPa for ALG+modCNCs). ε improved slightly as well. Addition of pristine or modified CNCs did not greatly affect *MC* of the films or their *WS*.

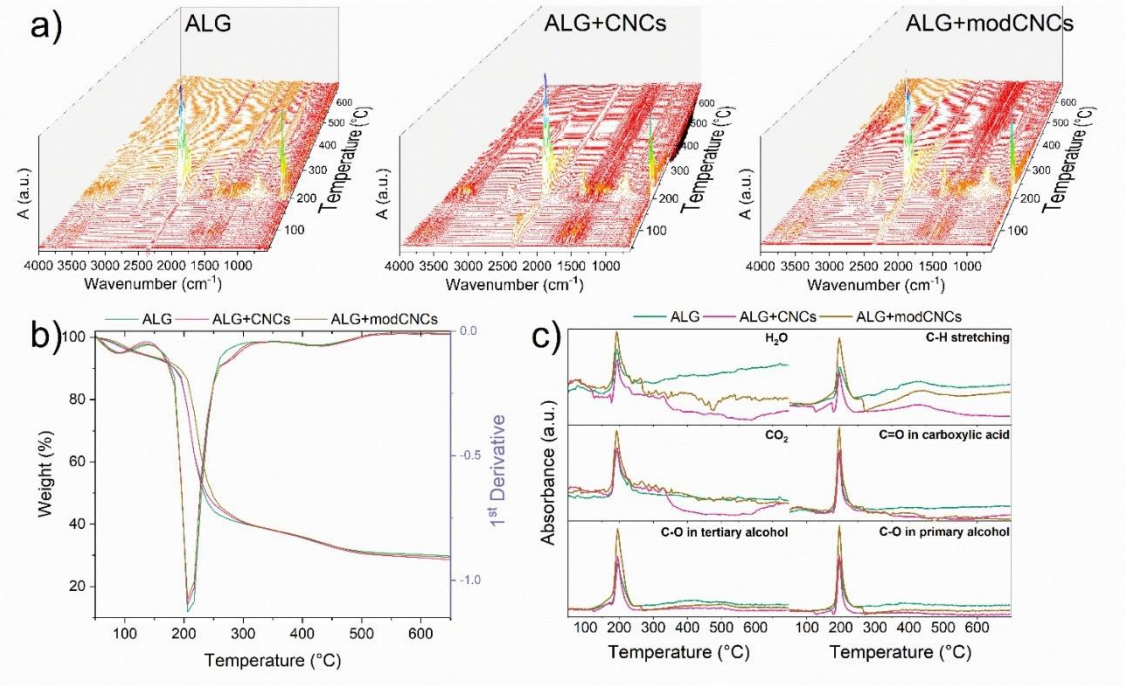

Fig. 3. Thermogravimetrical analysis of chitosan-based films coupled with FTIR. (a) FTIR spectra of exhaust in the cell while heating ALG, ALG+CNCs and ALG+modCNCs from 40 °C to 700 °C; (b) weight loss of the samples (left axis) and its first derivative (right axis); (c) temperature profiles of compounds found in exhaust during the thermal degradation.

Table 1: Analyzed physicochemical parameters of polysaccharide-based films: tensile strength (σ), elongation at break (ε), moisture content (*MC*), water solubility (*WS*) and swelling rate (*SWR*).

Sample	σ (MPa)	ε (%)	*MC* (%)	*WS* (%)
ALG	29 ± 0.5	2 ± 0.4	22 ± 1.0	69 ± 6.3
ALG+CNCs	25 ± 3.0	3 ± 0.6	19 ± 1.7	67 ± 8
ALG+modCNCs	36 ± 4.4	4 ± 0.5	23 ± 4.5	68 ± 7.4

CH	12 ± 3.6	51 ± 3.1	23 ± 1.6	14 ± 3.5
CH+CNCs	12 ± 1.5	24 ± 4.4	22 ± 2.2	18 ± 7.2
CH+modCNCs	17 ± 0.7	43 ± 7.0	26 ± 1.4	34 ± 2.1

3.3. Physicochemical and structural properties of the fabricated chitosan-based films

Chitosan-based films were sticky, slightly yellow and also transparent. No change detected with a naked eye occurred upon addition of CNCs and modified CNCs. However, CH+CNCs exhibit change in surface smoothness, as observed in SEM micrographs, due to aggregates of uneven shape with length approximately of 3 μm (Fig. 4 a). The potential reason behind the formation of such structures is incompatibility of pristine CNCs with chitosan matrix and formation of CNCs aggregates. ATR-FTIR spectrum of CH (blue line in Fig. 4 b) is characteristic for chitosan-based films and is in agreement with literature [38]. A broad peak between 3700 cm-1 and 3024 cm-1 corresponds to both O-H and N-H stretching, followed by a series of smaller peaks between 3020 cm-1 and 2840 cm-1 that are correlated to C-H stretching. Peaks at 1639 cm-1, 1570 cm-1 and 1371 cm-1 are characteristic for chitosan and are associated with C-O stretching (amide I), N-H bending (amide II) and C-N stretching vibrations (amide III), respectively [39]. A peak centered at 1729 cm-1 might be correlated to C=O stretching in lactic acid in which chitosan was dissolved to obtain FFS. The addition of CNCs into the chitosan matrix does not alter the shape of the spectra greatly. A small change is observed in peak at 1074 cm-1 that becomes more pronounced with integration of pristine CNCs and even further with incorporation of acetylated CNCs (orange and violet lines Fig. 4 b). XRD spectra of chitosan- based films (CH, CH+CNCs and CH+modCNCs) all exhibit the same peaks at $2\theta = 20.4\ ^\circ$ and $2\theta = 7.6\ ^\circ$ that are characteristic for chitosan (Fig. 4 c) [46]. Similar to alginate-based films, no additional cellulose-related peak was observed that would indicate phase separation.

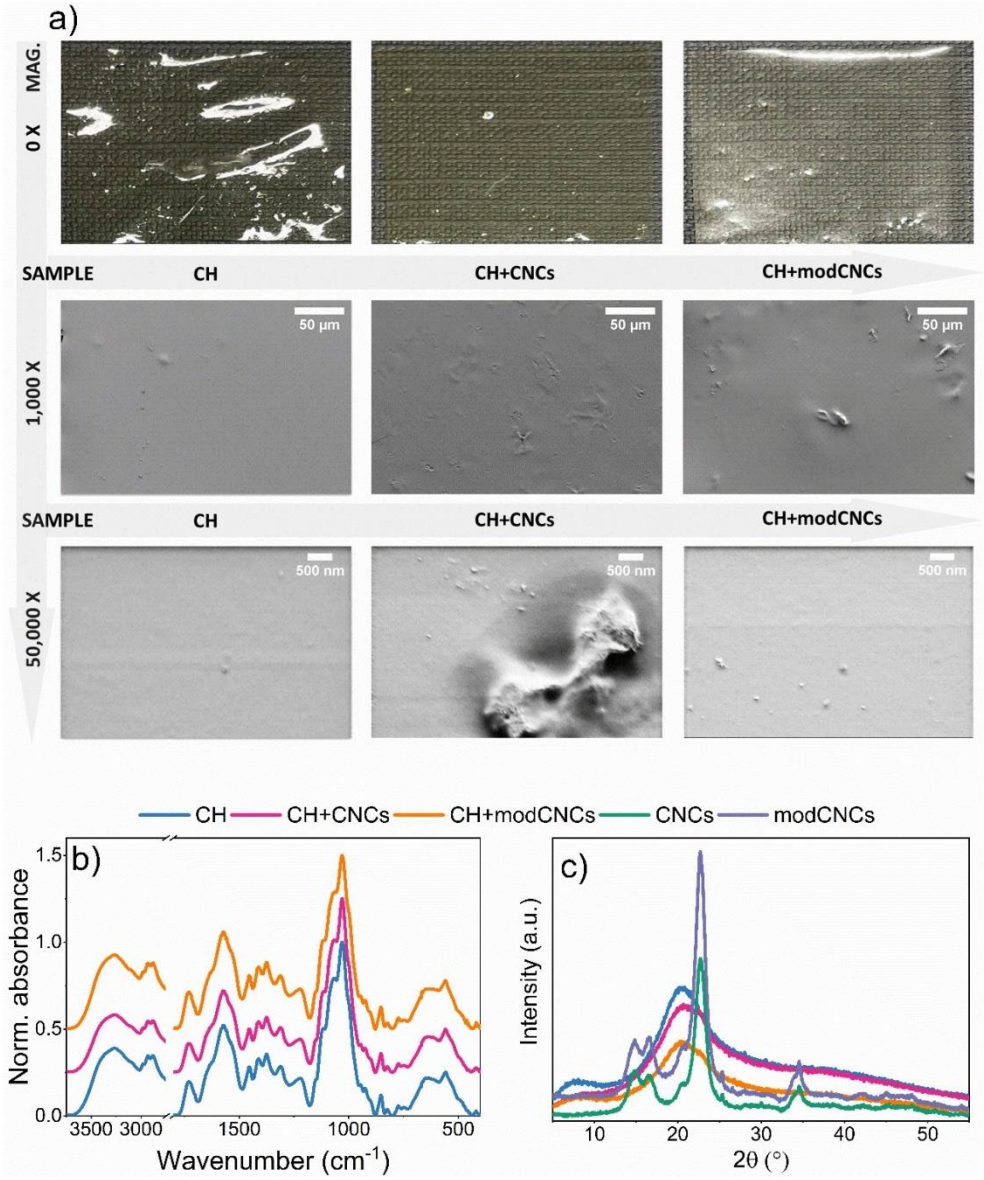

Fig. 4. (a) Photographs and SEM micrographs of chitosan-based films as seen with naked eye and at two different magnifications (0x, 1000x and 50000x); (b) ATR-FTIR spectra of chitosan-based films; (c) XRD analysis of chitosan-based films alongside with pristine and modified CNCs.

Again, TGA of chitosan-based films coupled with FTIR was carried out. Similar to alginate, the detected species were water (O-H stretching related peak at 3588 cm^{-1}), carbohydrates (peaks at 2944 cm^{-1}, 1785 cm^{-1}, 1110 cm^{-1} that are correlated to C-H stretching, C=O stretching in carboxylic acid and C-O, respectively) and CO_2 (peak centered at 2361 cm^{-1}) (Fig. 5 a). However, the thermal decomposition of chitosan-based films takes place in four stages (Fig. 5 b): i) up to 110 °C where the loss of mass can be accounted to the loss of water, ii) 180 – 240 °C, iii) 240 – 390 °C and iv) 400 -515 °C. Profiles of individual compounds through entire temperature range (Fig. 5 c) confirm loss of moisture in the first stage. According to literature, chitosan remains stable up to 250 °C, therefore the second stage of degradation is accounted to decomposition of glycerol to CO, CO_2, CH4 and C_2H_4 [47], followed by decomposition of chitosan to H_2O, CO, CO_2 and acetic acid (stage iii) and CH_4 (stage iv) [43,48].

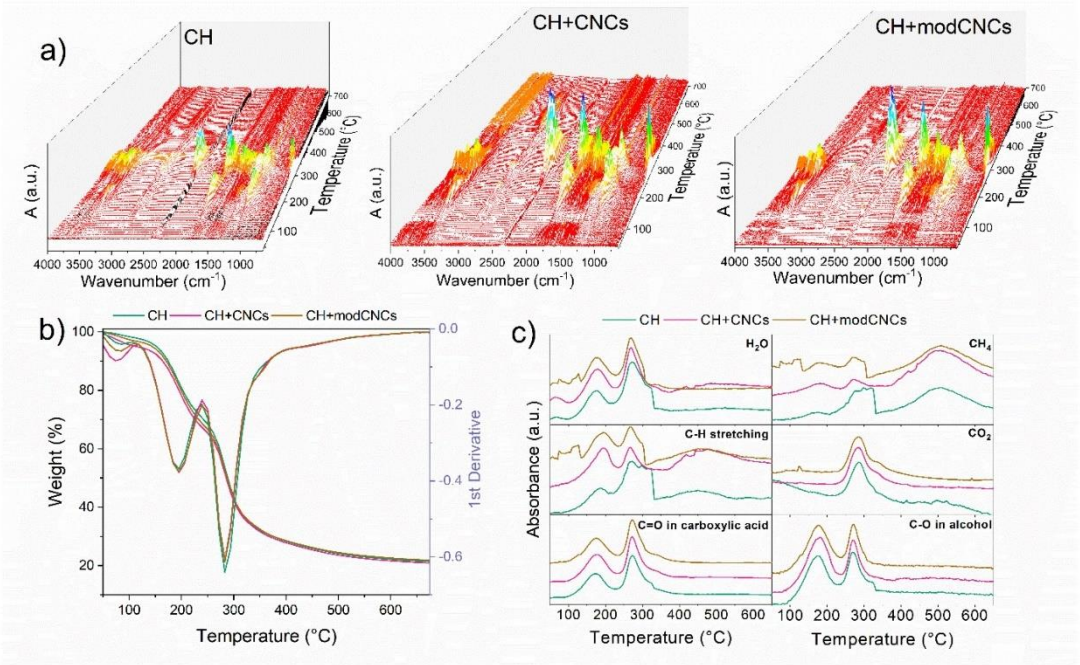

Fig. 5. Thermogravimetrical analysis of chitosan-based films. (a) FTIR spectra of exhaust in the cell while heating CH, CH+CNCs and CH+modCNCs from 40 °C to 700 °C; (b) weight loss of the samples

(left axis) and its first derivative (right axis); (c) temperature profiles of compounds found in exhaust during the thermal degradation.

Regarding properties relevant for packaging applications (Table 1), incorporation of modified CNCs slightly increased σ (from initial 12 ± 3.6 MPa to 17 ± 0.7 MPa), while addition of pristine CNCs did not have impact on mechanical strength of the biocomposite. On the other hand, ε was decreased in both instances: for 53 % in case of CH+CNCs and for 16 % in CH+modCNCs with respect to CH. Again, presence of CNCs in either form did not alter *MC* of the films, however *WS* did increase in CH+modCNCs from 14 ± 3.5 % to 34 ± 2 %.

3.4. Biodegradability studies of the fabricated polysaccharide-based films

The BOD OxiTop® system measures the amount of oxygen consumed during the degradation of organic matter by measuring changes in pressure. Biodegradability of biopolymer-based films was evaluated first through OxiTop® measurements that were later on accompanied with in situ FTIR, to obtain an insight into degradation mechanisms. During the experiment the pH value ranged between 6.9 and 7.5 and thus remained in optimal range between pH 6.5 and 8.0 [40]. To determine the degree of biodegradation at the end of the test, the amount of oxygen consumed by microorganisms in the test media (corrected for uptake by negative control, run in parallel) is expressed as a percentage.

The degradation kinetics of alginate-based and chitosan-based films showed some notable differences. As shown in the Fig. 6 a, the biocomposites film with alginate fully degraded (100 %) in the tested time period. Introduction of CNCs (either pristine or modified) did not greatly influence biodegradability of alginate-based films. The biodegradation rate of all alginate-based samples increased in a linear regime over the first 80 hours, after which the rate slowed down with complete degradation with no degradation plateau was achieved in 107 hours for ALG, and 112 hours for ALG+CNCs and ALG+modCNCs, as shown in Fig. 6 a. On the other hand, despite the faster initial

degradation rate of chitosan-based films, they are not fully degradable in activated sludge medium. The degradation rate of chitosan-based films plateaus, indicating that degradation rate does not continue to increase significantly beyond a certain point - 76 % for CH, 89 % for CH+CNCs and 92 % for CH+modCNCs (Fig. 6 b). The possible reason behind the difference in degradation kinetics could lie in higher *WS* of alginate compared to chitosan. Additionally, the presence of cellulose nanocrystals (CNCs), either pristine or modified, did not significantly influence the biodegradation of alginate-based films, while it appeared to enhance the degradation rate of chitosan-based films, possibly due to the swelling of chitosan in aqueous media and increased surface availability for microbial attack.

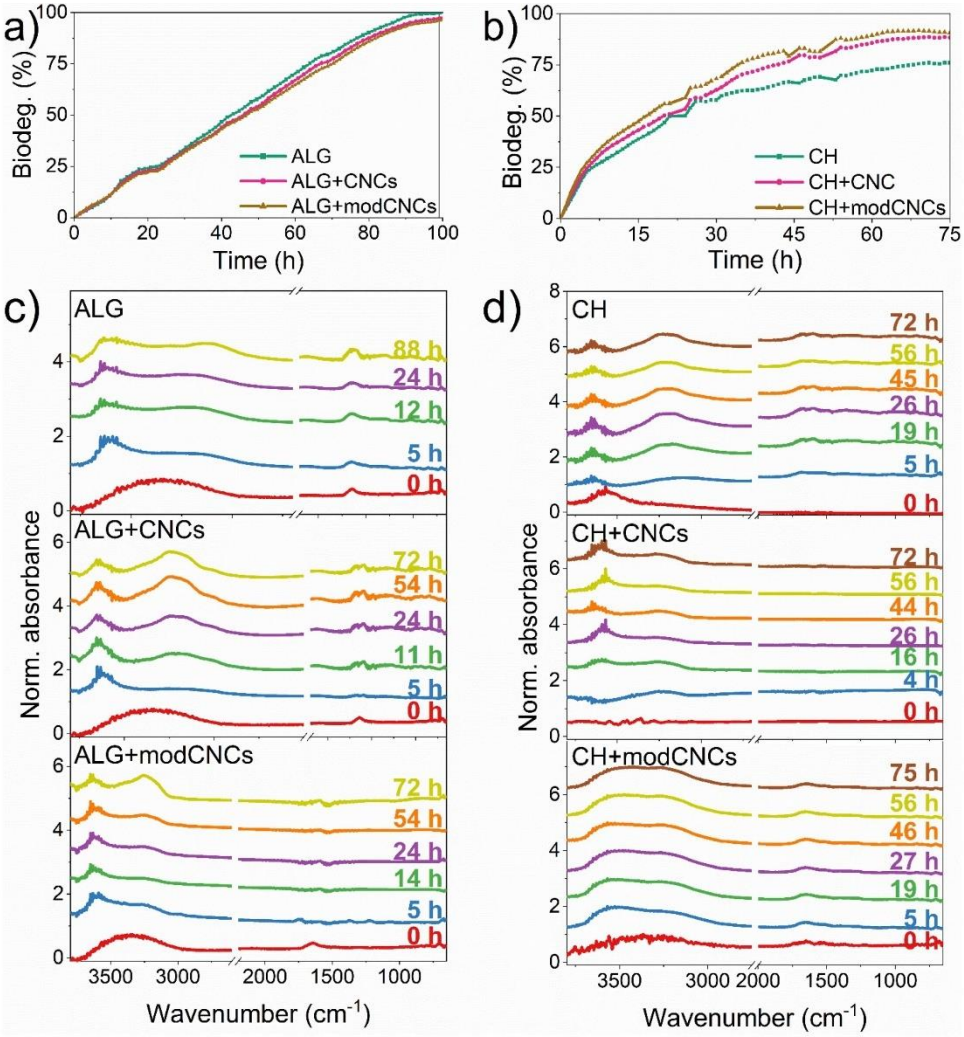

Fig. 6. Biodegradation progression of (a) alginate-based films and (b) chitosan-based films in activated sludge medium. Subfigures (c) and (d) present in situ FTIR spectra of activated sludge medium during degradation of alginate- and chitosan-based films, respectively.

To obtain a deeper insight into biodegradation mechanisms, in situ FTIR analysis of biodegradation process was carried out over the course of maximum 88 h. It should be noted, that the change in spectra of activated sludge medium was followed, with changes attributed to degradation of biopolymer-based films. Initially, at time 0, two peaks are defined in alginate-based samples (Fig. 6 c), which correspond

to N-H stretching vibrations (centered at 3356 cm^{-1}) and C=O stretching associated with proteins present in activated sludge [41], N-H bending and N-H_2 scissoring of primary amines located between 1830 cm^{-1} and 1510 cm^{-1}. During the process of degradation of all three alginate-based samples, the peak featuring N-H stretching vibrations is shifted to lower wavenumber (3275 cm^{-1}), while also becoming more pronounced in spectra of activated sludge with ALG+CNC, possibly pointing to presence of C-H species as well. A sharp peak centered at 3640 cm^{-1} newly appears is correlated to O-H stretching, possibly as a consequence of water loss in the film, indicating that water loss is responsible for the first part of alginate degradation or as a result of alginate solubility in aqueous media [42]. Additionally, a peak at 1640 cm^{-1} increases in intensity, pointing to higher abundancy of N-H and C=O species that could be related to growth of biomass in activated sludge medium.

Initial spectrum of activated sludge in which degradation of CH and CH+modCNCs samples proceeded, features a broad peak between 3750 cm^{-1} and 3350 cm^{-1} that is correlated to O-H as well as N-H stretching vibrations, while such peak was not detected in activated sludge prior to degradation of CH+CNCs (Fig. 6 d). By introduction of the sample into the activated sludge, the peak shifts to higher wavenumbers (between 3770 cm^{-1} and 3530 cm^{-1}) and a new broad peak emerges between 3450 cm^{-1} and 2950 cm^{-1} in all inspected samples. It could be attributed to N-H stretching vibrations in glucosamine and N-acetyl glucosamine that are the products of chitosan degradation, further pointing to the reasoning that faster degradation of CNCs is responsible for faster overall degradation, while the degradation mechanisms of CH, CH+CNCs and CH+modCNCs do not greatly differ [43]. Although in situ FTIR analysis of activated sludge medium offers an initial insight into the degradation mechanisms, it should be taken into an account, that certain limitations are present in the method, as only the composite itself is not recorded.

Use of advanced statistical analysis shed a light onto dependence of biodegradation process on physicochemical parameters of the films and therefore allowed the final comparison between the

various biocomposites. Multivariate analyses show that the large cumulative percentage variance in biodegradability-chemistry relation was effectively captured in the first two axes (73.9 % and 24 %). Conditional effects of environmental variables selected by forward selection in RDA as determined by Monte Carlo permutations under the full multivariate model showed that the selection of material (ALG vs CH), solubility of the material next to TGA (chemical characteristics) contributed 73 %, 18 % and 8 %, respectively, to the biodegradability-chemistry relationship (F=10.89; F=5.89; F=10.43). For other variables included in analyses collinearity was detected when fitting variable to the model and were hence omitted from the analyses. The approaches described here are fully within the scope of multivariate statistical analysis in chemometrics [53] as the type of data available does not confound to the parametric assumptions utilized in univariate statistical analysis: distributional assumptions are not fulfilled; the number of variables is often much higher than the number of objects; the variables are highly correlated, the data matrices are sparse (contain many zeroes), etc, as described recently [54,55] and an evaluation of such data provides significant additional insight that is urgently needed in the field of biomaterials.

4. Conclusions

Solutions regarding plastic waste treatment must be considered with regards to the whole supply and production chain, since the demand for it will continue to rise. Many different polysaccharides from various natural sources can be envisioned as a sustainable alternative to conventional packaging materials, following the 'zero-waste' and circular economy principles. Since these materials are renewable, locally available, easily accessible, non-antigenic, non-carcinogenic and immunogenic, they are considered as alternatives going beyond (bio)plastics. In this context, chitosan and alginate-based films reinforced with pristine and modified CNCs were characterized (XRD, SEM, TGA with FTIR, ATR-FTIR, mechanical properties, moisture content and water solubility) and studied in terms

of biodegradability in activated sludge medium. It was observed that modification of CNCs prior to incorporation into film of either matrix improves mechanical properties. With the OxiTop® method it was assessed that the initial rate of degradation was higher in chitosan-based films, although they did not fully degrade over the course of 120 h. On the other hand, alginate-based films were degraded in 107 h (neat alginate film) and 112 h (alginate films with incorporated CNCs). In situ FTIR analysis provided insight into biodegradation mechanisms, indicating water loss and solubility of alginate films and deacetylation as the first step in the degradation of chitosan films. Also, the adoption of multivariate approaches enabled us to connect and explore the complexities of biological and chemical datasets obtained in these experiments, indicating the prevalent dependence of biodegradability to biopolymer matrix (chitosan or alginate), followed by water solubility and thermal stability.

Such results can be employed to make a better correlation between microbial consortia and physio-chemical parameters during biodegradation process of biomaterials, which can be used as plastic alternatives. Additional studies are necessary to fully comprehend the correlation, as the current study exhibits limitations related to the controlled laboratory environment that may not accurately reflect the complexities of real-world wastewater treatment plants.

5. Conflict of interest

The authors declare that the research was conducted in the absence of any commercial or financial relationships that could be construed as a potential conflict of interest.

6. Author contributions

Beti Vidmar: Conceptualization, Investigation, Methodology, Data curation, Visualization, Writing – original draft, editing. **Ana Oberlintner**: Conceptualization, Investigation, Methodology, Visualization, Data curation, Writing – original draft, Writing – review and editing. **Blaž Stres:** Statistical analysis, Writing – review and editing. **Blaž Likozar**: Resources, Project administration,

Funding acquisition. **Uroš Novak**: Funding acquisition, Conceptualization, Project administration, Supervision, Writing – review and editing.

7. Funding

This study was funded by Slovenian Research Agency research core funding No. P2-0152 and PhD Grant (Ana Oberlintner) as well as by Horizon Europe projects ESTELLA (GA 101058371) and RURALITIES (GA 101060876). A.O is thankful to L'Oréal-UNESCO Slovenia for the fellowship granted to her under the program 'For Women in Science 2023'.

8. Acknowledgments

Dr. Anže Prašnikar and Edi Kranjc are acknowledged for capturing of SEM images and recording of XRD spectra, respectively. The authors would also like to acknowledge prof. Sabina Kolbl Repinc from Faculty of Civil and Geodetic Engineering, University of Ljubljana, Slovenia for assessment of the physicochemical parameters of activated sludge.

9. References

[1] Q. Xia, C. Chen, Y. Yao, J. Li, S. He, Y. Zhou, T. Li, X. Pan, Y. Yao, L. Hu, A strong, biodegradable and recyclable lignocellulosic bioplastic, Nat. Sustain. 4 (2021) 627–635. https://doi.org/10.1038/s41893-021-00702-w.

[2] J.-G. Rosenboom, R. Langer, G. Traverso, Bioplastics for a circular economy, Nat. Rev. Mater. 7 (2022) 117–137. https://doi.org/10.1038/s41578-021-00407-8.

[3] A. Krishnamurthy, P. Amritkumar, Synthesis and characterization of eco-friendly bioplastic from low-cost plant resources, SN Appl. Sci. 1 (2019) 1–13. https://doi.org/10.1007/s42452-019-1460-x.

[4] A. Agustien, M. Jannah, A. Djamaan, Screening polyethylene synthetic plastic degrading-

bacteria from soil, Der Pharm. Lett. 8 (2016) 183–187.

[5] Zeenat, A. Elahi, D.A. Bukhari, S. Shamim, A. Rehman, Plastics degradation by microbes: A sustainable approach, J. King Saud Univ. - Sci. 33 (2021) 101538. https://doi.org/10.1016/j.jksus.2021.101538.

[6] K. Ghosh, B.H. Jones, Roadmap to biodegradable plastics-current state and research needs, ACS Sustain. Chem. Eng. 9 (2021) 6170–6187. https://doi.org/10.1021/acssuschemeng.1c00801.

[7] N. Sakthipriya, Plastic waste management: A road map to achieve circular economy and recent innovations in pyrolysis, Sci. Total Environ. 809 (2022) 151160. https://doi.org/10.1016/j.scitotenv.2021.151160.

[8] X. Ren, Biodegradable plastics: A solution or a challenge?, J. Clean. Prod. 11 (2002) 27–40. https://doi.org/10.1016/S0959-6526(02)00020-3.

[9] J.H. Song, R.J. Murphy, R. Narayan, G.B.H. Davies, Biodegradable and compostable alternatives to conventional plastics, Philos. Trans. R. Soc. B Biol. Sci. 364 (2009) 2127–2139. https://doi.org/10.1098/rstb.2008.0289.

[10] G. Davis, J.H. Song, Biodegradable packaging based on raw materials from crops and their impact on waste management, Ind. Crops Prod. 23 (2006) 147–161. https://doi.org/10.1016/j.indcrop.2005.05.004.

[11] G. Lavrič, A. Oberlintner, I. Filipova, U. Novak, B. Likozar, U. Vrabič-Brodnjak, Functional nanocellulose, alginate and chitosan nanocomposites designed as active film packaging materials, Polymers (Basel). 13 (2021). https://doi.org/10.3390/polym13152523.

[12] A. Oberlintner, M. Bajić, G. Kalčíková, B. Likozar, U. Novak, Biodegradability study of active chitosan biopolymer films enriched with Quercus polyphenol extract in different soil types, Environ. Technol. Innov. 21 (2021). https://doi.org/10.1016/j.eti.2020.101318.

[13] E. Abraham, B. Deepa, L.A. Pothan, M. Jacob, S. Thomas, U. Cvelbar, R. Anandjiwala, Extraction of nanocellulose fibrils from lignocellulosic fibres: A novel approach, Carbohydr.

Polym. 86 (2011) 1468–1475. https://doi.org/10.1016/j.carbpol.2011.06.034.

[14] A. Isogai, Wood nanocelluloses: Fundamentals and applications as new bio-based nanomaterials, J. Wood Sci. 59 (2013) 449–459. https://doi.org/10.1007/s10086-013-1365-z.

[15] K. Jamshidi, S.H. Hyon, Y. Ikada, Thermal characterization of polylactides, Polymer (Guildf). 29 (1988) 2229–2234. https://doi.org/10.1016/0032-3861(88)90116-4.

[16] I.F. Wahab, S.I.A. Razak, Polysaccharides as Composite Biomaterials, in: Compos. from Renew. Sustain. Mater., InTech, 2016. https://doi.org/10.5772/65263.

[17] M. Lackner, Bioplastics, in: C. Ley (Ed.), Kirk-Othmer Encyclopedia of chemical technology, New Jersey, 2015, pp. 1-29. [18] U. Novak, M. Bajić, K. Kõrge, A. Oberlintner, J. Murn, K. Lokar, K.V. Triler, B. Likozar, From waste/residual marine biomass to active biopolymer-based packaging film materials for food industry applications- A review, Phys. Sci. Rev. 5 (2020) 1–24. https://doi.org/10.1515/psr-2019-0099.

[19] C. Zinge, B. Kandasubramanian, Nanocellulose based biodegradable polymers, Eur. Polym. J. 133 (2020) 109758. https://doi.org/10.1016/j.eurpolymj.2020.109758.

[20] N. Saba, P. Md. Tahir, K. Abdan, N.A. Ibrahim, Preparation and characterization of fire retardant nano-filler from oil palm empty fruit bunch fibers, BioResources. 10 (2015) 4530–4543. https://doi.org/10.15376/biores.10.3.4530-4543.

[21] M. Nasir, R. Hashim, O. Sulaiman, M. Asim, Nanocellulose: Preparation methods and applications, Elsevier Ltd, 2017. https://doi.org/10.1016/B978-0-08-100957-4.00011-5.

[22] S. Eyley, W. Thielemans, Surface modification of cellulose nanocrystals, Nanoscale. 6 (2014) 7764–7779. https://doi.org/10.1039/c4nr01756k.

[23] C. Xu, D. Wu, Q. Lv, L. Yan, Crystallization Temperature as the Probe to Detect Polymer-Filler Compatibility in the Poly(ε-caprolactone) Composites with Acetylated Cellulose Nanocrystal, 2017. https://doi.org/10.1021/acs.jpcc.7b05055.

[24] N. Jamaluddin, T. Kanno, T.A. Asoh, H. Uyama, Surface modification of cellulose nanofiber using acid anhydride for poly(lactic acid) reinforcement, Mater. Today Commun. 21 (2019) 100587. https://doi.org/10.1016/j.mtcomm.2019.100587.

[25] N. Lin, J. Huang, P.R. Chang, J. Feng, J. Yu, Surface acetylation of cellulose nanocrystal and its reinforcing function in poly(lactic acid), Carbohydr. Polym. 83 (2011) 1834–1842. https://doi.org/10.1016/j.carbpol.2010.10.047.

[26] T. V. Patil, D.K. Patel, S.D. Dutta, K. Ganguly, T.S. Santra, K.T. Lim, Nanocellulose, a versatile platform: From the delivery of active molecules to tissue engineering applications, Bioact. Mater. 9 (2022) 566–589. https://doi.org/10.1016/j.bioactmat.2021.07.006.

[27] T. Huq, S. Salmieri, A. Khan, R.A. Khan, C. Le Tien, B. Riedl, C. Fraschini, J. Bouchard, J. Uribe-Calderon, M.R. Kamal, M. Lacroix, Nanocrystalline cellulose (NCC) reinforced alginate based biodegradable nanocomposite film, Carbohydr. Polym. 90 (2012) 1757–1763. https://doi.org/10.1016/j.carbpol.2012.07.065.

[28] J.M.F. Pavoni, C.L. Luchese, I.C. Tessaro, Impact of acid type for chitosan dissolution on the characteristics and biodegradability of cornstarch/chitosan based films, Int. J. Biol. Macromol. 138 (2019) 693–703. https://doi.org/10.1016/j.ijbiomac.2019.07.089.

[29] APHA/AWWA/WEF, Standard Methods for the Examination of Water and Wastewater, (2005). https://www.standardmethods.org/.

[30] S.K. Repinc, B. Bizjan, V. Budhiraja, M. Dular, J. Gostiša, B. Brajer Humar, A. Kaurin, A. Kržan, M. Levstek, J.F.M. Arteaga, M. Petkovšek, G. Rak, B. Stres, B. Širok, E. Žagar, M. Zupanc, Integral analysis of hydrodynamic cavitation effects on waste activated sludge characteristics, potentially toxic metals, microorganisms and identification of microplastics, Sci. Total Environ. 806 (2022). https://doi.org/10.1016/j.scitotenv.2021.151414.

[31] M. Das Murtey, P. Ramasamy, Sample Preparations for Scanning Electron Microscopy – Life Sciences - Modern Electron Microscopy in Physical and Life Sciences, Milos Janecek and

Robert Kral, IntechOpen. (2016).

[32] P. Vähäoja, P. Piltonen, A. Hyvönen, J. Niinimäki, J. Jalonen, T. Kuokkanen, Biodegradability studies of certain wood preservatives in groundwater as determined by the respirometric BOD OxiTop method, Water. Air. Soil Pollut. 165 (2005) 313–324. https://doi.org/10.1007/s11270-005-6912-9.

[33] M. Karhu, J. Kaakinen, T. Kuokkanen, J. Rämö, Biodegradation of light fuel oils in water and soil as determined by the manometric respirometric method, Water. Air. Soil Pollut. 197 (2009) 3–14. https://doi.org/10.1007/s11270-008-9752-6.

[34] ISO 9408:1999, Water quality: evaluation of the aerobic biodegradability of organic compounds in an aquaeous medium by determination of oxygen demand in a closed respirometer - Static test (Zahn-Wellens method) (1999).

[35] P.R. Peres-Neto, P. Legendre, S. Dray, D. Borcard, Variation partitioning of species data matrices: Estimation and comparison of fractions, Ecology. 87 (2006) 2614–2625. https://doi.org/10.1890/0012-9658(2006)87[2614:vposdm]2.0.co;2.

[36] B. Stres, W.J. Sul, B. Murovec, J.M. Tiedje, Recently Deglaciated High-Altitude Soils of the Himalaya: Diverse Environments, Heterogenous Bacterial Communities and Long-Range Dust Inputs from the Upper Troposphere, PLoS One. 8 (2013). https://doi.org/10.1371/journal.pone.0076440. eCollection.

[37] T.W. Smith, J.T. Lundholm, Variation partitioning as a tool to distinguish between niche and neutral processes, Ecography. 33 (2010) 648–655. https://doi.org/10.1111/j.1600-0587.2009.06105.x [38] J.C. Tsai, Y.L. Lo, C.Y. Lin, H.M. Sheu, J.C. Lin, Feasibility of rapid quantitation of stratum corneum lipid content by Fourier transform infrared spectrometry, Spectroscopy. 18 (2004) 423–431. https://doi.org/10.1155/2004/401015.

[39] H. Aloui, A.R. Deshmukh, C. Khomlaem, B.S. Kim, Novel composite films based on sodium

alginate and gallnut extract with enhanced antioxidant, antimicrobial, barrier and mechanical properties, Food Hydrocoll. 113 (2021) 106508. https://doi.org/10.1016/j.foodhyd.2020.106508.

[40] G. Aydin, E.B. Zorlu, Characterisation and Antibacterial Properties of Novel Biodegradable Films Based on Alginate and Roselle (Hibiscus sabdariffa L.) Extract, Waste and Biomass Valorization. 13 (2022) 2991–3002. https://doi.org/10.1007/s12649-022-01710-3.

[41] H.E. Salama, M.S. Aziz Abdel, M.W. Sabaa, Novel biodegradable and antibacterial edible films based on alginate and chitosan biguanidine hydrochloride, Int. J. Biol. Macromol. 116 (2018) 443–450. https://doi.org/10.1016/j.ijbiomac.2018.04.183.

[42] B. Dou, V. Dupont, P.T. Williams, H. Chen, Y. Ding, Thermogravimetric kinetics of crude glycerol, Bioresour. Technol. 100 (2009) 2613–2620. https://doi.org/10.1016/j.biortech.2008.11.037.

[43] I. Corazzari, R. Nistico, F. Turci, M.G. Faga, F. Franzoso, S. Tabasso, G. Magnacca, Advanced physico-chemical characterization of chitosan by means of TGA coupled on-line with FTIR and GCMS: Thermal degradation and water adsorption capacity, Polym. Degrad. Stab. J. 112 (2015) 1–9. https://doi.org/10.1016/j.polymdegradstab.2014.12.006.

[44] A. Oberlintner, M. Huš, B. Likozar, U. Novak, Multiscale Study of Functional Acetylation of Cellulose Nanomaterials by Design: Ab Initio Mechanisms and Chemical Reaction Microkinetics, ACS Sustain. Chem. Eng. (2022). https://doi.org/10.1021/acssuschemeng.2c04686.

[45] M. Bajić, H. Jalšovec, A. Travan, U. Novak, B. Likozar, Chitosan-based films with incorporated supercritical CO2 hop extract: Structural, physicochemical, and antibacterial properties, Carbohydr. Polym. 219 (2019) 261–268. https://doi.org/10.1016/j.carbpol.2019.05.003.

[46] Y.X. Xu, K.M. Kim, M.A. Hanna, D. Nag, Chitosan-starch composite film: Preparation and characterization, Ind. Crops Prod. 21 (2005) 185–192.

https://doi.org/10.1016/j.indcrop.2004.03.002.

[47] T. Valliyappan, N.N. Bakhshi, A.K. Dalai, Pyrolysis of glycerol for the production of hydrogen or syn gas, Bioresour. Technol. 99 (2008) 4476–4483. https://doi.org/10.1016/j.biortech.2007.08.069.

[48] P. dos S. Araújo, G.B. Belini, G.P. Mambrini, F.M. Yamaji, W.R. Waldman, Thermal degradation of calcium and sodium alginate: A greener synthesis towards calcium oxide micro/nanoparticles, Int. J. Biol. Macromol. 140 (2019) 749–760. https://doi.org/10.1016/j.ijbiomac.2019.08.103.

[49] D.D. Baldwin, C.E. Campbell, Short-term effects of low pH on the microfauna of an activated sludge wastewater treatment system, Water Qual. Res. J. Canada. 36 (2001) 519–535. https://doi.org/10.2166/wqrj.2001.028.

[50] A.R. Badireddy, S. Chellam, P.L. Gassman, M.H. Engelhard, A.S. Lea, K.M. Rosso, Role of extracellular polymeric substances in bioflocculation of activated sludge microorganisms under glucose-controlled conditions, Water Res. 44 (2010) 4505–4516. https://doi.org/10.1016/j.watres.2010.06.024.

[51] Y. Liu, J. Zhao, C. Zhang, H. Ji, P. Zhu, The flame retardancy, thermal properties, and degradation mechanism of zinc alginate films, J. Macromol. Sci. Part B Phys. 53 (2014) 1074–1089. https://doi.org/10.1080/00222348.2014.891169.

[52] S. Beier, S. Bertilsson, Bacterial chitin degradation-mechanisms and ecophysiological strategies, Front. Microbiol. 4 (2013) 1–12. https://doi.org/10.3389/fmicb.2013.00149.

[53] K. Varmuza, P. Filzmoser, Introduction to Multivariate Statistical Analysis in Chemometrics, 1st ed., CRC Press, 2009. https://doi.org/https://doi.org/10.1201/9781420059496.

[54] R.G. Brereton, Chemometrics: Multivariate Statistical Analysis of Analytical Chemical and Biomolecular Data, in: Kunal Roy (Ed.), Chemom. Cheminformatics Aquat. Toxicol., John

Wiley & Sons, 2021: pp. 45–60. https://doi.org/10.1002/9781119681397.

[55] P. Oliveri, C. Malegori, M. Casale, Chemometrics: multivariate analysis of chemical data, in: Y. Pico (Ed.), Chem. Anal. Food, Academic Press, 2020: pp. 33–76. https://doi.org/https://doi.org/10.1016/B978-0-12-813266-1.00002-4.

Supplementary material: Biodegradation of polysaccharide-based biocomposites with acetylated cellulose nanocrystals, alginate and chitosan in aqueous environment

Beti Vidmar[a, †], Ana Oberlintner[a, b, †], Blaž Stres[a, c, d, e], Blaž Likozar[a], Uroš Novak[a, *]

[a] National Institute of Chemistry, Department of Catalysis and Chemical Reaction Engineering, Hajdrihova 19, SI-1000 Ljubljana, Slovenia

[b] Jožef Stefan International Postgraduate School, Jamova cesta 39, SI-1000 Ljubljana, Slovenia

[c] Jožef Stefan Institute, Department of Automation, Biocybernetics and Robotics, Jamova cesta 39, SI-1000 Ljubljana, Slovenia

[d] Faculty of Civil and Geodetic Engineering, Institute of Sanitary Engineering, Jamova 2, SI-1000 Ljubljana, Slovenia

[e] University of Ljubljana, Biotechnical Faculty, Jamnikarjeva 101, SI-1000 Ljubljana, Slovenia

[†] The authors contributed equally to this work and share first authorship

*Corresponding author

Phone no.: +386 1 4760 283

E-mail: uros.novak@ki.si

1. Physicochemical parameters of activated sludge

1.1. Determination of moisture content, total solids and volatile solids in activated sludge

Before the degradation the appropriate loading of the OxiTop® reactors was determined by measuring total solids, volatile solids, volatile suspended solids and total suspended solids for activated sludge samples, which were determined according to Standard Methods [1]. At first the samples of activated sludge were dried at 105 °C for approximately 24 h or at constant

weight. Moisture content was calculated according to Eq. (1) and expressed as the percentage of water content in the activated sludge:

$$\text{Moisture content (\%)} = \frac{(m_1 - m_2)}{m_1} * 100\ \% \quad (1)$$

where m_1 is the mass of the wet activated sludge sample and m_2 is the mass of the dried activated sludge.

TS and VS content were determined using annealing furnace at 550 °C overnight (to a constant mass) as described previously in official methods of analysis [1]. After annealing, the samples were transferred to a desiccator, cooled and weighed again on the analytical scale to get the final weight of dried residue. The percentage of total solids and volatile solids were calculated according to Eq. (2) and Eq. (3).

$$\text{\% total solids} = \frac{(A - B) * 100\ \%}{C - B} \quad (2)$$

$$\text{\% volatile solids} = \frac{(A - D) * 100\ \%}{A - B} \quad (3)$$

where A is the final weight of dried residue with dish included (in mg), B is weight of a dish (in mg), C is weight of the wet sample with dish included (in mg) and D is the final weight of residue with dish after annealing (in mg).

1.2. Determination of pH, redox potential and electrical conductivity of activated sludge

Redox potential and electrical conductivity of wastewater activated sludge were measured using portable multimeter HQ40D (Hach, USA). The pH-values of all OxiTop® reactors were measured at the beginning (t_0) and the end (t_5) of the experiment using a pH meter (Metrohm, Switzerland), previously calibrated between pH = 6 and pH = 8.

Table S1: Physicochemical parameters of activated sludge. COD (chemical oxygen demand), TOC (total organic carbon), TN (total nitrogen), TP (total phosphorus), TS (total solids), VS (volatile solids), TSS (total suspended solids), VSS (volatile suspended solids).

Parameters	Value
pH	6.9 ± 0.1
Moisture content (%)	88.2 ± 1.4
Electrical conductivity (mS/cm)	3.4 ± 0.01
Redox potential (mv)	136.4 ± 1.3
COD_{total} (g/L)	64.5 ± 0.5
$COD_{soluble}$ (g/L)	6.9 ± 0.02
$TOC_{soluble}$ (g/L)	3.5 ± 0.01
$NH^{+}_{4,\ soluble}$ (g/L)	0.3 ± 0.006
TN (g/L)	2.4 ± 0.2
$TN_{soluble}$ (g/L)	0.05 ± 0.0003
TP (mg/L)	4.0 ± 0.01
PO_4-P (mg/L)	3.9 ± 0.01
TS (g/L)	42.3 ± 1.1
VS (g/L)	30.0 ± 0.8
TSS (g/L)	45.0 ± 1.7
VSS (g/L)	33.8 ± 1.0

Table S2: Elemental analysis of activated sludge.

Elemental analysis	Content (wt %)
C	34.0 ± 0.03
H	5.5 ± 0.05
N	6.5 ± 0.02
S	0.7 ± 0.01

2. Schematic representation of the experimental set-up for biodegradation

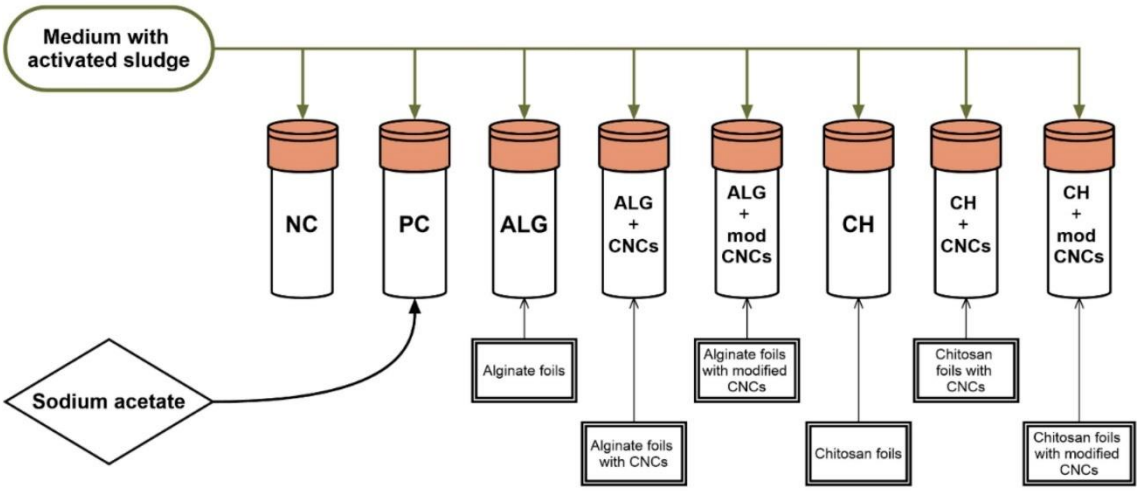

SI Fig. 1. Experimental set-up for biodegradation assay. NC – negative control (medium with activated sludge), PC – positive control respectively standard.

3. Supplementary analyses of CNCs

Freeze dried CNCs were analyzed by the means of ATR-FTIR (Omega 2, Perkin Elmer, USA) between wavenumbers 4000 cm^{-1} and 400 cm^{-1} with resolution of 4 cm^{-1} and accumulation of 16 scans. Successful modification of CNCs was confirmed with ATR-FTIR analysis that revealed two newly formed peaks at 1748 cm^{-1} and 1236 cm^{-1} that are correlated to C=O and C-O stretching. Additionally, the intensity of C-H stretching peak has increased due to C-H stretching vibrations in acetyl groups. Lastly, the decrease in O-H stretching related peak indicates substitution of surface OH groups with acetyl groups upon modification.

Crystallinity index (*CrI*) of pristine CNCs and modified CNCs was calculated from XRD spectra through Eq. 4 proposed by Segal et al. [2]:

$$CrI = \frac{I_{cryst} - I_{am}}{I_{200}} \, x \, 100 \, \% \quad (4)$$

I_{200} indicates maximum intensity at 2θ = 22.8 ° for CNCs and 2θ = 20.4 ° for chitosan-based composites (the diffraction of crystalline plane), while I_{am} stands for minimum intensity at 2θ=18.0 ° and 2θ=11.2 ° (diffraction of amorphous region).

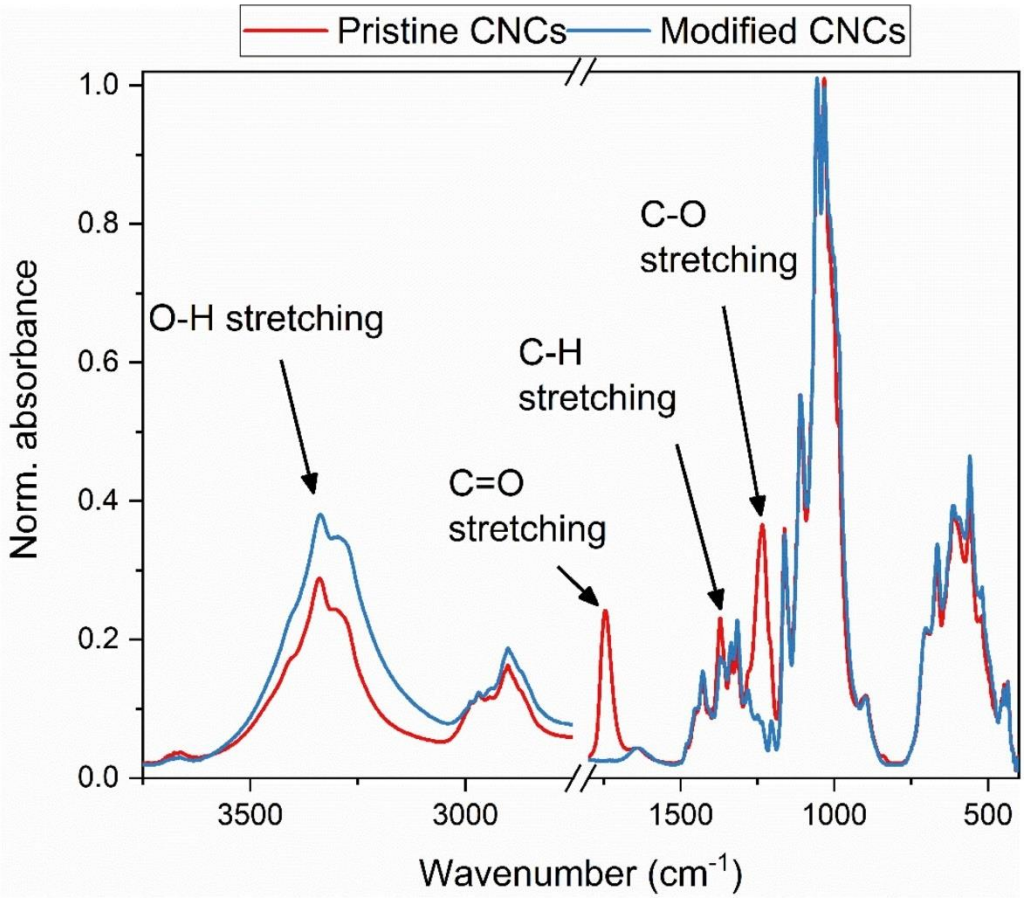

SI Fig. 2. ATR-FTIR spectra of pristine and modified CNCs.

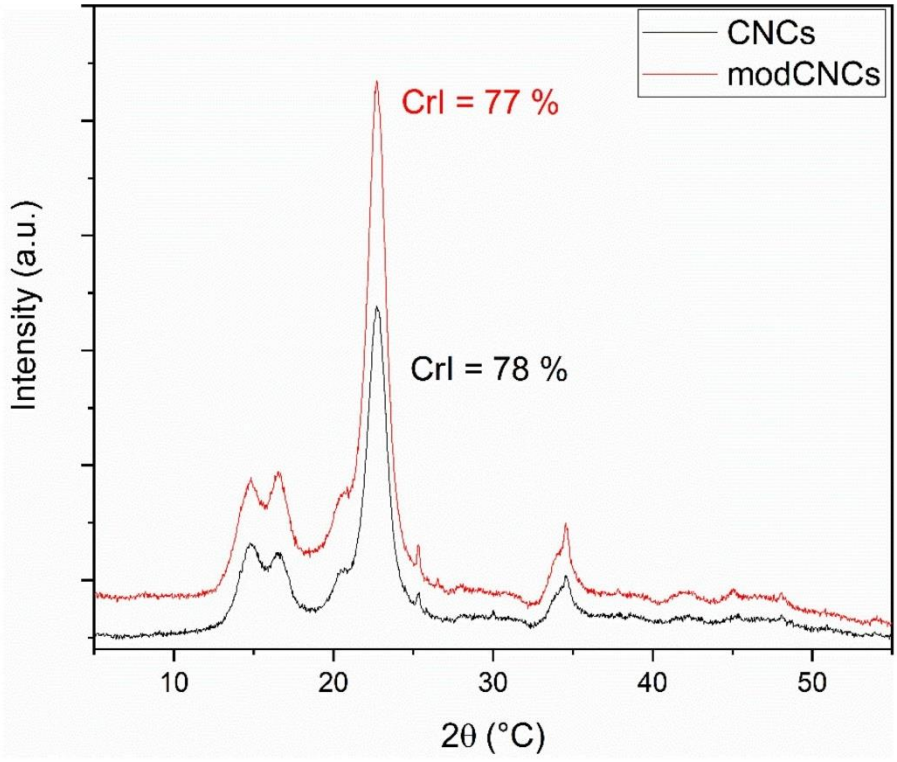

SI Fig. 3. XRD spectra of pristine and modified CNCs with calculated CrI.

4. References

[1] APHA/AWWA/WEF, Standard Methods for the Examination of Water and Wastewater, (2005). https://www.standardmethods.org/.

[2] L. Segal, J.J. Creely, A.E. Martin, C.M. Conrad, An Empirical Method for Estimating the Degree of Crystallinity of Native Cellulose Using the X-Ray Diffractometer, Text. Res. J. 29 (1959) 786–794. https://doi.org/10.1177/004051755902901003.

Chapter 5

Hydrophobization with Plasma Processing

The second limitation in cellulose nanomaterials hydrophobization research defined by the literature review (Chapter 3) are scarce reports on the use of plasma. Plasma, considered as the fourth state of matter, is generally obtained by excitement of gases by radio frequency (rf), microwave, or electrons from a hot filament discharge into energetic state (Chu et al. 2002). It has been shown that this technique enables fast processing without liquid waste and providing long-lasting effect. For hydrophobization purposes, fluorine or silane-containing gases are used, as well as inert gases such as argon along with monomers such as styrene, caprolactone and farnesene to induce surface polymerization (Alanis et al. 2019; Samanta et al. 2021).

However, plasma treatment was used mostly for surface treatment of cellulose fibers on the macro-scale, especially in the field of textile engineering, with smaller emphasis on nanostructured cellulose. Taking this into consideration, in this chapter, cellulose nanomaterials and their composites were treated with rf-generated plasma. The chapter is divided into 3 sections: 5.1 Hydrophilic to Hydrophobic: Ultrafast Conversion of Cellulose Nanofibrils by Cold Plasma Fluorination, 5.2 Permanent Hydrophobic Coating of Chitosan/Cellulose Nanocrystals Composite Film by Cold Plasma Processing, and 5.3 Use of Non-Fluorine Containing Plasma.

The chapter addresses Objective 5.

5.1 Hydrophilic to Hydrophobic: Ultrafast Conversion of Cellulose Nanofibrils by Cold Plasma Fluorination

In this section, rf-generated cold plasma in fluorine-containing gas (CF_4) is studied as a fast technique to hydrophobically modify the surface of CNFs films. It was demonstrated that conversion from hydrophilic (with WCA of 46°) to hydrophobic surface (WCA higher than 90°) can be reached in already 10 s, while maximum WCA (around 130°) was reached after 30 s of processing. Morphological analysis, carried out by the means of SEM, indicated increased nanoporosity with higher treatment times. More structured morphology might contribute to lower wettability by improving the surface tension between the water droplet and the substrate. Surface chemistry was inspected with XPS, ATR-FTIR and Raman spectroscopy, indicating the formation of C-F, C-F_2 and C-F_3 species that are responsible for the hydrophobic change. This study demonstrates that plasma presents an ultrafast technique to obtain highly hydrophobic cellulose-based surfaces.

Regarding my contribution: I fabricated CNFs films, participated in their treatment with plasma, measured WCA, carried out ATR-FTIR analysis and co-wrote the manuscript.

Applied Surface Science 581 (2022) 152276

Contents lists available at ScienceDirect

Applied Surface Science

journal homepage: www.elsevier.com/locate/apsusc

Full length article

Hydrophilic to hydrophobic: Ultrafast conversion of cellulose nanofibrils by cold plasma fluorination

Ana Oberlintner [a,b], Vasyl Shvalya [c], Aswathy Vasudevan [b,c], Damjan Vengust [c], Blaž Likozar [a], Uroš Cvelbar [b,c], Uroš Novak [a,*]

[a] Department of Catalysis and Chemical Reaction Engineering, National Institute of Chemistry, Hajdrihova 19, SI-1000 Ljubljana, Slovenia
[b] Jožef Stefan International Postgraduate School, Jamova cesta 39, SI-1000 Ljubljana, Slovenia
[c] Department of Gaseous Electronics, Jožef Stefan Institute, Jamova cesta 39, SI-1000, Ljubljana, Slovenia

ARTICLE INFO

Keywords:
Cellulose nanofibrils
Films
Functionalization
Hydrophobic
Fluorocarbon plasma

ABSTRACT

The cellulose-based products are gaining increased interest, especially as a top-choice material for replacing plastics in packaging-related fields. Nevertheless, the high inherent wettability often hinders its advancement in becoming an efficient substitute in packaging industry. To bridge this challenge,the fluorocarbon plasma processing was implemented for improvement of cellulose surface hydrophobicity. This was done on the example of nanofibrils films exposed to CF_4 plasma, in order to achieve hydrophilic to hydrophobic conversion in less than 10 s. The saturation of water contact angle (approximately 130 ± 5°) was obtained after only 30s of plasma processing. The surface fluorination was the result of the presence of newly formed C–F_3, C–F_2 and C–F bonds confirmed by high-resolution C 1s XPS spectra. A prolonged continuous plasma functionalization resulted in structural vibrational alterations associated mostly with intense IR and Raman active stretching C–F_2 mode. Simultaneously, ATR-FTIR revealed a formation of the surface-linked IR active H–F functional group. Our findings successfully demonstrate that the CF_4 plasma processing can be an effective way for ultrafast cellulose conversion from hydrophilic to hydrophobic surface.

1. Introduction

Among a variety of manufacture facilities the packaging industry remains one of the largest sectors responsible for plastic production/consumption and its piling in terrestrial and aquatic ecosystems [1]. Made of non-renewable resources, the packaging polymers being fragmented under environmental processes represent a serious threat to human health and surrounding biota [2]. Regarding the rising global ecological challenge created by plastics contamination, the alternative biopolymers such as cellulose, chitosan, alginate, starch are considered a promising substitution material to tackle the problem [3]. Within the listed compounds, cellulose is the most abundant, cheapest, is easily modified and its sources are not food-competing [4]. Originating from renewable lignocellulosic biomass, cellulose is a polymer consisting of β-1,4 linked D-glucopyranose units, each unit rotated for 180° around its axis [4]. Structured hierarchically, it enables extraction of smaller-scale materials, with improved intrinsic properties, namely rod-like nanocrystals sized from 30–500 nm in length and nanofibrils (CNFs) having diameter of the individual unit approximately 10–20 nm [5,6]. CNFs are known to be of better choice, compared to cellulose fibers, as they possess higher specific surface area and an ability to form films with tensile strength up to 214 MPa, elongation-at-break up to 10.1% and Young's modulus up to 17.5 GPa [7–9]. It allows them to be considered as a suitable material for packaging applications. However, being exposed to highly humid environment, the mechanical strength of CNFs drops over 90% of its initial property [10]. This natural hydrophilic character of cellulose and its nano-allotropes, attributed to the weakening of the hydrogen related bonds [5], prevents their broad exploitation in transportation and food-industry related packaging. For cellulose to be further employed for this specific use, the desired surface hydrophobicity, characterized by water contact angle exceeding 90°, can be achieved by two main principles: (i) decrease of the surface energy through wet or dry chemical modification or/and (ii) increase of surface roughness [11].

So far, the researchers have attempted to improve cellulose's water resistance behavior and its capability to protect the product from the surrounding humidity by means of esterification reactions [10], etherification [12], chemical vapor deposition [13], carbamation [14] and adsorption approaches [15]. The proposed strategies, however, require time consuming multi-step process, use of expensive chemicals

* Corresponding author.
E-mail address: uros.novak@ki.si (U. Novak).

https://doi.org/10.1016/j.apsusc.2021.152276
Received 30 July 2021; Received in revised form 24 November 2021; Accepted 17 December 2021
Available online 5 January 2022

and harmful organic solvents, or provided modifications are not stable upon the time [16]. On the other hand, plasma presents a tool for rapid and solvent-less controlled modification of the organic surfaces without loss of material, requiring no further separation steps and eliminating liquid discard. For industrial interest, the area of the treated material can easily be expanded by the scale-up of the low pressure plasma system. Furthermore, the same assembly enables use of various carrier gasses incorporating atoms such as fluorine, nitrogen, sulfur, or oxygen, tailoring the surface properties according to wide range of applications [17,18].

Recently, it was found that plasma hydrophobization enabling their faster processing without producing any chemical waste and ensuring long-lasting stability of modifications [19,20]. As was demonstrated, fluorine containing plasma induces hydrophobic features of the polymer composite surface. The observed findings were associated with the formation of new C–F, C–F_2 and C–F_3 bonds that were responsible for hydrophobic behavior [21]. Regarding the cellulose, plasma treatment was mainly applied to increase hydrophobicity of fibers at micro scale in the field of textile engineering. For instance, highly durable water resistant cellulose textiles were obtained upon helium/fluorocarbon and helium/1,3-butadiene direct plasma exposure [22–24]. Two-step process involving an activation of surface reactive species by oxygen plasma followed by a polymerization of monomer was also found to be helpful to improve water repulsing features of cellulose-based materials [25]. Other gases such as caprolactone, styrene, farnesene [26], oleic acid [27] and non-polymerizing argon gas accompanied or not with fluorocarbon [28–30] were successfully implemented as well.

However, to best of our knowledge, there is a lack of published studies concerning treatment of CNFs with fluorocarbon plasma and detailed inspection of the structural changes that are induced by modification. However, a little work was reported on nanosized cellulose so far [26].

To fill this gap, in the present report cellulose nanofibrils (CNFs) were studied focusing on the relevant improvement of their hydrophobic properties under fluorocarbon plasma processing. Prepared in the form of films, they were subjected to non-destructive CF_4 plasma exposure to convert their hydrophilic surface behavior to hydrophobic one. Starting with initial value of the water contact angle below 45°, the hydrophobic transformation occurred as fast as within 10 s, reaching its maximum value of about 130° right after half-minute. Followed by FTIR, XPS and Raman analysis, the nearly instant sample fluorination resulted in evident appearance of surface and structurally related FH_3, CF, CF_2 and CF_3 bondings, where contribution of fluorocarbon ones to the water repellent ultrafast conversion is more significant and increases with treatment time. Altogether, the findings suggest the use of fluor-containing plasma is highly efficient single-step facile approach for cellulose nanofibrils film hydrophobization improvement, required for their advance utilization in packaging related applications.

2. Materials and methods

2.1. Materials and film preparation

CNFs (3 wt%) were supplied by Sappi Valida (Maastricht, Netherlands). Previous studies have shown the necessity of plasticizer addition, in this study glycerol bought from Pharmachem Sušnik (Ljubljana, Slovenia) was used, to gain flexibility of the film that can be further used for hydrophobization [31].

1.15 wt% water dispersion of CNFs with glycerol in amount of 30 wt% with respect to CNFs was homogenized for 5 min at 10000 min^{-1} with UltraTurrax homogenizer (Ika, Staufen, Germany). The solution was cast into 12 *x* 12 cm petri dishes with silicon bottom. The final amount of CNFs was 25.6 g m^{-1}. The films were dried in the ventilation oven (Kambič, Slovenia) at 35 °C and 30% ventilation for 48 h. The films were covered and stored at room temperature and in the dark until the plasma treatment.

2.2. Surface treatment

The CNFs films treatment was conducted in plasma operating at radio-frequency (RF) (13.56 MHz). The plasma system consisted of 55 cm long glass tube with a diameter of 3.8 cm and a wall thickness of approximately 3 mm. The RF generator was inductively coupled by a nine-turn water-cooled copper coil. The samples were cut into rectangular pieces that were approximately 3 cm long and 2 cm wide, placed on glass substrate and inserted inside the glass tube, 10 cm from the center of the copper coil. CF_4 gas was used for the plasma discharge with flow rate of 80 sccm. Plasma power was set at constant power of 80 W. The samples were treated for 5, 10, 20, 30, 45 and 60 s.

Optical emission spectroscopy (OES) was employed to gain insight into the plasma composition. OES spectra were collected at 5 s, 15 s, 25 s, 35 s, 45 s and 55 s in wavelengths range from 200 to 800 nm. The spectral lines were identified using the NIST Atomic Spectra Database. For the analysis a broad-range spectrometer, model LR1 (ASEQ Instruments, Vancouver, Canada) was used.

2.2.1. Surface analyses

Contact angle analysis was carried out with Tensiometer Theta T200 (Biolin Scientific, Germany) in an hour after the plasma treatment. The samples were placed on the glass substrate. Distilled H_2O with the volume of the drop 4 μL was used. The water contact angle (WCA) was assessed with the sessile drop method 5 s after the drop was released onto the surface. The measurements were done in at least triplicates. To investigate the stability of the modification, the water contact angle on the sample treated for 60 s was determined 72 h after the treatment as well. In the meantime, it was kept in a plastic container at the room temperature and in the dark place.

Scanning electron micrographs were recorded with SEM Supra35V (Carl Zeiss, Jena, Germany). Film samples were placed onto the graphite tape before the analysis to ensure better conductivity. The homogeneity of the hydrophobic coating was studied using energy dispersive X-ray spectroscopy (EDS) with X-Max probe (Oxford Instruments, Abingdon, UK) equipped on JSM-7600F SEM (Jeol, Tokyo, Japan) under accelerating voltage of 5.0 kV and acquisition time 294 s.

Surface elemental composition and chemical bonding study was carried out on the selected samples immediately after the plasma modification with XPS PHI-TFA spectrometer (Physical Electronics Inc., Chanhassen, MN, USA) using an Al-monochromatic X-ray source operating at energy of 1486.6 eV.

FTIR-ATR analysis was performed after one hour the treatment at room temperature with Spectrum Two (PerkinElmer, USA) probing the range of wavelengths from 3800 cm^{-1} to 400 cm^{-1} with resolution of 4 cm^{-1}, accumulating 32 scans. The measurement was performed in duplicates and the average is reported.

Inelastic photon scattering study was conducted out by means of confocal Raman spectrometer (NTEGRA) collecting a signal in back-scattered geometry. A monochromatic 633 nm laser excitation was focused on the sample surface by applying x60 magnifying objective lens. Spectra of cellulose-based samples were acquired upon 10 s of exposure with and 5-times accumulation. In total 3 spectra from each sample were averaged, base-line subtracted, smoothed and normalized to form a final experimental curve.

3. Results and discussion

The produced CNFs films were white in color, opaque and had smooth surface. They did not stick on the silicon surface, that lead to the efficient detachment of the film. Initially, the film revealed hydrophilic behavior with WCA of 46°, which is already higher than WCA of CNF nanopaper described in literature [10]. The difference could be attributed to the addition of plasticizer (glycerol) that acts as a viscous matrix filler, enabling better mobility of the fibrils and decreasing porosity. This effect was previously observed in the films based

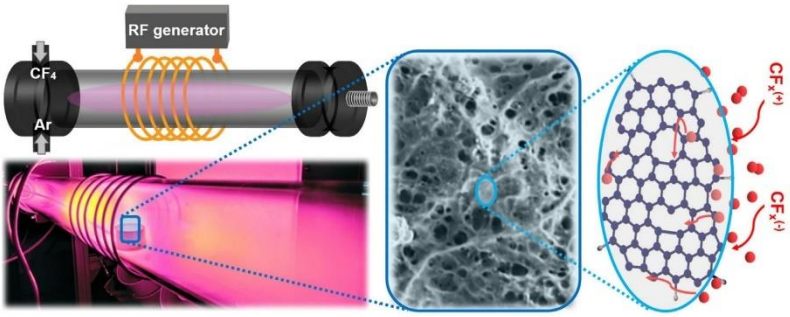

Fig. 1. Visualization of the plasma system applied for hydrophobization of cellulose nanofibrils and schematic presentation of the process of fluorination.

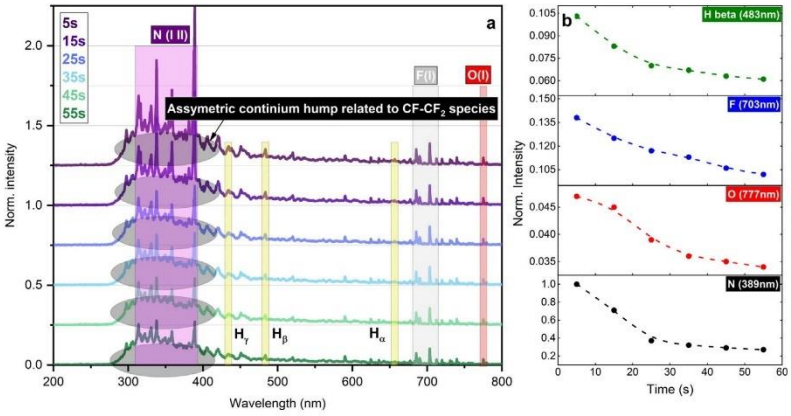

Fig. 2. (a) OES spectra of the plasma with the identified excited species and (b) time-evolution of the normalized intensity of H beta, F, O and *N* selected bands.

on cellulose nanofibers of bacterial origin [31]. To increase the water resistance and create a hydrophobic film surface, they were subjected to fluorination in a CF_4 plasma system visualized in Fig. 1. After the plasma treatment, there was no change in color or structure visible with the naked eye, regardless of the treatment duration. OES was applied to on-line analyze the excited species in plasma. The spectra presented in Fig. 2a are characterized by second positive molecular band of nitrogen in the wavelength range of 310–390 nm, hydrogen's Balmer series (alpha, beta and gamma lines) at 656.5 nm, 483.6 nm and 434.3 nm, respectively. Atomic fluorine was detected in the range of 680–715 nm and oxygen at 777 nm (Fig. 2a). The detected asymmetric continuum hump located between 300 and 400 nm are typically related to the presence CF–CF_2 species [32]. Analyzing Fig. 2b, it could be stated, that the intensity of the spectral lines steeply decreases in the first 25 s of the treatment and then stabilizes at 45 s.

After the processing, the WCA was evaluated to get an impression of the water resistance conversion. The results displayed in Fig. 3a, demonstrate an abrupt raise of the WCA (initially 46°) in the beginning of the treatment, followed by a stabilization of the curve at around 130° after 30 s. The observed ΔWCA ($WCA_{treated}$ - $WCA_{initial}$) was as high as 85°. In literature, previous reports regarding cellulose materials' water repelling improvement demonstrate the increase of WCA ranging from 60° to 150°, however none of them were able to reach the hydrophobic conversion within 10 s and ΔWCA of 85° in 30 s (Fig. 3b). Within Table 1, the most relevant studies were collected and the ΔWCA after the plasma modification is presented. It is worth to mention, that CNFs films already initially possess higher WCA (46°) compared to micro-scale cellulose fibers (as little as 0° for [22–24]), which makes it more challenging to reach comparable ΔWCA.

While the goal to convert hydrophilic CNFs surface to hydrophobic (WCA > 90°) was achieved already after 10 s of plasma exposure (Fig. 3), the WCA further increased steeply up to 30 s and then settled at about 130°. The stability of the newly obtained water repellent properties was confirmed, as the sample treated for 60 s exhibited WCA of 129 ± 7° after being aged at room temperature for 72 h.

In order to gain insight into the origin of WCA saturation, FTIR analysis was carried out. The treated samples exhibited alterations in VI regions compared to the untreated one (Fig. 4a). A newly formed peak that corresponds to FH_3 functional group raised between wavelengths of 3600 and 3750 cm^{-1} (Fig. 4b). The absorbance increases with the treatment time, indicating that this type of change affects the surface and is more prominent with shorter treatment times. The absorbance bands fallen within the range of wavelengths 2900 cm^{-1} - 3000 cm^{-1} correspond to CH_3 and CH_2 asymmetric stretching, while modes in wavelengths 2800 cm^{-1} - 2890 cm^{-1} correspond to CH_3 and CH_2 symmetrical stretching (Fig. 4c) [34,35]. After WCA saturation, a slight spectral shift to the longer vibrancies was observed. With a prolonged processing time, the asymmetric stretching starts to be more prominent. It is worth mentioning that the typical H–O–H banding vibration at 1600 cm^{-1} (Fig. 4d), that is typically associated to surface absorbed moisture, decreases with the treatment time and completely disappears after 60 s treatment. This behavior could be related to the newly obtained hydrophobic character of the treated CNFs film. The band centered at 1260 cm^{-1} (Fig. 4e), corresponding to a newly created C–F bonding [36,37] increases with time after continuous treatment.

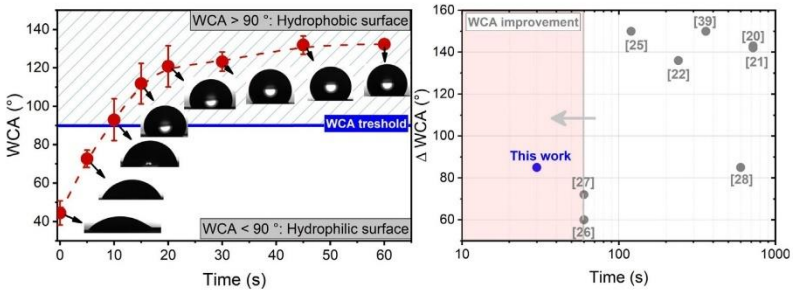

Fig. 3. (a) Time-evolution of water contact angle of CNFs films upon plasma exposure and (b) graphical presentation of ΔWCA reported in the literature so far.

Table 1
Comparison of the conducted research on hydrophobization by plasma in the means of WCA increase and processing time.

Material	Method	Increase in WCA	Treatment time	Reference
Cellulose triacetate electrospun mats	CF_4 plasma	60°	60 s	[28]
Cellulose acetate membranes	Ar/CH_2F_2 plasma	72°	60 s	[29]
Cellulose fiber	He/1,3-butadiene plasma	143°	720 s	[22]
Cotton fabric	Microwave plasma with hydrophobic agent	150°	120 s	[27]
Cellulose fiber	CF_4 plasma	142°	720 s	[23]
Cellulose fiber	CF_4 plasma	85°	600 s	[30]
Bagasse fiber	Hydrophobic coating followed by plasma etching	150°	360 s	[33]
Cellulose fiber	CF_4 plasma	136°	240 s	[24]
CNFs	CF_4 plasma	85°	30 s	This study

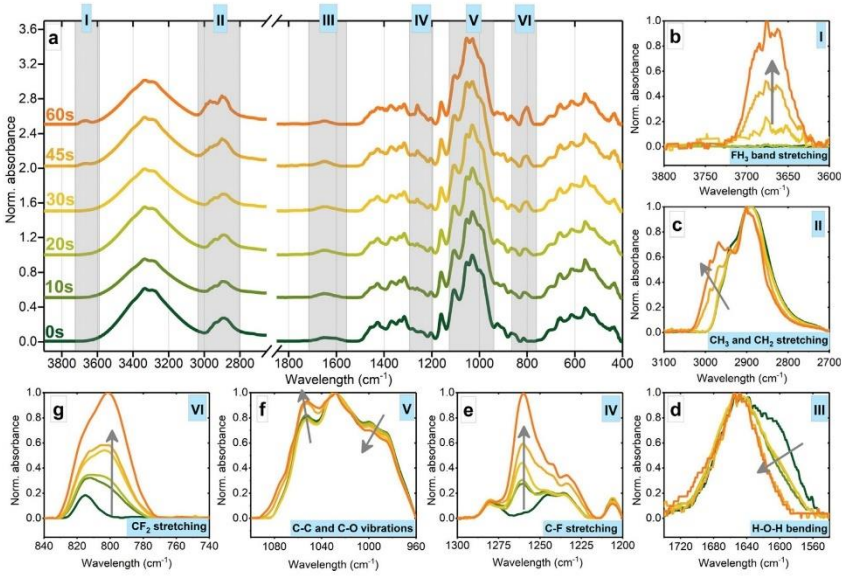

Fig. 4. FTIR spectra of the non-treated and treated samples, with detailed six regions where change was observed.

Furthermore, slight increase of the peak at 1055 cm^{-1} (Fig. 4f) corresponding to C–C and C–O stretch at C-6 in cellulose [38]. The shoulder placed in the range of 1000–980 cm^{-1} that is linked to H–C–H bending decreases with treatment time [39,40]. The vibrational mode located at 815 cm^{-1} assigned to C–C asymmetrical stretching is sharing the place with the newly formed band attributed to CF_2 stretching motion placed at 801 cm^{-1} (Fig. 4g) [36]. The peak intensity rises significantly with

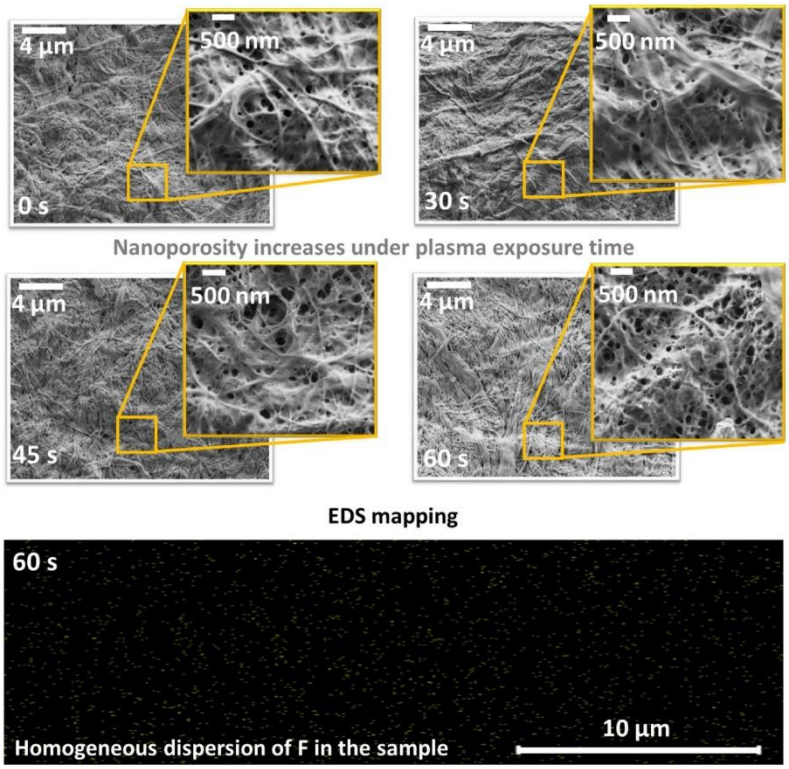

Fig. 5. The increasing porosity of the films after the treatment evident in SEM micrographs.

the treatment time, which suggests that prolonged exposure to plasma induces deeper structural modifications of CNFs film.

Since we are interested mostly in the surface changes after fluorine saturation, films treated for 30, 45 and 60 s were inspected in detail with SEM. The micrographs showed fibrilous structure in all samples. The surface of the untreated film was compared to the surface of films treated for 30 s, 45 s and 60 s (Fig. 5 upper part). It was observed, that treatment time longer than 45 s leads to etching of the surface and tearing of fibrils, resulting in higher porosity. The increase in surface roughness attributes to higher hydrophobicity. The homogeneity of the CF_4 plasma-produced hydrophobic coating was confirmed qualitatively through EDS mapping, as seen in the lower part of Fig. 5.

According to FTIR results essentially no change takes place in the first 20 s of the treatment, so only the samples processed for longer than 30 s, where the transition point occurs, were examined into more details. To explain the surface composition modifications after plasma processing, the XPS analysis was carried out. The survey spectrum of the untreated CNFs films includes the O KLL signal, O 1s and C 1s peaks with no detected impurities. Initially, carbon to oxygen atomic ratio was 60:40, which is in accordance with the stoichiometric ratio of glucose [41]. Upon modification, additional F KLL signal occurs indicating successful fluorination of the film surface. During the treatment the fluorine concentration increases with time, while the amount of oxygen and carbon gradually decrease (Fig. 6a and Fig. 6b). The saturation of the surface with fluorine is achieved after 30 s of treatment, reaching the maximum value of 41 at%. Furthermore, the deconvolution of C 1s peaks was performed to get insight into C–F related binding contributions.

First, in the non-treated sample, the presence of O–C–O (287.5 eV), C–O (286.1 eV), and both C–C and C–H (284.6 eV) bonds were detected confirming the composition of the cellulose (Fig. 6c). In accordance with the fittings, under the plasma, the oxygen associated carbon peaks O–C–O, C–O are affected to a much lesser extent compared to the C–C/C–H bonds, the fitted area of which decreased approximately by factor two after fluorine saturation. Furthermore, all the treated samples are featured by the newly created peaks centered at 289.3 eV, 291 eV and 292.5 eV, that are attributed to C–F, C–F_2 and C–F_3 chemical bondings, respectively, that have been observed previously by fluorination of commercial epoxy-based SU-8 polymer [42]. The fitted area of the latter increases with processing time and equals 0.30 ± 0.21, 0.36 ± 0.28 and 0.55 ± 0.16 for 30, 45 and 60 s, respectively. A typical non-splitted symmetrical cellulose backbone C–O related peak for oxygen 1s was found at 532.6 eV. After treatment, the intensity of the core level of oxygen declines with evident shouldering peak arising at 534.8 eV.

To gain a deeper insight into the vibrational changes, Raman spectroscopy was carried out. A typical vibrational cellulose spectra with four distinct regions presented in Fig. 7a. The peaks enclosed in the yellow-colored region stand for skeletal deformations and rings breathing modes, where the highest peak centered at 380 cm^{-1} (out of plane breathing of the glucopyranose ring) is typically related to the crystalline-like behavior of the CNFs [40]. The fingerprint region corresponding to the green-colored region is composed of multiple wagging, rocking, twisting molecular vibrations of C–C, C–O, C–O–H and C–H_2, with a dominant peak (1095 cm^{-1}) standing for C–O–C symmetric stretching movement [40,43]. The purple-colored area is characterized by various C–H modes, where the peak corresponding to C–H stretching (2900 cm^{-1}) one is the most prominent. A series of lower intensity peaks in orange-colored region correspond to O–H

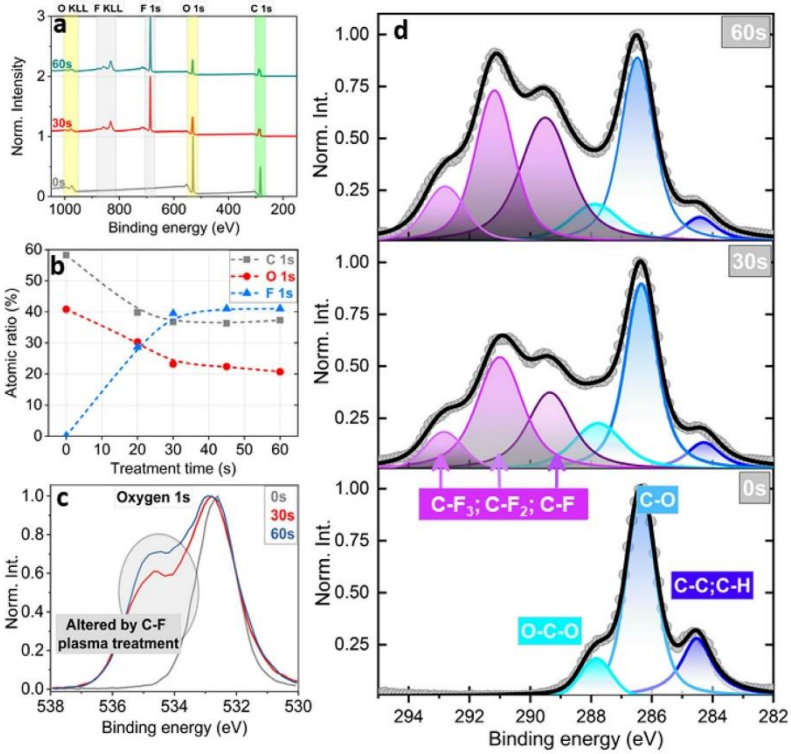

Fig. 6. (a) Survey spectra of the CNFs films treated with plasma; (b) the time-evolution of atomic concentrations of C, O and F; (c) high-resolution O 1s XPS spectra and (d) deconvoluted high-resolution C 1s spectra.

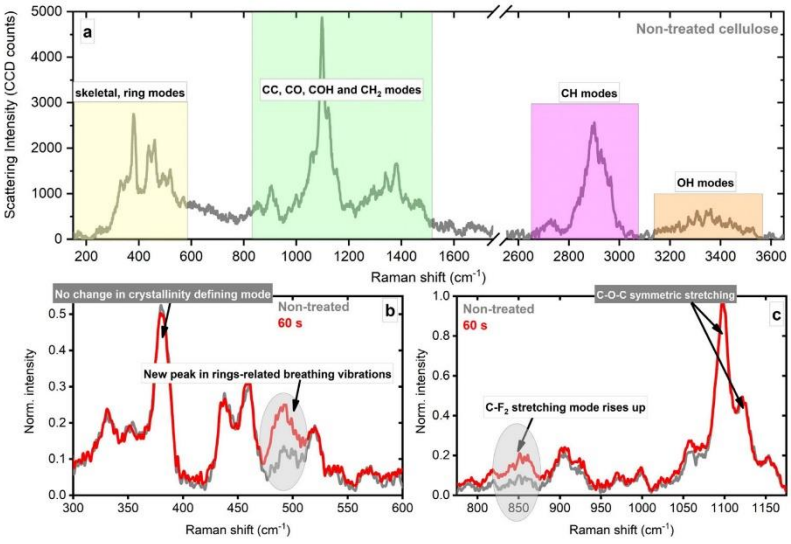

Fig. 7. (a) Room temperature Raman spectra of CNFs film, b and (c) selected ranges with observed spectral alterations.

stretching vibrations. After treatment all samples revealed similarities in the spectrum, with no visible differences in C–H and O–H regions. However, some changes were observed within fingerprint interval and skeletal deformations/rings breathing vibrations. Bearing in mind that

the changes are minor, for clarity, we compared the non-treated sample to sample treated for 60 s. In the ring breathing/deformation spectral range a new peak located at 490 cm^{-1} is observed (Fig. 7b), with its intensity being higher after continuous treatment. The appearance of this peak could be attributed to the structural fluorination of the cellulose, which affects C–C and C–O units within the glucopyranose ring [39]. It should be noted, that the crystallinity defining mode at 380 cm^{-1} is not affected by plasma treatment, pointing to the preservation of cellulose crystallinity. Further, in accordance to FTIR results, in the fingerprint interval, a new peak related to C–F_2 stretching modes was detected at 850 cm^{-1}. All other spectral features remained unchanged.

4. Conclusions

In the conducted research, hydrophobic CNFs films were successfully obtained by direct CF_4 plasma treatment, producing no liquid chemical waste. The desired ultrafast hydrophilic to hydrophobic nanofibrils conversion was confirmed by abrupt water contact angle (WCA) raise, over-preforming the required threshold of 90° already after 10 s of processing. Subsequent increase of WCA reached a plateau at about 130 ± 5° after 30 s, signaling that the surface gained its optimal water repellent properties. Morphologically, the treated samples were featured by prominent nanoporosity which affected the surface tension improvement between the water droplet and the substrate. Surface composition, analyzed by XPS confirmed gradual increment of the fluorine content reflected by the occurrence of C–F, C–F_2 and C–F_3 components within the deconvoluted high-resolution C 1s spectra. The detailed inspection by FTIR-ATR and Raman techniques demonstrated the presence of surface related F–H_3 band, which increases with time. Importantly, the processing time exceeding 30 s induced deeper molecular changes affecting significantly C–C, C–F_2 spectral range and structural rings breathing/deformation vibrations, however revealing virtually no influence on WCA improvement.

The elaborated plasma processing provides a facile, highly-controllable modification of cellulose-based nanomaterial, meeting a satisfactory level of surface water resistance required to be profitably applied to the packaging industry. Further effort should be made to examine the effect of formed C–F bonds, which are stronger than C–C bond, on the material behavior during usage and at end-of-life (biodegradability). To ensure that the final product as well as the process contribute to the greener future, thorough evaluation of such cellulose packaging's impact on the environment is needed, as well as establishing the recycling process in line with the trends of circular economy.

CRediT authorship contribution statement

Ana Oberlintner: Conceptualization, Investigation, Methodology, Data curation, Formal analysis, Visualization, Writing – original draft. **Vasyl Shvalya:** Investigation, Methodology, Data curation, Formal analysis, Visualization, Writing – review & editing. **Aswathy Vasudevan:** Investigation, Methodology. **Damjan Vengust:** Investigation, Methodology. **Blaž Likozar:** Writing – review & editing, Supervision, Project administration, Funding acquisition. **Uroš Cvelbar:** Conceptualization, Writing – review & editing, Supervision, Project administration, Funding acquisition. **Uroš Novak:** Conceptualization, Writing - Review & Editing, Supervision, Project administration, Funding acquisition.

Declaration of competing interest

The authors declare that they have no known competing financial interests or personal relationships that could have appeared to influence the work reported in this paper.

Acknowledgments

The authors acknowledge Sappi for CNFs donation. The authors are thankful to Andrea Jurov for OES measurements, dr. Janez Kovač for XPS measurements and Anže Prašnikar for SEM images. The research was funded by PhD research grant (Ana Oberlintner), Slovenian Research Agency (ARRS) program P2-0152 and PEGASUS (Plasma Enabled and Graphene Allowed Synthesis of Unique Nano-structures, No. 766894); grant G5814 – NOOSE.

References

[1] A. Isobe, S. Iwasaki, K. Uchida, T. Tokai, Abundance of non-conservative microplastics in the upper ocean from 1957 to 2066, Nature Commun. 10 (2019) 417, http://dx.doi.org/10.1038/s41467-019-08316-9.

[2] X. Guo, J. Wang, The chemical behaviors of microplastics in marine environment: A review, Mar. Pollut. Bull. 142 (2019) 1–14, http://dx.doi.org/10.1016/j.marpolbul.2019.03.019.

[3] U. Novak, M. Bajić, K. Kõrge, A. Oberlintner, J. Murn, K. Lokar, K.V. Triler, B. Likozar, From waste/residual marine biomass to active biopolymer-based packaging film materials for food industry applications – a review, Phys. Sci. Rev. 5 (2020) http://dx.doi.org/10.1515/psr-2019-0099.

[4] T. Heinze, Cellulose chemistry and properties: Fibers, nanocelluloses and advanced materials, in: O.J. Rojas (Ed.), Cellulose: Structure and Properties, Springer International Publishing, Cham, 2016, pp. 1–52, http://dx.doi.org/10.1007/12{_2015{_}319}.

[5] L. Thompson, J. Azadmanjiri, M. Nikzad, I. Sbarski, J. Wang, A. Yu, Cellulose nanocrystals: Production, functionalization and advanced applications, Rev. Adv. Mater. Sci. 58 (2019) 1–16, http://dx.doi.org/10.1515/rams-2019-0001.

[6] M.T. Postek, R.J. Moon, A.W. Rudie, M.A. Bilodeau, Foreword, in: M.T. Postek, R.J. Moon, A.W. Rudie, M.A. Bilodeau (Eds.), Production and Applications of Cellulose Nanomaterials, Tappi Press, Peachtree Corners, U.S.A, 2013, p. 1.

[7] M. Henriksson, L.A. Berglund, P. Isaksson, T. Lindström, T. Nishino, Cellulose nanopaper structures of high toughness, Biomacromolecules 9 (2008) 1579–1585, http://dx.doi.org/10.1021/bm800038n.

[8] K. Syverud, P. Stenius, Strength and barrier properties of MFC films, Cellulose 16 (2008) 75–85, http://dx.doi.org/10.1007/s10570-008-9244-2.

[9] K. Lee, Y. Jeon, D. Kim, G. Kwon, U.J. Kim, C. Hong, J.W. Choung, J. You, Double-crosslinked cellulose nanofiber based bioplastic films for practical applications, Carbohydr. Polymers 260 (2021) 117817, http://dx.doi.org/10.1016/j.carbpol.2021.117817.

[10] H. Sehaqui, T. Zimmermann, P. Tingaut, Hydrophobic cellulose nanopaper through a mild esterification procedure, Cellulose 21 (2014) 367–382, http://dx.doi.org/10.1007/s10570-013-0110-5.

[11] A. Raman, J.S. Jayan, B.D.S. Deeraj, A. Saritha, K. Joseph, Electrospun nanofibers as effective superhydrophobic surfaces: A brief review, Surf. Interfaces 24 (2021) 101140, http://dx.doi.org/10.1016/j.surfin.2021.101140.

[12] Y. Qi, S. Lin, J. Lan, Y. Zhan, J. Guo, J. Shang, Fabrication of super-high transparent cellulose films with multifunctional performances via postmodification strategy, 2021, http://dx.doi.org/10.1016/j.carbpol.2021.117760.

[13] F. Rafieian, M. Hosseini, M. Jonoobi, Q. Yu, Development of hydrophobic nanocellulose-based aerogel via chemical vapor deposition for oil separation for water treatment, Cellulose 25 (2018) 4695–4710, http://dx.doi.org/10.1007/s10570-018-1867-3.

[14] G. Siqueira, J. Bras, A. Dufresne, Cellulose whiskers versus microfibrils: Influence of the nature of the nanoparticle and its surface functionalization on the thermal and mechanical properties of nanocomposites, Biomacromolecules 10 (2009) 425–432, http://dx.doi.org/10.1021/bm801193d.

[15] M. Salajková, L.A. Berglund, Q. Zhou, Hydrophobic cellulose nanocrystals modified with quaternary ammonium salts, J. Mater. Chem. 22 (2012) 19798–19805, http://dx.doi.org/10.1039/c2jm34355j.

[16] A. Oberlintner, B. Likozar, U. Novak, Hydrophobic functionalization reactions of structured cellulose nanomaterials: Mechanisms, kinetics and in silico multi-scale models, Carbohydr. Polymers 259 (2021) 117742, http://dx.doi.org/10.1016/j.carbpol.2021.117742.

[17] O. Baranov, K. Bazaka, H. Kersten, M. Keidar, U. Cvelbar, S. Xu, I. Levchenko, Plasma under control: Advanced solutions and perspectives for plasma flux management in material treatment and nanosynthesis, Appl. Phys. Rev. 4 (2017) 041302, http://dx.doi.org/10.1063/1.5007869.

[18] N. M. Santhosh, G. Filipič, E. Kovacevic, A. Jagodar, J. Berndt, T. Strunskus, H. Kondo, M. Hori, E. Tatarova, U. Cvelbar, N-graphene nanowalls via plasma nitrogen incorporation and substitution: The experimental evidence, Nano-Micro Lett. 12 (2020) 53, http://dx.doi.org/10.1007/s40820-020-0395-5.

[19] S. Amirabadi, J.M. Milani, F. Sohbatzadeh, Application of dielectric barrier discharge plasma to hydrophobically modification of gum arabic with enhanced surface properties, Food Hydrocolloids 104 (2020) 105724, http://dx.doi.org/10.1016/j.foodhyd.2020.105724.

[20] L. Xu, J. Deng, Y. Guo, W. Wang, R. Zhang, J. Yu, Fabrication of super-hydrophobic cotton fabric by low-pressure plasma-enhanced chemical vapor deposition, Text. Res. J. 89 (2019) 1853–1862, http://dx.doi.org/10.1177/0040517518780000.

[21] H. Puliyalil, N. Recek, G. Filipič, M. Čekada, I. Jerman, M. Mozetič, S. Thomas, U. Cvelbar, Mechanisms of hydrophobization of polymeric composites etched in CF4 plasma, Surf. Interface Anal. 49 (2017) 334–339, http://dx.doi.org/10.1002/sia.6104.

[22] K.K. Samanta, G.J. Amish, J. Manjeet, K.A. Aswini, Study of hydrophobic finishing of cellulosic substrate using he_1, 3-butadiene plasma at atmospheric pressure_Elsevier enhanced reader. pdf, Surf. Coat. Technol. 213 (2012) 65–76.

[23] K.K. Samanta, T.N. Gayatri, S. Saxena, S. Basak, S.K. Chattopadhyay, A. Arputharaj, V. Prasad, Hydrophobic functionalization of cellulosic substrates using atmospheric pressure plasma, Cellul. Chem. Technol. 50 (2016) 745–754.

[24] K.K. Samanta, A.G. Joshi, M. Jassal, A.K. Agrawal, Hydrophobic functionalization of cellulosic substrate by tetrafluoroethane dielectric barrier discharge plasma at atmospheric pressure, Carbohydr. Polymers 253 (2021) 117272, http://dx.doi.org/10.1016/j.carbpol.2020.117272.

[25] S. Ercegović, R. Čunko, L. Bautista, V. Bukošek, Plasma effect on the chemical structure of cellulose fabric for modification of some functional properties, in: 3rd International Conference on Natural Fibers: Advanced Materials for a Greener World, ICNF 2017, 21-23 2017, Braga, Portugal, 2017, pp. 333–340.

[26] A. Alanis, J.H. Valdés, .N.-V. María Guadalupe, R. Lopez, R. Mendoza, A.P. Mathew, R.Díaz.De. León, L. Valencia, Plasma surface-modification of cellulose nanocrystals: A green alternative towards mechanical reinforcement of ABS, RSC Adv. 9 (2019) 17417–17424, http://dx.doi.org/10.1039/c9ra02451d.

[27] L. Cabrales, N. Abidi, Microwave plasma induced grafting of oleic acid on cotton fabric surfaces, Appl. Surf. Sci. 258 (2012) 4636–4641, http://dx.doi.org/10.1016/j.apsusc.2011.12.130.

[28] Y.I. Yoon, H.S. Moon, W.S. Lyoo, T.S. Lee, W.H. Park, Superhydrophobicity of cellulose triacetate fibrous mats produced by electrospinning and plasma treatment, Carbohydr. Polymers 75 (2009) 246–250, http://dx.doi.org/10.1016/j.carbpol.2008.07.015.

[29] C. Huang, C.-Y. Tsai, R.-S. Juang, H.-C. Kao, Tailoring surface properties of cellulose acetate membranes by low-pressure plasma processing, J. Appl. Polymer Sci. 118 (2010) 3227–3235, http://dx.doi.org/10.1002/app.32604.

[30] A. Tursi, N. De Vietro, A. Beneduci, A. Milella, F. Chidichimo, F. Fracassi, G. Chidichimo, Low pressure plasma functionalized cellulose fiber for the remediation of petroleum hydrocarbons polluted water, J. Hazard. Mater. 373 (2019) 773–782, http://dx.doi.org/10.1016/j.jhazmat.2019.04.022.

[31] G. Lavrič, A. Oberlintner, I. Filipova, U. Novak, B. Likozar, U. Vrabič-Brodnjak, Functional nanocellulose alginate and chitosan nanocomposites designed as active film packaging materials, Polymers 13 (2021) 1–15, http://dx.doi.org/10.3390/polym13152523.

[32] M.F. Cuddy, E.R. Fisher, Contributions of CF and CF2 species to fluorocarbon film composition and properties for CxFy plasma-enhanced chemical vapor deposition, ACS Appl. Mater. Interfaces 4 (2012) 1733–1741, http://dx.doi.org/10.1021/am2018546.

[33] M.Z. Yao, Y. Liu, C.N. Qin, X.J. Meng, B.X. Cheng, H. Zhao, S.F. Wang, Z.Q. Huang, Facile fabrication of hydrophobic cellulose-based organic/inorganic nanomaterial modified with POSS by plasma treatment, Carbohydr. Polymers 253 (2021) 117193, http://dx.doi.org/10.1016/j.carbpol.2020.117193.

[34] J.-C. Tsai, Y.-L. Lo, C.-Y. Lin, H.-M. Sheu, J.-C. Lin, Feasibility of rapid quantitation of stratum corneum lipid content by Fourier transform infrared spectrometry, Spectroscopy 18 (2004) 401015, http://dx.doi.org/10.1155/2004/401015.

[35] S. Karimi, J. Feizy, F. Mehrjo, M. Farrokhnia, Detection and quantification of food colorant adulteration in saffron sample using chemometric analysis of FT-IR spectra, RSC Adv. 6 (2016) 23085–23093, http://dx.doi.org/10.1039/c5ra25983e.

[36] M. Salado, S. Lanceros-Mendez, E. Lizundia, Free-standing intrinsically conducting polymer membranes based on cellulose and poly(vinylidene fluoride) for energy storage applications, Eur. Polymer J. 44 (2021) http://dx.doi.org/10.1016/j.eurpolymj.2020.110240.

[37] X. Wang, W. Wang, Y. Liu, M. Ren, H. Xiao, X. Liu, Characterization of conformation and locations of C–F bonds in graphene derivative by polarized ATR-FTIR, Anal. Chem. 88 (2016) 3926–3934, http://dx.doi.org/10.1021/acs.analchem.6b00115.

[38] S. Cichosz, A. Masek, IR Study on cellulose with the varied moisture contents: Insight into the supramolecular structure, Materials 13 (2020) 1–22, http://dx.doi.org/10.3390/ma13204573.

[39] M. Szymańska-Chargot, J. Cybulska, A. Zdunek, Sensing the structural differences in cellulose from apple and bacterial cell wall materials by Raman and FT-IR spectroscopy, Sensors (Basel, Switzerland) 11 (2011) 5543–5560.

[40] S.A. Brandán, Vibrational characterization of monomers and dimers of cellulose by usinf DFT calculations and the SQM methodology, J. Comput. Chem. Mol. Modell. 1 (2017) 51–85, http://dx.doi.org/10.15436/JCCMM.1.2.4.

[41] K.L. Kostov, E. Belamie, B. Alonso, T. Mineva, Surface chemical states of cellulose, Chitin and Chitosan studied by density functional theory and high-resolution photoelectron spectroscopy, Bulg. Chem. Commun. 50 (2018) 135–146.

[42] B. Bêche, P. Papet, D. Debarnot, E. Gaviot, J. Zyss, F. Poncin-Epaillard, Fluorine plasma treatment on SU-8 polymer for integrated optics, Opt. Commun. 246 (2005) 25–28, http://dx.doi.org/10.1016/j.optcom.2004.10.081.

[43] M. Makarem, C.M. Lee, K. Kafle, S. Huang, I. Chae, H. Yang, J.D. Kubicki, S.H. Kim, Probing cellulose structures with vibrational spectroscopy, Cellulose 26 (2019) 35–79, http://dx.doi.org/10.1007/s10570-018-2199-z.

5.2 Permanent Hydrophobic Coating of Chitosan/Cellulose Nanocrystals Composite Film by Cold Plasma Processing

Based on the findings in the previous section, in this section, the use of plasma for hydrophobization is expanded to chitosan/CNCs composite film. First, the screening for the optimal treatment time was carried out, suggesting 5 s treatment to be sufficient to reach WCA over 120°. Surface structural analyses XPS and ATR-FTIR were employed and fluorine-related bonds (CF-CF_2, CF_2-CF_2, C-CF, CF_3, O-CF_2 ad O-CF_3) were identified to be responsible for the decrease in surface wettability. However, for packaging applications, stability of films is essential. With this in mind, the treated films (along with control) were aged in a controlled environment (room temperature, RH 50 %). WCA and elemental analysis that were carried out every five days revealed there was no change on the surface of the biocomposite films. Tensile strength, elongation-at-break and water vapor transmission were analyzed right after the treatment and after ageing over 31 days as well. Lastly, to evaluate possible leaching of fluorine-related compounds into the liquid environment, the films were incubated in water, aqueous solution of acetic acid and aqueous solution of ethanol. The liquids were analyzed with LC-MS, whereas no fluorine-related species were detected (either not present or under the limit of detection). The results of this study present that plasma treatment is a very fast technique that provides a stable hydrophobic coating while not compromising mechanical properties of the biocomposite films.

Regarding my contribution: I fabricated the chitosan/CNCs films, treated them with plasma, carried out ATR-FTIR and LC-MS analysis, determined the mechanical properties and co-wrote the manuscript.

Applied Surface Science 597 (2022) 153562

Contents lists available at ScienceDirect

Applied Surface Science

journal homepage: www.elsevier.com/locate/apsusc

Full length article

Permanent hydrophobic coating of chitosan/cellulose nanocrystals composite film by cold plasma processing

Ana Oberlintner [a,b], Alenka Vesel [c], Katerina Naumoska [d], Blaž Likozar [a], Uroš Novak [a,*]

[a] Department of Catalysis and Chemical Reaction Engineering, National Institute of Chemistry, Hajdrihova 19, SI-1000 Ljubljana, Slovenia
[b] Jožef Stefan International Postgraduate School, Jamova cesta 39, SI-1000 Ljubljana, Slovenia
[c] Department of Surface Engineering, Jožef Stefan Institute, Jamova cesta 39, SI-1000 Ljubljana, Slovenia
[d] Department of Analytical Chemistry, Laboratory for Food Chemistry, National Institute of Chemistry, Hajdrihova 19, SI-1000 Ljubljana, Slovenia

ARTICLE INFO

Keywords:
Chitosan/Cellulose nanocrystals film
Biocomposite packaging
Functionalization with cold plasma processing
Permanent hydrophobic Coating
Shelf-life of modification

ABSTRACT

A highly effective ultrafast chemical modification of chitosan/cellulose nanocrystals composite film surface is presented in the present research. Added value properties were achieved by the use of a few seconds' treatment with RF-generated low-temperature fluorocarbon plasma. Drastic increase of the water-repelling character of the completely natural-based biocomposite foil were observed, with contact angle reaching up to 121°. Surface fluorination occurred through formation of irreversible fluorine-related bonds (CF-CF_2, CF_2-CF_2 and C-CF, CF_3 and O-CF_2, O-CF_3) detected by the means of X-ray photoelectron spectroscopy. Surface structural changes were further confirmed with ATR-FTIR. With packaging application in mind, the films were subjected to analysis of mechanical and water-related properties, showing an improvement upon fluorination. Further the stability of the modification was followed by measurements of water contact angle and atomic composition, as well as mechanical properties, water content and water vapor transmission after at least 31 days of storage in controlled environment. Lastly, no leaching of fluorinated components into liquid environments was detected by the means of HILIC LC-MS analyses in ESI(+) and ESI(-) modes. The presented method rapidly enhances the hydrophobic character of chitosan/nanocellulose biocomposite films without receding mechanical strength and provides a long-lasting surface coating.

1. Introduction

An alarming amount of plastic packaging is produced and discarded every year. Worldwide manufacture of plastic reached 368 million tonnes in 2019, with packaging sector taking up 39.6% of overall demand [1]. Plastic intended for packaging also has the shortest life cycle with average of only one year and includes non-recyclable plastics such as LDPE and PS [1,2]. Additionally, the conventional plastic is based on non-renewable resources, which emphasizes the need for an alternative even further.

Chitosan, obtained by deacetylation of chitin, that is found in food-processing industry waste, is one of the promising sustainable materials of the future [3]. Owing to its film-forming ability, focus on chitosan-based films as a potential packaging material is emerging. Besides being non-toxic, bio-compatible and biodegradable, these films exhibit not only sufficient mechanical strength and elasticity, but also antioxidant and antimicrobial properties [3–5]. Furthermore, the desired characteristics can be tuned by incorporation of various additives, namely plant extracts [6–8], essential oils [9–11] into chitosan matrix and was proven to extend the shelf life of various fresh foods [12,13]. Mechanical properties can be improved by incorporation of cellulose nanocrystals, rod-like shaped nanoparticles isolated from cellulose, the most abundant polymer on earth [14].

Yet, one of the crucial roles of packaging is to protect its content from environmental factors, hence water resistance and low water vapor transmission are desired. Chitosan film exhibits poor moisture barrier, which limits its wider use [15]. For reference, LDPE, PVC and PLA transmit 1.5 g m^{-2}, 3 g m^{-2} and 40 g m^{-2} of water vapor daily, respectively, while chitosan water vapor transmission rate is as much as 150 g m^{-2} day^{-1} [16]. To tackle this drawback, two approaches of film modification have been researched: i- introducing hydrophobic components such as fatty acids into a film-forming solution [17–19], or ii- chemically modify polysaccharide [17], while modification of the bio-polymer itself before obtaining a film-forming solution was generally shown not to be suitable, as these derivates often do not exhibit film-forming properties [17]. The first described path to hydrophobization of chitosan leads to composite materials derived

* Corresponding author.
E-mail address: uros.novak@ki.si (U. Novak).

https://doi.org/10.1016/j.apsusc.2022.153562
Received 2 February 2022; Received in revised form 16 April 2022; Accepted 30 April 2022
Available online 16 May 2022

from emulsion which can negatively influence other properties, or to multilayer materials [17,18]. For chemical modification of chitosan surface, various polymer grafting paths were proposed. Up to date literature describes grafting of N-acetyl cysteine to chitosan (resulted in hydrated films with improved tensile properties) [20], alkyl chains to chitosan with intention to improve water resistance for bonding applications [21] and grafting of poly(2-hydroxyethyl methacrylate) chains on chitosan followed by esterification with a fluorinated compound, which is responsible for hydrophobicity [15]. In the latter, the rise in contact angle was 16° and was stable through 10 min of wetting. The drawback of such modification is that the process involves several steps, can be quite time-consuming and produce liquid chemical waste. On the contrary, plasma processing is a single-step modification, eliminating subsequent separation techniques and producing no liquid discard. RF-generated plasma is a multifunctional tool for etching of the surface or plasma-enhanced chemical vapor deposition, with thermal energy of the electrons being few eV, bringing the atoms to excited state and inducing chemical reaction. Still, the temperature of the electron gas remains low (near room-temperature), allowing modifications of sensitive surfaces, such as biopolymers [22,23]. The closed reactor system offers the possibility of gas capturing and recycling, preventing harmful gas exhaust into the environment [24,25]. Furthermore, the possibility of scale-up and utilization of the same assembly system for tailoring the materials surface properties with various dopants (nitrogen, oxygen, sulfur, or fluorine) highlights the industrial applicability of the technique [26–28].

Despite simplicity, effectiveness and rapidity of plasma treatment, only limited amount of studies concerning chitosan surface functionalization are taking this approach. Several researchers treated chitosan with argon plasma yielding a more hydrophilic surface required in adhesives and coatings, but is not desired for packaging [19,29–31]. Slight increase in hydrophobicity, water contact angle rose from initial 13° to 23°, was achieved with alkane vapor plasma technique [32]. On the example of cellulose textiles and films, it has already been demonstrated that plasma using fluorinated compounds as a carrier gas successfully modifies surface and enhances its hydrophobic character [28, 33–36].

Chow et al. [37] reported general non-cytotoxicity of fluorinated chitin derivates, leading to increased interest in use of these materials as wound dressing agents or topical medication, taking in advantage their antibacterial activity [38,39]. Furthermore, as demonstrated on example of fluorine-modified cellulose [40], fluorinated biopolymers can be enzymatically degraded by dehalogenases in several microorganisms, that are present in soil and aqueous environment [41, 42].

With respect to these facts, the present study focuses on utilization of RF-generated plasma in fluorocarbon (CF_4) for improvement of water-related properties of chitosan-based films reinforced with cellulose nanocrystals (CNCs) as a fast, efficient, non-destructive and stable modification process, to best of our knowledge, for the first time. The samples were treated for 5 s, which was the optimal treatment time as determined according to water contact angle measurement, and subjected to surface analyses with XPS, FTIR-ATR and SEM. Further, physicochemical properties relevant for packaging application were considered (mechanical properties, moisture content and water vapor transmission. To prove stability of modification, which can be deemed as uncertain, the water contact angle was followed through a period of 40 days, while other properties were re-evaluated after 31 days of storage in controlled environment. Finally, the hydrophobized films stability and possible migration of fluorinated species into liquid environments was examined, to validate applicability of plasma-treated chitosan-based films as packaging.

2. Experimental section

2.1. Materials

High molecular weight chitosan (85% deacetylated), lactic acid (85% aqueous solution) and ammonium formate (for LC-MS) were bought from Sigma-Aldrich (Steinheim, Germany). Cellulose nanocrystals were supplied by Navitas (Stari trg pri Ložu, Slovenia). Glycerol was acquired from Pharmachem Sušnik (Ljubljana, Slovenia), while ethanol (absolute), acetic acid (glacial 100% and 100%, for LC-MS) and ammonia solution (32%) were purchased from Merck (Darmstadt, Germany). Acetonitrile for LC-MS was obtained from Honeywell (North Carolina, USA) and ultrapure water (18 $M\Omega^{-1}$ cm) was supplied by a Milli-Q water purification system (Millipore, Bedford, MA, USA).

2.2. Fabrication of chitosan-based films with incorporated CNCs

Chitosan-based films were prepared according to a previously described protocol [14]. Detailed description can be found in Appendix A.

2.3. Hydrophobization of films by fluorocarbon (CF_4) plasma treatment

Chitosan-based films with incorporated CNCs were cut out in different sizes, according to the further analysis. One sample at the time was placed on the microscopic glass and fixed with carbon tape. The sample was then introduced into the 80 cm long discharge tube made of borosilicate glass with diameter 4 cm. The tube was pumped with a two-stage rotary pump of a nominal pumping speed of 80 $m^3\ h^{-1}$. The base pressure was 1 Pa. Plasma was sustained by a coil with six turns which was connected to the RF generator via a matching network. The generator operated at the standard frequency of 13.56 MHz. The output power was set to 150 W, which was found to be the optimal among preliminary tested 150 W, 200 W and 400 W (data not shown). At these conditions, diffusing plasma expanded far away from the coil. The sample was positioned 7 cm away from the coil. The treatment was carried out with CF_4 gas at 50 Pa for 0.5 s, 1 s, 3 s, 5 s, 10 s, 20 s and 30 s.

2.4. Films surface analyses

Water contact angle (WCA), analyzed with Drop Shape Analyser DSA-100 (Krüss GmbH, Hamburg, Germany), was measured at two points in this study: immediately after the treatment on all of the samples and through period of 40 days on the selected sample (treated for 5 s). A static contact angle was determined using a sessile drop method. MilliQ water with the volume of the drop of 1 μL was used for the measurements. The first set of measurements was applied to select the optimal treatment time and the second to follow the effect of aging onto the newly reached hydrophobic character of the surface.

The surface chemical composition of the samples was analyzed by means of X-ray Photoelectron Spectroscopy (XPS) using instrument TFA XPS (Physical Electronics, Munich, Germany). Monochromatic Al $K\alpha_{1,2}$ radiation at 1486.6 eV over an area of 400 μm^2 was used as a source for excitement. Hemispherical analyzer positioned at an angle of 45° with respect to the sample surface was applied for the detection of photoelectrons. The survey spectra were measured at a pass energy of 187 eV with an energy step of 0.4 eV. High-resolution XPS spectra of carbon C1s were measured at a pass energy of 29.35 eV with an energy step of 0.125 eV. For surface charge neutralization an additional electron source was used. The C–C component in C1s was set to the binding energy of 284.8 eV. Analysis of the obtained spectra was carried out using MultiPak v8.1c software (Physical Electronics, Munich, Germany). The C1s spectra were fitted with the Gauss–Lorentzian function, where the width and positions of the peaks were fixed during the fitting procedure.

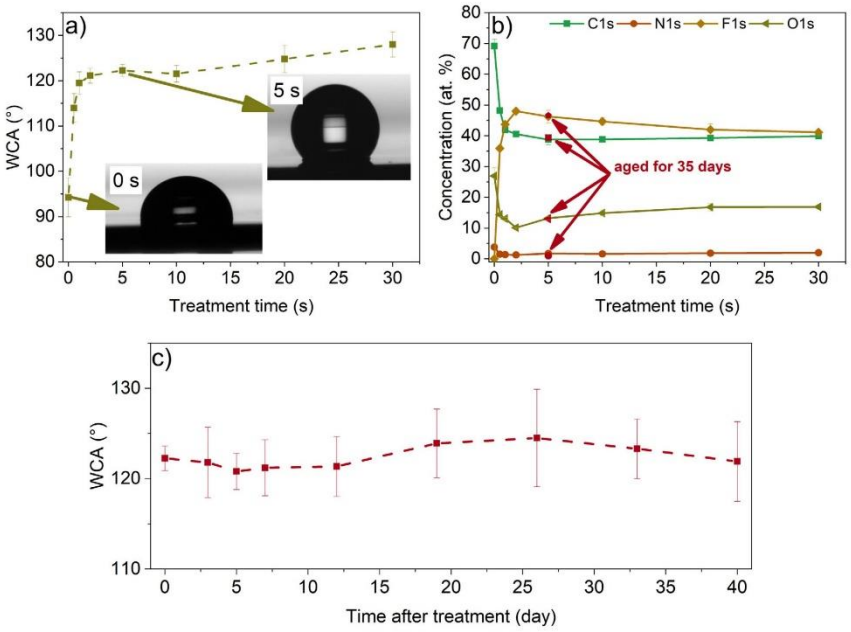

Fig. 1. (a) WCA of the samples with respect to treatment time, (b) atomic composition at various treatment times and atomic composition of the sample treated for 5 s after 35 days (marked in red) and (c) stability of WCA over a period of 40 days.

FTIR spectra of the untreated samples, treated samples right after the treatment and after 31 days were recorded with ATR-FTIR Spectrum Two (Perkin Elmer, Germany) from 4000 cm^{-1} to 400 cm^{-1} with 4 cm^{-1} step, accumulation of 64 scans. All measurements were done in parallels. Treated and untreated samples were coated with 10 nm layer of gold and were subjected to SEM analysis with Supra 35VP electron microscope (Carl Zeiss, Jena, Germany).

2.5. Film physico-chemical properties

Film thickness and mechanical properties of the film samples were determined according to Bajić et al. (2020), with slight modification in the latter (size of the samples was 6 × 2 cm and gauge length segment was 4 cm). For a detailed description of the analysis the reader is referred to Appendix A. Protocol described by [5] was followed for assessment of water vapor transmission (WVT). Brief description can also be found in Appendix A. During the aging process the samples were stored at 50% RH and room temperature.

2.6. Film stability in liquid environments

To observe stability of fluorinated compounds in liquid environments, processed sample was cut into smaller pieces with mass approximately 10 mg and submerged into liquid media (water, 5% acetic $acid_{(aq)}$, 10% $ethanol_{(aq)}$) of appropriate volume so the final concentration was 2 mg_{film} mL^{-1}. The samples were collected after 144 h (this time was selected to achieve the longest possible submersion time while avoiding disintegration of the sample, visible after 168 h), dried under nitrogen flow and the solid residues were redissolved in 70% acetonitrile and analyzed with LC-ESI-MS system in positive and negative ionization mode. UHPLC-MS system (Accela 1250, coupled to an LTQ Velos MS, Thermo Fisher Scientific, Waltham, MA, USA) was used to analyze liquid media upon contact with reference and CF_4 treated films). HILIC LC-MS analyses in ESI(+) and ESI(−) mode were carried out on Phenomenex Luna NH_2 (100 Å, 100 × 2.0 mm i.d., 3 µm) column using 0.05% ammonia in water solution (mobile phase A) and acetonitrile (mobile phase B) with gradient elution from 10% to 40% A in 10 min at a flow rate of 300 µL min^{-1}. Re-equilibration of the column with initial conditions was applied from 11th to 20th min before each next injection. Column oven and autosampler temperature were set at 25 °C and 5 °C, respectively. Injection volume was 2 µL. Alternative HILIC and RP methods are described in Appendix A. MS parameters were optimized using glucosamine standard (25 µg/mL) and were as follows: heater temperature 300 °C, sheath gas 41 a.u., auxiliary gas 35 a.u., sweep gas to 0 a.u., spray current 5 µA, capillary temperature 200 °C and S-Lens RF Level 49%. The MS spectra were acquired in the *m/z* range of 50–2000. The collected chromatograms and spectra were evaluated using the Xcalibur software (version 2.1.0, Thermo Fisher Scientific).

3. Results and discussion

3.1. Film surface analyses

The produced chitosan/cellulose nanocrystals films subjected to CF_4 plasma for various time duration (0.5 s, 1 s, 2 s, 5 s, 10 s, 20 s and 30 s). Water contact angle (WCA), that was evaluated immediately after the treatment, increased abruptly from 94 ± 4° to 121 ± 2° in the first two seconds and then stabilized between 122° and 125° with further processing as shown in Fig. 1a. WCA reached with treatment is higher than water repelling of bio-polymer films (75° for chitosan-only, 58° for alginate reinforced with CNCs, 23° for cellulose nanofibrils films and around 52° for starch film) [14,43], as well as conventional polymers (PE 102°, PS 91°, PVC 87° and PET 81°) [44]. To reveal the cause of this occurrence, the samples were inspected with XPS that showed the saturation of the surface with fluorine in the first two seconds of processing, which correlates to the increase of WCA and its stabilization (Fig. 1b). The initial C:O:N ratio (69:27:4), was notably altered upon

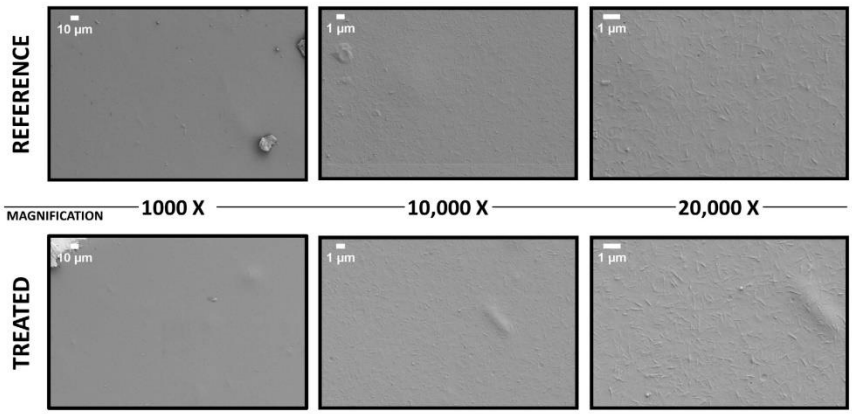

Fig. 2. SEM images of reference and treated sample at three different magnifications.

fluorination. The composition at saturation with fluorine, that is after two seconds of processing, was 41% carbon, 48% fluorine, 10% oxygen and 1% nitrogen. It was also observed that the ratios slightly change, namely higher carbon, oxygen and nitrogen content and lower fluorine percentage, when plasma is operating longer, which could be attributed to the etching of the surface. Based on these observations, 5 s was chosen as an optimal treatment time and was used for further analyses.

The treated films remained semi-transparent, slightly brown in color and slightly sticky, indicating that plasma treatment had no effect detected with a naked eye. However, plasma treatment can cause etching on the surface of the film, surface morphology was closely inspected with SEM before and after processing. The micrographs shown in Fig. 2 are taken at magnifications 1k, 10k and 20k from left to right. At the smallest magnification, the reference and the treated surface seem smooth with no visible roughness or porosity. Further magnification, however, reveals the structure of rod-like shaped CNCs in the film. The particles seem to be evenly distributed in the chitosan matrix. The surface retained the same morphological properties after the modification.

Alternative to conventional polymers used for packaging applications is required to exhibit stable composition and water repelling character over longer period of time. Observations based on the following of WCA over the period of 40 days showed that it remained constant at around 120°. Additionally, the composition was shown to remain the same after 35 days of aging with C:F:O:N ratio 39:47:13:1. Hereby, the interest in the surface chemistry throughout the plasma treatment arose, so high-resolution XPS carbon spectra of samples processed for various times were recorded (Fig. 3a). To gain a deeper insight into C–F related binding contributions the deconvolution of the C 1s peaks was performed for the reference sample and sample treated for 5 s. In the untreated sample, the C–C (284.8 eV), C–O (286.5 eV), O–C–O (288.0 eV) and O–C=O (289.0 eV) bonds were detected. The intensity of the peak corresponding to initially prevalent C–C bond decreases with plasma processing, while at the same time, peaks related to various C–F bindings start to increase. With longer treatment times the peaks at higher binding energies, that correspond to carbon atoms binding to more than one fluorine, become more prominent. It can be observed that the intensity of the peak at 293.5 eV, corresponding to CF_3 bond, is increasing in the first five seconds of the treatment but this trend takes a turn and the peak starts to decrease with further processing. On the other hand, at the same time, the peak featuring the C–C bond starts to increase after initial decrease in the first 10 s of the treatment that, again, could be due to the etching of the already treated surface and is in alignment with the previously described alteration of atomic ratios. Further, the high-resolution C 1s XPS spectrum of sample treated for 5 s was inspected into detail (Fig. 3c). The shape of the treated sample's spectrum differentiates greatly compared to the reference because of the formation of various fluorine groups. Decrease in the intensity of the initially present peaks corresponding to C–C, C–O and O–C=O bonding was detected, with the latter completely disappearing upon treatment, while the peak positioned at 288.0 eV met a slight increase. However, this same peak can be associated with CF–CF binding as well which is most possibly responsible for the inflation. The treated sample is featured by the newly developed peaks attributed to CF–CF_2 (289.5 eV), CF_2–CF_2 and CF–CF_2 (291.5 eV), CF_3 (293.4 eV) and O–CF_2, O–CF_3 (295.0 eV).

To further understand possible structural changes upon fluorination, the sample treated for 5 s were additionally analyzed by means of FTIR-ATR and compared to the reference spectrum. Both spectra exhibited characteristic peaks for chitosan namely: the broad peak between 3500 cm^{-1} and 3030 cm^{-1} (corresponds to O–H and N–H bands in chitosan), the two weak bands located between 2820 cm^{-1} and 3015 cm^{-1} (attributed to C–H stretching in alkane groups), peaks appearing between 1490 cm^{-1} and 1750 cm^{-1} (assigned to C=O stretching — carbonyl and amide I, and N–H bending — amide II, respectively) [45, 46]. The shapes of the treated and non-treated spectra differentiate in the four different regions marked I–IV in Fig. 4. The peaks in region positioned between 2830 cm^{-1} and 3000 cm^{-1}, that are attributed to alkane C–H stretching, the absorbance decreases upon plasma processing pointing to lower abundance of these groups. Similar trend is visible in regions II and III, both corresponding to C–O stretching, where the peak positioned at 1287 cm^{-1} disappears and the peaks between 1130 cm^{-1} and 1060 cm^{-1} straighten after fluorine treatment. Similarly, examining region IV, corresponding to C–H bending, it can be observed that the intensity decreases.

3.2. Physico-chemical properties

For packaging important properties, namely tensile strength (TS), elongation at break (ϵ) and water vapor transmission (WVT) were measured immediately after the treatment as well as after 31 days of aging in the controlled environment. As seen in Fig. 5, TS and ϵ did not decline with hydrophobization, which was of concern with this treatment. On the contrary, TS improved by 68% (from initial 1.38 ± 0.37 MPa to 2.32 ± 0.51 MPa after the treatment). Similarly, the ϵ increased from the original 63 ± 13% to 78 ± 10%. It is worth noting, that both of the measured mechanical properties are strongly influenced by the thickness of the film and moisture content (MC). While the thickness of the films (0.10 ± 0.01 mm) did not deviate upon modification, MC decreased in the fluorinated samples from initial 11.6 ± 0.4% to 9.2 ±

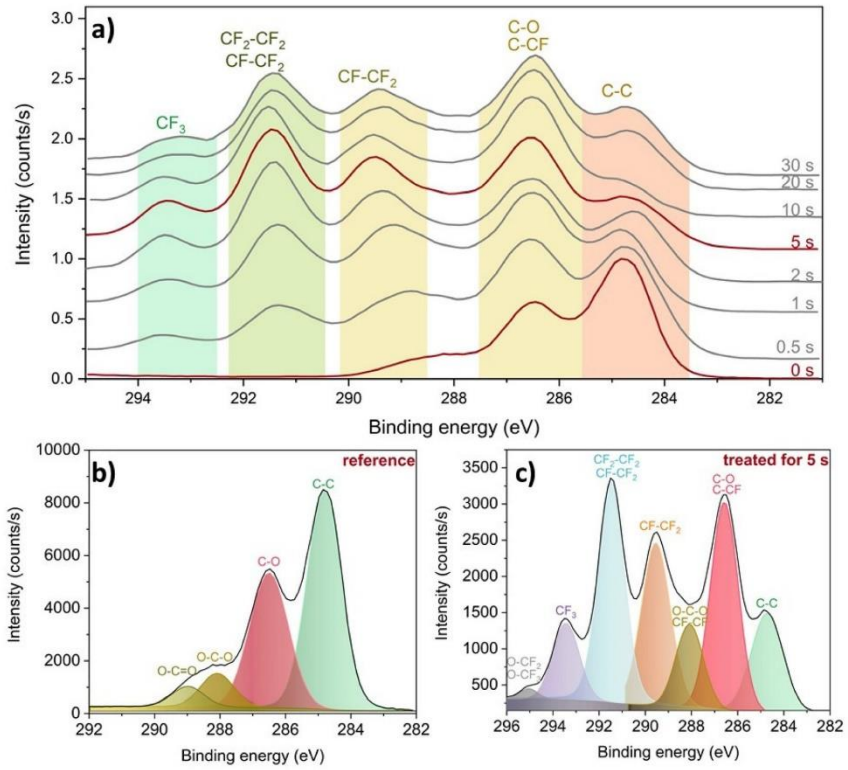

Fig. 3. (a) Evolution of high resolution XPS carbon spectra according to plasma processing time; (b) and (c) deconvolution of high-resolution C 1s XPS spectrum of reference material and sample treated for 5 s, respectively.

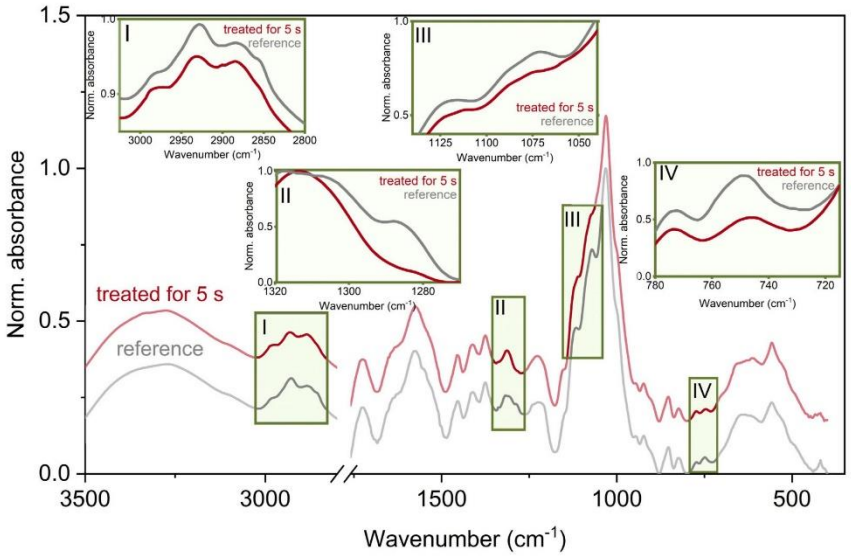

Fig. 4. FTIR-ATR spectra of reference and sample treated for 5 s immediately after processing with marked regions where the structural changes were observed.

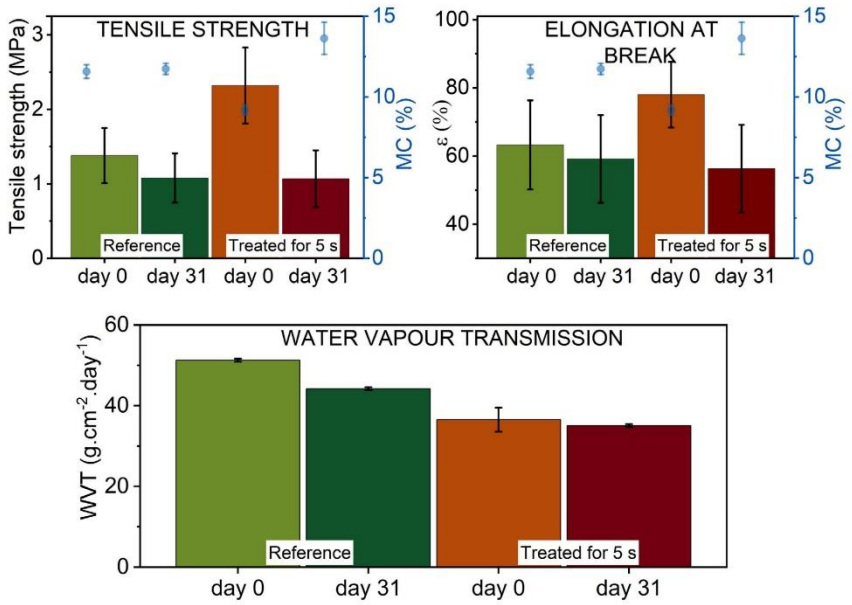

Fig. 5. TS, ϵ and WVT of the reference and sample treated for 5 s immediately after processing and after aging in controlled environment for 31 days.

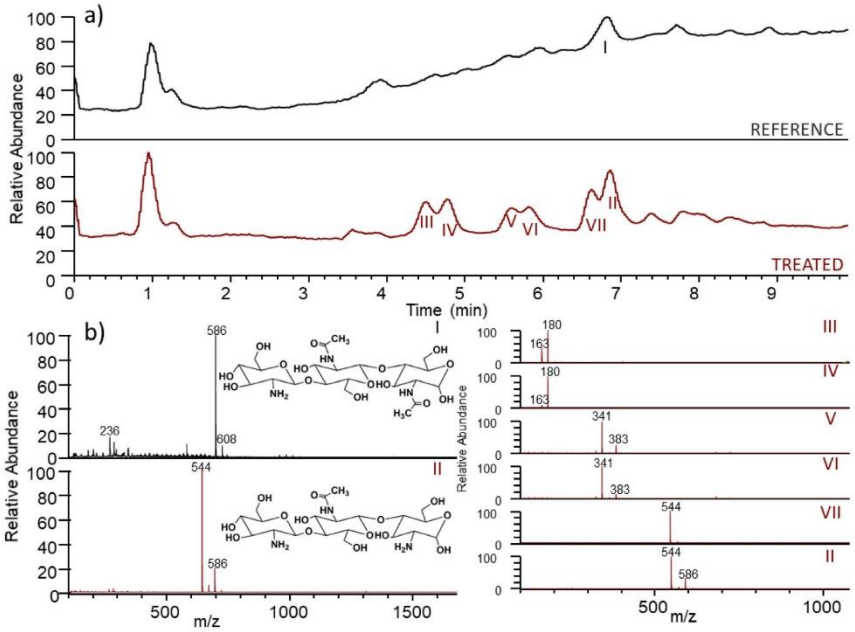

Fig. 6. HILIC LC-ESI(+)-MS chromatograms of water leachates in which reference (black) and sample treated for 5 s (red) were submerged for 144 h (a) with marked peaks further analyzed with MS and their corresponding spectra (b).

0.3%. The water is bound in the sample through hydrogen bonding sites in chitosan (Bajić et al. 2020), so the lower amount of moisture after treatment might be attributed to saturation of hydrogen binding sites of chitosan and CNCs with fluorine. As moisture has a plasticizing effect on the film, TS and MC are in inverse correlation [47], which explains the increase in TS of the treated sample well. However, generally, elongation rate has positive correlation to MC, which is not the case in the fluorinated samples. The newly formed bonds between fluorine and chitosan-CNCs might contribute to higher stiffness of the material. The mechanical properties of biopolymer films strongly relate to free

and bound water [7]. Leceta et al. suggest that the water bound inside the crosslinked composite matrix tends to form hydrogen bonds with more polar functional groups, which are in this case the newly added fluorine-related groups on the surface. With this, the internal film structure is damaged, resulting in loss of strength, stiffness and lower stretching [48]. Furthermore, high resolution spectrum of the aged sample was thoroughly inspected (Fig. A2), suggesting that the bonds, disrupted during the aging process, are in the backbone of the polymer chains, which could negatively affect the mechanical properties shown in Fig. 5. Aging of the films leads to loss of the advantage in mechanical properties gained by treatment. MC in the reference sample remains constant, whereas in the fluorinated one the moisture content increased to 13 ± 1.0% and consequently a drop in TS was seen. Based on assumption that the moisture content was lower in the treated film because of formation of hydrogen bonds between chitosan-CNCs and fluorine, the increase over time could be attributed to substitution of these binding with water-chitosan again. Both reference and processed films age into a stiffer material with ϵ 59 ± 14% and 56 ± 13%, respectively. Important role of packaging is to shelter the contents from loss of moisture or to prevent the moisture from the environment to breach into the inside and effect the contents. Upon treatment, water vapor transmission (WVT) lowered (from initial 51.3 ± 0.4 g cm^{-2} day^{-1} to 36.5 ± 3.0 g cm^{-2} day^{-1}) as shown in Fig. 5, which could be attributed to increase in hydrophobic character. Comparing to other available materials, the processed sample is better at preventing water transmission than PVA, nanocellulose-based films, cellophane and PCL and comparable to PS, Nylon 6 and PLA [16]. With aging, WVT slightly decreases in both samples, with treated sample still performing better than the reference.

3.3. Film stability in liquid environments

To further demonstrate suitability of the plasma treated material in packaging industry, which was suggested by the measured physicochemical properties and long-term stable hydrophobicity, the interaction of the films with liquid environments was evaluated. The main concern related to material′ s adequacy as packaging is potential leaching of fluorinated compounds into the environment, which was explored with an untargeted analysis of film leachates in water, 5% acetic $acid_{aq}$, 10% $ethanol_{aq}$ in both HILIC and RP modes using ESI(+)-MS and ESI(−)-MS. Two HILIC methods and an RP method were used to analyze the samples. LC-MS chromatograms of treated samples were compared with those of reference (blank) samples to reveal the potential leaching of fluorinated compounds. Both HILIC methods showed comparable results. In RP method, all peaks eluted in dead time (as expected for polar compounds such as glucosamine and N-acetyl glucosamine, potentially present in the simulants as monomer units of chitosan). The experiments showed no difference between the reference and treated sample, except for the water samples (LC-ESI(+)-MS chromatograms and MS spectra shown in Fig. 6; supplementary LC-MS chromatograms of the leachates are presented in Fig. A2. In the reference sample, the peak at t_R 6.8 min (marked with I) corresponds to the signal at m/z 586, which matches a formula of a trimer consisting of one glucosamine (GlcN) unit and two *N*-acetyl-D-glucosamine (GlcNAc) units. LC-MS analysis of treated water sample showed three split peaks, for which the MS analysis revealed that both parts correspond to the same m/z, so the splitting could be attributed to the existence of isomerism or aminosugar anomerism. The peaks with t_Rs between 4.2–5.0 min (peaks III and IV) correlate to m/z 180, which is attributed to protonated GlcN. The following two peaks with t_Rs between 5.6–6.0 min (peaks V and VI) and between 6.6–7.2 min (peaks VII and II) correspond to m/z at 341 (protonated GlcN/GlcN dimer) and m/z at 544 (protonated GlcN/GlcN/GlcNAc trimer), respectively [49]. Additionally, the peak with t_R 6.8 min in the treated sample (peak II) that coincide with the t_R of peak I in the control sample showed additional mass peak of lower intensity (m/z at 586), which was attributed to GlcN/GlcNAc/GlcNAc [49]. There were no detected peaks pointing to traces of fluorinated compounds in both HILIC and RP using either positive or negative ionization mode, however some limitations apply to this approach. The MS parameters were tuned using glucosamine as a standard due to the non-commercially available fluorinated standards. Moreover, taking into consideration that only surface was modified, it can be assumed that the concentration of potential fluorinated compounds leached into the liquid media is rather low, and may be under the limit of detection (LOD) of our methods, however LODs cannot be calculated due to the absence of standards.

4. Conclusions

Hydrophobization of bioplastic bio-composite formed from chitosan with incorporated cellulose nanocrystals have been achieved using ultrafast and efficient RF-generated plasma treatment. The main effect of the hydrophobization was to improve water-related properties and raise the material's suitability for packaging applications. After only 5 s of treatment, the increase of WCA by 28° was achieved. The insight into the surface chemistry behind these changes was provided, with XPS revealing newly formed fluorine-related bonds, while a decrease in C–H and C–O stretching and C–H bending was detected with FTIR-ATR. It is worth noting, that the surface was not damaged by the treatment. Plasma processing decreased MC in the fabricated films, which influenced TS, ϵ and WVT. However, for the role of packaging, the modified sample performed better than the reference one. Stability of the hydrophobic coating, an important aspect for this application, was demonstrated by following WCA over 40 days as well as determining comparable atomic composition with XPS after 35 days of aging. On the other hand, TS, ϵ and WVT all decreased in both, treated and reference sample with time, causing the processed material to lose its superiority. Lastly, to investigate the material's interaction with liquid environments and potential leaching of fluorinated compounds, the films were immersed in three different liquid environments (water, 5% acetic acid, 10% ethanol) and analyzed by means of LC-MS. No evidence pointing to presence of fluorinated compounds were found.

CRediT authorship contribution statement

Ana Oberlintner: Conceptualization, Investigation, Methodology, Data curation, Formal analysis, Visualization, Writing – original draft. **Alenka Vesel:** Conceptualization, Investigation, Methodology, Data curation, Formal analysis, Visualization, Writing – review & editing. **Katerina Naumoska:** Investigation, Methodology, Data curation, Formal analysis, Writing – review & editing. **Blaž Likozar:** Writing – review & editing, Supervision, Project administration, Funding acquisition. **Uroš Novak:** Conceptualization, Writing – review & editing, Supervision, Project administration, Funding acquisition.

Declaration of competing interest

The authors declare that they have no known competing financial interests or personal relationships that could have appeared to influence the work reported in this paper.

Acknowledgments

The authors acknowledge Anže Prašnikar for SEM images. The research was funded by Ph.D. research grant (Ana Oberlintner) and Slovenian Research Agency (ARRS) programs P2-0152, P2-0151 and P1-0005.

Appendix A. Supplementary data

Supplementary material related to this article can be found online at https://doi.org/10.1016/j.apsusc.2022.153562.

References

[1] Plastic Europe - Association of Plastics Manufactures, Plastics – the Facts 2020: An Analysis of European Plastics Production, Demand and Waste Data, Tech. Rep., Plastics Europe, Brussels, Belgium, 2020, pp. 1–64, URL https://www.plasticseurope.org/application/files/3416/2270/7211/Plastics{_}the{_}facts-WEB-2020{_}versionJun21{_}final.pdf{%}0Ahttps://www.plasticseurope.org/en/resources/publications/4312-plastics-facts-2020.

[2] Plastic Europe - Association of Plastics Manufactures, Plastics - the Facts 2019: An Analysis of European Plastics Production, Demand and Waste Data, Tech. Rep., Plastics Europe, Brussels, Belgium, 2019, http://dx.doi.org/10.31025/2611-4135/2019.13894, URL https://www.plasticseurope.org/application/files/9715/7129/9584/FINAL{_}web{_}version{_}Plastics{_}the{_}facts2019{_}14102019.pdf.

[3] U. Novak, M. Bajić, K. Kõrge, A. Oberlintner, J. Murn, K. Lokar, K.V. Triler, B. Likozar, From waste/residual marine biomass to active biopolymer-based packaging film materials for food industry applications – a review, Phys. Sci. Rev. 5 (3) (2020) http://dx.doi.org/10.1515/psr-2019-0099.

[4] L.A.M. van den Broek, R.J.I. Knoop, F.H.J. Kappen, C.G. Boeriu, Chitosan films and blends for packaging material, Carbohydr. Polymers 116 (2015) 237–242, http://dx.doi.org/10.1016/j.carbpol.2014.07.039.

[5] A. Oberlintner, M. Bajić, G. Kalčikova, B. Likozar, U. Novak, Biodegradability study of active chitosan biopolymer films enriched with quercus polyphenol extract in different soil types, Environ. Technol. Innov. (2020) http://dx.doi.org/10.1016/j.eti.2020.101318.

[6] M. Bajić, T. Ročnik, A. Oberlintner, F. Scognamiglio, U. Novak, B. Likozar, Natural plant extracts as active components in chitosan-based films: A comparative study, Food Pack. Shelf Life 21 (2019) 100365, http://dx.doi.org/10.1016/j.fpsl.2019.100365.

[7] M. Bajić, A. Oberlintner, K. Kõrge, B. Likozar, U. Novak, Formulation of active food packaging by design: Linking composition of the film-forming solution to properties of the chitosan-based film by response surface methodology (RSM) modelling, 2020, http://dx.doi.org/10.1016/j.ijbiomac.2020.05.186.

[8] K. Rambabu, G. Bharath, F. Banat, P.L. Show, H.H. Cocoletzi, Mango leaf extract incorporated chitosan antioxidant film for active food packaging, Int. J. Biol. Macromol. 126 (2019) 1234–1243, http://dx.doi.org/10.1016/j.ijbiomac.2018.12.196.

[9] J. Hafsa, M. ali Smach, M.R. Ben Khedher, B. Charfeddine, K. Limem, H. Majdoub, S. Rouatbi, Physical, antioxidant and antimicrobial properties of chitosan films containing eucalyptus globulus essential oil, 2016, http://dx.doi.org/10.1016/j.lwt.2015.12.050.

[10] L. Sánchez-González, C. González-Martínez, A. Chiralt, M. Cháfer, Physical and antimicrobial properties of chitosan-tea tree essential oil composite films, 2010, http://dx.doi.org/10.1016/j.jfoodeng.2010.01.026.

[11] N.M. Hromiš, V.L. Lazić, S.L. Markov, Ž.G. Vaštag, S.Z. Popović, D.Z. Šuput, N.R. Džinić, A.S. Velićanski, L.M. Popović, Optimization of chitosan biofilm properties by addition of caraway essential oil and beeswax, 2015, http://dx.doi.org/10.1016/j.jfoodeng.2015.01.001.

[12] K. Kõrge, H. Šeme, M. Bajić, B. Likozar, U. Novak, Reduction in spoilage microbiota and cyclopiazonic acid mycotoxin with chestnut extract enriched chitosan packaging : Stability of inoculated gouda cheese, Foods 9 (2020) 1645, http://dx.doi.org/10.3390/foods9111645.

[13] K. Kõrge, M. Bajić, B. Likozar, U. Novak, Active chitosan–chestnut extract films used for packaging and storage of fresh pasta, Int. J. Food Sci. Technol. 55 (2020) 3043–3052, http://dx.doi.org/10.1111/ijfs.14569.

[14] G. Lavrič, A. Oberlintner, I. Filipova, U. Novak, B. Likozar, U. Vrabič-Brodnjak, Functional nanocellulose, alginate and chitosan nanocomposites designed as active film packaging materials, Polymers 13 (15) (2021) 2523, http://dx.doi.org/10.3390/polym13152523.

[15] B. Lepoittevin, T. Elzein, D. Dragoe, A. Bejjani, F. Lemée, J. Levillain, P. Bazin, P. Roger, I. Dez, Hydrophobization of chitosan films by surface grafting with fluorinated polymer brushes, Carbohydr. Polymers 205 (October 2018) (2019) 437–446, http://dx.doi.org/10.1016/j.carbpol.2018.10.044.

[16] S.S. Ahankari, A.R. Subhedar, S.S. Bhadauria, A. Dufresne, Nanocellulose in food packaging: A review, Carbohydr. Polymers 255 (2021) 117479, http://dx.doi.org/10.1016/j.carbpol.2020.117479.

[17] N. Bordenave, S. Grelier, V. Coma, Hydrophobization and antimicrobial activity of chitosan and paper-based packaging material, Biomacromolecules 11 (1) (2010) 88–96, http://dx.doi.org/10.1021/bm9009528.

[18] P.K. Binsi, C.N. Ravishankar, T.K. Srinivasa Gopal, Development and characterization of an edible composite film based on chitosan and virgin coconut oil with improved moisture sorption properties, J. Food Sci. 78 (4) (2013) http://dx.doi.org/10.1111/1750-3841.12084.

[19] A. Niemczyk, A. Goszczyńska, M. Gołda-Cępa, A. Kotarba, P. Sobolewski, M. El Fray, Biofunctional catheter coatings based on chitosan-fatty acids derivatives, Carbohydr. Polymers 225 (2019) 115263, http://dx.doi.org/10.1016/j.carbpol.2019.115263.

[20] K.B. Miles, R.L. Ball, H.W.T. Matthew, Chitosan films with improved tensile strength and toughness from N-acetyl-cysteine mediated disulfide bonds, Carbohydr. Polymers 139 (2016) 1–9, http://dx.doi.org/10.1016/j.carbpol.2015.11.052.

[21] N. Mati-Baouche, C. Delattre, H. de Baynast, M. Grédiac, J.-D. Mathias, A.V. Ursu, J. Desbrières, P. Michaud, Alkyl-chitosan-based adhesive: Water resistance improvement, Molecules 24 (10) (2019) 1987, http://dx.doi.org/10.3390/molecules24101987.

[22] A. Piel, Plasma generation, Springer Berlin Heidelberg, Berlin, Heidelberg, 2010, pp. 323–350, http://dx.doi.org/10.1007/978-3-642-10491-6_11.

[23] S. Han, Y. Lee, Y.-W. Kim, Y. Kim, H. Chun, J. Lee, Plasma source ion implantation using high-power pulsed RF plasma, Surf. Coat. Technol. 186 (1) (2004) 177–181, http://dx.doi.org/10.1016/j.surfcoat.2004.04.045.

[24] F.X. Lu, W.Z. Tang, T.B. Huang, J.M. Liu, J.H. Song, W.X. Yu, Y.M. Tong, Large area high quality diamond film deposition by high power DC arc plasma jet operating at gas recycling mode, Diam. Relat. Mater. 10 (9) (2001) 1551–1558, http://dx.doi.org/10.1016/S0925-9635(01)00407-1.

[25] C.A. Santos, N.H. Phuong, M.J. Park, S.B. Kim, Y.M. Jo, Decomposition of indoor VOC pollutants using non-thermal plasma with gas recycling, Korean J. Chem. Eng. 37 (1) (2020) 120–129, http://dx.doi.org/10.1007/s11814-019-0406-8.

[26] O. Baranov, K. Bazaka, H. Kersten, M. Keidar, U. Cvelbar, S. Xu, I. Levchenko, Plasma under control: Advanced solutions and perspectives for plasma flux management in material treatment and nanosynthesis, Appl. Phys. Rev. 4 (4) (2017) 041302, http://dx.doi.org/10.1063/1.5007869.

[27] M.N. Santhosh, G. Filipič, E. Kovacevic, A. Jagodar, J. Berndt, T. Strunskus, H. Kondo, M. Hori, E. Tatarova, U. Cvelbar, N-graphene nanowalls via plasma nitrogen incorporation and substitution: The experimental evidence, Nano-Micro Lett. 12 (1) (2020) 53, http://dx.doi.org/10.1007/s40820-020-0395-5.

[28] A. Oberlintner, V. Shvalya, A. Vasudevan, D. Vengust, B. Likozar, U. Cvelbar, U. Novak, Hydrophilic to hydrophobic: Ultrafast conversion of cellulose nanofibrils by cold plasma fluorination, Appl. Surf. Sci. (2022) 152276, http://dx.doi.org/10.1016/j.apsusc.2021.152276.

[29] Z. Sheikhi, L. Mirmoghtadaie, K. Abdolmaleki, M.R. Khani, M. Farhoodi, E. Moradi, B. Shokri, S. Shojaee-Aliabadi, Characterization of physicochemical and antimicrobial properties of plasma-treated starch/chitosan composite film, Pack. Technol. Sci. 34 (7) (2021) 385–392, http://dx.doi.org/10.1002/pts.2559.

[30] U.V. Brodnjak, A. Jesih, D. Gregor-Svetec, Chitosan based regenerated cellulose fibers functionalized with plasma and ultrasound, Coatings 8 (4) (2018) 9–14, http://dx.doi.org/10.3390/coatings8040133.

[31] P. Wanichapichart, R. Sungkum, W. Taweepreda, M. Nisoa, Characteristics of chitosan membranes modified by argon plasmas, Surf. Coat. Technol. 203 (17) (2009) 2531–2535, http://dx.doi.org/10.1016/j.surfcoat.2009.02.069.

[32] H. Wang, Y.-E. Fang, Y. Yan, Surface modification of chitosan membranes by alkane vapor plasma, J. Mater. Chem. 11 (5) (2001) 1374–1377, http://dx.doi.org/10.1039/B009688L.

[33] K.K. Samanta, G.J. Amish, J. Manjeet, A. Aswini K., Study of hydrophobic finishing of cellulosic substrate using he_1,3-butadiene plasma at atmospheric pressure _ elsevier enhanced reader.pdf, Surf. Coat. Technol. 213 (2012) 65–76.

[34] K.K. Samanta, T.N. Gayatri, S. Saxena, S. Basak, S.K. Chattopadhyay, A. Arputharaj, V. Prasad, Hydrophobic functionalization of cellulosic substrates using atmospheric pressure plasma, Cellul. Chem. Technol. 50 (7–8) (2016) 745–754.

[35] O. Mauger, S. Westphal, S. Klöpzig, A. Krüger-Genge, W. Müller, J. Storsberg, J. Bohrisch, Plasma activation as a powerful tool for selective modification of cellulose fibers towards biomedical applications, Plasma 3 (4) (2020) 196–203, http://dx.doi.org/10.3390/plasma3040015.

[36] K.K. Samanta, A.G. Joshi, M. Jassal, A.K. Agrawal, Hydrophobic functionalization of cellulosic substrate by tetrafluoroethane dielectric barrier discharge plasma at atmospheric pressure, Carbohydr. Polymers 253 (2021) 117272, http://dx.doi.org/10.1016/j.carbpol.2020.117272.

[37] K.S. Chow, E. Khor, New flourinated chitin derivatives: synthesis, characterization and cytotoxicity assessment, Carbohydr. Polymers 47 (4) (2002) 357–363, http://dx.doi.org/10.1016/S0144-8617(01)00190-4.

[38] A. Wijekoon, N. Fountas-Davis, N.D. Leipzig, Fluorinated methacrylamide chitosan hydrogel systems as adaptable oxygen carriers for wound healing, Acta Biomater. 9 (3) (2013) 5653–5664, http://dx.doi.org/10.1016/j.actbio.2012.10.034.

[39] Z.E.D. Cele, A.M. Somboro, D.G. Amoako, L.F. Ndlandla, M.O. Balogun, Fluorinated quaternary chitosan derivatives: Synthesis, characterization, antibacterial activity, and killing kinetics, ACS Omega 5 (46) (2020) 29657–29666, http://dx.doi.org/10.1021/acsomega.0c01355.

[40] F.E. Tabaght, A. El Idrissi, M. Aqil, A. Elbachiri, A. Tahani, A. Maaroufi, Grafting method of fluorinated compounds to cellulose and cellulose acetate: Characterization and biodegradation study, Cellul. Chem. Technol. 55 (5–6) (2021) 511–528, http://dx.doi.org/10.35812/CelluloseChemTechnol.2021.55.46.

[41] T.-F. Ang, J. Maiangwa, A.B. Salleh, Y.M. Normi, T.C. Leow, Dehalogenases: From improved performance to potential microbial dehalogenation applications, Molecules 23 (5) (2018) 1100, http://dx.doi.org/10.3390/molecules23051100.

[42] C.L. Amorim, M.F. Carvalho, C.M.M. Afonso, P.M.L. Castro, Biodegradation of fluoroanilines by the wild strain labrys portucalensis, Int. Biodeterioration Biodegrad. 80 (2013) 10–15, http://dx.doi.org/10.1016/j.ibiod.2013.02.001.

[43] E. Ojogbo, R. Blanchard, T. Mekonnen, Hydrophobic and melt processable starch-laurate esters: Synthesis, structure–property correlations, J. Polym. Sci. A 56 (23) (2018) 2611–2622, http://dx.doi.org/10.1002/pola.29237.

[44] S. Wu, Surface and interfacial tensions of polymer melts. II. Poly(methyl methacrylate), poly(n-butyl methacrylate), and polystyrene, J. Phys. Chem. 74 (3) (1970) 632–638, http://dx.doi.org/10.1021/j100698a026.

[45] H. Liu, R. Adhikari, Q. Guo, B. Adhikari, Preparation and characterization of glycerol plasticized (high-amylose) starch–chitosan films, J. Food Eng. 116 (2) (2013) 588–597, http://dx.doi.org/10.1016/j.jfoodeng.2012.12.037.

[46] R. Varma, S. Vasudevan, Extraction, characterization, and antimicrobial activity of chitosan from horse mussel modiolus modiolus, ACS Omega 5 (32) (2020) 20224–20230, http://dx.doi.org/10.1021/acsomega.0c01903.

[47] R.Y. Aguirre-Loredo, A.I. Rodríguez-Hernández, E. Morales-Sánchez, C.A. Gómez-Aldapa, G. Velazquez, Effect of equilibrium moisture content on barrier, mechanical and thermal properties of chitosan films, Food Chem. 196 (2016) 560–566, http://dx.doi.org/10.1016/j.foodchem.2015.09.065.

[48] I. Leceta, M. Peñalba, P. Arana, P. Guerrero, K. de la Caba, Ageing of chitosan films: Effect of storage time on structure and optical, barrier and mechanical properties, Eur. Polym. J. 66 (2015) 170–179, http://dx.doi.org/10.1016/j.eurpolymj.2015.02.015.

[49] C.L. Allison, A. Lutzke, M.M. Reynolds, Identification of low molecular weight degradation products from chitin and chitosan by electrospray ionization time-of-flight mass spectrometry, Carbohydr. Res. 493 (2020) 108046, http://dx.doi.org/10.1016/j.carres.2020.108046.

Supplementary Information: Permanent Hydrophobic Coating of Chitosan/Cellulose Nanocrystals Composite Film by Cold Plasma Processing

Ana Oberlintner[a,b], Alenka Vesel[c], Katerina Naumoska[d], Blaž Likozar[a], Uroš Novak[a]
[a]Department of Catalysis and Chemical Reaction Engineering, National Institute of Chemistry, Hajdrihova 19, SI-1000 Ljubljana, Slovenia
[b] Jožef Stefan International Postgraduate School, Jamova cesta 39, SI-1000 Ljubljana, Slovenia
[c] Department of Surface Engineering, Jožef Stefan Institute, Jamova cesta 39, SI-1000 Ljubljana, Slovenia
[d]Department of Analytical Chemistry, Laboratory for Food Chemistry, National Institute of Chemistry, Hajdrihova 19, SI-1000 Ljubljana, Slovenia

Methods

1- Fabrication of Chitosan-Based Films with Incorporated CNCs

Briefly, 1.5 wt % of chitosan powder was dissolved in 1 *v/v* % aqueous solution of lactic acid. Glycerol in amount of 30 wt % with respect to chitosan was used as a plasticizer. The mixture was filtered through four layers of medical gauze. CNCs were added in the form of suspension in water in amount of 3 wt % according to the weight of chitosan and homogenized with UltraTurrax (Ika, Straufen, Germany) for three minutes at 600 rpm. 50 g of the film-forming solution was poured into Petri dishes in size of 12 × 12 cm and dried in the ventilation oven (Kambič, Slovenia) at ventilation rate 30 % and 30 °C for 48 h.

2- Film Physico-Chemical Properties

Film thickness was measured at eight different points on the film and the average was reported. ABS Digital Thickness Gauge (Mitutoyo, Aurora, USA) was used.

Film samples of rectangular shape, 6 cm long and 2 cm wide, were analyzed with XLW Auto Tensile Rester (Labthink® Instruments, Jinan, China) equipped with a 100 N load cell. The gauge length segment was 4 cm and the cross-head speed 25 mm min^{-1}. Tensile strength (TS) was calculated by division of the maximal load with the average cross-sectional area in the gauge segment (4 cm) of the sample. Elongation at break (ε) was expressed as a ratio between the increase in the length of the sample and original cross-sectional area in the sample gauge length segment.

For determination of WVT, $CaCl_2$ was first activated in the oven at 105 °C for two hours and then filled into glass flask (diameter 5 cm, height 10 cm, volume 150 mL). Samples were cut into 3 x 3 cm rectangular pieces and tightened over the flask. A circular area with diameter 2.1 cm was carved out from the top of the flask which was used to cover the flask over the film. These flasks were then put into a 150 mL bottle with 50 mL of saturated NaCl solution. Approximately 5 g of NaCl was additionally added into the NaCl solution, to ensure saturation at all times. The flasks with sample and $CaCl_2$ were weighted daily over the period of 8 days. Water vapor transmission was then calculated according to Equation 1:

$$WVT = k / S \qquad \text{Eq. A1}$$

where k represents the slope of the time (h)/Δ mass (g) plot, and S represents the area of the film through which the water can migrate in m^2 (1.84×10^{-4} m^2). WVT is expressed in g m^2 24 h^{-1}.

3- Leaching of film substances into liquid environments

An alternative, HILIC LC-MS analyses in ESI(+) and ESI(-) mode were also performed. The mobile phase was composed of 10 mM ammonium formate with pH 3 (mobile phase A) and acetonitrile: ammonium formate buffer with ratio 90 % : 10 % (mobile phase B). A gradient elution from 0 % to 30 % A in 10 min was employed to elute the compounds in the samples and the mobile phase

remained at 30 % A for further 10 min (cleaning step) before returning to initial conditions (in 1 min). The re-equilibration step was 15 min long. The mobile phase flow rate was 300 µL min^{-1}. Column oven and autosampler temperature were set at 25 °C and 5 °C, respectively. Injection volume was 2 µL. The MS parameters were as described in the main text. The samples were dried under nitrogen flow and redissolved in 70 % acetonitrile before injection into the LC-MS.

Further, RP LC-MS analyses in ESI(+) and ESI(-) mode were also performed using the above equipment. The separation occurred on ThermoScientific Hypersil Gold (150 × 2.1 mm i.d., 3 µm). The mobile phase was composed of 0.1% acetic $acid_{(aq)}$ (mobile phase A) and acetonitrile (mobile phase B). Isocratic method was used for compounds elution (A : B = 90 % : 10 %) with mobile phase flow rate at 300 µL min^{-1}. The MS parameters were as described in the main text and the samples were injected into the LC-MS without additional sample preparation steps.

Supplementary results

1- High resolution spectra of CF_4 plasma treated and aged sample

The high resolution XPS spectra of treated and aged (40 days) sample revealed, that compared to samples immediately after the CF_4 plasma treatment, the intensity of the peaks located at 284.7 eV (corresponding to C-C bond) and at 286.7 eV (C-O and C-F bonds) has increased slightly, while the peaks correlating to O-C-O/CF-CF, CF-CF_2 and CF_2-CF_2/CF_2-CF decreased. On the other hand, the intensity correlated to CF_3 peak was retained.

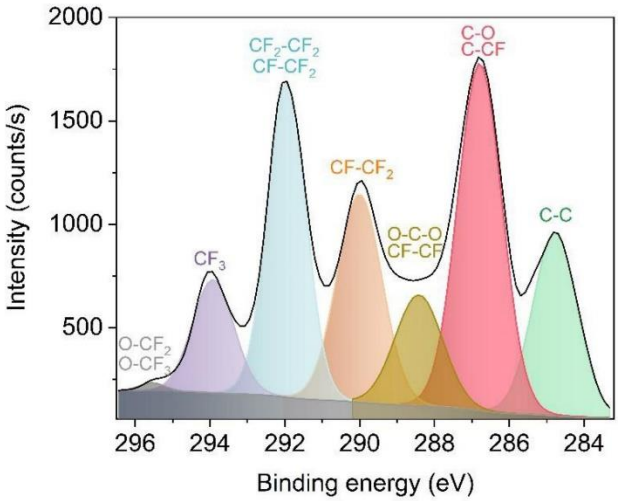

Fig. A1: Deconvolution of high resolution C 1s XPS spectrum of the plasma treated and aged sample.

2- Leaching of film substances into liquid food simulants

Alternative HILIC analysis by comparing LC-MS chromatograms of the tested liquids, revealed mass peaks at *m/z* 167 in all three leachates. This *m/z* suggests the presence of protonated diglycerol molecule $[2M - H_2O + H]^+$ [1]. The *m/z* at 297 detected in peak IV may correspond to $[4M - 4H_2O + H]^+$, originating from glycerol molecule as well. This is in line with the composition of the prepared biofilm. In water, additional compounds at *m/z* 180, 341 and 544 are found, corresponding to GlcN, GlcN/GlcN dimer and GlcN/GlcN/GlcNAc trimer, respectively (Fig. A2). In RP analysis, all compounds eluted in dead time.

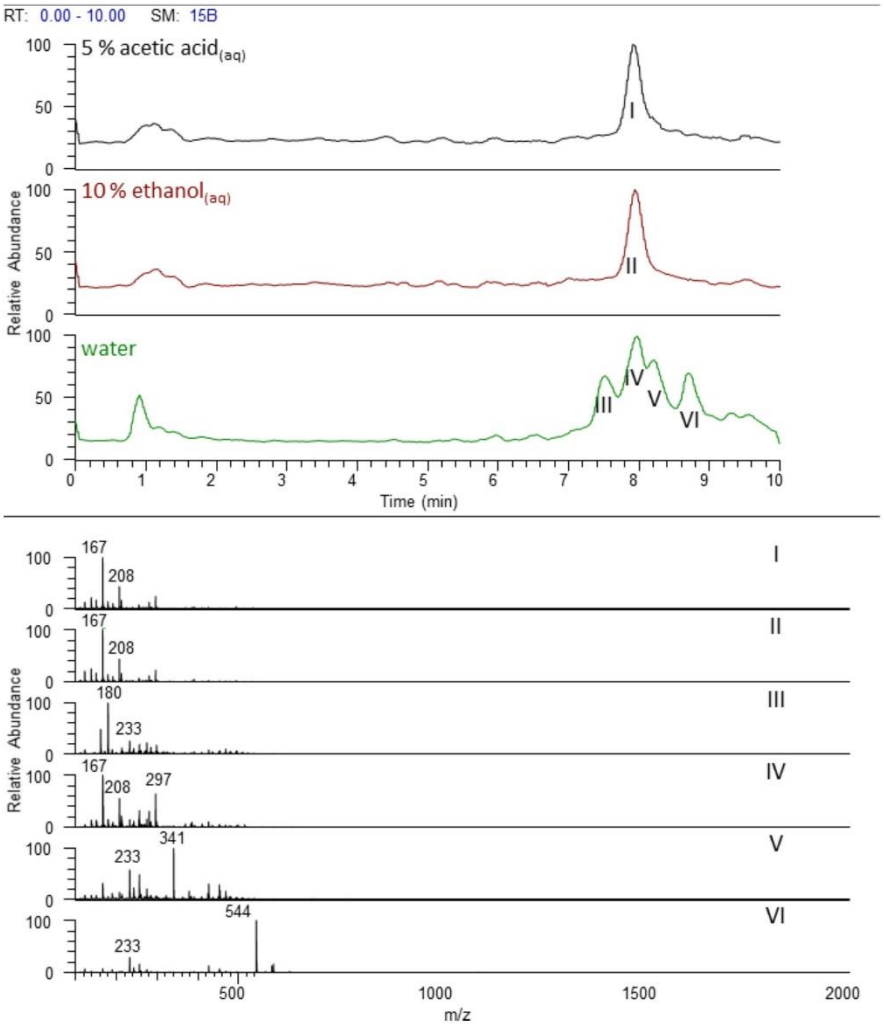

Fig. A2: HILIC LC-ESI(+)-MS chromatograms of leachates prepared using different liquid environments (5 % acetic acid$_{(aq)}$ - top, 10 % ethanol$_{(aq)}$ - middle, water – bottom), separated on Phenomenex Luna NH_2 column (using the alternative HILIC method), in which fluorinated sample was immersed for 144 h and their corresponding MS spectra.

Supplementary References

(1) Medeiros, M. A.; Araujo, M. H.; Augusti, R.; De Oliveira, L. C. A.; Lago, R. M. Acid-Catalyzed Oligomerization of Glycerol Investigated by Electrospray Ionization Mass Spectrometry. *J. Braz. Chem. Soc.* **2009**, *20* (9), 1667–1673. https://doi.org/10.1590/S0103-50532009000900015.

5.3 Use of Non-Fluorine Containing Plasma

The last section in Chapter 5 investigates the use of other gases for hydrophobization of cellulose nanomaterials by plasma processing. Table 1 provides an insight into plasma modifications of cellulose substrates, sorted by carrier gas and with described final result regarding wettability and change in WCA after treatment. Air, Ar, O_2 and N_2 are generally utilized for increasing hydrophilicity in cellulose substrates, while fluorine- and silane-containing reactants yield hydrophobic surface. Pretreatment with O_2 is often carried out to etch the substrate and provide higher specific surface for subsequent hydrophobic polymerization (Balu, Breedveld, and Hess 2008; Leal et al. 2020). Although fluorine/silane-containing plasma or polymerization of fluorine/silane-containing monomers on the surface of (nano)cellulose was shown to provide ultrafast conversion, stable coating and that fluorine-related compounds do not leach into liquid environment, fluorine is toxic to humans in higher concentrations and should best be avoided in sustainable applications. Furthermore, it has to be taken into account that CF_4 is a potent greenhouse gas. To align with green chemistry principles, a search for more sustainable gas continues. Literature suggests that processing with plasma produced from H_2 results in a hydrophobic surface, however such change is visible only after 8 min of continuous treatment, which also causes destruction of surface morphology (Carlsson and Stroem 1991). On the other hand, Deslandes et al. (1998) and Pertile et al. (2010) suggest that N_2 plasma might induce hydrophobic behavior on the surface of cellulose substrate, showing an increase of WCA for 15°.

With this in mind, in this section, nitrogen for hydrophobization of cellulose nanomaterials by plasma processing is investigated. Additionally, the effect accumulating treatment, pretreatment with oxygen plasma and reversibility to initial hydrophilic state are explored.

Table 1: Up-to-date literature review on plasma processing of cellulose substrates with the goal to modify their wettability. ΔWCA represents the highest/lowest value depending on the type of functionalization (hydrophobic/hydrophilic).

Substrate	Carrier gas	Conditions	Result	Reference
Cellulose	Air	DBD plasma, 500 W	Increased wettability (ΔWCA = -20°)	(Flynn, Byrne, and Meenan 2013)
Bacterial cellulose	Ar	10 W, 240 s	Increased wettability (ΔWCA = - 43°)	(Kutová et al. 2021)
CNCs film	Ar/CH_4 (2 %) and Ar/SiH_4 (0.02 %)	DBD plasma, 200 sccm and 100 sccm, 1–30 min and 1–3 min	Decreased wettability (ΔWCA = + 50 ° for CH_4 and +110 ° for SiH_4)	(Matouk et al. 2020)
CNCs powder	Ar/CH_4 (2 %) and Ar/SiH_4 (0.02 %) and Ar/SiH_4/ CH_4 (2 %) (0.02 %)	DBD plasma, 7.2 kV	Decreased wettability (Ar/CH_4: ΔWCA = + 50°; Ar/SiH_4: ΔWCA = + 120°; Ar/SiH_4/ CH_4: ΔWCA = + 110°)	(Matouk et al. 2021)
CNCs film	Ar/NH_3 (10 %)	DBD plasma, 200 sccm, 1–60 min	Increased wettability (ΔWCA = -45°)	(Matouk et al. 2020)
Cellulose	Ar/C_4F_8	75 sccm/ 15 sccm, 30 W	Decreased wettability **	(Vaswani, Koskinen, and Hess 2005)

Bacterial cellulose	CF_4	20 W, 60 s	Decreased wettability (ΔWCA = + 92°)	(Kurniawan, Lai, and Wang 2012)
CNFs	CF_4	30 s, 100 W	Decreased wettability (ΔWCA = + 85°)	This thesis, Section 5.1
Regenerated cellulose	CF_4	40 W, 60 s, 10 sccm	Decreased wettability (ΔWCA = + 90°)	(Kawano, Wang, and Andou 2022)
Cellulose	H_2	100 W, 10 sccm, 8 min	Decreased wettability **	(Carlsson and Stroem 1991)
Bacterial cellulose	N_2	20 W, 60 s	Increased wettability (ΔWCA = -12°)	(Kurniawan et al. 2012)
Bacterial cellulose	N_2	30 min, 85 W, 10 sccm	Slightly decreased wettability (ΔWCA = -+15°) *	(Pertile et al. 2010)
Cellulose	N_2	2–60 s, 20 sccm, 33 W, 27 Pa	Slightly decreased wettability (WCA was not measured) *	(Deslandes et al. 1998)
Regenerated cellulose	N_2	10 W, 240 s, 10 sccm	Increased wettability (ΔWCA = - 30°)	(Kawano et al. 2022)
TEMPO-CNFs	N_2 (with deposition of hexamethyl disiloxane)	150 slm, 400 W	Decreased wettability (ΔWCA = + 80°)	(Khakalo et al. 2020)
TEMPO-CNFs	N_2 (with deposition of (3-aminopropyl)triethoxy silane)	150 slm, 400 W	Decreased wettability (ΔWCA = + 45°)	(Khakalo et al. 2020)
Cellulose	NH_3/N_2	DBD plasma, 1000 W	Increased wettability (ΔWCA = -15°)	(Flynn et al. 2013)
Bacterial cellulose	O_2	20 W, 60 s	Increased wettability (ΔWCA = -18°)	(Kurniawan et al. 2012)
Cellulose	O_2	5 W/20 W, 20 sccm/5 sccm, 60–960 s	Increased wettability **	(Carlsson and Stroem 1991)
Regenerated cellulose	O_2	40 W, 120 s, 10 sccm	Increased wettability (ΔWCA = - 29°)	(Kawano et al. 2022)
Cellulose	O_2 (with subsequent deposition of C_2HF_5)	6 sccm, 150 W, 30 min	Decreased wettability (ΔWCA = + 84°)	(Balu et al. 2008)
Bacterial cellulose	O_2 (with subsequent deposition of CH_3Cl_3Si)	100 W, 100 Pa, 15 min	Decreased wettability (ΔWCA = + 108°)	(Leal et al. 2020)

Cellulose	Ar/ C_2HF_5	75 sccm/20 sccm, 30 W	Decreased wettability (ΔWCA = + 82°)	(Vaswani et al. 2005)
CNFs	SF_6	150 W, 15 min, 0.1–0.3 Torr	Decreased wettability (ΔWCA = + 96°)	(Silva et al. 2016)

* The decrease in wettability was accounted to vacuuming.
** The initial value was not measured or WCA analysis was not carried out.

5.3.1 Materials and methods

5.3.1.1 Materials

Valida S CNFs were obtained from Sappi (Maastricht, Netherlands). Glycerol was bought from Pharmachem (Ljubljana, Slovenia). Ultrapure water (18 MΩ cm) was used throughout the experiments. For the determination of free surface energy and oleophobicity, diiodomethane and n-hexadecane were purchased from Sigma Aldrich (Darmstadt, Germany), while formamide was obtained from Thermo Scientific (Waltham, MA, USA).

5.3.1.2 Fabrication of CNFs Films

CNFs films were fabricated according to the protocol described in Section 5.1. Briefly, to decrease the viscosity of the 3 wt% suspension of CNFs and enable casting, it was diluted with ultrapure water to reach 1.152 wt%. Glycerol was added in the amount to reach 30 wt% based on CNFs solid weight. Finally, 32 g of suspension was casted to a 12x12 cm petri dish, reaching the final solid weight of CNFs 0.367 g per petri dish. The films were dried in an oven (Kambič, Slovenija) at 40 °C with 30 % ventilation for 48 hours and stored at room temperature before treatment.

5.3.1.3 Surface Treatment of the Fabricated Films

The films were cut to pieces with a size of approximately 2x2.5 cm and placed onto a microscope glass slide and fixated on the sides with pieces of cracked glass that were attached with carbon tape. The glass covered a minimal surface area of the sample. The experiments were carried out in a borosilicate glass tube with a diameter of 4 cm and with 80 cm in length, using radio frequency generator operating at 13.56 MHz RF power. The samples were treated under different conditions with parameters that were varying being power, time, flow and position inside the tube. The flushing was carried out using argon. The tested parameters are indicated in Table 2.

Table 2: Tested gases and parameters for hydrophobization of CNFs films.

Gas	Power (W)	Treatment time (s)	Distance (cm from the center of coil)	Flow (sccm)
Nitrogen	100	5	10	100
Nitrogen	100	10	10	100
Nitrogen	100	15	10	100
Nitrogen	100	20	10	100
Nitrogen	100	30	10	100
Nitrogen	100	40	10	100
Nitrogen	100	50	10	100
Nitrogen	100	60	10	100
Nitrogen	100	120	10	100
Nitrogen	50	20	10	100

Nitrogen	100	20	10	100
Nitrogen	200	20	10	100
Nitrogen	300	20	10	100
Nitrogen	400	20	10	100
Nitrogen	500	20	10	100
Nitrogen	100	20	10	50
Nitrogen	100	20	10	100
Nitrogen	100	20	10	150
Nitrogen	100	20	10	200
Nitrogen	100	20	10	300
Nitrogen	100	20	10	400
Nitrogen	100	20	10	500
Nitrogen	100	20	- 20*	100
Nitrogen	100	20	- 10*	100
Nitrogen	100	20	0	100
Nitrogen	100	20	10	100
Nitrogen	100	20	20	100
Nitrogen	100	20	30	100
Nitrogen	100	20**	10	100
Nitrogen	100	40**	10	100
Nitrogen	100	60**	10	100
Nitrogen	100	80**	10	100
Nitrogen	100	100**	10	100
Nitrogen	100	120**	10	100
Nitrogen + Oxygen	100 (N_2), 500 (O_2)	20 (both)	10 (both)	150 (both)
Oxygen + Nitrogen	100 (N_2), 500 (O_2)	20 (both)	10 (both)	150 (both)
Oxygen	100	20	10	100
Oxygen	200	20	10	100
Oxygen	300	20	10	100
Oxygen	400	20	10	100
Oxygen	500	20	10	100
Oxygen	600	20	10	100

* Negative value indicates position before coil.

** Treatments were carried out in a pulsating regime with 20 s of treatment and 20 s cooldown. The total accumulated treatment time is reported.

5.3.1.4 Measurement of Water Contact Angle, Lipophobicity and Determination of Surface Free Energy

All analyses were carried out on Tensiometer Theta T200 (Biolin Scientific, Germany), in the frame of 6 h after the treatment. The samples were placed on a microscope glass substrate and contact angle between films surface and the liquid was evaluated 5 s after the release of drop onto the surface by sessile drop analysis. On the selected samples, n-Hexadecane was used to determine lipophilicity of the surface, while diiodomethane and formamide were used for the calculation of free surface energy following Good and van Oss theory (Good and van Oss 1992). All samples were measured at least three times.

5.3.1.5 ATR-FTIR Analysis

Structural analysis of the treated films was carried out using ATR-FTIR Spectrum Two (Perkin Elmer, USA), scanning between wavelengths 4000 cm^{-1} and 400 cm^{-1}, with step 4 cm^{-1} and accumulation of 16 scans. All samples were measured in parallels, where the mean value is reported. All spectra were normalized and had the baseline subtracted.

5.3.2 Results and Discussion

Although literature suggests that nitrogen plasma only offers hydrophilic surface modifications of cellulose substrates and their nanosized counterparts or that it does not affect surface wettability at all (Kurniawan et al. 2012; Mortazavi, Ghoranneviss, and Sari 2011; Pertile et al. 2010; Vesel et al. 2008), we discovered that it can be used for hydrophobization of CNFs film surface. To determine the optimal treatment time, power, position of the sample inside the tube and flow, the parameters were scanned over a wide operating range. The main indicator of hydrophilicity/hydrophobicity of the sample surface is WCA, while the insight into structure is offered by ATR-FTIR.

Firstly, various treatment times from 5 s to 120 s were tested. The results are presented in Figure 5. It was observed that hydrophobic surface is reached in already 5 s of treating the surface of CNFs with nitrogen plasma, and it further increases up to 20 s, where WCA reaches 134°. Continuing with treatment, the WCA decreases (to minimum of 110° after continuous treatment for 120 s) but does not fall under the hydrophobic threshold (Figure 5a). However, at such conditions the surface of CNFs film becomes damaged showing in SEM micrographs in the form of smooth patches that are not present in the control sample (Figure 9).

ATR-FTIR spectrum of control sample (blue line in Figure 5b, as well as in Figure 6b, Figure 7b and Figure 8b), presents a characteristic spectrum of cellulose, featuring a broad peak between 3622 cm^{-1} and 3020 cm^{-1} corresponding to stretching of free (3337 cm^{-1}) and intermolecularly bonded (3282 cm^{-1}) hydroxyl groups, a weak broad peak centered at 2900 cm^{-1} correlated to C-H stretching vibrations and intermolecularly bonded hydroxyl groups, peaks located at 1657 cm^{-1} (O-H bending of adsorbed water), 1429 cm^{-1} (C-H_2 symmetric bending in crystalline region), 1361 cm^{-1} (tertiary C-H bending), 1315 cm^{-1} (symmetric CH_2 wagging), 1105 cm^{-1} (in-plane ring stretching), 1162 cm^{-1} (C-O-C asymmetric stretching vibration at β-glucosidic linkage) and two characteristic peaks for cellulose associated with C-O stretching at C3 and C-O asymmetric stretching deformation at C6 centered at 1055 cm^{-1} and 1030 cm^{-1}, respectively. Furthermore, in the fingerprint region, weak peaks located at 664 cm^{-1}, 558 cm^{-1} and 435 cm^{-1} that are related to C-O-H out-of-plane bending, C-H vibrational modes that are characteristic for cellulose I and C-O bonds vibrations, respectively (Cichosz, Masek, and Dems-Rudnicka 2022; Gulmine et al. 2002; Guo et al. 2018; Soliman, Díaz Baca, and Fatehi 2023).

Upon treatment with nitrogen-containing plasma, the majority of previously existing peaks became more pronounced. The broad peak between 3622 cm^{-1} and 3020 cm^{-1} narrowed and sharpened into one peak centered at 3304 cm^{-1} with a shoulder at 3197 cm^{-1}, which is the result of surface modification and decrease of surface hydroxyl groups in all nitrogen plasma-treated samples (Figures 4-7b). The peaks centered at 1603 cm^{-1} and 1581 cm^{-1} associated with N-H bending vibrations of primary amines become better defined with treatment time. A new peak centered at 1513 cm^{-1} associated with N-O stretching develops already in 10 s of the treatment and increases in intensity with longer treatment time. As this peak is visible in all morphologically unchanged samples, we believe it is one of the responsible for the initial change in surface wettability. However, after 15 s of treatment, with further increase of the WCA, another peak, corresponding to C-N stretching (centered at 1219 cm^{-1}), is formed. Also associated with C-N stretching vibrations, two peaks are formed between 1279 cm^{-1} and 1236 cm^{-1} and are overlapping with a peak assigned to C-O stretching (1262 cm^{-1}), that is present in the control sample. With longer treatment time, deformation and decrease of characteristic cellulose peaks at 1056 cm^{-1} and 1021 cm^{-1}, which is also slightly shifted, was observed, pointing to deeper structural changes in the cellulose chain.

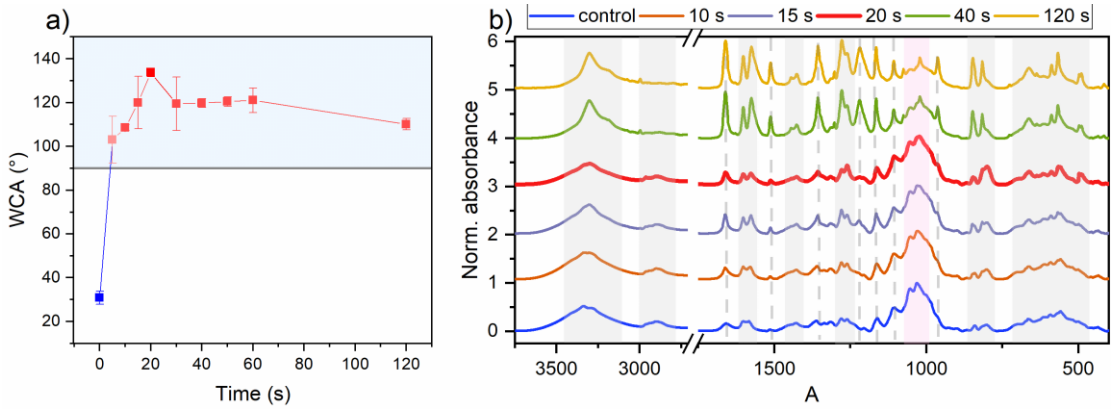

Figure 5: a) WCA of CNFs films after various treatment times, and b) the corresponding ATR-FTIR spectra of the selected samples.

WCA analysis of the samples treated with various operational powers revealed that hydrophobic effect can be reached at lower power (50W, 100W and 200 W), as shown in Figure 6a, while further increase of power yields in hydrophilic surface. It is worth noting that the samples treated at higher powers (300 W and 500 W) were visibly changed – previously whitish surface became yellow-brown, indicating surface destruction that was visible in SEM micrographs as well (Figure 9). ATR-FTIR analysis confirmed the trends observed in the analysis of the effect of treatment time – increased intensity and better resolution of majority of the peaks, formation of N-O stretching-related peak at 1512 cm^{-1}, and formation of C-N-related peaks at 1278 cm^{-1} and 1210 cm^{-1}. The main difference in prolonging the treatment and increasing power is observed at 1427 cm^{-1}, 1225 cm^{-1} and in the region between 1075 cm^{-1} and 951 cm^{-1} corresponding to vibrations of the cellulose ring. As opposed to time, increasing of power does not greatly modify C-O-C and C-O bonds in cellulose backbone, indicating that substitution on the ring does not occur to the same extent.

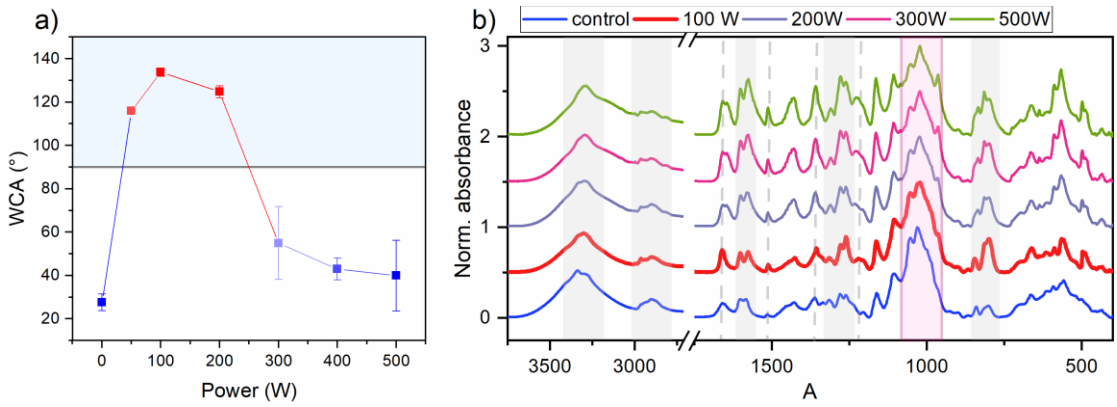

Figure 6: a) WCA of CNFs films after various treatment powers, and b) the corresponding ATR-FTIR spectra of the selected samples.

Hydrophobic behavior of the surface was reached regardless of the sample position inside the glass tube, however the placement 10 cm from the center of the coil in the afterglow was shown to be optimal, reaching WCA of 134°. Position before the glow resulted in damage of the surface that was visible with SEM (Figure 9). ATR-FTIR analysis further confirmed the formation of N-O- and C-N-related bonds, however deformation of the characteristic cellulose peak indicated disruption in C-O bonding pointing to substitution of O-H groups at C3 and C2 with nitrogen-related species. Additionally, it can be assumed that higher WCA is achieved when nitrogen is not attached directly to the cellulose chain.

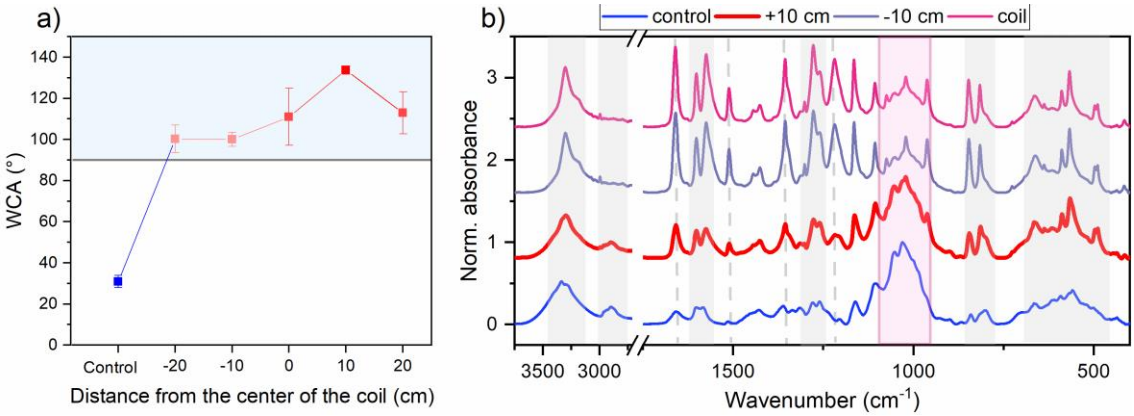

Figure 7: a) WCA of CNFs films after treatment at various positions inside the glass tube, and b) the corresponding ATR-FTIR spectra of the selected samples.

Lastly, treatment under various nitrogen flows was screened. Hydrophobic behavior of surface was obtained under flows in the range from 50 sccm to 400 sccm, with the highest WCA achieved at 100 sccm (Figure 8a), while the treatment under 500 sccm resulted in conversion back to hydrophilicity. ATR-FTIR spectra displays the same features as the analysis of the previous samples. To observe the switch between hydrophobic and hydrophilic surface, spectra of samples treated under 400 sccm and under 500 sccm are presented (Figure 8b). The main difference observed is the decrease of the cellulose characteristic peak at 1052 cm^{-1} and 1022 cm^{-1}, while other features remain the same. Higher ratio of C-N- or N-O-related peaks and peak associated with C-O-C stretching vibrations indicates higher degree of substitution. SEM inspection of the samples did not reveal any visible damage to the surface by increase of nitrogen flow (Figure 9).

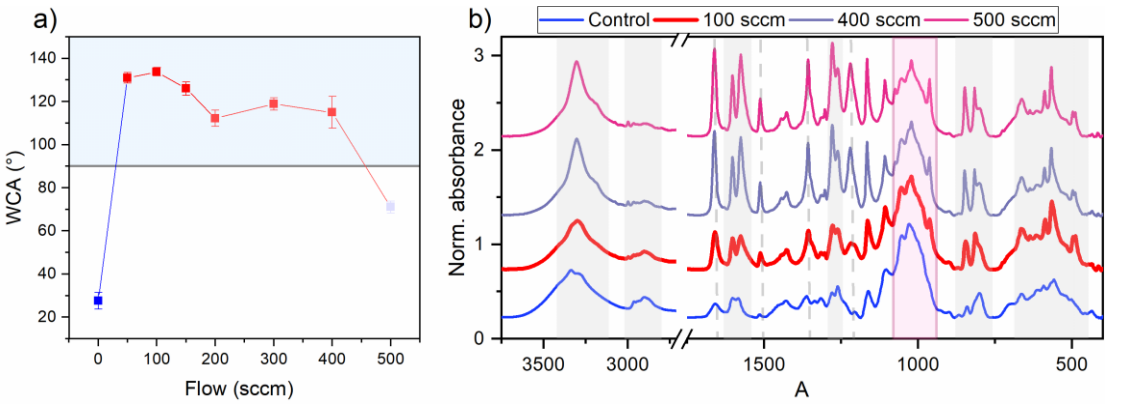

Figure 8: a) WCA of CNFs films after treatment under various nitrogen flows, and b) the corresponding ATR-FTIR spectra of the selected samples.

By screening various conditions (time, power, position of the sample in the glass tube and flow), optimal conditions for achieving the highest WCA were determined to be: 20 s, 100 W, 10 cm in the afterglow and 100 sccm achieving WCA of 134°. Inspection of such a sample under SEM did not indicate any surface damage (Figure 9), therefore it can be reasoned that the surface modification is purely chemical and hydrophobicity is the result of lowering of surface free energy. To confirm this, the surface free energy of the sample treated under optimal conditions was calculated through van Oss model (Good and van Oss 1992). Initial SFE of CNFs film is 37 mJ m^{-2} and decreases to 20 mJ m^{-2} upon plasma treatment. To gain an insight of surface interaction with liquids exhibiting low surface tension, contact angle with n-hexadecane was measured While the oleophilic effect was decreased – contact angle with n-hexadecane increased from initial 10 ± 2.7° to 31 ± 3.0°, the surface is not classified as oleophobic.

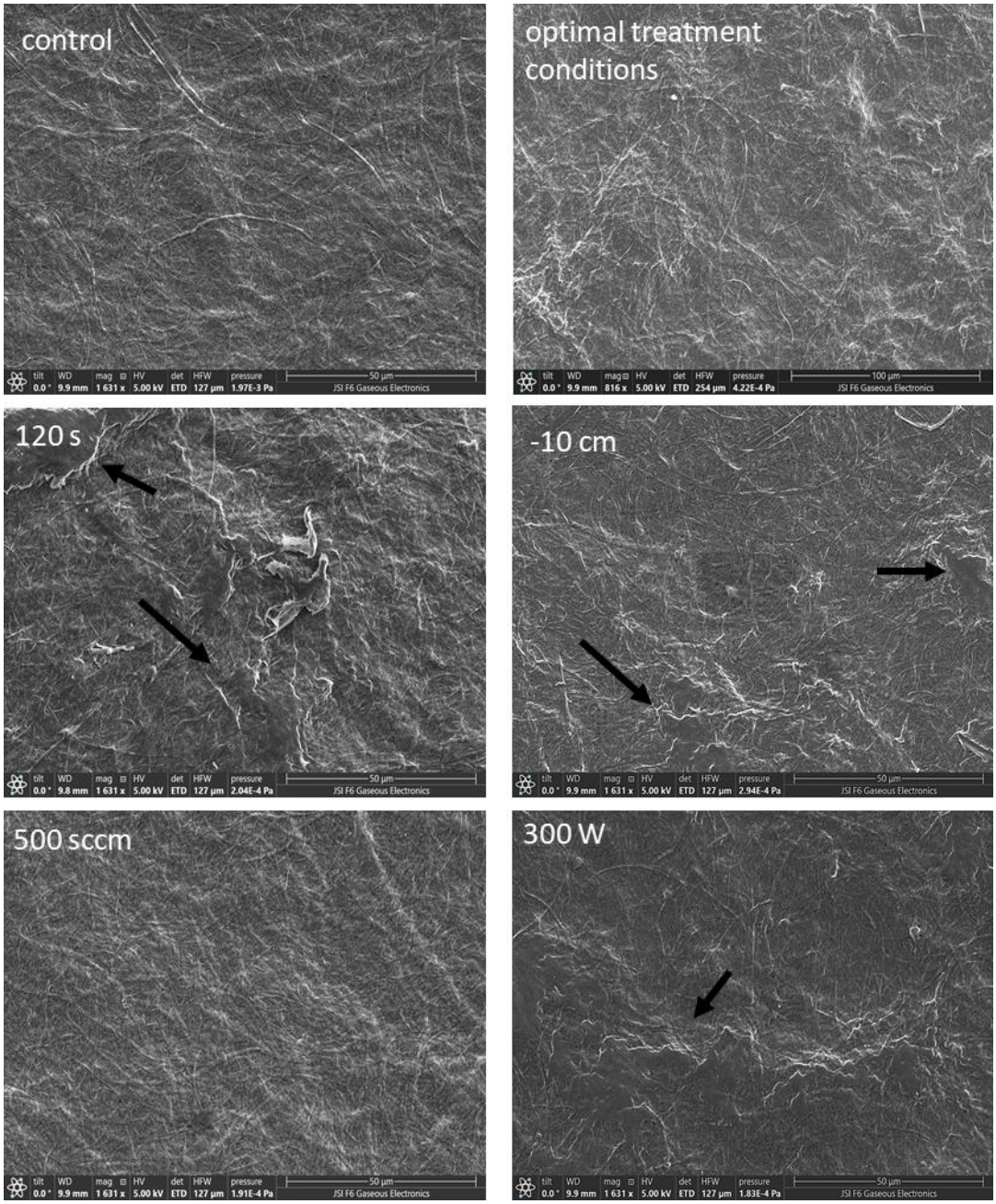

Figure 9: SEM micrographs of control sample, sample treated under optimal conditions (20 s, 100 W, 10 cm in the afterglow and 100 sccm) and selected samples that exhibit surface damage and decrease in WCA (120 s, 10 cm in the beforeglow (-10 cm), 500 sccm and 300 W).

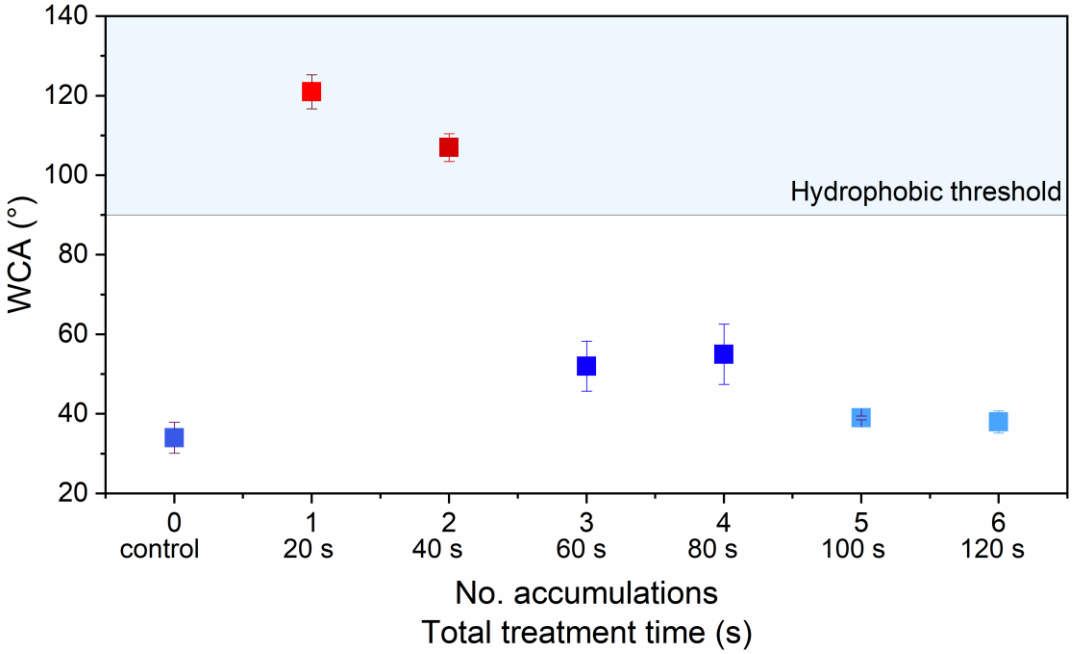

Figure 10: WCA in pulsating treatment regime.

Recovery of initially high wettability was investigated as well. Literature suggests that oxygen plasma enhances hydrophilic behavior of cellulosic materials (Kurniawan et al. 2012). To explore switching between hydrophilic/hydrophobic/hydrophilic surface, CNFs films were treated with plasma generated in oxygen at different powers. While treatments with power in the range from 100 W to 400 W did not alter surface wettability, power of 500 W treatment resulted in additional lowering of WCA (Figure 11a). As any higher power caused destruction of the sample visible with a naked eye, the power of 500 W was chosen for further experiments. The samples were first treated with nitrogen and then consequently with oxygen according to conditions specified in Table 2. While processing with nitrogen plasma increases WCA and decreases wettability of the sample, subsequent treatment with oxygen plasma decreases WCA to its initial value (Figure 11). These results demonstrate that by applying plasma generated in different gases, surface wettability can be tailored.

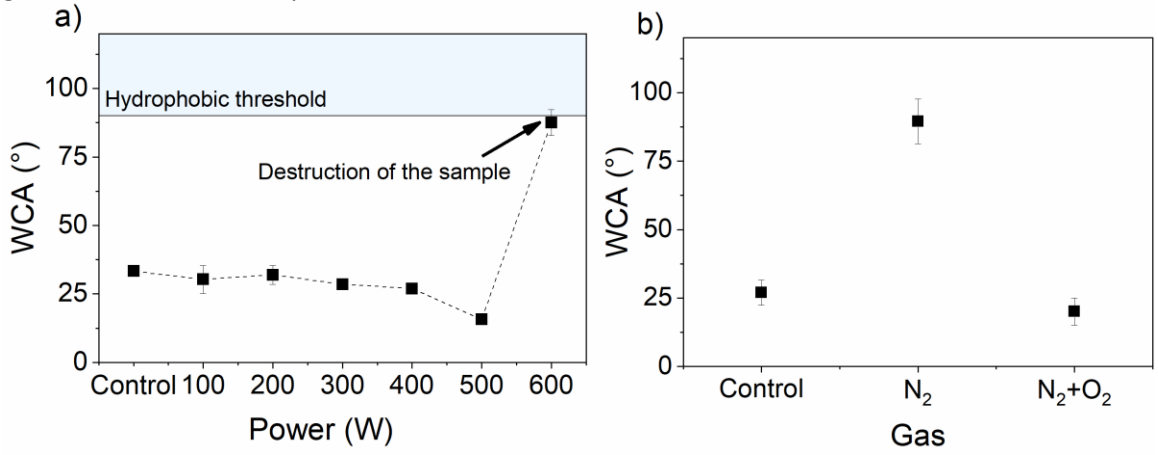

Figure 11: a) WCA of CNFs films after being treated with oxygen plasma at different powers, and b) hydrophilic-hydrophobic-hydrophilic switch by use of nitrogen and oxygen plasma.

Chapter 6

Conclusions and Outlook

Cellulose nanomaterials, found in two forms, CNCs and CNFs, exhibit high mechanical strength, biocompatibility and biodegradability that advances them to be an indispensable material of the future. Furthermore, originating from the most plentiful source on the planet, they are easily accessible, cheap and highly renewable. Yet, their hydrophilic character and this high interaction with water limits their potential in wider utilization. To address this, in the thesis, cellulose nanomaterials are explored as standalone biopolymer film or as a filler in bio-based composites films intended for flexible packaging, with emphasis on their hydrophobization reactions, mechanisms, kinetics and application as flexible films for e.g. packaging.

Firstly, various formulations of chitosan, alginate and cellulose nanomaterials as standalone films or as biocomposites were fabricated and evaluated from mechanical, barrier (water vapor and oxygen) and morphological point of view. It was shown that the most prospective combinations for packaging purposes are chitosan, alginate, chitosan with 3 wt. % of CNCs, alginate with 5 wt. % of CNCs, bacterial nanocellulose, and CNFs films, which would be suitable for packing of various ready-to-eat foods with short storage time. Alginate-based films exhibited the highest oxygen barrier, chitosan-based films with incorporated CNCs posed as the best barrier for water vapors and nanocellulose-based films exhibited the highest tensile strength. The latter were also the most sensitive to water, due to their hydrophilic nature. To minimize this drawback, various surface modifications can be carried out.

In the second objective, comprehensive review of literature published in the field of hydrophobic modifications indicated that the esterification, carbamation, silylation, polymers grafting (grafting to and grafting from approaches) and adsorption are commonly applied and relatively well researched, yet there is a lack of studies regarding kinetics and mechanisms of such reactions. Additionally, it was demonstrated that although plasma is a fast and efficient tool to hydrophobization, there is a lack of studies dealing with hydrophobization of nano-structured cellulose with plasma treatment.

Based on these findings, in the third objective, the dissertation explores mechanisms and kinetics of acetylation reaction through a joint computational-experimental study of acetylation of both CNCs and CNFs. Firstly, the cellulose nanomaterials were characterized in terms of morphology with SEM and TEM, crystallinity (XRD analysis) and accessibility of surface hydroxyl groups through ^{31}P NMR. After the reaction that was carried out with acetic anhydride in the presence of pyridine at various temperatures and reactants ratios to study the kinetics, the samples were characterized with ATR-FTIR, from which acetyl content was determined. Additionally, the successful modification and possible change in crystallinity was confirmed with solid-state NMR, while for the latter, XRD analysis was carried out as well. First principles revealed the mechanism of reaction, which occurs through two competitive steps: direct conversion to final product or through an active intermediate acetopyridinium. The proposed mechanism and calculated activation energies were used as a basis in the development of microkinetic model describing acetylation reaction of CNCs and CNFs that yielded true kinetic parameters, which is crucial information in the transfer to a larger scale.

Acetylated CNCs were then used as a reinforcing filler in biopolymer composites. Acetylated to various degrees, they were incorporated into chitosan and alginate matrix and studied with regards to structure (with ATR-FTIR), morphology, water contact angle, water vapor transmission rate and thermal stability. Furthermore, mechanical properties, namely tensile

strength and elongation at break, were studied in respect to environmental humidity. The results of the study indicate that acetylation of CNCs prior to incorporation to chitosan matrix improves their compatibility resulting in improved properties relevant for packaging applications: smooth surface, increase in mechanical properties, better thermal stability and lower water vapor permeability. On the other hand, for alginate-based biocomposites, acetylation pretreatment is not needed as pristine CNCs already provide homogeneous dispersion in alginate matrix. Regarding environmental humidity, it was observed that the mechanical strength of such materials is the highest upon the samples being dry, and while higher environmental humidity causes its decline, elongation at break increases.

To ensure that materials, which are newly introduced to broader commercial use, are in-line with green chemistry and circular economy principles, it is of uttermost importance to study their end-of-life. Although they originate from nature and are biodegradable in their natural ecosystem, it might not be the case with biocomposites and in other environments, such as communal wastewater treatment plants. With this in mind, biodegradability of chitosan and alginate-based films with or without incorporated pristine or acetylated CNCs was studied in activated sludge medium through respirometric test method. It was observed that chitosan-based films showed higher initial rate of degradation, however they did not fully degrade over the period of 120 hours. On the contrary, alginate-based films degraded over 107 hours (for neat alginate film) and 112 hours (alginate films with incorporated CNCs). In combination with *in situ* FTIR analysis, an insight into biodegradation mechanisms was gained. In films with alginate matrix, the first step of degradation was shown to be water loss and dissolution, while in chitosan-based films, the first step is deacetylation. These findings can help establish a better correlation between microbial consortia and physio-chemical parameters during the biodegradation process of such biocomposites, suitable alternatives to conventional plastic packaging. Yet, additional studies are necessary to fully comprehend this correlation, as the study carried out in the frame of this doctoral thesis still has limitations related to the controlled laboratory environment that may not accurately reflect the complexities of real-world wastewater treatment plants.

The second research direction was to explore plasma as a fast and efficient tool for surface hydrophobization of biopolymer films. By direct CF_4 plasma treatment, initially highly hydrophilic CNFs were converted to hydrophobic as fast as in 10 s, while optimal water-repellent properties were reached in 30 s with WCA 130 ± 5°. SEM analysis revealed notable nanoporosity upon processing, leading to improved surface tension between the substrate and water droplet. XPS analysis indicated gradual increase of fluorine content that is bound to the surface through C-F, C-F_2 and C-F_3 bonds. Occurrence of these species was further confirmed with spectroscopic techniques (ATR-FTIR and Raman), which have also shown the presence of surface-related F-H_3 band that increases with treatment time and deeper molecular changes affecting C-C, C-F_2 and cellulose ring that are detectable after 30 s of treatment. This research demonstrated that plasma processing provides ultrafast and highly-controllable surface hydrophobization of CNFs films.

To further expand and prove applicability of plasma processing for hydrophobization of biopolymer surface, chitosan/CNCs biocomposite films were fabricated and processed in CF_4 plasma. Such biocomposites exhibit relatively high WCA (85°), however their water barrier capacity is not sufficient. An improvement in water-related properties was achieved, making the material more suitable for packaging applications. After a short treatment of only 5 seconds, the water contact angle (WCA) increased by 28°. XPS analysis revealed newly formed fluorine-related bonds, while FTIR-ATR detected a decrease in C–H and C–O stretching and C–H bending. The surface of the material surface was not damaged by the treatment as confirmed with SEM. Plasma processing decreased the moisture content (MC) in the films, which influenced tensile strength and water vapor transmission. However, the modified sample still performed better than the reference sample in terms of packaging. The stability of the hydrophobic coating was demonstrated over 40 days, and there was no evidence of the presence of fluorinated compounds after immersion in three different liquid environments (water, 5% acetic acid, 10% ethanol) as analyzed by LC-MS. Although the TS and WVT decreased in both the treated and reference samples over time, the processed material still had an advantage to the non-processed one.

Finally, to avoid the use of fluorine (greenhouse gas), other gases were tested for hydrophobization of surface of CNFs films. Treatment with plasma generated in nitrogen was

shown to be efficient and is superior to fluorine- and silane-containing plasmas as well as other chemical modifications of the surface, as it is an inert gas and such treatment does not produce any liquid chemical discarge. Optimal treatment conditions were determined by systematic study of various treatment times, powers, nitrogen flows and position of the sample inside the chamber and were shown to be 20 s, 100 W, 100 sccm and 10 cm from the center of the coil, respectively, yielding WCA as high as 134°. Through ATR-FTIR analysis, structural changes following the increase in hydrophobicity were followed, indicating C-N bonds are responsible for this change. At harsher conditions (longer treatment time, higher power, higher flow, placement inside the coil), when the WCA decreased or the surface even switched back to hydrophilic, change in the cellulose backbone was visible, indicating modifications directly on the ring. As surface roughness also impacts WCA, the samples were inspected with SEM. In the micrographs, no change in surface morphology was visible on the sample treated at optimal conditions, while some damages were noted at samples treated for a longer time (120 s), at higher power (300 W and 500 W), higher flow (500 sccm) and placement before coil (10 cm in the beforeglow). Attempts were made to further increase the hydrophobicity by a pulsating regime of 20 s treatments with 20 s intermittent cooling, however the WCA dropped already after the first cycle. Finally, in combination with oxygen plasma, return of the surface to initial hydrophobicity was obtained, demonstrating that plasma processing enables switching from hydrophilic to hydrophobic and back to hydrophilic behavior.

In frame of EU Green Deal, more specifically the Chemicals Strategy for Sustainability, phasing out harmful substances and finding sustainable alternatives is crucial. However, while developing these alternatives, a safe and sustainable by design approach should be applied: substances that might be (eco)toxic and persistent in the environment should be avoided, the impact on the environmental footprint (climate change, resource use, ecosystems and biodiversity) of the final product from cradle-to-grave or cradle-to-cradle should be assessed prior to introduction to the wider market (Caldeira et al. 2022). With this in mind, to ensure safe and sustainable production and use of cellulose nanomaterials and their composites as a safe and sustainable by design packaging, the above-mentioned methodologies should be considered in further research expanding the work of this thesis. Detailed studies of kinetics and mechanisms of hydrophobic reactions carried out in aqueous medium, eliminating harmful solvents and their liquid waste, as well as reducing the cost of the process should be a starting point to consider when introducing new biomaterials. Many of these plastic-free material innovations shown in this doctoral thesis have been exemplified as a systems change driven towards wholesale shift to materials that are considerably less toxic than conventional plastic. Furthermore, biodegradability in real-world wastewater treatment plants, compost, marine environment and terrestrial environment as well as life cycle assessment of such materials, their composites and final products as well as hydrophobization processes should always be studied prior to commercial use in order to eliminate their potential negative effect on ecosystems. Many of these hydrophobized plastic-free biomaterials knowledge gaps explained and innovations presented will hopefully pave the way to reach the market applications and are successfully winning market share away from their petrochemical counterparts.

References

Abdelmouleh, M., S. Boufi, M. N. Belgacem, and A. Dufresne. 2007. "Short Natural-Fibre Reinforced Polyethylene and Natural Rubber Composites: Effect of Silane Coupling Agents and Fibres Loading." *Composites Science and Technology* 67(7):1627–39. doi: https://doi.org/10.1016/j.compscitech.2006.07.003.

Agulló, Enrique, María Susana Rodríguez, Viviana Ramos, and Liliana Albertengo. 2003. "Present and Future Role of Chitin and Chitosan in Food." *Macromolecular Bioscience* 3(10):521–30. doi: https://doi.org/10.1002/mabi.200300010.

Ahmadi, Mobina, Tayebeh Behzad, and Rouhallah Bagheri. 2017. "Reinforcement Effect of Poly (Methyl Methacrylate)-g-Cellulose Nanofibers on LDPE/Thermoplastic Starch Composites: Preparation and Characterization." *Iranian Polymer Journal* 26(10):733–42. doi: 10.1007/s13726-017-0558-5.

Alanis, Andrés, Josué Hernández Valdés, Neira Velázquez María Guadalupe, Ricardo Lopez, Ricardo Mendoza, Aji P. Mathew, Ramón Díaz De León, and Luis Valencia. 2019. "Plasma Surface-Modification of Cellulose Nanocrystals: A Green Alternative towards Mechanical Reinforcement of ABS." *RSC Advances* 9(30):17417–24. doi: 10.1039/c9ra02451d.

Anastas, Paul T., and John Charles Warner. 1998. *Green Chemistry: Theory and Practice*. Oxford University Press.

Aranaz, Inmaculada, Niuris Acosta, Concepción Civera, Begoña Elorza, Javier Mingo, Carolina Castro, María De los Llanos Gandía, and Angeles Heras Caballero. 2018. "Cosmetics and Cosmeceutical Applications of Chitin, Chitosan and Their Derivatives." *Polymers* 10(2). doi: 10.3390/polym10020213.

Aravamuthan, R. G. 2004. "PULPING | Chemical Pulping." Pp. 904–10 in *Encyclopedia of Forest Sciences*, edited by J. Burley. Oxford: Elsevier.

Aziz, Muhammad Arif, Mukarram Zubair, and Muhammad Saleem. 2021. "Development and Testing of Cellulose Nanocrystal-Based Concrete." *Case Studies in Construction Materials* 15:e00761. doi: 10.1016/j.cscm.2021.e00761.

Bajić, Marijan, Helena Jalšovec, Andrea Travan, Uroš Novak, and Blaž Likozar. 2019. "Chitosan-Based Films with Incorporated Supercritical CO2 Hop Extract: Structural, Physicochemical, and Antibacterial Properties." *Carbohydrate Polymers* 219(December 2018):261–68. doi: 10.1016/j.carbpol.2019.05.003.

Bajić, Marijan, Tina Ročnik, Ana Oberlintner, Francesca Scognamiglio, Uroš Novak, and Blaž Likozar. 2019. "Natural Plant Extracts as Active Components in Chitosan-Based Films: A Comparative Study." *Food Packaging and Shelf Life* 21:100365. doi: 10.1016/j.fpsl.2019.100365.

Balu, Balamurali, Victor Breedveld, and Dennis W. Hess. 2008. "Fabrication of 'Roll-off' and 'Sticky' Superhydrophobic Cellulose Surfaces via Plasma Processing." *Langmuir* 24(9):4785–90. doi: 10.1021/la703766c.

Biranje, Santosh Shivaji, Jianzhong Sun, Yifei Shi, Sujie Yu, Haixin Jiao, Meng Zhang, Qianqian Wang, Jin Wang, and Jun Liu. 2021. "Polysaccharide-Based Hemostats: Recent Developments, Challenges, and Future Perspectives." *Cellulose* 28(14):8899–8937. doi: 10.1007/s10570-021-04132-x.

Caldeira, Carla, Lucian R. Farcal, Irantzu Garmendia Aguirre, Lucia Mancini, Davide Tosches, Antonio Amelio, Kirsten Rasmussen, Hubert Rauscher, Juan Riego Sintes, and Serenella Sala. 2022. *Safe and Sustainable by Design Chemicals and Materials: Framework for the Definition of Criteria and Evaluation Procedure for Chemicals and Materials*. LU: Publications Office of the European Union. https://data.europa.eu/doi/10.2760/487955

Cao, Shujun, Gan Xu, Qiujing Li, Shukun Zhang, Yifan Yang, and Jingdi Chen. 2022. “Double Crosslinking Chitosan Sponge with Antibacterial and Hemostatic Properties for Accelerating Wound Repair.” *Composites Part B: Engineering* 234:109746. doi: https://doi.org/10.1016/j.compositesb.2022.109746.

Carlsson, C. M. Gilbert, and Goeran Stroem. 1991. “Reduction and Oxidation of Cellulose Surfaces by Means of Cold Plasma.” *Langmuir* 7(11):2492–97. doi: 10.1021/la00059a016.

Chu, P. K., J. Y. Chen, L. P. Wang, and N. Huang. 2002. “Plasma-Surface Modification of Biomaterials.” *Materials Science and Engineering: R: Reports* 36(5):143–206. doi: 10.1016/S0927-796X(02)00004-9.

Cichosz, Stefan, Anna Masek, and Katarzyna Dems-Rudnicka. 2022. “Original Study on Mathematical Models for Analysis of Cellulose Water Content from Absorbance/Wavenumber Shifts in ATR FT-IR Spectrum.” *Scientific Reports* 12(1):19739. doi: 10.1038/s41598-022-24097-6.

Costa, C., A. Conte, G. G. Buonocore, M. Lavorgna, and M. A. Del Nobile. 2012. “Calcium-Alginate Coating Loaded with Silver-Montmorillonite Nanoparticles to Prolong the Shelf-Life of Fresh-Cut Carrots.” *Food Research International* 48(1):164–69. doi: 10.1016/j.foodres.2012.03.001.

Cunha, Ana G., Carmen S. R. Freire, Armando J. D. Silvestre, Carlos Pascoal Neto, Alessandro Gandini, Elina Orblin, and Pedro Fardim. 2007. “Highly Hydrophobic Biopolymers Prepared by the Surface Pentafluorobenzoylation of Cellulose Substrates.” *Biomacromolecules* 8(4):1347–52. doi: 10.1021/bm0700136.

Deslandes, Y., G. Pleizier, E. Poiré, S. Sapieha, M. R. Wertheimer, and E. Sacher. 1998. “The Surface Modification of Pure Cellulose Paper Induced by Low-Pressure Nitrogen Plasma Treatment.” *Plasmas and Polymers* 3(2):61–76. doi: 10.1023/B:PAPO.0000005939.84830.44.

Draget, K. I. 2009. “Alginates.” Pp. 807–28 in *Handbook of Hydrocolloids (Second Edition)*, *Woodhead Publishing Series in Food Science, Technology and Nutrition*, edited by G. O. Phillips and P. A. Williams. Woodhead Publishing.

Dufresne, Alain. 2012. *Nanocellulose: From Nature to High Performance Tailored Materials*. De Gruyter.

Dufresne, Alain. 2019. “Nanocellulose Processing Properties and Potential Applications.” *Current Forestry Reports* 5(2):76–89. doi: 10.1007/s40725-019-00088-1.

Ensikat, Hans J., Petra Ditsche-Kuru, Christoph Neinhuis, and Wilhelm Barthlott. 2011. “Superhydrophobicity in Perfection: The Outstanding Properties of the Lotus Leaf.” *Beilstein Journal of Nanotechnology* 2:152–61. doi: 10.3762/bjnano.2.19.

Espino-Pérez, Etzael, Julien Bras, Giana Almeida, Cédric Plessis, Naceur Belgacem, Patrick Perré, and Sandra Domenek. 2018. “Designed Cellulose Nanocrystal Surface Properties for Improving Barrier Properties in Polylactide Nanocomposites.” *Carbohydrate Polymers* 183:267–77. doi: https://doi.org/10.1016/j.carbpol.2017.12.005.

Ferreira, Filipe V., Lucas P. Souza, Thais M. M. Martins, João H. Lopes, Bruno D. Mattos, Marcos Mariano, Ivanei F. Pinheiro, Thalita M. Valverde, Sébastien Livi, José A. Camilli, Alfredo M. Goes, Rubia F. Gouveia, Liliane M. F. Lona, and Orlando J. Rojas. 2019. “Nanocellulose/Bioactive Glass Cryogels as Scaffolds for Bone Regeneration.” *Nanoscale* 11(42):19842–49. doi: 10.1039/C9NR05383B.

Flynn, C. N., C. P. Byrne, and B. J. Meenan. 2013. “Surface Modification of Cellulose via Atmospheric Pressure Plasma Processing in Air and Ammonia–Nitrogen Gas.” *Surface and Coatings Technology* 233:108–18. doi: 10.1016/j.surfcoat.2013.04.007.

Foday Jr, Edward Hingha, Taiwo Sesay, Emmanuel Bartholomew Koroma, Anthony Amara Golia Seseh Kanneh, Ekeoma Bridget Chineche, Alpha Yayah Jalloh, and John Mambu Koroma. 2022. “Biotemplate Replication of Novel Mangifera Indica Leaf (MIL) for Atmospheric Water Harvesting: Intrinsic Surface Wettability and Collection Efficiency.” *Biomimetics* 7(4):147. doi: 10.3390/biomimetics7040147.

Gällstedt, Mikael, and Mikael S. Hedenqvist. 2002. “Oxygen and Water Barrier Properties of Coated Whey Protein and Chitosan Films.” *Journal of Polymers and the Environment* 10(1):1–4. doi: 10.1023/A:1021068304169.

Geyer, Roland, Jenna R. Jambeck, and Kara Lavender Law. 2017. “Production, Use, and Fate of All Plastics Ever Made.” *Science Advances* 3(7):e1700782. doi: 10.1126/sciadv.1700782.

Goh, Cheong Hian, Paul Wan Sia Heng, and Lai Wah Chan. 2012. “Alginates as a Useful Natural Polymer for Microencapsulation and Therapeutic Applications.” *Carbohydrate Polymers* 88(1):1–12. doi: https://doi.org/10.1016/j.carbpol.2011.11.012.

Good, Robert J., and Carel J. van Oss. 1992. “The Modern Theory of Contact Angles and the Hydrogen Bond Components of Surface Energies.” Pp. 1–27 in *Modern Approaches to Wettability*, edited by G. I. Loeb and M. E. Schrader. New York: Springer US.

Gulmine, J. V., P. R. Janissek, H. M. Heise, and L. Akcelrud. 2002. “Polyethylene Characterization by FTIR.” *Polymer Testing* 21(5):557–63. doi: 10.1016/S0142-9418(01)00124-6.

Guo, Xin, Liu Liu, Junjie Wu, Jia Fan, and Yiqiang Wu. 2018. “Qualitatively and Quantitatively Characterizing Water Adsorption of a Cellulose Nanofiber Film Using Micro-FTIR Spectroscopy.” *RSC Advances* 8(8):4214–20. doi: 10.1039/C7RA09894D.

Habibi, Youssef. 2014. “Key Advances in the Chemical Modification of Nanocelluloses.” *Chemical Society Reviews* 43(5):1519–42. doi: 10.1039/C3CS60204D.

Hay, Iain D., Zahid Ur Rehman, M. Fata Moradali, Yajie Wang, and Bernd H. A. Rehm. 2013. “Microbial Alginate Production, Modification and Its Applications.” *Microbial Biotechnology* 6(6):637–50. doi: https://doi.org/10.1111/1751-7915.12076.

Heimbuck, Abitha M., Tyler R. Priddy-Arrington, Madison L. Padgett, Claire B. Llamas, Haley H. Barnett, Bruce A. Bunnell, and Mary E. Caldorera-Moore. 2019. “Development of Responsive Chitosan–Genipin Hydrogels for the Treatment of Wounds.” *ACS Applied Bio Materials* 2(7):2879–88. doi: 10.1021/acsabm.9b00266.

Heinze, Thomas. 2016. “Cellulose: Structure and Properties.” Pp. 1–52 in *Cellulose Chemistry and Properties: Fibers, Nanocelluloses and Advanced Materials*, edited by O. J. Rojas. Cham: Springer International Publishing.

Hosseini, Seyede Mahtab, Majid Abdouss, Saeedeh Mazinani, Azim Soltanabadi, and Mohammadreza Kalaee. 2022. “Modified Nanofiber Containing Chitosan and Graphene Oxide-Magnetite Nanoparticles as Effective Materials for Smart Wound Dressing.” *Composites Part B: Engineering* 231:109557. doi: https://doi.org/10.1016/j.compositesb.2021.109557.

Hou, Weixin, and Qihua Wang. 2009. “Stable Polytetrafluoroethylene Superhydrophobic Surface with Lotus-Leaf Structure.” *Journal of Colloid and Interface Science* 333(1):400–403. doi: 10.1016/j.jcis.2009.01.027.

Hu, Chuhuan, Wei Lu, Analucia Mata, Katsuyoshi Nishinari, and Yapeng Fang. 2021. “Ions-Induced Gelation of Alginate: Mechanisms and Applications.” *International Journal of Biological Macromolecules* 177:578–88. doi: https://doi.org/10.1016/j.ijbiomac.2021.02.086.

International Organization for Standardization. 2017. “Standard Terms and Their Definition for Cellulose Nanomaterial - ISO Standard No. 20477:2017(En).”

Inukai, Shunya, Naruki Kurokawa, and Atsushi Hotta. 2020. “Mechanical Properties of Poly(ε-Caprolactone) Composites with Electrospun Cellulose Nanofibers Surface Modified by 3-Aminopropyltriethoxysilane.” *Journal of Applied Polymer Science* 137(17):48599. doi: https://doi.org/10.1002/app.48599.

Jamaluddin, Naharullah, Tomonari Kanno, Taka-Aki Asoh, and Hiroshi Uyama. 2019. “Surface Modification of Cellulose Nanofiber Using Acid Anhydride for Poly(Lactic Acid) Reinforcement.” *Materials Today Communications* 21:100587. doi: 10.1016/j.mtcomm.2019.100587.

Jele, Thabisile Brightwell, Prabashni Lekha, and Bruce Sithole. 2022. “Role of Cellulose Nanofibrils in Improving the Strength Properties of Paper: A Review.” *Cellulose* 29(1):55–81. doi: 10.1007/s10570-021-04294-8.

Ji, Maocheng, Jianyong Li, Yi Wang, Fangyi Li, Jia Man, Jianfeng Li, Chuanwei Zhang, Sixian Peng, and Shiqing Wang. 2022. “Advances in Chitosan-Based Wound Dressings: Modifications, Fabrications, Applications and Prospects.” *Carbohydrate Polymers* 297:120058. doi: https://doi.org/10.1016/j.carbpol.2022.120058.

Jiang, Lei, Yong Zhao, and Jin Zhai. 2004. “A Lotus-Leaf-like Superhydrophobic Surface: A Porous Microsphere/Nanofiber Composite Film Prepared by Electrohydrodynamics.” *Angewandte Chemie - International Edition* 43(33):4338–41. doi: 10.1002/anie.200460333.

Jiang, Tianjia. 2013. “Effect of Alginate Coating on Physicochemical and Sensory Qualities of Button Mushrooms (Agaricus Bisporus) under a High Oxygen Modified Atmosphere.” *Postharvest Biology and Technology* 76:91–97. doi: 10.1016/j.postharvbio.2012.09.005.

Jiang, Yao, Chuhan Fu, Sihui Wu, Guihua Liu, Jiao Guo, and Zhengquan Su. 2017. “Determination of the Deacetylation Degree of Chitooligosaccharides.” *Marine Drugs* 15(11). doi: 10.3390/md15110332.

Kalantari, Katayoon, Amalina M. Afifi, Hossein Jahangirian, and Thomas J. Webster. 2019. “Biomedical Applications of Chitosan Electrospun Nanofibers as a Green Polymer – Review.” *Carbohydrate Polymers* 207:588–600. doi: https://doi.org/10.1016/j.carbpol.2018.12.011.

Kalaycıoğlu, Zeynep, Emrah Torlak, Gülşen Akın-Evingür, İlhan Özen, and F. Bedia Erim. 2017. “Antimicrobial and Physical Properties of Chitosan Films Incorporated with Turmeric Extract.” *International Journal of Biological Macromolecules* 101:882–88. doi: 10.1016/j.ijbiomac.2017.03.174.

Kargarzadeh, Hanieh, Marcos Mariano, Deepu Gopakumar, Ishak Ahmad, Sabu Thomas, Alain Dufresne, Jin Huang, and Ning Lin. 2018. *Advances in Cellulose Nanomaterials*. Vol. 25. Springer Netherlands.

Kawano, Tessei, Meng-Jiy Wang, and Yoshito Andou. 2022. “Surface Modification of a Regenerated Cellulose Film Using Low-Pressure Plasma Treatment with Various Reactive Gases.” *ACS Omega* 7(48):44085–92. doi: 10.1021/acsomega.2c05499.

Khakalo, Alexey, Tapio Mäkelä, Leena-Sisko Johansson, Hannes Orelma, and Tekla Tammelin. 2020. “High-Throughput Tailoring of Nanocellulose Films: From Complex Bio-Based Materials to Defined Multifunctional Architectures.” *ACS Applied Bio Materials* 3(11):7428–38. doi: 10.1021/acsabm.0c00576.

Khan, Ruhul A., Stephanie Beck, Dominic Dussault, Stephane Salmieri, Jean Bouchard, and Monique Lacroix. 2013. “Mechanical and Barrier Properties of Nanocrystalline Cellulose Reinforced Poly(Caprolactone) Composites: Effect of Gamma Radiation.” *Journal of Applied Polymer Science* 129(5):3038–46. doi: https://doi.org/10.1002/app.38896.

Kim, Dabum, Youngsang Ko, Goomin Kwon, Ung-Jin Kim, and Jungmok You. 2018. “Micropatterning Silver Nanowire Networks on Cellulose Nanopaper for Transparent Paper Electronics.” *ACS Applied Materials & Interfaces* 10(44):38517–25. doi: 10.1021/acsami.8b15230.

Kim, Tae-Young, Bialuch Ingmar, Klaus Bewilogua, Kyu Hwan Oh, and Kwang-Ryeol Lee. 2007. “Wetting Behaviours of A-C:H:Si:O Film Coated Nano-Scale Dual Rough Surface.” *Chemical Physics Letters* 436(1):199–203. doi: 10.1016/j.cplett.2007.01.036.

Kontominas, Michael G. 2020. “Use of Alginates as Food Packaging Materials.” *Foods* 9(10):1440. doi: 10.3390/foods9101440.

Kurniawan, Hengky, Jinn-Tsyy Lai, and Meng-Jiy Wang. 2012. “Biofunctionalized Bacterial Cellulose Membranes by Cold Plasmas.” *Cellulose* 19(6):1975–88. doi: 10.1007/s10570-012-9785-2.

Kutová, Anna, Lubica Staňková, Kristýna Vejvodová, Ondřej Kvítek, Barbora Vokatá, Dominik Fajstavr, Zdeňka Kolská, Antonín Brož, Lucie Bačáková, and Václav Švorčík. 2021. “Influence of Drying Method and Argon Plasma Modification of Bacterial Nanocellulose on Keratinocyte Adhesion and Growth.” *Nanomaterials* 11(8):1916. doi: 10.3390/nano11081916.

Leal, Salomé, Cecília Cristelo, Sara Silvestre, Elvira Fortunato, Aureliana Sousa, Anabela Alves, D. M. Correia, S. Lanceros-Mendez, and Miguel Gama. 2020. “Hydrophobic Modification of Bacterial Cellulose Using Oxygen Plasma Treatment and Chemical Vapor Deposition.” *Cellulose* 27(18):10733–46. doi: 10.1007/s10570-020-03005-z.

Lee, Kuen Yong, and David J. Mooney. 2012. “Alginate: Properties and Biomedical Applications.” *Progress in Polymer Science* 37(1):106–26. doi: https://doi.org/10.1016/j.progpolymsci.2011.06.003.

Lepore, Emiliano, and Nicola Pugno. 2011. “Superhydrophobic Polystyrene by Direct Copy of a Lotus Leaf.” *BioNanoScience* 1(4):136–43. doi: 10.1007/s12668-011-0017-2.

Lin, Ning, Jin Huang, Peter R. Chang, Jiwen Feng, and Jiahui Yu. 2011. “Surface Acetylation of Cellulose Nanocrystal and Its Reinforcing Function in Poly(Lactic Acid).” *Carbohydrate Polymers* 83(4):1834–42. doi: 10.1016/j.carbpol.2010.10.047.

Maftoonazad, Neda, Hosahalli S. Ramaswamy, and Michelle Marcotte. 2008. “Shelf-Life Extension of Peaches through Sodium Alginate and Methyl Cellulose Edible Coatings.” *International Journal of Food Science & Technology* 43(6):951–57. doi: 10.1111/j.1365-2621.2006.01444.x.

Matouk, Zineb, Rocío Rincón, Badr Torriss, Amir Mirzaei, Joëlle Margot, Annie Dorris, Stephanie Beck, Richard M. Berry, and Mohamed Chaker. 2021. “Functionalization of Cellulose Nanocrystal Powder by Non-Thermal Atmospheric-Pressure Plasmas.” *Cellulose* 28(10):6239–52. doi: 10.1007/s10570-021-03927-2.

Matouk, Zineb, Badr Torriss, Rocio Rincón, Annie Dorris, Stephanie Beck, Richard M. Berry, and Mohamed Chaker. 2020. “Functionalization of Cellulose Nanocrystal Films Using Non-Thermal Atmospheric –Pressure Plasmas.” *Applied Surface Science* 511:145566. doi: 10.1016/j.apsusc.2020.145566.

Mortazavi, S. Hamideh, Mahmood Ghoranneviss, and A. H. Sari. 2011. “Low Pressure Hexamethyldisiloxane (HMDSO)/Nitrogen Plasma Treatment on the Wettability and Surface Free Energy of Biaxial-Oriented Polypropylene (BOPP) Films.” *Journal of Fusion Energy* 30(1):83–88. doi: 10.1007/s10894-010-9336-5.

Murthy, Aditya, Punna Rao Ravi, Himanshu Kathuria, and Rahul Vats. 2020. “Self-Assembled Lecithin-Chitosan Nanoparticles Improve the Oral Bioavailability and Alter the Pharmacokinetics of Raloxifene.” *International Journal of Pharmaceutics* 588:119731. doi: https://doi.org/10.1016/j.ijpharm.2020.119731.

Nechyporchuk, Oleksandr, Mohamed Naceur Belgacem, and Julien Bras. 2016. “Production of Cellulose Nanofibrils: A Review of Recent Advances.” *Industrial Crops and Products* 93:2–25. doi: https://doi.org/10.1016/j.indcrop.2016.02.016.

Oberlintner, Ana, Marijan Bajić, Gabriela Kalčikova, Blaž Likozar, and Uroš Novak. 2020. “Biodegradability Study of Active Chitosan Biopolymer Films Enriched with Quercus Polyphenol Extract in Different Soil Types.” *Environmental Technology & Innovation*. doi: https://doi.org/10.1016/j.eti.2020.101318.

Oladzadabbasabadi, Nazila, Abdorreza Mohammadi Nafchi, Fazilah Ariffin, M. M. Jeevani Osadee Wijekoon, A. A. Al-Hassan, Mohammed Ali Dheyab, and Mehran Ghasemlou. 2022. “Recent Advances in Extraction, Modification, and Application of Chitosan in Packaging Industry.” *Carbohydrate Polymers* 277:118876. doi: https://doi.org/10.1016/j.carbpol.2021.118876.

Oyekanmi, Adeleke A., N. I. Saharudin, Che Mohamad Hazwan, Abdul Khalil H. P. S., Niyi G. Olaiya, Che K. Abdullah, Tata Alfatah, Deepu A. Gopakumar, and Daniel Pasquini. 2021. “Improved Hydrophobicity of Macroalgae Biopolymer Film Incorporated with Kenaf Derived CNF Using Silane Coupling Agent.” *Molecules* 26(8):2254. doi: 10.3390/molecules26082254.

Pawar, Siddhesh N., and Kevin J. Edgar. 2012. “Alginate Derivatization: A Review of Chemistry, Properties and Applications.” *Biomaterials* 33(11):3279–3305. doi: https://doi.org/10.1016/j.biomaterials.2012.01.007.

Pei, Ying, Lu Wang, Keyong Tang, and David L. Kaplan. 2021. “Biopolymer Nanoscale Assemblies as Building Blocks for New Materials: A Review.” *Advanced Functional Materials* 31(15):2008552. doi: https://doi.org/10.1002/adfm.202008552.

Pereira, Pedro Miguel Matos, Ana Sofia Moita, Gabriel Amaro Monteiro, and Duarte Miguel França Prazeres. 2014. “Characterization of the Topography and Wettability of English Weed Leaves and Biomimetic Replicas.” *Journal of Bionic Engineering* 11(3):346–59. doi: 10.1016/S1672-6529(14)60048-2.

Pertile, Renata A. N., Fábia K. Andrade, Clodomiro Alves, and Miguel Gama. 2010. “Surface Modification of Bacterial Cellulose by Nitrogen-Containing Plasma for Improved Interaction with Cells.” *Carbohydrate Polymers* 82(3):692–98. doi: 10.1016/j.carbpol.2010.05.037.

Raeisi, Mojtaba, Alijan Tabaraei, Mohammad Hashemi, and Nasser Behnampour. 2016. “Effect of Sodium Alginate Coating Incorporated with Nisin, Cinnamomum Zeylanicum, and Rosemary Essential Oils on Microbial Quality of Chicken Meat and Fate of Listeria Monocytogenes during Refrigeration.” *International Journal of Food Microbiology* 238:139–45. doi: 10.1016/j.ijfoodmicro.2016.08.042.

Raghavendran, Vijayendran, Emmanuel Asare, and Ipsita Roy. 2020. “Bacterial Cellulose: Biosynthesis, Production, and Applications.” Pp. 89–138 in *Advances in Microbial Physiology*. Vol. 77. Academic Press.

Riseh, Roohallah Saberi, Mohadeseh Hassanisaadi, Masoumeh Vatankhah, Somayeh Abdani Babaki, and Essaid Ait Barka. 2022. “Chitosan as a Potential Natural Compound to Manage Plant Diseases.” *International Journal of Biological Macromolecules* 220:998–1009. doi: https://doi.org/10.1016/j.ijbiomac.2022.08.109.

Saedi, Shahab, Coralia V. Garcia, Jun Tae Kim, and Gye Hwa Shin. 2021. “Physical and Chemical Modifications of Cellulose Fibers for Food Packaging Applications.” *Cellulose* 28(14):8877–97. doi: 10.1007/s10570-021-04086-0.

Samanta, Kartick Kumar, Amish G. Joshi, Manjeet Jassal, and Ashwini K. Agrawal. 2021. “Hydrophobic Functionalization of Cellulosic Substrate by Tetrafluoroethane Dielectric Barrier Discharge Plasma at Atmospheric Pressure.” *Carbohydrate Polymers* 253:117272. doi: https://doi.org/10.1016/j.carbpol.2020.117272.

Shojaeiarani, Jamileh, Dilpreet S. Bajwa, and Saptaparni Chanda. 2021. “Cellulose Nanocrystal Based Composites: A Review.” *Composites Part C: Open Access* 5:100164. doi: https://doi.org/10.1016/j.jcomc.2021.100164.

Silva, Barbara Estefania de Almeida, Aparecido Junior de Menezes, Adriana Oliveira Delgado, Nilson Cristino Cruz, and Elidiane Cipriano Rangel. 2016. “Modification of the Wettability of Nanocellulose Films by SF6 Plasma Treatment.” Brazil.

Soliman, Ahmed I. A., Jonathan A. Díaz Baca, and Pedram Fatehi. 2023. “One-Pot Synthesis of Magnetic Cellulose Nanocrystal and Its Post-Functionalization for Doxycycline Adsorption.” *Carbohydrate Polymers* 308:120619. doi: 10.1016/j.carbpol.2023.120619.

Song, E. H., J. Shang, and D. M. Ratner. 2012. “Polysaccharides.” Pp. 137–55 in *Polymer Science: A Comprehensive Reference*, edited by K. Matyjaszewski and M. Möller. Amsterdam: Elsevier.

Šturcová, Adriana, Geoffrey R. Davies, and Stephen J. Eichhorn. 2005. “Elastic Modulus and Stress-Transfer Properties of Tunicate Cellulose Whiskers.” *Biomacromolecules* 6(2):1055–61. doi: 10.1021/bm049291k.

Surya, Indra, C. M. Hazwan, H. P. S. Abdul Khalil, Esam Bashir Yahya, A. B. Suriani, Mohammed Danish, and Azmi Mohamed. 2022. “Hydrophobicity and Biodegradability of Silane-Treated Nanocellulose in Biopolymer for High-Grade Packaging Applications.” *Polymers* 14(19):4147. doi: 10.3390/polym14194147.

Talón, Emma, Kata T. Trifkovic, Viktor A. Nedovic, Branko M. Bugarski, María Vargas, Amparo Chiralt, and Chelo González-Martínez. 2017. “Antioxidant Edible Films Based on Chitosan and Starch Containing Polyphenols from Thyme Extracts.” *Carbohydrate Polymers* 157:1153–61. doi: 10.1016/j.carbpol.2016.10.080.

Tangpasuthadol, Varawut, Noppong Pongchaisirikul, and Vipavee P. Hoven. 2003. “Surface Modification of Chitosan Films.: Effects of Hydrophobicity on Protein Adsorption.” *Carbohydrate Research* 338(9):937–42. doi: 10.1016/S0008-6215(03)00038-7.

Vanderfleet, Oriana M., and Emily D. Cranston. 2021. “Production Routes to Tailor the Performance of Cellulose Nanocrystals.” *Nature Reviews Materials* 6(2):124–44. doi: 10.1038/s41578-020-00239-y.

Vaswani, Sudeep, Jere Koskinen, and Dennis W. Hess. 2005. “Surface Modification of Paper and Cellulose by Plasma-Assisted Deposition of Fluorocarbon Films.” *Surface and Coatings Technology* 195(2):121–29. doi: 10.1016/j.surfcoat.2004.10.013.

Verma, Madan L., Sandeep Kumar, Anamika Das, Jatinder S. Randhawa, and Munusamy Chamundeeswari. 2020. “Chitin and Chitosan-Based Support Materials for Enzyme Immobilization and Biotechnological Applications.” *Environmental Chemistry Letters* 18(2):315–23. doi: 10.1007/s10311-019-00942-5.

Vesel, Alenka, Ita Junkar, Uros Cvelbar, Janez Kovac, and Miran Mozetic. 2008. “Surface Modification of Polyester by Oxygen- and Nitrogen-Plasma Treatment.” *Surface and Interface Analysis* 40(11):1444–53. doi: 10.1002/sia.2923.

Vicente, Filipa A., Sonia P. M. Ventura, Helena Passos, Ana C. R. V. Dias, Mario A. Torres-Acosta, Uroš Novak, and Blaž Likozar. 2022. “Crustacean Waste Biorefinery as a Sustainable Cost-Effective Business Model.” *Chemical Engineering Journal* 442:135937. doi: https://doi.org/10.1016/j.cej.2022.135937.

Wang, Hongxia, Jun Qian, and Fuyuan Ding. 2018. “Emerging Chitosan-Based Films for Food Packaging Applications.” *Journal of Agricultural and Food Chemistry* 66(2):395–413. doi: 10.1021/acs.jafc.7b04528.

Wang, Xudong, Chunhua Yao, Fei Wang, and Zhaodong Li. 2017. “Cellulose-Based Nanomaterials for Energy Applications.” *Small* 13(42):1702240. doi: https://doi.org/10.1002/smll.201702240.

Wei, Han, Yan Yingting, Gu Jingjing, Yi Wenshi, and Tang Junhong. 2017. “Lignocellulosic Biomass Valorization: Production of Ethanol.” Pp. 601–4 in *Encyclopedia of Sustainable Technologies*. Elsevier.

Yuan, Xueming, and Gang Cheng. 2015. “From Cellulose Fibrils to Single Chains: Understanding Cellulose Dissolution in Ionic Liquids.” *Phys. Chem. Chem. Phys.* 17(47):31592–607. doi: 10.1039/C5CP05744B.

Zhang, Min, Mao Yang, Meng Wai Woo, Yanchun Li, Wenjia Han, and Xugang Dang. 2021. “High-Mechanical Strength Carboxymethyl Chitosan-Based Hydrogel Film for Antibacterial Wound Dressing.” *Carbohydrate Polymers* 256:117590. doi: https://doi.org/10.1016/j.carbpol.2020.117590.

Zheng, R., J. Arora, B. Boonkaew, S. R. Raghavan, D. L. Kaplan, J. He, N. S. Pesika, and V. T. John. 2014. “Liposomes Tethered to a Biopolymer Film through the Hydrophobic Effect Create a Highly Effective Lubricating Surface.” *Soft Matter* 10(46):9226–29. doi: 10.1039/C4SM01692K.

Zhu, Y., J. Zhang, Y. Zheng, Z. Huang, L. Feng, and L. Jiang. 2006. “Stable, Superhydrophobic, and Conductive Polyaniline/Polystyrene Films for Corrosive Environments.” *Advanced Functional Materials* 16(4):568–74. doi: 10.1002/adfm.200500624.

Zugenmeier, Peter. 2021. “Order in Cellulosics: Historical Review of Crystal Structure Research on Cellulose.” *Carbohydrate Polymers* 254:117417. doi: https://doi.org/10.1016/j.carbpol.2020.117417.

Bibliography

Publications Related to the Thesis

Journal Articles

Lavrič, G., Oberlintner, A., Filipova, I., Novak, U., Likozar, B, & Vrabič-Brodnjak, U. (2021). Functional Nanocellulose, Alginate and Chitosan Nanocomposites Designed as Active Film Packaging Materials. *Polymers,* 13(15), 2523. doi: 10.3390/polym13152523.

Oberlintner, A., Likozar, B., & Novak, U. (2021). Hydrophobic Functionalization Reactions of Structured Cellulose Nanomaterials: Mechanisms, Kinetics and in Silico Multi-Scale Models. *Carbohydrate Polymers,* 259, 117742. doi: 10.1016/j.carbpol.2021.117742.

Oberlintner, A., Huš, M., Likozar, B., & Novak, U. (2022). Multiscale Study of Functional Acetylation of Cellulose Nanomaterials by Design: Ab Initio Mechanisms and Chemical Reaction Microkinetics. *ACS Sustainable Chemistry & Engineering*, 10(47), 15480–89. doi: 10.1021/acssuschemeng.2c04686.

Oberlintner, A., Likozar, B., & Novak, U. (2023). Effect of Environment on Acetylated Cellulose Nanocrystal-Reinforced Biopolymers Films. *Polymers,* 15, 1663. doi: 0.3390/polym15071663

Vidmar, B.[#], Oberlintner, A.[#], Likozar, B., Novak, U. (2023). Biodegradation of Polysaccharide-based Biocomposites with Acetylated Cellulose Nanocrystals, Alginate and Chitosan in Aqueous Environment. Submitted to *International Journal of Biological Macromolecules* (Under review)

(# equal contribution)

Oberlintner, A., Shvalya, V., Vasudevan, A., Vengust, D., Likozar, B., Cvelbar, U. & Novak, U. (2022). Hydrophilic to Hydrophobic: Ultrafast Conversion of Cellulose Nanofibrils by Cold Plasma Fluorination. *Applied Surface Science,* 581, 152276. doi: 10.1016/j.apsusc.2021.152276.

Oberlintner, A., Vesel, A., Naumoska, K., Likozar, B. & Novak, U. (2022). Permanent Hydrophobic Coating of Chitosan/Cellulose Nanocrystals Composite Film by Cold Plasma Processing. *Applied Surface Science,* 597, 153562. doi: 10.1016/j.apsusc.2022.153562.

Conference Paper

Oberlintner, A., Vesel, A., Likozar, B., Novak, U. (2021) Radio frequency plasma in CF4 as a fast and efficient tool for obtaining and retaining a long-term hydrophobicity of cellulose nanocrystals-reinforced chitosan films. In Proceedings of the 2nd International Conference on Circular Packaging. Slovenj Gradec, Slovenia and online: Pulp and Paper Institute; Faculty of Polymer Technology.

Other Publications

Isailović, J., Oberlintner, A., Novak, U., Finšgar, M., Oliviera, F. M., Paštika, J., Zdeněk S., Tasić, N., Gusmão, R., Hočevar, S. (2023). Study of Chitosan-Stabilized $Ti_3C_2T_x$ MXene for Ultrasensitive and Interference-Free Detection of Gaseous H_2O_2. ACS Applied Materials & Interfaces. doi: 10.1021/acsami.3c05314.

Naumoska, K., Jug, U., Kõrge, K., Oberlintner, A., Golob, M., Novak, U., Vovk, I., Likozar, B., (2022). Antioxidant and antimicrobial biofoil based on chitosan and Japanese knotweed (Fallopia japonica, Houtt.) : rhizome bark extract. Antioxidants, 11(6), 1-22. doi: 10.3390/antiox11061200

Olugbemide, A.D., Likozar, B., Oberlintner, A., Novak, U., Ekebafe, L. (2022). Reaction kinetics modelling for dry anaerobic digestion of hura crepitans invasive species lignocellulosic biomass. Chemical papers, 76(10), 6263–6269. doi: 10.1007/s11696-022-02312-y

Oberlintner, A., Bajić, M., Kalčíková, G., Likozar, B., Novak, U. (2021). Biodegradability study of active chitosan biopolymer films enriched with Quercus polyphenol extract in different soil types. Environmental technology & innovation. 21, 101318-1-101318-12. doi: 10.1016/j.eti.2020.101318

Olugbemide, A. D.[#], Oberlintner, A.[#], Novak, U., Likozar, B. (2021). Lignocellulosic corn stover biomass pre-treatment by Deep Eutectic Solvents (DES) for Biomethane production process by bioresource anaerobic digestion. Sustainability, 13(19), 1-13. doi: 10.3390/su131910504

(# equal contribution)

Bajić, M., Oberlintner, A., Kõrge, K., Likozar, B., Novak, U. (2020). Formulation of active food packaging by design: linking composition of the film-forming solution to properties of the chitosan-based film by response surface methodology (RSM) modelling. International journal of biological macromolecules, 160, 971-978. doi: 10.1016/j.ijbiomac.2020.05.186

Novak, U., Bajić, M., Kõrge, K., Oberlintner, A., Murn, J., Lokar, K., Triler, K. V., Likozar, B. (2020). From waste/residual marine biomass to active biopolymer-based packaging film materials for food industry applications: a review. Physical sciences reviews, 5(3), 20190099-1-20190099-24. doi: 10.1515/psr-2019-0099

Bajić, M., Ročnik, T., Oberlintner, A., Scognamiglio, F., Novak, U., Likozar, B. (2019). Natural plant extracts as active components in chitosan-based films: a comparative study. Food packaging and shelf life, 21, 100365-1-100365-8. doi: 10.1016/j.fpsl.2019.100365

Biography

The author of this thesis graduated from Chemical Engineering in 2019 at the Faculty of Chemistry and Chemical Technology, University of Ljubljana. She finished her Master studies with the thesis titled “Degradation of chitosan-based bioplastics in terrestrial environment” that was awarded The Prešeren Award for Students of Faculty of Chemistry and Chemical Technology. Since 2019, she has been a Young Researcher at the Department of Catalysis and Chemical Reaction Engineering. In her research, she is focusing on cellulose nanomaterials, their characterization, hydrophobic modifications and their incorporation into biocomposites. Her work also includes characterization of such biocomposites in terms of morphology, properties relevant for packaging applications, such as mechanical and barrier, and biodegradability. During her PhD studies, she collaborated with national and international researchers, resulting altogether in 14 peer-reviewed scientific publications and 14 poster or oral presentations at conferences. She received the “For Women in Science 2023” Fellowship awarded by L’Oréal - UNESCO. Additionally, she contributed to presenting science to a wider public by participating at workshops for children and holding presentations at events such as “Noč raziskovalcev”.